Autonomous Supervision and Control of Parametric Roll Resonance

Galeazzi, Roberto; Blanke, Mogens; Jensen, Jørgen Juncher

Publication date:
2010

Document Version
Publisher's PDF, also known as Version of record

Technical University of Denmark

Roberto Galeazzi

Autonomous Supervision and Control of Parametric Roll Resonance

PhD thesis, October 2009

DTU Electrical Engineering
Department of Electrical Engineering

Autonomous Supervision and Control of Parametric Roll Resonance

Roberto Galeazzi

DTU Elektro – PhD Thesis
Kongens Lyngby October 2009

Technical University of Denmark
DTU Electrical Engineering
Automation and Control
Building 326, DK-2800 Kongens Lyngby, Denmark
Phone +45 45 25 35 50, Fax +45 45 88 12 95
info@elektro.dtu.dk
www.elektro.dtu.dk

DTU Elektro-PhD: ISBN 978-87-92465-16-0

[This page intentionally left blank]

Summary

When ships sail in longitudinal waves, and the encounter frequency and wave length satisfy certain conditions, passage of wave crest and wave trough along the hull continuously amplifies the roll motion at half the frequency of encounter. This gives the onset of a resonance condition. The phenomenon can induce a rapid increase in roll motion that can reach 40 degrees or more. Recent incidents have shown that modern container ships and some fishing vessels are particularly prone to this due to their hull shape. Such incidents can result in damages counting to millions of USD. Theoretically, the resonance behaviour is well understood and it can be reproduced by quasi-periodic changes in parameters of nonlinear differential equations that describe ship motion. Practically, the challenge is whether detection and stabilization can be achieved in time to avoid damage. The research in this thesis has therefore two objectives. The first is to develop methods for detection of the inception of parametric roll resonance. The second is to develop control strategies to stabilize the motion after parametric roll has started.

Stabilisation of parametric roll resonance points to two possible courses of action. One is a direct stabilisation through an increase of damping in roll, which increases the threshold that triggers the resonant motion. A second is to obtain a change in wave encounter frequency by means of changes in ship forward speed and/or heading. As direct stabilisation, this thesis considers the increase of roll damping by using fin stabilisers, which are controlled using integrator backstepping methods. As indirect stabilisation, a shift in the encounter frequency is considered by varying the ship forward speed. The speed controller is designed using nonlinear Lyapunov methods. The two control strategies are then combined to stabilise parametric roll resonance within few roll cycles. Limitations on the maximum stabilisable roll angle are analysed and linked to the

slew rate saturation and hydrodynamic stall characteristics of the fin stabilisers.

The study on maximum stabilisable roll angle leads to the requirements for early detection. Two novel detectors are proposed, which work within a short-time prediction horizon, and issue early warnings of parametric roll inception within few roll cycles from its onset. The main idea behind these detection schemes is that of exploiting the link between the second harmonic of roll angle and the first harmonic of heave or pitch motions. A nonlinear energy flow indicator, which measures the transfer of energy from the first harmonic of heave or pitch into the second harmonic of roll, is at the core of the first detector. The second detector relies on a driving signal that carries information about the phase correlation between either pitch or heave and roll. A generalised likelihood ratio test is designed to detect a change in distribution of the driving signal. The detectors are validated against experimental data of tests of a 1:45 scale model of a container ship. The validation shows excellent performance in terms of time to detect and false-alarm rate for both the proposed detectors. The detectors are the main contribution of this research.

The thesis also offers a contribution regarding modeling. A 3 degree-of-freedom nonlinear model in heave-pitch-roll of a container ship suitable for parametric roll resonance study is proposed. The model, which has been developed in collaboration with other researchers, provides a benchmark for the study and simulation of parametric roll over a large range of ship speeds and sea states.

The results of this research have been published in articles enclosed in this dissertation and in an international patent application.

Dansk Resumé

Når et skib sejler i bølger hvis mødefrekvens og bølgelængde opfylder visse betingelser, kan rulning exiteres af en mødefrekvense som er den dobbelte af den naturlige rulningsfrekvens. En såkaldt parametrisk resonnans kan starte. Dette fænomen er forårsaget af at det oprettende moment fra bølger varierer så bølgetoppe og -dale vedblivende forstærker rulningen under deres passage af skroget. En parametrisk rulning kan nå 40 grader eller mere. Hændelser gennem de seneste år har vist at moderne container skibe og fiskefartøjer er særligt udsatte for dette fænomen på grund af deres specielle skrogform, og tilfælde af parametrisk rulning har forårsaget skader, der opgøres i millioner af USD. Et skibs dynamiske opførsel under en sådan resonnans kan beskrives som periodiske ændringer i parametre i de ulineære differentialligninger, der beskriver skibets dynamik, og teoretisk er det velbeskrevet hvordan parametrisk resonnans opstår. Udfordringen er om man kan detektere og dæmpe en parametrisk rulning inden den forårsager skader. Forskningsarbejdet har derfor haft to formål. Det første at udvikle metoder for detektion af starten af parametrisk rulning, det andet at udvikle reguleringsstrategier, som kan dæmpe parametrisk rulning.

Stabilisering af parametrisk resonnans kan opnås på to måder. Den ene er direkte dæmpning af rulningsbevægelsen gennem forøgelse af den grænse hvor parametrisk rulning kan indtræde. Den anden er en indirekte dæmpning gennem ændring i mødefrekvens. I denne afhandling benyttes finner til direkte stabilisering. Indirekte stabilisering opnås gennem ændring i skibets fart. Regulatorer designes med henholdsvis *integrator backstepping* og *Lyapunov* design metoder. De to reguleringsstrategier kombineres og det vises at stabilisering opnås på ganske få rulningsperioder. Afhandlingen analyserer også hvilke begrænsninger der er i opnåelig stabilisering og relaterer disse til begrænsninger i drejehastighed og løftekarakteristik for finner.

Studiet i stabiliserbarhed viser at der er krav om hurtig detektion af at parametrisk rulning er startet for at man kan opnå at stabilisere skibets bevægelser. Der er udviklet to nye metoder til at detektere at en parametrisk rulning er startet. Dedikeret signalprocessering og statistisk hypotesetest udnyttes og det vises at detektion kan ske indenfor få perioder af rulningsbevægelsen, hvilket rigeligt opfylder kravene til at opnå stabilisering. I den ene algoritme udnyttes at første harmoniske af duvning eller stampning skal give et positivt flow ind i anden harmoniske af rulning for at give resonnans. Den anden detektor er en indikator for fasekorrelation mellem rulning og duvning eller stampning. Der designes derefter en generaliseret sandsynligheds test (GLRT) til at afgøre hvilken statistiske fordeling indikatoren har og dermed detektere om parametrisk ressonans er indtrådt. Detektorerne er valideret med modeltank data fra test med en model af et containerskib i skala 1:45. Valideringen viser at begge detektorer fint opfylder kravene til hurtig detektion og at de begge har tilfredsstillende performance med hensyn til lavt niveau for falske alarmer. I forening har de to detektorer fremragende egenskaber og udgør et signifikant bidrag på området.

Afhandlingen indeholder også et bidrag vedrørende modellering. En matematisk model er udviklet for et containerskib i tre frihedsgrader, hævning-duvning-rulning. Modellen, som er udviklet i et internationalt samarbejde, gør det muligt at simulere og studere parametrisk rulning over et bredt område af fart og bølgehøjde.

Hovedresultaterne af dette forskningsarbejde er offentliggjort i artikler, som indgår i afhandlingen, samt i en international patentansøgning.

Preface

This thesis was prepared at the Department of Electrical Engineering, the Technical University of Denmark in partial fulfillment of the requirements for acquiring the Ph.D. degree in engineering.

The thesis deals with the design of a system for the supervision and control of large roll motion due to parametric resonance. Statistical change detection techniques are applied to design detectors capable of issuing early warnings of parametric roll inception. In this perspective the thesis focuses on signal based approaches, which do not require neither a model of the system to be monitored nor the estimation of the sea state parameters. Linear and nonlinear control strategies are employed to stabilise the roll motion, acting directly on roll or indirectly on surge to detune the resonance condition.

The thesis consists of a summary report and a collection of five research papers written during the period 2006–2009, and elsewhere published.

Lyngby, October 2009

Roberto Galeazzi

Papers included in the thesis

[A] C. Holden, R. Galeazzi, C. Rodríguez, T. Perez, T. I. Fossen, M. Blanke, M. A. S. Neves. "Nonlinear Container Ship Model for the Study of Parametric Roll Resonance." *Modeling, Identification and Control*, **28**, pp. 87-113, 2007.

[B] R. Galeazzi, M. Blanke. "On the Feasebility of Stabilizing Parametric Roll with Active Bifurcation Control." *Proceedings of the 7th IFAC International Conference on Control Applications in Marine Systems*, 2007.

[C] R. Galeazzi, C. Holden, M. Blanke, T. I. Fossen. "Stabilisation of Parametric Roll Resonance by Combined Speed and Fin Stabiliser Control." *Proceedings of the 10th European Control Conference*, 2009.

[D] R. Galeazzi, M. Blanke, N. K. Poulsen. "Parametric Roll Resonance Detection on Ships from Nonlinear Energy Flow Indicator." *Proceedings of the 7th IFAC International Symposium on Fault Detection, Supervision and Safety of Technical Processes*, 2009.

[E] R. Galeazzi, M. Blanke, N. K. Poulsen. "Parametric Roll Resonance Detection using Phase Correlation and Log-likelihood Testing Techniques." *Proceedings of the 8th IFAC International Conference on Manoeuvring and Control of Marine Craft*, 2009.

Other Publications

- R. Galeazzi, J. Vidic-Perunovic, M. Blanke, J. J. Jensen. "Stability Analysis of the Parametric Roll Resonance under Non-Constant Ship Speed" *Proceedings of the 9th Biennial ASME Conference on Engineering Systems Design and Analysis*, 2008.
- C. Holden, R. Galeazzi, T. Perez, T. I. Fossen. "Stabilization of Parametric Roll Resonance with Active U-tanks via Lyapunov Control Design" *Proceedings of the 10th European Control Conference*, 2009.
- R. Galeazzi, M. Blanke, N. K. Poulsen. "Prediction of Resonant Oscillations" *Patent Application: EP09157857.5, US61/169,154*, April 2009. Patent application writer: B. Andersen, Plougmann & Vingtoft - Intellectual property consulting.

Acknowledgements

1st August 2006 I "jumped aboard" of my PhD studies: I was a fresh mariner approaching his first voyage through the exciting world of research. Standing at the quay of this journey the way to go appeared very blurred, like in one those very foggy days. As in every long and challenging travel it is important to have an experienced master who can suggest the path to follow when the mariner is facing a completely new field of research, which is as wide as an ocean to his green eyes, and to guide through the sea mist when the right direction seems to be temporally lost. I personally retain myself extremely lucky of having had Prof. Mogens Blanke as mentor during the past three years. He introduced me to the fascinating world of research, fostering since the very beginning the desire of deeply and widely investigating into the problems at hand, and encouraging me throughout the PhD project to always achieve higher results. I sincerely enjoyed his attitude to openly confront each other during the numerous conversations we had about research issues and every day life. I really appreciated his way of supervising my PhD studies constantly increasing the amount of responsibilities I had to face myself, but at the same time never leaving me alone in those moments where the results were mostly needed. I will never forget his positive spirit in exchanging e-mails at 2 a.m. while a deadline was inexorably approaching and the paper was still missing a result. Therefore in these three years I had not only the luck of having a great mentor but I also had the pleasure of finding a sincere and valid friend.

I would like to gratefully thank my co-supervisor Prof. Jørgen J. Jensen to disclose some of the secrets of marine hydrodynamics to me. Thanks to his wide knowledge and fruitful advises I had a very smooth entrance in the marine engineering field, a completely unknown world at the beginning of this project.

Many thanks goes to Prof. Thor I. Fossen for hosting me at the Department of Engineering Cybernetics - Norwegian University of Science and Technology during the fall 2007. His guidance during my research stay has been source of many ideas, which resulted as strong basis for a part of this thesis.

Truthfully thanks goes to my "journey mates" Ole F. Hansen and Rufus Blas: I had the great opportunity to share the office with two excellent guys always ready for some good brainstorming as well as for a refreshing good beer. We started as colleagues, we ended up as friends. Special thanks goes to Martin B. Larsen for proof-reading the thesis when it was still a "wild draft", and pointing out the numerous typos which were hidden to my eyes.

Hearty thanks go to "min kæreste" Vibeke for showing huge patience and understanding especially during the last months of this voyage, when, although feeling neglected by me, she never refuses me a warm smile.

Last but not least important, I gratefully thank my Family who continuously supported me during these years I spent away from home. You always encouraged me to proceed along this difficult but at the same time exciting voyage, sharing morally with me the tough moments and the more joyful ones. Undoubtedly I can say that I constantly felt your presence beside me.

[This page intentionally left blank]

Contents

List of Symbols

Acronyms

DOF	degree-of-freedom
GLRT	generalised likelihood ratio test
MLE	maximum likelihood estimate
PDF	probability density function
TEU	twenty-foot equivalent unit

Greek letters

$\boldsymbol{\tau}_{\mathrm{hs}}$	vector of the hydrostatic forces and moments
χ	encounter angle of the wave
γ	threshold set by the desired probability of false alarms
$\hat{\sigma}_x^2$	estimate of the signal variance
λ_w	wave length
μ_0	signal mean value before a change takes place in the signal
Ω	frequency of the excitation
ω_0	natural frequency of the system
ω_e	encounter frequency of the wave

ω_w	wave frequency
$\phi_{\max}$	maximum roll angle
ρ	water density
σ	de-tuning parameter
σ_0^2	signal variance before a change takes place in the signal
σ_1^2	signal variance after a change takes place in the signal
σ_x^2	variance of the signal x
$\tau_{i,\mathrm{hs}}$	i-th component of $\boldsymbol{\tau}_{\mathrm{hs}}$ where $i = 1, \ldots, 6$

Roman letters

$\bar{e}$	energy threshold
$\bar{h}_s$	ship dependent threshold
$\bar{P}$	power threshold
GM_a	amplitude of the variations of the metacentric height in waves
∇	displaced volume
$\overline{\mathrm{GM}}$	metacentric height in calm water
A_w	wave amplitude
B	beam of the ship
e_f	energy flow coefficient
g	acceleration of gravity
H_s	significant wave height
h_w	wave height
I_{xx}	inertia in roll
I_{yy}	inertia in pitch
k	wave number
K_p	linear roll damping coefficient (also addressed by $K_{\dot{\phi}}$)
$K_{\dot{p}}$	added inertia coefficient in roll (also addressed by $K_{\ddot{\phi}}$)
$K_{\phi\phi\phi}$	cubic coefficient of the roll restoring moment

K_ϕ	linear roll restoring moment coefficient
L_{PP}	ship length between perpendiculars
m	mass of the ship
$M_{\ddot{\theta}}$	added inertia coefficient in pitch
$M_{\ddot{z}}$	added inertia coefficient in pitch due to heave acceleration
$M_{\dot{\theta}}$	linear pitch damping coefficient
$M_{\dot{z}}$	linear pitch damping coefficient due to heave speed
N	window length
$P_{x,y}$	cross-spectrum of the signal x with the signal y
S_{W_0}	water plane area in calm water
S_{W}	water plane area in waves
T_e	wave encounter period
T_p	peak period
T_ϕ	roll natural period
X_u	linear surge damping coefficient
$Z_{\ddot{\theta}}$	added mass coefficient in heave due to pitch acceleration
$Z_{\ddot{z}}$	added mass coefficient in heave
$Z_{\dot{\theta}}$	linear heave damping coefficient due to pitch rate
$Z_{\dot{z}}$	linear heave damping coefficient

Chapter 1

Introduction

According to the Review of Maritime Transport 2008 [80], maritime transportation is the backbone supporting international trade and globalization, carrying more than 80% of the world merchandize trade by volume. In the last 20 years the container trade in TEUs (twenty-foot equivalent unit) has approximately increased by a factor of five (Fig. 1.1) reaching 143 million TEUs in 2007, and the container business is estimated to double by 2016 and more than double by 2020 exceeding 371 million TEUs.

This unceasing growth of the container trade obviously affected the structure of the world fleet: in the period 2005-2008 the container ships fleet increased by 12.7%, the largest increment among the principal types of vessel. The increasing number of container carriers and their ceaseless transit over the major trading routes brought about a great risk of accidents. According to the European Maritime Safety Agency [16] accidents happened to 8% of the container ships in and around EU waters[1] in 2008 (Fig. 1.2).

The main concern related to container ships is the loss of containers overboard, a worry to shippers and insures due to the high value cargoes carried. Containers lost overboard are estimated to range between 2000 and 10000 units per year [67], and, although cargo losses at sea are as old as the shipping industry, this is becoming a problem since modern container vessels transport a large

[1] Including Norway and Iceland

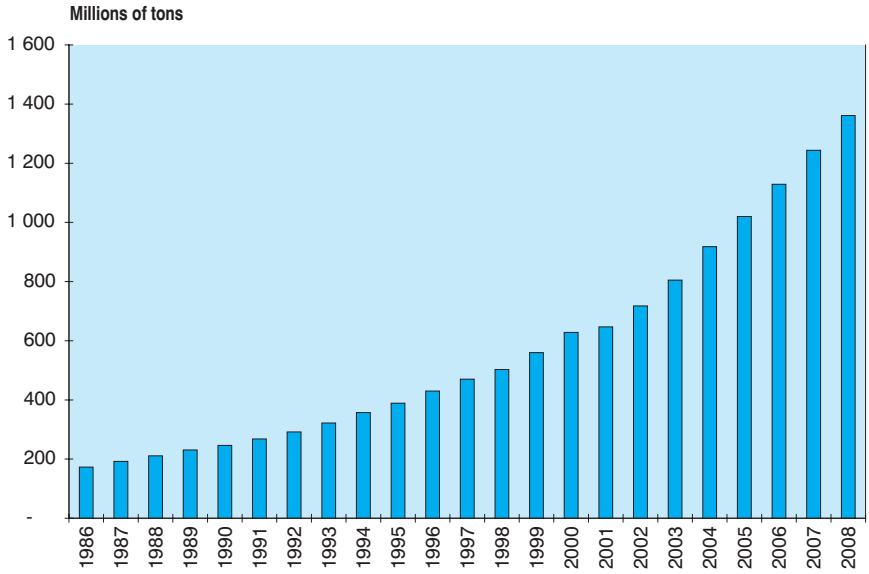

Figure 1.1: International containerized trade growth (source: [80]).

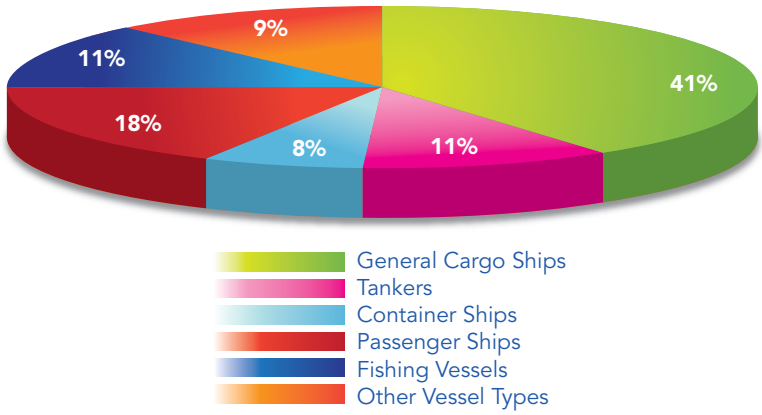

Figure 1.2: Breakdown of accidents by ship type in 2008. Percentages per vessel type have been rounded down, hence the total is 98% (source: [16]).

part of their cargo stacked above deck. Despite correct loading and fastening, containers regularly fell overboard during the stormy months of the year.

Harsh weather conditions can be retained a major cause for cargo losses, and recent incidents have shown that the natural reaction of ship's masters is to reduce speed and steer the vessels into the waves, in order to protect the ship and the cargo. However this has laid the vessel itself open to the attack of unexpected large roll oscillations whose amplitude was greater than that estimated at the shipbuilding stage. This phenomenon, identified as head seas parametric rolling, has been found to afflict modern container carriers due to the particular hull forms used – pronounced bow flare, flat transom stern, wall-sided midships sections – which were designed to achieve an optimal trade-off between high service speeds and maximum container payload above deck.

Although head seas parametric rolling has not yet sunk a ship, its existence challenges the insurance industry with the possibility of catastrophic losses, and it aggravates the risk of containers falling overboard, increasing in turn the marine litter[2].

1.1 The Unexpected Oscillation

An initial understanding of how parametric roll is expereinced can be obtained through two brief descriptions of incidents happened to container vessels:

October 1998 – APL China [20, 29]: "A laden, post-Panamax, C11 class containership, eastbound from Kaohsiung to Seattle, was overtaken by a violent storm in the North Pacific Ocean. ... Port and starboard rolls as great as 35° to 40° were reported to have occurred simultaneously with the extreme pitching. The master later described the ship as absolutely out of control during the worst storm conditions. ... Of the almost 1300 on-deck containers, one-third, with their cargoes, had been lost overboard. Another one-third, with their cargoes, were in various stages of damage and destruction. Containers and cargoes hung over both sides of the vessel. ... Cargo, container and vessel owners and their underwriters confronted the largest container casualty in history."

"At this early stage, lawyers are estimating that the lost cargo was worth more than the value of the China ship, more than $50 million."

[2]Human-created waste that has deliberately or accidentally become afloat in an ocean

January 2003 – Maersk Carolina [13]: "A Panamax container vessel encountered a storm in the North Atlantic en route from Algeciras, Spain, to Halifax, Nova Scotia, Canada. The vessel experienced gale-force winds and seas in excess of 10 m. During one particularly violent rolling and pitching event, the vessel quickly and unexpectedly began rolling upwards of 47°. During this incident 133 containers were lost overboard, and 50 others sustained moderate to severe water damage but remained on board. Cargo claims exceeded 4 million dollars. The vessel itself sustained moderate structural damage."

Three main aspects are evinced from these excerpts:

1. the roll motion onsets completely unexpectedly, and the vessel reaches large roll angles in a very short time
2. the large roll oscillations come together, or as a consequence of extreme pitching
3. the vessel becomes/seems to be completely out of control

which address the main issue: safety. Large roll oscillations combined with intense pitch motion can lead to structural damages of the ship hull, and in extreme cases reducing, or annulling the margins of safety for the ship.

A distinct image of the damages produced by parametric roll are illustrated by pictures of container vessels at quay after having experienced this phenomenon. Figure 1.3 illustrates the level of devastation suffered by the cargo.

1.2 Literature Survey

Parametric roll is a nonlinear phenomenon that belongs to the category of parametric resonance, a type of resonance that takes place in systems characterized by periodic variations of some of its coefficients. The first observations of parametric resonance phenomena date back to 1831 when Faraday [17] reported crispations produced when a large glass of water was made to sound by passing a wet finger around the edge. Later, in 1859, Melde [53] observed that a periodic variation in the tension of a taut string parametrically excites transverse waves in the string when the frequency of the change of the tension is about twice the natural frequency of any transverse mode. A mathematical description of

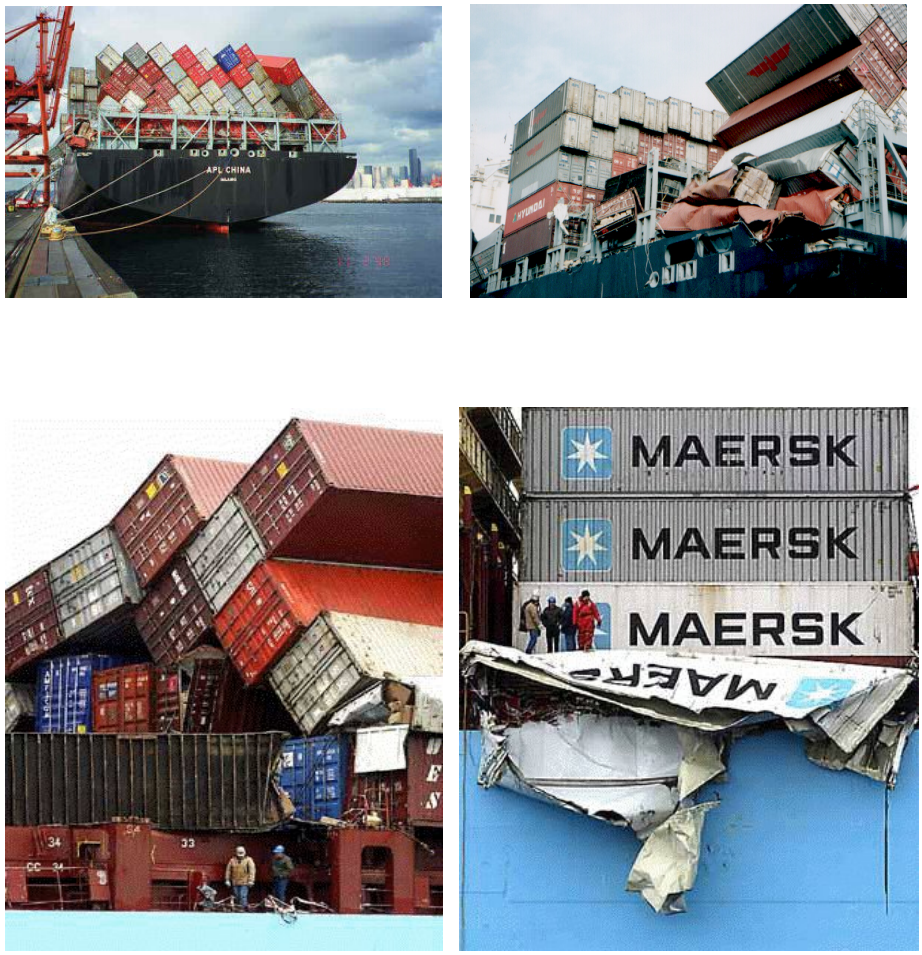

Figure 1.3: Devastation of on-deck containers after the vessels underwent parametric roll resonance phenomenon: (top) APL China, (bottom) Maersk Carolina. (`http://www.cargolaw.com/`)

parametric resonance was given by Mathieu [51], whose differential equations arise when the wave equation is written in elliptic form, followed by a separation of variables [4].

Observations of parametric resonance on ships were first done by Froude [23, 24], in 1861, who reported that a vessel, whose natural frequency in heave/pitch is twice its natural frequency in roll, shows undesirable seakeeping characteristics, which can lead to the possibility of exciting large roll oscillations. Indeed, this oscillatory motion can determine capsizing if the ship sails in longitudinal regular waves. Although from that moment on parametrically induced roll in longitudinal seas has been present on the agenda of the marine research community, which in the second half of the 20^{th} century moved important steps in order to gather full understanding of this phenomenon, it was only after the report presented by France et al. [20] at the SNAME[3] Annual Meeting in 2001 about the causes determining the mammoth losses suffered by APL China, that parametric roll resonance reached the top of the priority list among the ships' stability related phenomena.

The amount of publications explicitly devoted to parametric roll increased rapidly in the period 2001-2008 with contributions from research groups over the world. More than forty publications, half of which consider container ships as object of the investigation, have been presented at international conferences or published in leading journals. Therefore, the parametric resonance incident of the APL China has in a certain sense set the year zero for the marine community in toto, and this event is used to divide the following literature survey in two main branches in order to better emphasize what has been the focus of the research about parametric roll before and after October 1998.

1.2.1 Parametric Roll - A Historic Perspective

In 1955 Kerwin [47] was among the firsts addressing stability issues related with possible large roll motion in longitudinal seas. Under the assumptions of fore-aft symmetry of the hull, and of regular waves, he investigated the possibility of triggering severe rolling using 1-DOF (degree-of-freedom) model. The periodicity of the encounter wave determined sinusoidal variations of the metacentric height and, in turn, allowed Kerwin to rewrite the roll equation as the Mathieu's equation, which has unstable solutions for certain values of its parameters. In particular the author addressed the responsibility of the resonant roll motion to the periodic fluctuations of the restoring moment, and by means of the stability chart of the Mathieu's equation, he revealed the unstable regions and

[3]The Society of Naval Architects and Marine Engineers, `http://www.sname.org/`

the dangerous encounter frequencies, which may trigger the onset of the resonance. Kerwin tried also to confirm his theoretical conclusions by experiments, which highlighted an important property: the roll motion took several hundreds oscillations to build up. This suggested the author to consider the study of parametric roll in regular seas of no practical interest due the infinitesimal probability for a ship of encountering hundreds of waves with the same period and phase. However, he started questioning whether a state of instability could exist under certain irregular seas conditions.

Few years later, Paulling and Rosenberg [69] broadened the investigations to a 3-DOF nonlinearly coupled system, including the motions in the vertical plane on the analysis of the development of large rolling. Due to the complexity at hand, the authors renounced to look for general solutions of the system and, instead, they investigated stability properties of the subsystems heave-roll, heave-pitch, and pitch-roll. The authors demonstrated that the energy transfer from the longitudinal waves to the roll motion is due to a nonlinear coupling between either heave and roll or pitch and roll. These couplings were shown to generate time-varying coefficients in the roll equation, which was rewritten as the Mathieu's equation. Furthermore, the heave-pitch subsystem exhibited parametric resonance. Here both heave and pitch can be the exciting mode, whereas in the heave-roll and pitch-roll subsystems roll cannot excite the motions in the vertical plane. Paulling and Rosenberg verified their analytical results through experiments of the heave-roll case. By comparison between theoretical and experimental results two main conclusions were drawn: first parametric roll was a real phenomenon since it had been observed experimentally; second the qualitative agreement was found to be good with the phenomenon being dependent on parameters as predicted by the theory.

In 1980 Blocki [8] investigated the possibility of assessing the probability of capsizing due to the parametric roll resonance in a given loading condition and for a certain sea state. The author supplied a tool suitable for calculating this probability for both heave-roll and pitch-roll couplings, which was intended for the use of classification societies. Starting from the same nonlinear rolling model of the ship, ten years later Sanchez and Nayfeh [74] identified by a qualitative analysis, followed by numerical simulations, the regions of parameter space where the trivial solutions of the roll equation lose their stability. Further they determined the typology of motions that arise inside these regions, and they characterized the danger that such behaviors pose to the overall seaworthiness of the ship.

Oh et al. [64, 65] continued the work of Sanchez and Nayfeh, relaxing the constraint of fore-aft symmetry and adding a third degree of freedom, namely pitch. The authors demonstrated theoretically and experimentally that a vessel sailing in longitudinal waves (both head and following seas) can spontaneously

develop large roll oscillations. In particular they emphasized the possibility that the energy supplied by the wave motion to heave and pitch may be transferred to the roll motion through nonlinear couplings among these three modes. The loss of dynamic stability and the onset of severe roll motion was investigated by setting up a 3-DOF model, where heave and pitch motions were assumed to be independent of the roll motion; they focused the analysis on the principal parametric resonance, i.e. the resonance which arises when the frequency of the wave excitation is about twice the roll natural frequency. Force-response diagrams of the supercritical and subcritical pitchfork bifurcations were found, addressing the coexistence of multiple solutions, which can switch from stable to unstable for different values of the forcing term. Experiments run with a tanker model validated the theoretical findings about the possibility of triggering unstable phenomena, although some discrepancies were also reported.

In 1999 Neves et al. [61] treated the link between parametric roll resonance and ship safety, emphasizing how some particular hull forms may increase the susceptibility of severe roll motion in longitudinal seas. By means of experimental and numerical investigations they compared the roll responses of two trawlers, which differed in the shape of the stern. The conclusions from their study were mainly two: first the experiments showed how a transom stern may have a clear destabilizing effect, determining high levels of parametric excitations; second both model tests and numerical simulations reported large roll oscillations in the $1:2$ zone of resonance, pointing out that parametric roll may be responsible for the capsizing of some small fishing vessels. The authors also remarked the crucial importance of experimental evidence in the area. Two years later Francescutto [21] presented an experimental investigation on parametric rolling in head seas for a destroyer naval class. The author was among the firsts who pointed out the risk of the onset of parametric roll resonance in head seas, a condition partially neglected by previous works since merchant ships are more prone to this phenomenon in following seas. By means of 1-DOF roll model recast as the linear damped Mathieu equation, and the assumption of sinusoidal time variation of the transversal metacentric height, the author compared the experimental results with the stability chart of the aforementioned equation finding a very good agreement. This confirmed the potential danger of parametric roll in head seas for ships with relatively long roll period, and it urged a more extensive and thorough experimental campaign aimed at developing consistent mathematical models for forecasting maximum roll amplitudes.

1.2.2 Parametric Roll - Recent Experiences

At the SNAME Annual Meeting in 2001 France et al. [20] presented a detailed analysis of the incident of the post-Panamax container ship APL China in Octo-

ber 1998. By means of extensive model tests and omplex numerical simulations of the full 6-DOF ship model the authors were able to assess with no doubts that head sea parametric roll resonance was the cause of the massive losses suffered by APL China. The model tests highlighted the influence of wave heading and ship speed on the roll angle; in particular the wave heading affected the amplitude of the roll oscillations through the variations of the metacentric height and through the speed reduction, which in turn determined a decrease in roll damping. The comparison between theory, once again based on the Mathieu's equation, and the model tests allowed France et al. to list four major conditions for parametric roll to occur:

1. the roll natural period is approximately equal to twice the period of the encounter wave ($T_\phi \approx 2T_e$)
2. the wave length is approximately equal to the ship length ($\lambda_w \approx L_{\text{PP}}$)
3. the wave height is greater than a critical level ($h_w > \bar{h}_s$)
4. the ship's roll damping is low

Moreover, the authors pointed out that particular hull shapes, flat transom stern and significant bow flare, determine a higher susceptibility to parametric roll due to the large stability variations these vessels undergo during wave passage in head seas. They also showed that the larger the stability variation is the broader is the bandwidth in which parametric roll can develop.

The report presented by France et al. was a turning point in the research about parametric roll resonance: if in the previous fifty years parametric roll was considered a minor problem for small vessels with intrinsic marginal stability – e.g. small fishing vessels – sailing in following seas, and seen mainly as a "good benchmark" to test nonlinear techniques for stability investigations, all the sudden it became a very concrete phenomenon able to threaten some of the giants of the sea in common passage conditions, which previously were considered of no danger. Although diverse directions of research were then taken, mainly two types of marine craft became the object of further investigations: container ships ([2, 3, 12, 33, 42–45, 49, 71, 75, 76, 78, 79]) and fishing vessels ([57–60]).

Modeling: The development of high-fidelity models for studying the roll motion in parametric resonance and predicting its largest oscillations for specific naval classes has been the main area of investigation of the marine community after the accident happened to the APL China container ship. Mainly two directions of research have been pursued: on the one hand

low/medium-complexity models have been proposed for investigating the onset conditions of parametric roll in head seas and assessing the stability conditions behind this triggering event. In this class of models there are: 1-DOF models where the roll motion is rewritten as the linear/nonlinear damped Mathieu equation and stability conditions are derived starting from Floquet theory (e.g. [33, 75, 78]); 1.5-DOF models where the roll motion is implicitly coupled with the motions in the vertical plane through the pre-computation of the righting lever $\mathrm{GZ}(\phi, t)$ by hydrostatic calculation of the heave and/or pitch responses (e.g. [9, 11, 22, 42, 43]); 3-DOF models where heave and pitch are fully nonlinearly coupled with roll and the wave forcing explicitly appears as non homogenous term in the equation of motions [57–59, 77]. On the other hand numerical models taking into account the whole ship dynamics in 5 or 6-DOF were used for assessing susceptibility of specific hull forms to parametric roll resonance in [20, 71, 75].

The modeling of the nonlinearities of the roll restoring moment in regular seas condition has also received attention. Hashimoto and Umeda [33], Umeda et al. [78] proposed a 1-DOF roll model, where the roll restoring moment is modeled as a function of wave steepness from captive model experiments. Comparing model tests with theoretical derivations, it was noticed that by applying the Froude-Krylov prediction [68] the roll restoring moment could be overestimated, and a higher danger of capsizing due to parametric rolling could exist. A reliable approximation of the restoring moment was also in focus of Bulian [9], who expressed the righting arm as a Fourier series expansion of the wave crest with main period equal to the wave length, assuming regular waves.

Forecasting: A probabilistic approach that aimed at assessing statistical properties of the roll motion in parametric resonance, and probabilistic indicators to predict the likelihood and the magnitude of large roll events were proposed in Belenky et al. [3], Bulian et al. [12], Jensen [42], Jensen and Pedersen [43], Levadou and Palazzi [49].

Belenky et al. [3], on the base of numerical simulations of ship motion in head seas, appraised that parametric roll can be assumed to be a stationary process within the period of quasi-stationarity of the sea state, the period of time in which the sea changes its statistical properties, but it is not an ergodic process although the heave and pitch motions are ergodic. Moreover the roll motion in parametric resonance was found to be not normally distributed. Bulian et al. [12] agreed on the non-Gaussian behavior of the roll motion in parametric resonance, highlighting also a non-Rayleigh behavior of the roll peaks; conversely from Belenky et al. they assessed that parametric roll is likely to be ergodic by the analysis of the coefficient of variation of the running standard deviation.

Combining the weather statistics with a parametric roll database, which provides the probability of occurrence of large roll motion for given vessel and wave parameters, Levadou and Palazzi [49] made a first attempt to quantify the operational risk of parametric roll resonance. Using wave scatter diagrams the authors determined that the probability of parametric roll in head seas at low speed ($2.5 - 5$ knot) ranges between 9% and 6%; at higher cruising speed the likelihood drops significantly. Based on these results Levadou and Palazzi drew the conclusion that C11 class post-Panamax container ships have a non negligible risk of meeting conditions in which parametric roll can develop. Jensen and Pedersen [43] and Jensen [42] using the standard first-order reliability method (FORM), a statistical procedure from structural mechanics, computed the time-invariant peak distribution associated with the reliability index that minimizes the probability of the roll angle to exceed a given threshold. Further, the authors showed the sensitivity of the reliability index to ship and wave parameters such as ship speed and heading, significant wave height and zero-crossing period. Jensen and Pedersen [43] suggested that these results could be used to derive operational polar diagrams.

Risk reduction: The effect of ship's forward speed on the probability of occurrence of parametric roll was studied by Ribeiro e Silva et al. [71], and more extensively by Jensen et al. [44, 45]. Ribeiro e Silva et al. [71] analyzed the parametric roll response in irregular sea as a function of the forward speed. The outcomes of this study showed that the probability of exceeding a given roll angle decreases significantly while increasing ship's advance speed; therefore the authors identified the increase of cruise speed as the first action to be taken when the ship is under parametric roll, and based on that they suggested to revise the "*Guidance to the Master for Avoiding Dangerous Situations in Following and Quartering Seas*"[39]. Jensen et al. [44, 45] applied the first-order reliability method to evaluate the influence of ship's forward speed on parametric roll, and they reported an increase in the reliability index when surge motion is accounted for. This reduction in probability of occurrence was in agreement with theoretical expectation since a speed variation affects the encounter wave frequency and in turn tends to violate the parametric roll resonance frequency condition. Nevertheless in an irregular waves scenario, the probability of the onset of parametric roll is only slightly depending on the ship speed due to the large spread in wave frequencies.

Susceptibility to parametric roll: A deterministic approach for the determination of susceptibility criteria for the onset of parametric roll was proposed by Shin et al. [75]. By means of approximations of the first region of instability of the Ince-Strutt diagram associated with the Mathieu's equation, the authors derived the susceptibility criteria in terms of the

parameters of the aforesaid equation. The criteria consist of two conditions: a frequency condition stating that the frequency of parametric excitation should be approximately twice the roll natural frequency; a damping threshold condition assessing that the roll damping should be smaller than a damping threshold. Spyrou et al. [76] made a "step-by-step" evaluation of these susceptibility criteria, which were adopted by ABS[4] [1], and they found that these analytical formulae can successfully characterize parametric roll described as a Mathieu-type system; however as the mathematical model becomes more complex, e.g. accounting for non harmonic variation of the restoring moment, their prediction potential prominently decreases. The authors, hence, introduced the method of continuation of nonlinear dynamics in order to achieve a better identification of the stability boundary, and a more reliable prediction of the steady amplitudes of the roll oscillations in parametric resonance.

Passive anti-rolling devices: Shin et al. [75] proposed the use of passive anti-roll tanks to increase damping in the roll equation and hence reduce the ship's susceptibility to parametric rolling. From a preliminary numerical study they pointed out that passive U-tanks might be an effective technology to mitigate/avoid the consequences of parametric roll resonance. Umeda et al. [79] assessed experimentally the effectiveness of using anti-roll tanks and sponsons[5] to prevent parametric rolling: sponsons showed a limited capability of reducing roll oscillation in parametric resonance condition, beside the increased difficulty that such device will introduce in berthing and loading operations; anti-roll tanks, instead, may lead to complete vanishing of parametric roll, although their installation determines a reduction of onboard containers.

The APL China disaster also pushed the classification societies and the marine industry to investigate on parametric roll resonance in order to find adequate strategies and technologies capable of dealing with it. International organizations, like IMO[6], and SNAME, together with classification societies, like ABS, DNV[7], and Lloyd's Register[8], have spent remarkable efforts to support the ship industry with means capable of reducing the likelihood of occurrence of parametric roll resonance, and in turn to decrease the risks for the crew, the cargo and the ship.

[4] American Bureau of Shipping, `http://www.eagle.org/`

[5] Projections from the sides of a watercraft, for protection, stability, or the mounting of equipment; they extend the hull dimension at or below the waterline and serve to increase flotation or add lift when underway

[6] International Maritime Organization, `http://www.imo.org/`

[7] Det Norske Veritas, `http://www.dnv.com/`

[8] `http://www.lr.org/`

In August 2003 Lloyd's Register [50] suggested possible long term solutions that should focus on reducing the likelihood of occurrence of parametric roll. Two possible ways were taken into account: modification of the hull form, or enhancement of the ship's roll damping. Both solutions would have affected the vessel performance in terms of speed, stability and container carrying capacity. Nevertheless, due to the absence of reliable methods for decreasing the probability of occurrence at that time, Lloyd's Register proposed that ship owners and designers had to focus on the reduction of the consequences of the extreme motion addressing two main aspects: container lashing systems, and machinery systems. One year later, ABS issued the "*Guide for the assessment of parametric roll resonance in the design of container carriers*" [1] where for the first time an optional class notation was proposed specifically for parametric roll. Moreover an operational guidance based on polar diagrams (Fig. 1.4) was suggested to be supplied to the masters of ships found to be susceptible to parametric roll.

During the first half of 2006 DNV [15] pointed out the necessity of developing second generation warning systems capable to deal with the onset of critical roll in a short prediction horizon, to be integrated with the first generation warning systems based on guidelines for mariners and polar diagrams. In January 2007 IMO [40] issued a guidance to the masters for avoiding dangerous situations in severe sea and weather conditions, where again a kind of polar diagram was proposed as a tool to be used by the master in order to plan routes with low risk of parametric roll resonance. Later the same year DNV [14] presented its parametric rolling simulation model, which is a representation of a 2800 TEU Panamax beam container ship which has been trading in the North Atlantic for several years.

Looking at the off-the-shelf products it is clear that the maritime industry followed pretty much the requests from the classification societies in terms of prevention systems. Several companies provide onboard software that assess the operational risk for the onset of parametric roll. All these systems share the common approach of supplying the master with polar diagrams that show the conditions at which large ship motions can be expected (OCTOPUS Resonance[9], ARROW[10], VVOS[11], SeaSense [63]).

Figure 1.5 illustrates a screen shot from the SeaSense system: in the top right corner the polar diagram for parametric roll condition is displayed. The color-coded diagram shows the probability of the onset of parametric roll for a given

[9] `http://www.amarcon.com/products/index.html?main=http://www.amarcon.com/products/office6_voy.html`

[10] Avoidance of Roll Resonance or Wave Impact `http://www.marsig.com/software_arrow.html`

[11] Vessel and Voyage Optimization Solutions `http://www.jeppesen.com/industry-solutions/marine/high_seas/VVOS_Service_Page.jsp`

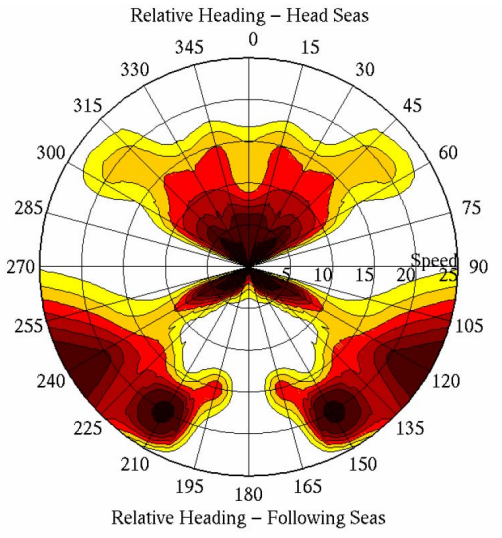

Figure 1.4: Polar diagram of predicted roll motion (source: [2]). Color-coded areas address combinations of ship's heading and forward speed that could trigger parametric roll.

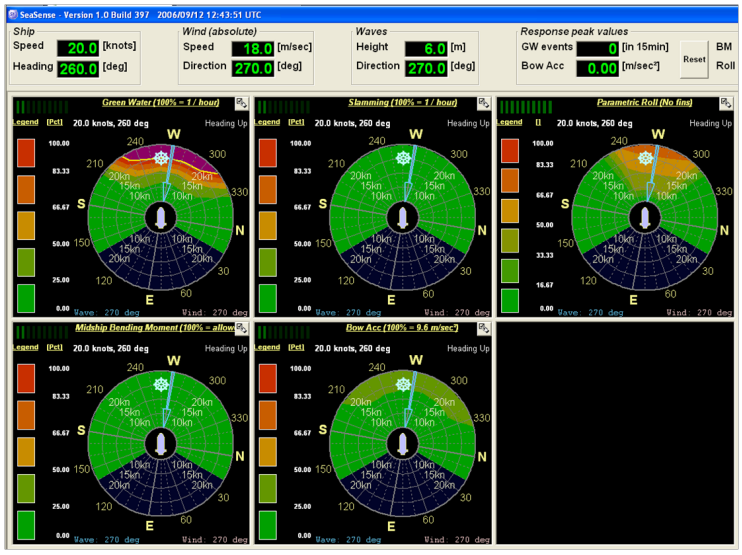

Figure 1.5: Screen shot of the SeaSense decision support system (courtesy of Lyngsø Marine).

ship heading and speed based on the estimated wave spectrum. These decision support systems all belongs to the first generation warning systems, since they provide the master with a probabilistic assessment of the risk of parametric roll resonance in a long time horizon and, therefore, the master can use them for eventual re-routing.

On the control side industry seemed to be less active, allotting marginal interest to the development of dedicated control solutions for counteracting the phenomenon. Only one ad-hoc solution was found, the IPRP[12]. This system consists of several pairs of U-tanks and pneumatically controlled air valves, together with a control unit equipped with pitch and roll sensors. The manufacturer claims that the IPRP system shifts the critical wave threshold to such high values that the possibilities of encountering such a sea state during a vessel's lifetime is very low. In order to achieve this the controller uses the damping effect of the tanks fluid's oscillations to raise the wave threshold and counteract the development of parametric rolling.

1.3 Scope and Contributions of the Thesis

This work has the aim of investigating possibilities to improve safety of container ships which undergo parametric roll resonance, preferably without re-routing that currently is scheduled on just the possibility of facing this critical phenomenon. This could be achieved by means of short time horizon detection of parametric roll and subsequent control action. The paradigm is that ability of detecting the onset of resonant motion in a time frame of few minutes would avoid the need of scheduling a new route, and at the same time it would allow to take the proper control action at the proper time. The thesis focuses on two strongly connected scopes:

- **detection** of the onset of parametric rolling
- **control** of parametric roll resonance once the phenomenon has onset.

The literature survey points out that these two directions of research have been left in the darkness. The marine community seemed to be completely devoted to the design of more complex models, which should better catch the characteristics of the roll motion in parametric resonance, leaving out almost any other aspect of the research.

[12]Intering Parametric Roll Prevention `http://www.rolls-royce.com/Images/3029_steer_stab_br_tcm92-8656.pdf`

Although the development of high-fidelity models is important since a new control system needs a good model to be tested, especially in marine engineering where tests are extremely expensive, developing the most representative model seemed to completely forget the large amount of ships afloat that can obtained very little benefit from a better model and subsequent new hull designs. These vessels can enhance their safety against parametric roll only through novel onboard systems, which are capable of giving an early warning of the onset of the resonant phenomenon, and that are ready to switch control strategies to counteract its development. Unnecessary re-routing could also be avoid if existing warning systems are integrated and/or replaced by second generation warning systems, which should be able to issue an alarm in a short time horizon, few minutes before critical oscillations take place.

The main contributions of this thesis can be summarized as follow:

Control: Paper [B] introduces the problem of parametric roll in the classical framework of the damped Mathieu equation and it identifies the damping as the critical parameter that can change the shape of the regions of stability diagram. In particular by increasing the level of the damping in the system the solution of the aforementioned equation can be brought back to the stable region. The feasibility of stabilizing parametric roll resonance is then shown by implementing a P controller, which actuates a fin stabilizer. Limitations on the control action are the saturation of the actuator due to the large roll moment induced by the parametric resonance.

Paper [C] continues along the direction of Paper [B] integrating the fin stabilizer with a speed controller, through nonlinear Lyapunov control design. By varying ship forward speed it is shown possible to de-tune the period coupling condition, i.e. $T_\phi \approx 2T_e$, and in turn to bring the system out of the principal parametric resonance region. Moreover, by increasing the speed it is possible to enhance the control action of the fin stabilizer, whose effectiveness increases with the ship speed. The combined action of the two controllers seems to be very effective in stabilizing the roll motion, which is driven to zero in few roll cycles, according to simulations.

Detection: Papers [D] and [E] address the detection problem in a completely novel framework that is characterized by:

1. a signal-based approach, which does not require a model of the system to be monitored, only the natural roll period needs to be known
2. detection achieved in a short-time horizon, and time to detect is less than two minutes for an irregular seas scenario
3. real-time detection
4. no need of estimating sea state parameters.

Paper [D] introduces a frequency-based detector, which uses an indicator of the energy flow from the modes in the vertical plane, directly excited by the waves, to the roll motion. This detector is compared against a standard sinusoidal detector on an experimental data set: in the regular wave scenario the two detection schemes perform equally well with the sinusoidal detector being somewhat faster in issuing the warnings; conversely in the irregular wave scenario the energy flow indicator shows greater robustness than the sinusoidal detector.

Paper [E] faces the detection problem in the time domain, proposing a detector that exploit the phase correlation between the second harmonic of roll and the first harmonic of heave/pitch. A driving signal carrying this phase information is designed and a GLRT (generalised likelihood ratio test) detector for non-Gaussian distributed signals is proposed and implemented. The detection performances are completely comparable with the energy flow detector, showing the same robustness in the regular and irregular wave scenario.

Paper [E] has been awarded as the "Best Regular Paper" at the 8th IFAC International Conference on Manoeuvring and Control of Marine Craft.

The methods presented in these two papers are covered by patents pending: EP 09157857.5 and US 61/169,154.

Finally, the thesis also offers a minor contribution in the field of modeling. Paper [A] presents a 3-DOF nonlinear coupled heave-pitch-model of a container ship for the study of parametric roll resonance. The main goal of this work has been to provide a benchmark for simulating parametric roll of a container ship over a large range of ship speeds and sea states. This benchmark has been designed to be a fully integrated part of Matlab/Simulink Toolbox for marine systems [54].

Chapter 2

Resonance and Parametric Resonance

Parametric roll is above all a nonlinear oscillation, which belongs to a class of systems called *parametrically excited systems*. This type of oscillation distinguishes itself from the forced oscillations because its onset is not due to the presence of an external forcing driving the system but it is caused by the presence of time-varying parameters in the equation of motion. Therefore it is of primal importance to unequivocally distinguish between externally excited systems, where resonant motions arise for the effect of the external forcing, and parametrically excited systems, where resonant behaviors appear due to variations in the parameters of the system. This is achieved by considering two well-known nonlinear differential equations: the forced Duffing equation, which belongs to the class of externally excited systems; the nonlinear Mathieu equation that appertains to the class of parametrically excited systems.

The last part of the chapter is dedicated to the introduction of another class of systems called *autoparametric systems*. Despite of the nonlinear Mathieu equation is a valuable tool to investigate parametric roll, it allows to consider the roll motion as 1-DOF system completely uncoupled from the rest of the ship dynamics. Autoparametric systems, instead, are interconnected systems, where parametric resonance origins from the vibrations of one of the constituting subsystems. Hence they provide a multi-degrees of freedom framework where the roll motion can be coupled with the modes responsible for the onset of

parametric resonance, namely heave and pitch.

The following analysis is based on the books by Nayfeh and Mook [55], Grimshaw [31], and Tondl et al. [77].

2.1 Externally Excited System

Consider the nonautonomous system governed by

$$\ddot{x} + \omega_0^2 x = \varepsilon f(x, \dot{x}) + E \tag{2.1}$$

where $\varepsilon \ll 1$ is a small parameter, f is a nonlinear function of the state x and its first time derivative, and E is an externally applied force, namely the excitation. In this analysis the excitation is restrained to be an ideal source of energy, which is featured by an unlimited amount of energy that makes the excited system have a negligible effect on the source itself. Thus $E = E(t)$, i.e. E is not a function of the system state.

Assuming that the nonlinear function f accounts for a cubic nonlinearity, and linear viscous damping, that is

$$f(x, \dot{x}) = -2\mu\dot{x} - \alpha x^3, \tag{2.2}$$

and assuming a single frequency excitation with amplitude and frequency constant, that is

$$E(t) = K\cos(\Omega t) \tag{2.3}$$

then Eq. (2.1) reads as the forced Duffing equation

$$\ddot{x} + \omega_0^2 x = -2\varepsilon\mu\dot{x} - \varepsilon\alpha x^3 + K\cos(\Omega t). \tag{2.4}$$

If the amplitude of the solution is small, then the nonlinear term can be neglected. The resulting system is linear and its response consists of two parts:

- *free-oscillation term*, which is the solution of the associated homogeneous equation

$$\begin{aligned} x_{\text{H}}(t) &= C_1 e^{-\varepsilon\mu t}\cos\left(\sqrt{\varepsilon^2\mu^2 - \omega_0^2}\right) + C_2 e^{-\varepsilon\mu t}\sin\left(\sqrt{\varepsilon^2\mu^2 - \omega_0^2}\right) \\ &= C_3 e^{-\varepsilon\mu t}\cos\left(\sqrt{\varepsilon^2\mu^2 - \omega_0^2} + C_4\right) \end{aligned} \tag{2.5}$$

  where C_j are determined from the initial conditions

- *steady-state response*, which is the particular solution

$$x_{\mathrm{P}}(t) = \frac{K}{\sqrt{(\omega_0^2 - \Omega^2)^2 + 4\Omega^2\varepsilon^2\mu^2}} \cos(\Omega t + \theta) \tag{2.6}$$

where $\theta = \arctan\left(-\frac{2\Omega\varepsilon\mu}{\omega_0^2 - \Omega^2}\right)$.

Equation (2.6) shows that the steady-state response has the same frequency of the excitation, but its phase θ is shifted from that of $E(t)$ a quantity, which depends on the damping and the relative magnitudes of ω_0 and Ω. Further the particular solution does not depend on the initial conditions. Then the complete solution of the linear damped harmonic oscillator is

$$\begin{aligned} x(t) &= x_{\mathrm{H}}(t) + x_{\mathrm{P}}(t) \qquad (2.7)\\ &= C_3 e^{-\varepsilon\mu t} \cos\left(\sqrt{\varepsilon^2\mu^2 - \omega_0^2} + C_4\right) + \frac{K}{\sqrt{(\omega_0^2 - \Omega^2)^2 + 4\Omega^2\varepsilon^2\mu^2}} \cos(\Omega t + \theta) \end{aligned}$$

From the steady-state response (2.6) it is noted that large motions occur when the amplitude K of the external force is large and/or the frequency of the excitation is approximately equal to the system natural frequency, i.e. $\Omega \approx \omega_0$. The latter condition is called *primary resonance* of the system.

2.1.1 Primary Resonance $\Omega \approx \omega_0$

The linear undamped theory predicts unbounded oscillations when $\Omega = \omega_0$, but in the actual case the oscillations are bounded by the presence of the damping and the nonlinearity. In order to determine the form of the solution of Eq. (2.4) at primary resonance the de-tuning parameter σ is introduced to quantitatively measure the closeness of the excitation frequency to the natural frequency of the system

$$\Omega = \omega_0 + \varepsilon\sigma, \qquad \sigma = O(1). \tag{2.8}$$

An approximate solution can be found applying, for example, the method of multiple scales, where the solution is expressed in terms of different time scales as

$$x(t;\varepsilon) = x_0(T_0, T_1) + \varepsilon x_1(T_0, T_1) + \ldots, \tag{2.9}$$

where $T_0 = t$ is the fast time, and $T_1 = \varepsilon t$ is the slow time. The excitation $E(t)$ is also expressed in terms of T_0 and T_1

$$E(t) = \varepsilon k \cos\left(\omega_0 T_0 + \sigma T_1\right), \tag{2.10}$$

where the amplitude K has been rewritten as εk. Substituting Eq. (2.9) and Eq. (2.10) into Eq. (2.4) and equating the coefficients of ε^0 and ε^1, the following system is obtained

$$\varepsilon^0 : \; D_0^2 x_0 + \omega_0^2 x_0 = 0 \tag{2.11}$$

$$\varepsilon^1 : \; D_1^2 x_1 + \omega_0^2 x_1 = -2D_0 D_1 x_0 - 2\mu D_0 x_0 - \alpha x_0^3 + k\cos(\omega_0 T_0 + \sigma T_1) \tag{2.12}$$

where $D_i = \frac{dT_i}{dt}\frac{\partial}{\partial T_i}$.

Nayfeh and Mook [55] showed that the first-order approximation to the steady-state response is given by

$$\begin{aligned} x(t) &= a\cos(\omega_0 t + \varepsilon\sigma t - \varsigma) + O(\varepsilon) \\ &= a\cos(\Omega t - \varsigma) + O(\varepsilon), \end{aligned} \tag{2.13}$$

that is the steady-state solution is exactly tuned at the frequency of the excitation Ω, but its phase is shifted of an amount equal to $-\varsigma$. The parameters a and ς are solutions of the first-order system

$$\begin{aligned} a' &= -\mu a + \frac{1}{2}\frac{k}{\omega_0}\sin\varsigma \\ a\varsigma' &= \sigma a - \frac{3}{8}\frac{\alpha}{\omega_0}a^3 + \frac{1}{2}\frac{k}{\omega_0}\cos\varsigma \end{aligned} \tag{2.14}$$

where the apex addresses differentiation with respect to T_1. At steady-state the amplitude a and the phase shift ς are constants, which depends on the frequency and the amplitude of the excitation, and in some circumstances on the initial conditions. The dependency of the amplitude a of the response on the amplitude K and frequency σ of the excitation can be evaluated by the *frequency-response equation*, which for the forced Duffing equation reads as

$$\left[\mu^2 + \left(\sigma - \frac{3}{8}\frac{\alpha}{\omega_0}a^2\right)^2\right] a^2 = \frac{k^2}{4\omega_0^2} \tag{2.15}$$

and by the *frequency-response curve* where each point corresponds to a different singular point[1] in the state plane.

Figures 2.1(a)-2.1(b) show the effect of the nonlinearity and the excitation amplitude on the frequency response curve, respectively. Hard springs, i.e. $\alpha > 0$, bend the curve to the right side with respect to the linear case ($\alpha = 0$), whereas soft springs, i.e. $\alpha < 0$ bend the curve to the left. The effect of

[1] Given the system $\dot{x} + f(x) = 0$, a singular point is a point $x = x^\star$ that is a solution of the equation $f(x) = 0$. Thus singular points correspond to the vanishing of the first derivative of the state, and therefore they are equilibrium points of the system.

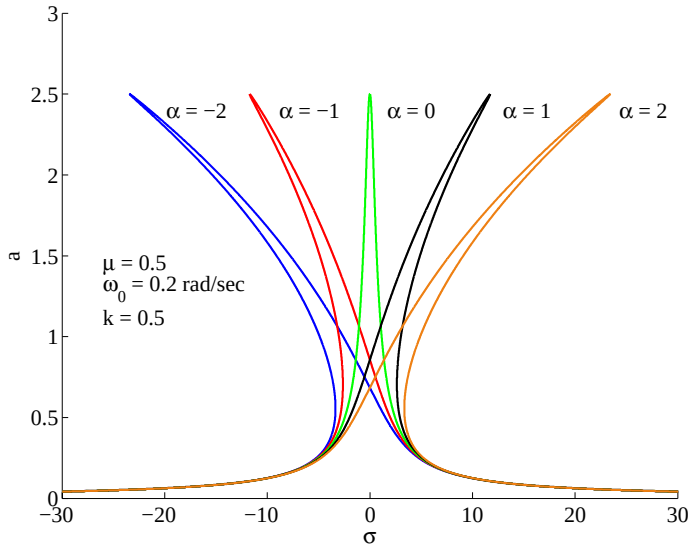

(a)

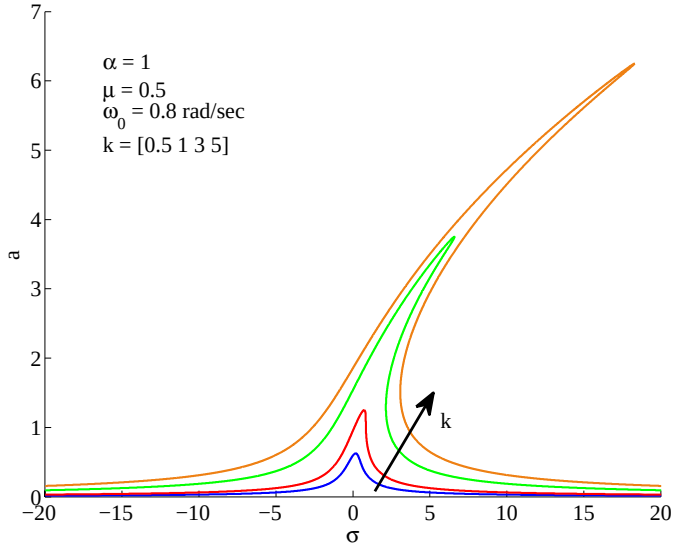

(b)

Figure 2.1: Frequency-response curves of the forced Duffing equation for different values of the nonlinear spring (a), and the excitation amplitude (b).

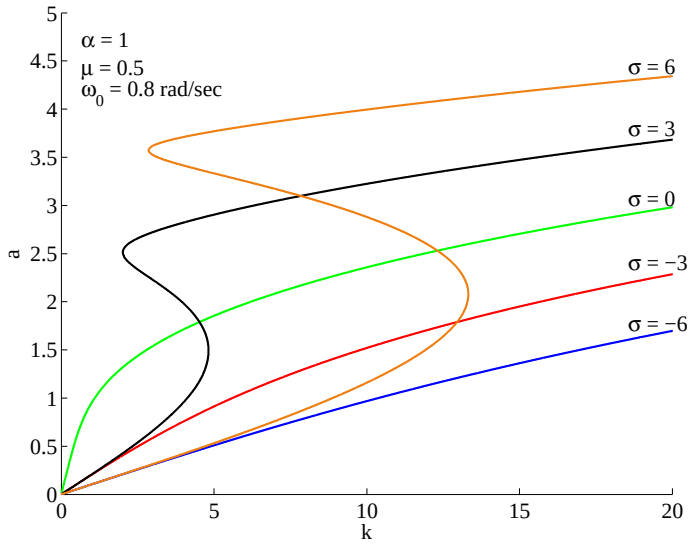

Figure 2.2: Response amplitude as a function of the excitation amplitude for different values of the de-tuning σ.

increasing the amplitude of the excitation is, instead, to bend away the curves from the $\sigma = 0$ axis; further it is possible to notice that, depending on the value of k, some of the frequency-response curves are single-valued whereas others are multivalued. Multivaluedness of the amplitude of the response can be also observed in Fig. 2.2, where the response amplitude a has been plotted as a function of the amplitude of the excitation k for several values of de-tuning.

The multivaluedness of the response curves bring about jump phenomena, which are distinctive of nonlinear systems; in particular Fig. 2.1(a) and Fig. 2.2 show that jumps may occur both by keeping the external excitation constant and varying the de-tuning σ, and by keeping fixed the frequency Ω of the excitation and varying its amplitude. Examples of how large oscillations may be generated by resonance condition ($\sigma = 0$), and by a jump phenomenon induced through the increase of the excitation amplitude are shown in Fig. 2.3.

2.1.2 Stability of the Steady-State Solution

According to Khalil [48] a nonautonomous system $\dot{x} = g(x,t)$ has a singular point at the origin at $t = 0$ if $g(t,0) = 0$ for all $t > 0$; but Eq. (2.4) has no

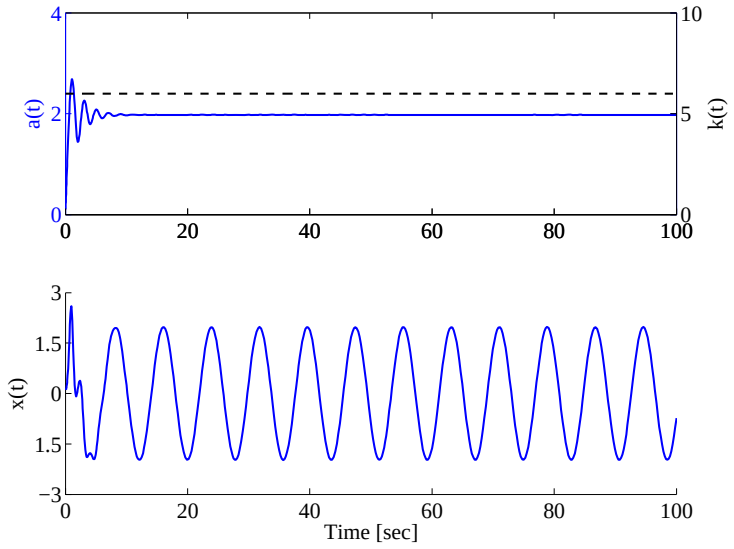

(a)

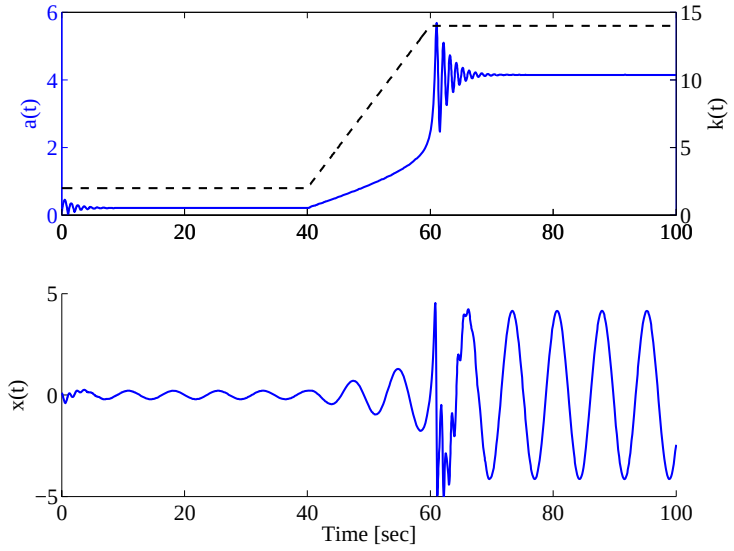

(b)

Figure 2.3: Large oscillations of the solution of the Duffing equation: (a) resonant response at $\Omega = \omega_0$ and $k = 6$, (b) jump phenomenon for $\sigma = 6$ and k raising from 2 to 14.

singular point at the origin since $g(t,0) = K\cos\Omega t$ for all $t > 0$. Hence to establish the stability of the steady-state solution (2.13) means to investigate the nature of the singular points of the system (2.14), whose solution is the amplitude and the phase shift of the steady-state response for a given set of parameters.

The local stability of the solution at steady-state can be assessed by investigating the nature of the singular points of the associated linear system. Therefore assuming that the pair $(a_{\rm ss}, \varsigma_{\rm ss})$ is a steady-state solution of the system (2.14), its stability is examined by looking at the behavior of the system in a neighborhood defined as

$$\begin{aligned} a &= a_{\rm ss} + a_1 \\ \varsigma &= \varsigma_{\rm ss} + \varsigma_1 \end{aligned} \tag{2.16}$$

where a_1 and ς_1 represent small perturbations. Substituting a and ς into the system (2.14) and linearizing in a_1 and ς_1, the following equations are obtained

$$\begin{aligned} a_1' &= -\mu a_1 + \left(\frac{1}{2}\frac{k}{\omega_0}\cos\varsigma_{\rm ss}\right)\varsigma_1 \\ \varsigma_1' &= -\left(\frac{3}{4}\frac{\alpha a_{\rm ss}}{\omega_0} + \frac{1}{2}\frac{k}{\omega_0 a_{\rm ss}^2}\cos\varsigma_{\rm ss}\right)a_1 - \left(\frac{1}{2}\frac{k}{\omega_0 a_{\rm ss}}\sin\varsigma_{\rm ss}\right)\varsigma_1. \end{aligned} \tag{2.17}$$

Hence the stability of the steady-state solution depends on the eigenvalues of the coefficient matrix of the perturbed system (2.17)

$$\mathbf{A} = \begin{bmatrix} -\mu & \left(\frac{1}{2}\frac{k}{\omega_0}\cos\varsigma_{\rm ss}\right) \\ -\left(\frac{3}{4}\frac{\alpha a_{\rm ss}}{\omega_0} + \frac{1}{2}\frac{k}{\omega_0 a_{\rm ss}^2}\cos\varsigma_{\rm ss}\right) & -\left(\frac{1}{2}\frac{k}{\omega_0 a_{\rm ss}}\sin\varsigma_{\rm ss}\right) \end{bmatrix}, \tag{2.18}$$

which can be found computing the roots of the characteristic polynomial

$$\begin{aligned} \det(\mathbf{A} - \rho\mathbf{I}) &= \rho^2 + 2\mu\rho + \mu^2 + \left(\sigma - \frac{3}{8}\frac{\alpha a_{\rm ss}}{\omega_0}\right)\left(\sigma - \frac{9}{8}\frac{\alpha a_{\rm ss}}{\omega_0}\right) \\ \rho_{1,2} &= -\mu \pm \sqrt{-\left(\sigma - \frac{3}{8}\frac{\alpha a_{\rm ss}}{\omega_0}\right)\left(\sigma - \frac{9}{8}\frac{\alpha a_{\rm ss}}{\omega_0}\right)}, \end{aligned} \tag{2.19}$$

where some of the coefficients of $\mathbf{A}$ have been replaced exploiting the relations (2.14) for $a' = \varsigma' = 0$. Equation (2.19) shows that if

$$\left(\sigma - \frac{3}{8}\frac{\alpha a_{\rm ss}}{\omega_0}\right)\left(\sigma - \frac{9}{8}\frac{\alpha a_{\rm ss}}{\omega_0}\right) < 0 \tag{2.20}$$

$$\left(\sigma - \frac{3}{8}\frac{\alpha a_{\rm ss}}{\omega_0}\right)\left(\sigma - \frac{9}{8}\frac{\alpha a_{\rm ss}}{\omega_0}\right) + \mu^2 < 0 \tag{2.21}$$

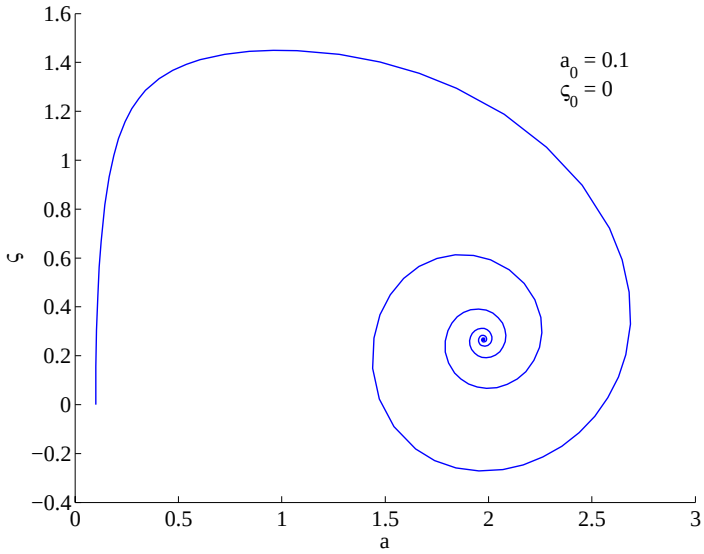

Figure 2.4: Phase plane of the resonant response in Fig. 2.3(a): the steady-state solution is stable as shown by the stable focus.

then one eigenvalue is positive and one is negative characterizing the singular point as a saddle; therefore the steady-state solution is unstable. Conversely, both eigenvalues are complex numbers with negative real part and, hence, there is a stable focus, which ensures stability of the steady-state solution.

Example 2.1 *Consider the steady-state solution shown in Fig. 2.3(a), which was obtained for these values of the parameters:* $\mu = 0.5$, $\omega_0 = 0.8\,\text{rad/sec}$, $k = 6$, $\alpha = 1$, $\sigma = 0$, *and* $\varepsilon = 0.01$. *The coefficient matrix associated with this response is*

$$\mathbf{A} = \begin{bmatrix} -0.5 & 4.5186 \\ -3.4729 & -0.5 \end{bmatrix} \tag{2.22}$$

whose eigenvalues are $\rho_{1,2} = -0.5 \pm 3.9614\text{i}$. *Therefore the singular point* $(a_{\text{ss}}, \varsigma_{\text{ss}}) = (1.9757, 0.2664)$ *is a stable focus, as it is also shown by the phase plane in Fig. 2.4.*

2.2 Parametrically Excited System

In a parametrically excited system the excitation appears as variations in the parameters; hence the system is mathematically described by differential equations with time-varying coefficients. In this case the excitation is called parametric excitation.

The first difference that comes into light comparing externally excited systems with parametrically excited systems is the amplitude of the response for a small amplitude of the excitation. In Section 2.1, Eq. (2.6), it has been pointed out that small excitation amplitudes K cannot determine large oscillations of the system response unless the excitation frequency is near to the natural frequency of the system, i.e. primary resonance condition. Conversely, a parametrically excited system can evidence large amplitude oscillations in response to a small parametric excitation when the frequency of the excitation is close to twice the natural frequency of the system. This frequency coupling is called *principal parametric resonance*.

The dynamics of parametrically excited systems can be inferred by analyzing the solutions behavior of the following system

$$\ddot{x} + p(t)x = \varepsilon f(x, \dot{x}) \tag{2.23}$$

where $p(t)$ is a periodic function, i.e. $p(t+T) = p(t)$, $\varepsilon \ll 1$ is a small parameter, and f is a nonlinear function of the state. In contrast with the analysis of the forced Duffing equation where the nonlinearity has been taken into account since the beginning, the study of Eq. (2.23) is carried out in three steps:

- analysis of the linear undamped system

  $$\ddot{x} + p(t)x = 0, \tag{2.24}$$

  where by means of Floquet theory [31, 55] stability properties of the solutions will be assessed

- inclusion of the linear viscous damping

  $$\ddot{x} + \mu\dot{x} + p(t)x = 0 \tag{2.25}$$

  to establish its effects on the stability of the solutions

- analysis of the effects of the nonlinearities on the behavior of the solutions.

2.2.1 Floquet Theory and Linear Hill-Mathieu Equation

Floquet theory was developed by Floquet [18] in order to characterize the functional behavior of linear systems with periodic coefficients. Obviously there is no intention of making a comprehensive excursus of this theory, but only two main theorems are stated, taken from [31]. The proofs are omitted, but the author addresses the interested reader to refer to [31].

Given the linear homogeneous system with periodic coefficients

$$\dot{x} = \mathbf{A}(t)x \tag{2.26}$$

where $\mathbf{A}(t+T) = \mathbf{A}(t)$ for all t, the following theorem holds

Theorem 2.1 *Let $\mathbf{X}(t)$ be the fundamental matrix of the system (2.26). Then $\mathbf{X}(t+T)$ is also a fundamental matrix, and there exist a non-singular constant matrix $\mathbf{B}$ such that*

$$\mathbf{X}(t+T) = \mathbf{X}(t)\mathbf{B} \qquad \forall\, t \tag{2.27}$$

Also,

$$\det \mathbf{B} = \exp \int_0^T \mathrm{tr}\mathbf{A}(s)\, \mathrm{d}s \tag{2.28}$$

Equation (2.27) states that in general the fundamental matrix $\mathbf{X}(t)$ is not periodic and, hence, in general the solution of the system (2.26) is not periodic although the presence of periodic coefficients in the matrix $\mathbf{A}(t)$. This can be shown with a simple example:

Example 2.2 *Consider the scalar equation*

$$\dot{x} = (\alpha + \beta \cos t)x, \qquad \alpha \neq 0 \tag{2.29}$$

which has a periodic coefficient with period $T = 2\pi$. The general solution can be obtained by separation of variables and it reads

$$x(t) = C_1 e^{\alpha t + \beta \sin t} \tag{2.30}$$

where C_1 is an arbitrary constant. It is evident that the solution is not periodic because

$$\lim_{t\to\infty} x(t) = \begin{cases} +\infty & \text{if } \alpha > 0 \\ 0 & \text{if } \alpha < 0 \end{cases} \tag{2.31}$$

Definition 2.2 Let the eigenvalues of $\mathbf{B}$ be $\rho_1, \ldots, \rho_n$ called *characteristic multipliers* for the system (2.26). The *characteristic exponents* $\lambda_1, \ldots, \lambda_n$ are defined by

$$\rho_1 = e^{\lambda_1 T}, \qquad \ldots, \qquad \rho_n = e^{\lambda_n T} \tag{2.32}$$

The characteristic multipliers and, therefore, the characteristic exponents do not depend on the specific selection of the fundamental matrix $\mathbf{X}(t)$, but they are intrinsic properties of the system (2.26). The second important result is asserted in the following theorem

Theorem 2.3 *Let ρ be a characteristic multiplier for the system* (2.26) *and let λ be the corresponding characteristic exponent so that $\rho = e^{\lambda T}$. Then there exists a solution $x(t)$ of the system* (2.26) *such that*

$$x(t+T) = \rho x(t) \qquad \forall\, t \tag{2.33}$$

Further, there exists a periodic function $q(t)$ such that

$$x(t) = e^{\lambda t} q(t) \qquad \forall\, t \tag{2.34}$$

Theorem 2.3 provides the general form of the solutions of the system (2.26) when the characteristic exponent has algebraic multiplicity one, and it points out that the key component is the exponential factor $e^{\lambda t}$, which fully determines the behavior of the solution. Therefore by knowing the sign of the characteristic exponent λ it is possible to infer the stability of the solution; λ can be straightforwardly computed inverting the relation (2.32)

$$\lambda_i = \frac{1}{T} \ln \rho_i \qquad i = 1, \ldots, n. \tag{2.35}$$

Consider the second-order differential equation

$$\ddot{x} + p(t)x = 0 \tag{2.36}$$

where $p(t)$ is a periodic function of period T. Equation (2.36) was first discussed by Hill [34] and therefore it is called Hill's equation. Applying Floquet theory, the stability of the solutions of Eq. (2.36) can be inferred by computing the eigenvalues of the constant matrix $\mathbf{B}$. Since the relationship (2.27) holds for all t, the matrix $\mathbf{B}$ can be expressed in terms of the fundamental matrix $\mathbf{X}(t)$ by putting $t = 0$

$$\mathbf{B} = \mathbf{X}^{-1}(0)\mathbf{X}(T), \tag{2.37}$$

further if $\mathbf{X}(t)$ is chosen as the principal fundamental matrix, i.e. $\mathbf{X}(0) = \mathbf{I}$ where $\mathbf{I}$ is the identity matrix, then $\mathbf{B} = \mathbf{X}(T)$. First Eq. (2.36) is rewritten as a first-order system

$$\begin{bmatrix} \dot{x}_1 \\ \dot{x}_2 \end{bmatrix} = \begin{bmatrix} 0 & 1 \\ -p(t) & 0 \end{bmatrix} \begin{bmatrix} x_1 \\ x_2 \end{bmatrix}, \tag{2.38}$$

where $x_1 = x$ and $x_2 = \dot{x}$. Then the principal fundamental matrix is formed

$$\mathbf{X} = \begin{bmatrix} x_1 & x_2 \\ \dot{x}_1 & \dot{x}_2 \end{bmatrix}, \tag{2.39}$$

where x_1 and x_2 are linearly independent solutions of Eq. (2.36) so that $\mathbf{X}(0) = \mathbf{I}$. The constant matrix $\mathbf{B}$ is, hence, given by Eq. (2.37)

$$\mathbf{B} = \begin{bmatrix} x_1(T) & x_2(T) \\ \dot{x}_1(T) & \dot{x}_2(T) \end{bmatrix}. \tag{2.40}$$

From $\mathrm{tr}\mathbf{A} = 0$ two implications can be derived:

- $\det \mathbf{B} = 1$
- the Wronskian of the fundamental matrix (2.39) is constant, and hence

$$W(t) \triangleq \det \mathbf{X} = x_1\dot{x}_2 - x_2\dot{x}_1 = W(0) = 1, \tag{2.41}$$

  where the rightmost-hand side derives from the fact that $\mathbf{X}$ has been selected as the principal fundamental matrix.

The characteristic exponents of $\mathbf{B}$ can then be computed as roots of the characteristic polynomial

$$\begin{aligned} \det(\mathbf{B} - \rho\mathbf{I}) &= \rho^2 - (x_1(T) + \dot{x}_2(T))\rho + x_1(T)\dot{x}_2(T) - x_2(T)\dot{x}_1(T) \\ &= \rho^2 - 2\varphi\rho + 1, \end{aligned} \tag{2.42}$$

where

$$\varphi \triangleq \frac{1}{2}(x_1(T) + \dot{x}_2(T)). \tag{2.43}$$

Hence $\rho_{1,2}$ are functions of the parameter φ and they are given by

$$\rho_{1,2} = \varphi \pm \sqrt{\varphi^2 - 1}. \tag{2.44}$$

Last the stability of the solutions of Eq. (2.36) can be assessed by the sign of the characteristic exponents associated with the roots $\rho_{1,2}$:

$|\varphi| > 1$ both roots are real and positive but the absolute value of one root is larger than unity, whereas that of the other one is less than one. Therefore one characteristic exponent is positive and one is negative determining the unbounded behavior of one of the solutions, and the instability of the Hill equation

$|\varphi| < 1$ the roots $\rho_{1,2} \in \mathbb{C}$ and they have unit modulus, i.e. $|\rho_{1,2}| = 1$; the characteristic exponents are both imaginary numbers, that is $\lambda = \mathrm{i}\upsilon$ where υ is the phase of the complex root. Therefore the solutions are both bounded, and the Hill equation is stable

$|\varphi| = 1$ there is a single root of multiplicity 2 at $\rho = \pm 1$, hence the characteristic exponent is $\lambda = 0$ and the solutions are periodic. When $\rho_{1,2} = 1$ the Hill equation has a periodic solution of period T, whereas when $\rho_{1,2} = -1$ there exists a periodic solution of period $2T$.

From this analysis two major conclusions may be drawn: first, the boundary between stable and unstable behavior is identified by the presence of periodic solutions; second, the onset of instability is caused by the existence of a resonance condition between the period of the parametric variation and some natural period of the system. The latter concept is explored further by considering a special case of the Hill equation, namely the Mathieu equation [51].

When the periodic function $p(t)$ is set equal to $\delta + \varepsilon \cos 2t$ the Hill equation reads as the Mathieu equation

$$\ddot{x} + (\delta + \varepsilon \cos 2t)x = 0, \tag{2.45}$$

where $\sqrt{\delta} = \omega_0$ is the natural frequency of the system, and the periodic coefficient has a period $T = \pi$. According to the previous analysis, the characteristic exponents of the Mathieu equation are still function of φ, which, in turn, is function of the parameters δ and ε, i.e. $\varphi = \varphi(\delta, \varepsilon)$. The pairs (δ, ε) for which $|\varphi| > 1$ are called unstable values, whereas those for which $|\varphi| = 1$ are called transition values. These determine the transition curves, which divide the $\delta\varepsilon$-plane into regions of stability and instability usually referred to as tongues, as shown by the Ince-Strutt diagram in Fig 2.5. Figure 2.6 shows two examples of solutions of the linear Mathieu equation for two different pairs of the parameters δ and ε: the solution on the top of the plot is oscillatory and unbounded, while that on the bottom is oscillatory but bounded.

In order to find the origin of the transition curves it is noted that for $\varepsilon = 0$ Eq. (2.45) reduces to the linear harmonic oscillator whose general solution is

$$x(t) = C_1 \cos \sqrt{\delta} t + C_2 \sin \sqrt{\delta} t, \tag{2.46}$$

which is a linear combination of the two independent periodic solutions of period $T_0 = 2\pi/\sqrt{\delta}$

$$x_1(t) = \cos \sqrt{\delta} \tag{2.47}$$

$$x_2(t) = \frac{1}{\sqrt{\delta}} \sin \sqrt{\delta} \tag{2.48}$$

found by imposing on the fundamental matrix $\mathbf{X}(t)$ to be the principal fundamental matrix. Hence, the conditions for parametric resonance, and in turn the

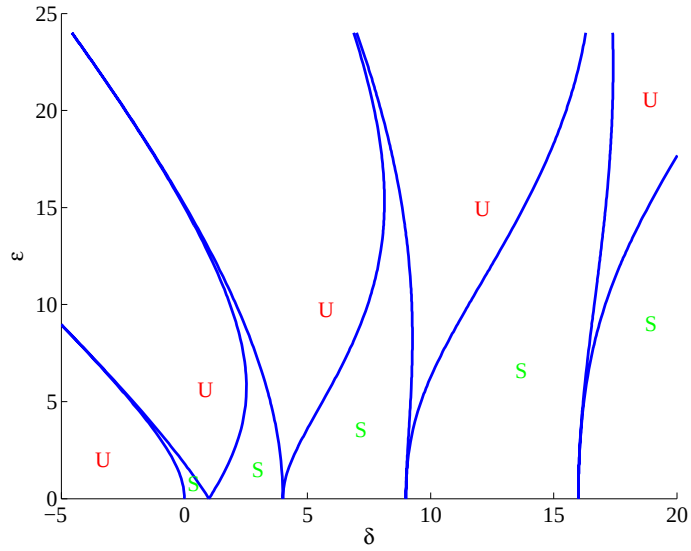

Figure 2.5: Ince-Strutt diagram of the linear Mathieu equation: the transition curves divide the $\delta\varepsilon$-plane in stable (S) and unstable (U) regions.

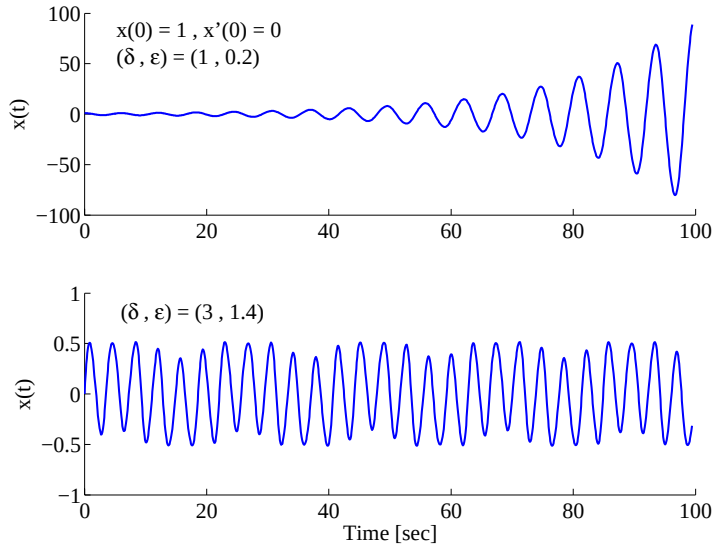

Figure 2.6: Unbounded and bounded solutions of the linear Mathieu equation.

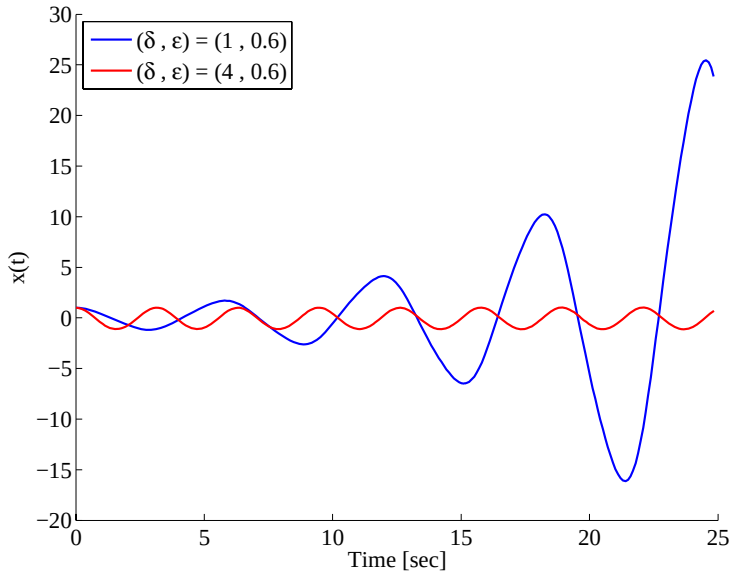

Figure 2.7: Responses of the linear Mathieu equation for the same magnitude of the excitation in two distinct resonance conditions.

origin on the δ-axis of the transition curves, can then be found by applying the relation (2.43), i.e. $\varphi = \cos\sqrt{\delta}T$, on the stability boundaries. In particular

$$\begin{array}{llll} \sqrt{\delta}T = 2n\pi & \Rightarrow & T = nT_0 & \text{if } \varphi = 1 \\ \sqrt{\delta}T = (2n+1)\pi & \Rightarrow & 2T = (2n+1)T_0 & \text{if } \varphi = -1 \end{array} , \qquad n \in \mathbb{N}. \tag{2.49}$$

When $\varphi = -1$ and $n = 0$ the Mathieu equation is in the resonance condition called principal parametric resonance, which is a sub-harmonic resonance characterized by $T_0 = 2T$ or $\omega_0 = \frac{1}{2}\omega$, that is the forcing frequency is twice the natural frequency. The principal parametric resonance is the most threatening resonance condition for the Mathieu equation since large amplitude oscillations can be generated for very small amplitude of the forcing. In Fig. 2.7 two responses of the Mathieu equation are plotted for the same magnitude of the excitation ε but at different resonance conditions, that is $\delta = 1$ and $\delta = 4$. In about eight periods of the parametric variation the amplitude of the response in principal parametric resonance has grown more than twenty times of the amplitude of the response in the second unstable region.

2.2.2 Effect of Linear Damping

Let us consider the linear Mathieu equation (2.45) where a small viscous damping term is added

$$\ddot{x} + \mu\dot{x} + (\delta + \varepsilon\cos 2t)x = 0 \tag{2.50}$$

with $\mu > 0$ being the damping coefficient. Applying the Floquet theory, stability conditions analogous to those obtained for the undamped case could be obtained, but in order to easily grasp the effect of the damping term on the stability of the solutions the transformation of variables proposed by Gunderson et al. [32]

$$y(t) = x(t)e^{-\mu t} \tag{2.51}$$

is applied to rewrite Eq. (2.50) as

$$\ddot{y} + (\delta - \mu^2 + \varepsilon\cos 2t)y = 0. \tag{2.52}$$

Therefore the effects of including linear damping are basically two:

- to decrease the growth rate of the response by a factor equal to μ
- to shift the natural frequency of the system from $\omega_0 = \sqrt{\delta}$ to $\omega_0 = \sqrt{\delta - \mu^2}$.

The presence of the viscous damping changes also the shape of the transition curves of the Ince-Strutt diagram; in particular to increase the value of the damping has the effect of enlarging the stability regions of the Mathieu equation and setting a minimum threshold for the parameter variation in order to trigger the parametric resonance, as shown in Fig. 2.8. For the first region of instability an approximation of the threshold is given by [31]

$$\varepsilon_{\min} \approx \sqrt{4[\mu^2 + (\delta - 1)^2]}, \tag{2.53}$$

which at the principal parametric resonance ($\delta = 1$) reduces to $\varepsilon_{\min} = 2\mu$, that is the parametric variation must be larger than twice the damping of the system to trigger the resonance motion.

2.2.3 Effect of Nonlinearities

To illustrate the effect of the nonlinearities on the behavior of the solutions, the following modified Mathieu equation is considered

$$\ddot{x} + (\delta + \varepsilon\cos 2t)x = \varepsilon f(x, \dot{x}). \tag{2.54}$$

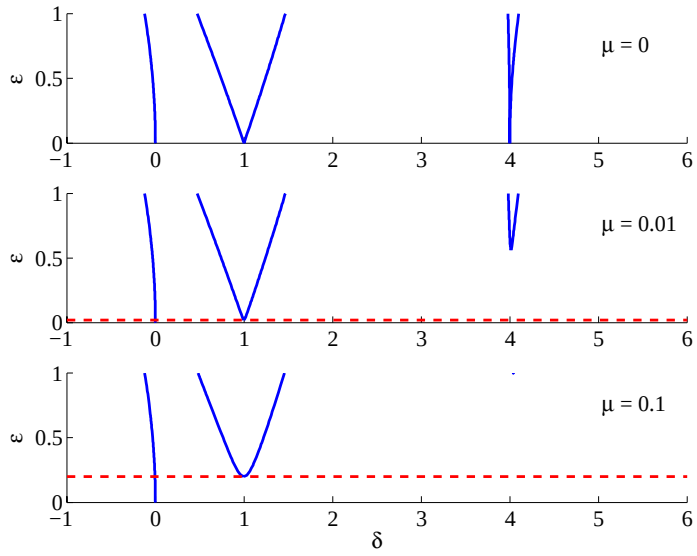

Figure 2.8: Ince-Strutt diagram of the linear damped Mathieu equation: the viscous damping has a stabilizing effect on the system since it enlarges the regions of stability and it sets a threshold on the minimum parametric variation needed to trigger the unstable motion (dashed red line).

In particular by choosing $f = -\mu\dot{x} - \alpha x^3$, Eq. (2.54) becomes a Duffing-type equation with a time-varying parameter in the linear term of the spring and without the external forcing

$$\ddot{x} + \varepsilon\mu\dot{x} + (\delta + \varepsilon\cos 2t)x + \alpha x^3 = 0. \tag{2.55}$$

Restricting the analysis to the case of principal parametric resonance, and applying the method of multiple scales, Nayfeh and Mook [55] showed that to first-order approximation the solution of Eq. (2.55) is given by

$$x(t) = a\cos\left(t - \frac{1}{2}\varsigma\right) + O(\varepsilon), \tag{2.56}$$

where α and ς are solutions of the autonomous system

$$\begin{aligned} a' &= -\frac{a}{2\omega}\sin\varsigma - \frac{1}{2}\mu a \\ a\varsigma' &= 2\varsigma a - \frac{a}{2\omega}\cos\varsigma - \frac{3}{4}\frac{\alpha}{\omega}a^3. \end{aligned} \tag{2.57}$$

The system (2.57) shows that the nonlinear spring term affects the amplitude of the response indirectly through varying the phase ς. In fact assuming that the

pair (δ, ε) corresponds to a point above the transition curve in Fig. 2.8 the amplitude of the response starts growing due to the parametric excitation, which pumps energy into the system. The increase of the amplitude a, however, determines a variation of the phase ς through the nonlinearity and, as consequence, a change in the rate of energy being pumped into the system. The system reaches the steady-state solution when the rate at which energy is being pumped into the system is balanced by the rate at which viscous damping dissipates energy; therefore the amplitude of the solution is limited by the nonlinearity to a finite value.

2.3 Autoparametric System

Tondl et al. [77] defined an autoparametric system as follows:

> "Autoparametric systems are vibrating systems that consist of at least two constituting subsystems. One is a *primary system* that will generally be in a vibrating state. This primary system can be externally forced, self-excited, parametrically excited, or a combination of these. ... The second constituting subsystem is called the *secondary system*. The secondary system is coupled to the primary system in a nonlinear way, but such that the secondary system can be at rest while the primary is vibrating."

More precisely an autoparametric system can be characterized by these four points:

- (at least) two nonlinearly coupled subsystems
- existence of a semitrivial solution defined as

$$\sum_{i=1}^{N} \left[x_i(t) + \dot{x}_i(t)\right]^2 \neq 0$$

$$y_i(t) = \dot{y}_i(t) = 0, \qquad i = 1, \ldots, M$$

  where x is the N-dimensional state of the primary system, and y is the M-dimensional state of the secondary system
- existence of intervals of the excitation frequency in which the semitrivial solution can become unstable

- autoparametric resonance onsets in the instability intervals of the semitrivial solution: the vibrations of the primary system act as parametric excitation of the secondary system, which stops being at rest.

An autoparametric system is, hence, the combination of a secondary system, which is always a parametrically excited one, with a primary system that belongs to one of the system classes aforementioned. Thus the stability of the semitrivial solution can be investigated using the same analysis carried out for the Hill/Mathieu equation in Section 2.2.1.

Of particular interest for the analysis of the phenomenon at hand is the autoparametric system that consists of a primary system externally forced by a sinusoidal excitation [77], that is

$$\begin{aligned} x'' + \mu_1 x' + x + \alpha_1 y^2 &= k\cos\eta\tau \\ y'' + \mu_2 y' + q^2 y + \alpha_2 xy &= 0 \end{aligned} \tag{2.58}$$

where $\mu_{1,2} > 0$ are the linear damping coefficients, $\alpha_{1,2}$ are the nonlinear coupling coefficients, $q = \omega_2/\omega_1$ is the tuning parameter that connotes the ratio of the natural frequencies of the linearized undamped secondary system ω_2 and the primary system ω_1, k is the amplitude of the external forcing, $\eta = \Omega/\omega_1$ is the forcing frequency, and $\tau = \omega_1 t$ is the time variable with respect to which differentiation is done. The nonlinear coupling between the primary and the secondary system is achieved through the term $\alpha_1 y^2$, which is the lowest order term that triggers a resonant interaction when ω_1 and ω_2 are in the $2:1$ ratio, that is the principal parametric resonance condition.

The semitrivial solution of the system (2.58) can be determined by posing

$$\begin{aligned} x(\tau) &= R\cos(\eta\tau + \varsigma) \\ y(\tau) &= 0 \end{aligned} \tag{2.59}$$

and by substituting $x(\tau)$ and $y(\tau)$ into the system's equations. This yields

$$R = R_0 = \frac{k\eta^2}{\sqrt{(1-\eta^2)^2 + \mu_1^2\eta^2}}. \tag{2.60}$$

The stability of the semitrivial solution is investigated by looking at its behaviour in a neighborhood defined as

$$\begin{aligned} x(\tau) &= R\cos(\eta\tau + \varsigma) + x_1(\tau) \\ y(\tau) &= 0 + y_1(\tau) \end{aligned} \tag{2.61}$$

where $x_1(\tau)$ and $y_1(\tau)$ are small perturbations. Substituting Eq. (2.61) into the system (2.58) and linearizing in $x_1(\tau)$ and $y_1(\tau)$ the following system is obtained

$$\begin{aligned} x_1'' + \mu_1 x_1' + x_1 &= 0 \\ y_1'' + \mu_2 y_1' + [q^2 + \alpha_2 R_0 \cos(\eta\tau + \varsigma_1)] y_1 &= 0. \end{aligned} \tag{2.62}$$

The first equation of the system (2.62) has solution $x_1 = 0$, which is asymptotically stable. Therefore the stability of the semitrivial solution is fully determined by the second equation, which is a Mathieu equation. As shown in Section 2.2.1, this equation has its principal instability region for $q \approx \frac{1}{2}\eta$ and its boundary is given by

$$\left(q^2 - \frac{1}{4}\eta^2\right)^2 + \frac{1}{4}\mu_2^2\eta^2 = \frac{1}{4}\alpha_2^2 R_0^2. \tag{2.63}$$

The boundary condition (2.63) can be used to determine the critical value k_c of the external excitation, which triggers the parametric resonance in the secondary system. In particular substituting Eq. (2.60) into Eq. (2.63) we obtain

$$k_c = 2\frac{\sqrt{(1-\eta^2)^2 + \mu_1^2\eta^2}}{\alpha_2\eta^2}\sqrt{\left(q^2 - \frac{1}{4}\eta^2\right)^2 + \frac{1}{4}\mu_2^2\eta^2} \tag{2.64}$$

which is analogue to the threshold condition found in Eq. (2.53) after posing $\eta = 1$, $\varepsilon = \alpha_2 R_0$, $\delta = q^2$, and $\mu = \mu_2$.

For $k > k_c$ the semitrivial solution becomes unstable, and a non trivial solution appears which is given by

$$\begin{aligned} x(\tau) &= R_1 \cos(\eta\tau + \varsigma_1) \\ y(\tau) &= R_2 \cos\left(\frac{1}{2}\eta\tau \ + \varsigma_2\right) \end{aligned} \tag{2.65}$$

where

$$R_1 = \frac{2}{\alpha_2}\sqrt{\left(q^2 - \frac{1}{4}\right)^2 + \frac{1}{4}\mu_2^2} \tag{2.66}$$

and R_2 grows over time.

Note that the system (2.58) shows a saturation phenomenon. In fact for values of the excitation amplitudes between 0 and k_c the semitrivial solution is stable and its amplitude grows linearly with k, as shown in Eq. (2.60). When the amplitude of the external excitation becomes greater than k_c then the semitrivial solution loses stability and a non trivial solution appears. In particular, Eq. (2.66) shows that the amplitude of the solution of the primary system stays constant, whereas the amplitude of the secondary system grows with increasing k. Therefore, when the excitation amplitude increases the amount of energy supplied by the external excitation to the primary system stays constant and the whole energy rise flows to secondary system.

Chapter 3

Modeling of Parametric Roll on Ships

Modeling plays an important role in control system design and testing, since the availability of a model of the process to be controlled provides the designer the possibility of predicting the impact of certain design choices. The prominence of models in control engineering is thus summarized by Goodwin et al. [30]:

> "The power of a mathematical model lies in the fact that it can be simulated in hypothetical situations, be subject to states that would be dangerous in reality, and it can be used as a basis for synthesizing controllers."

The development of mathematical models of any complexity to describe a physical phenomenon relies on the basic understanding of the phenomenological laws, which govern the system itself. Although phenomenological insights are often crucial for the understanding of key dynamical features of the real system, the level of complexity of the model should be chosen in accordance with its scope. Therefore, models are classified in [30]

- **nominal models** which provide an approximate description of the real process and they are used for control system design

- **calibration models** which give a more comprehensive description of the physical system; they usually include features that have not been used for the design of the controller but which have a direct connection on the achieved performance.

Parametric roll is an unstable resonant phenomenon which belongs to the class of parametrically excited systems. In Chapter 2 we have seen that parametrically excited systems are driven by the presence of a periodic coefficient; moreover it was pointed out that the resonance conditions may origin when the period of the parameter fluctuations is a multiple integer of the system period. In particular the resonance condition $T_0 = 2T$ was addressed as the most dangerous one since responses with large amplitude oscillations are generated for very small amplitude of the parametric excitation. Therefore, first two main points have to be clarified: how the principal parametric resonance condition translates into the parametric roll motion, i.e. which are the periods linked together; what is the time-varying parameter in the roll dynamics that determines the onset of the unstable oscillations. Subsequently models of different complexity can be developed for the study of parametric roll resonance.

This chapter is divided in five sections:

Section 3.1 offers a very short overview of the definitions of the ship motions with respect to inertial and non-inertial reference frames to make the green reader a bit familiar with some of the marine terminology.

Section 3.2 approaches parametric roll from a qualitative point of view, and it elucidates the two aspects above mentioned.

Section 3.3 presents a 1-DOF model and it shows how starting from the uncoupled roll equation it is possible to recast it as the linear/nonlinear damped Mathieu equation.

Section 3.4 introduces a 2-DOF surge-roll model in order to analyse the influence of variations in ship forward speed on the development of parametric roll. Both the 1-DOF model and the 2-DOF model are nominal models.

Section 3.5 presents a 3-DOF heave-pitch-roll model derived for a specific container ship. This model that represents parametric roll as an autoparametric system has been used for the testing of nonlinear controllers since it is considered a calibration model.

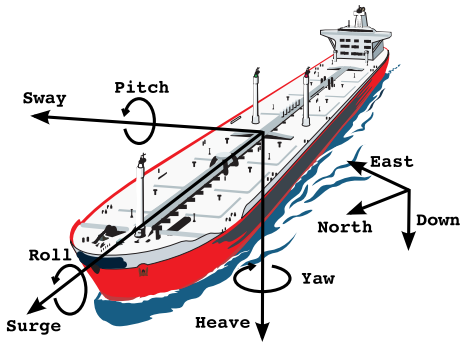

Figure 3.1: Definition of ship motions [A].

3.1 Ship Motions

A ship is a rigid body that moves in 6-DOF, therefore its motion is completely determined by six coordinates: three of them used to define the translations and the other three to define the orientation [19, 70]. Two kind of reference frames are adopted to denote these coordinates – see Fig. 3.1:

- **North-east-down (n-frame)** that is an inertial reference frame fixed to the Earth. The positive directions of the x_n, y_n, z_n-axis point towards the North, the East, and the center of the Earth, respectively. Its origin is positioned on the mean water free surface at an appropriate location
- **Body-fixed frame (b-frame)** which is fixed to the ship hull and, therefore, it moves at the average speed of the vessel following its path. The positive directions of the x_b, y_b, z_b-axis point towards the bow, starboard, and the bottom of the sea bed, respectively. The position of the origin of this reference frame is determined by making the axes to coincide with the principal axes of inertia of the ship.

The n-frame is used to determine the position of the vessel, and together with the b-frame it also defines the orientation. Therefore the north-east-down position of the ship is given by the coordinates of the origin of the b-frame relative to the n-frame

$$\mathbf{r}_{o_b}^{n} \triangleq \begin{bmatrix} n & e & d \end{bmatrix}^T, \tag{3.1}$$

whereas its attitude is determined by the orientation of the b-frame relative to n-frame, that is using the vector of Euler angles

$$\boldsymbol{\Theta}_{nb} \triangleq \begin{bmatrix} \phi & \theta & \psi \end{bmatrix}^T. \tag{3.2}$$

	n-frame		b-frame	
DOF	**Coordinate**	**Name**	**Coordinate**	**Name**
1	n	North position	u	Surge velocity
2	e	East position	v	Sway velocity
3	d	Down position	w	Heave velocity
4	ϕ	Roll angle	p	Roll rate
5	θ	Pitch angle	q	Pitch rate
6	ψ	Yaw angle	r	Yaw rate

Table 3.1: Nomenclature for the description of the ship motion in 6-DOF.

Thus according to the notation of Fossen [19], the *generalized position vector* is defined as

$$\boldsymbol{\eta} \triangleq \begin{bmatrix} \mathbf{r}_{o_b}^n \\ \boldsymbol{\Theta}_{nb} \end{bmatrix} = \begin{bmatrix} n & e & d & \phi & \theta & \psi \end{bmatrix}^T . \tag{3.3}$$

The b-frame is instead exploited to express linear and angular velocities. The linear velocity vector defining the velocity of the origin of the b-frame is given by

$$\mathbf{v}_{o_b}^b = \begin{bmatrix} u & v & w \end{bmatrix}^T , \tag{3.4}$$

while the angular velocity vector defining the velocity of rotation of the b-frame with respect to the n-frame in the b-frame is given by

$$\boldsymbol{\omega}_{nb}^b = \begin{bmatrix} p & q & r \end{bmatrix}^T . \tag{3.5}$$

Hence, the *generalized velocity vector* is defined as

$$\boldsymbol{\nu} \triangleq \begin{bmatrix} \mathbf{v}_{o_b}^b \\ \boldsymbol{\omega}_{nb}^b \end{bmatrix} = \begin{bmatrix} u & v & w & p & q & r \end{bmatrix}^T . \tag{3.6}$$

A summary of the adopted notation can be found in Table 3.1.

3.2 Parametric Roll in Head Seas: the Underlying Physics

In order to capture the sparkle that induces the development of parametric roll consider a vessel sailing in moderate head regular seas. The wave elevation is

modeled as a single frequency sinusoid (written w.r.t. the b-frame)

$$\zeta(t) = A_w \cos(kx \cos\chi - ky \sin\chi - \omega_e t), \tag{3.7}$$

and the waves are coming from the bow ($\chi = 180°$), then

$$\zeta(t) = A_w \cos(kx + \omega_e t), \tag{3.8}$$

where A_w is the wave amplitude, ω_e the encounter frequency of the wave, k the wave number, and χ the wave encounter angle.

The incident wave gives rise to forces and moments acting on the hull, which are divided into [62, 70]:

- 1^{st}**-order wave excitation forces** that are the zero-mean oscillatory forces generated by the waves. These forces consist of two components: the *Froude-Krylov forces*, which are caused by the incident wave under the assumption that the hull is restrained from moving and that its presence does not disturb the flow field; the *diffraction forces*, which account for the modification of the flow field due to the presence of the hull
- 2^{nd}**-order wave excitation forces** that account for mean wave-drift loads, slowly varying (difference of frequencies) and rapidly varying (sum of frequencies) wave loads.

In the present analysis 2^{nd}-order effects have been neglected, leaving the external forces and moments to be proportional to 1^{st}-order wave motion. In the nominal models only the Froude-Krylov forces have been considered, neglecting the diffraction component. This simplification is possible because the Froude-Krylov exciting force and moment are the leading-order contributions in the vertical plane, i.e. for surge, heave, and pitch, when the wavelength is large compared to the beam of the ship [62]. For parametric roll this condition is fulfilled since the onset of the phenomenon is possible if $\lambda_w \approx L_{\text{PP}} \gg B$.

Due to the wave heading the roll mode cannot be excited by the sea motion since forces and moments generated by the wave pressure on the hull have no lateral components; hence only the motions in the vertical plane (heave, pitch, and surge) can be provoked. Heaving and pitching cause periodic variations of the submerged hull geometry; in particular, during a wave passage the intercepted water plane area S_{W} changes from the still water case S_{W_0}, resolving in a variation of the position of the center of buoyancy [41, 62]. This in turn determines a modification of the transverse metacentric height GM due to the new position of the metacentre M – the centre of gravity G is assumed to be

fixed since it depends only upon the ship's loading condition. Consequently the periodic fluctuation of GM, which can be deemed sinusoidal

$$\mathrm{GM}(t) = \overline{\mathrm{GM}} + \mathrm{GM}_a \cos \omega_e t, \tag{3.9}$$

influences the stability properties of the vessel through the roll restoring moment that for small roll angle is approximated by

$$\tau_{4,\mathrm{hs}}(t) \approx \rho g \nabla \mathrm{GM}(t) \phi, \tag{3.10}$$

where $\overline{\mathrm{GM}}$ is the mean value of the metacentric height, GM_a is the amplitude of the variations of the metacentric height in waves.

These two situations alternates:

- a wave trough is amidships: in this case $S_{\mathrm{w}} > S_{\mathrm{w}_0}$ causing a larger restoring moment ($\tau_{4,\mathrm{hs}} > \tau_{4,\mathrm{hs}_0}$) and, hence, an increased stability
- a wave crest is amidships: in this case $S_{\mathrm{w}} < S_{\mathrm{w}_0}$ inducing a smaller restoring moment ($\tau_{4,\mathrm{hs}} < \tau_{4,\mathrm{hs}_0}$) and, hence, a reduced stability.

If a disturbance, like a wind gust, occurs in roll when the ship is between the wave crest and trough at amidships position, then its response will be greater than in calm water since it is approaching a situation of instantaneous increased stability. Therefore the vessel will roll back to a larger angle than it would have done in calm water condition, as illustrated in Fig. 3.2. After the first quarter of the roll period T_ϕ the vessel has rolled back to the zero degree attitude but it continues towards port side due to the inertia. However now the ship encounters a wave crest amidships, which determines a reduced restoring moment with respect to the calm water one; therefore the ship rolls to a larger angle than it would have done in calm water condition. As a result the roll angle is increased again over the second quarter of the roll period, reaching a higher value than at the end of the first quarter. This alternate sequence of instantaneous increased and reduced restoring moment causes the roll angle to keep increasing unless some other factors start counteracting it.

Established that it is the metacentric height GM the time-varying parameter exciting the roll dynamics, to determine how the principal parametric resonance condition translates into the parametric roll phenomenon is trivial. In fact assuming that the metacentric height varies periodically with period $T_e = 2\pi/\omega_e$, then the principal parametric resonance condition becomes $T_\phi = 2T_e$, or $\omega_e = 2\omega_\phi$, that is the frequency of the fluctuations of GM must be twice the roll natural frequency. Note that this relation can be relaxed since the onset of the resonant roll motion can happen if $\omega_e \approx 2\omega_\phi$. As a matter of fact

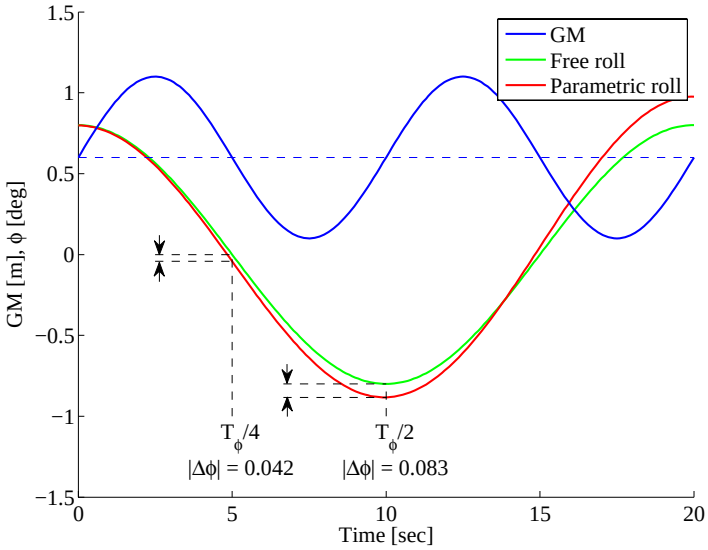

Figure 3.2: Development of parametric roll. The dashed blue line is the value of GM in calm water.

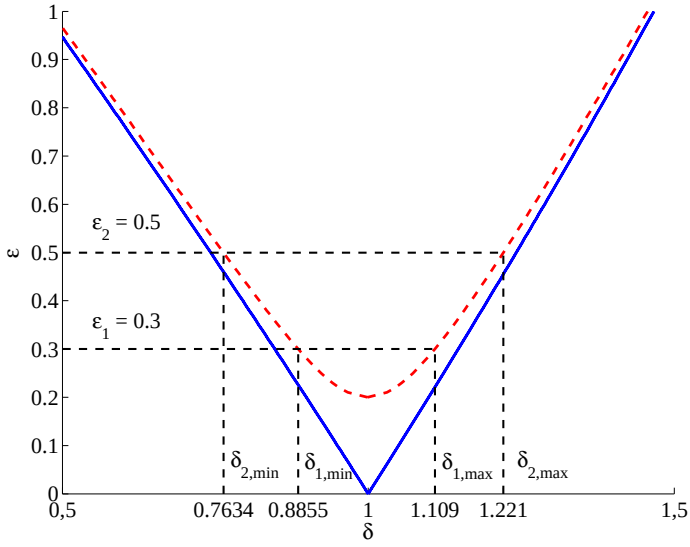

Figure 3.3: Principal parametric resonance region: the different magnitudes of the excitation and the level of damping determine the range of frequencies inside which parametric roll resonance can develop.

the encounter frequency can be included in a range whose amplitude depends on the magnitude of the excitation and the amount of damping of the roll system. Figure 3.3 shows that for a given level of damping, the value of the parameter δ for which parametric resonance is triggered ranges in an interval $[\delta_{\min}\ ,\ \delta_{\max}]$ that depends on the magnitude of the excitation ε.

Last, the surge motion determines oscillations around the working point of the ship forward speed U through the relation

$$U = \sqrt{u^2 + v^2}, \tag{3.11}$$

which resolves in $U \approx u$ if the sway velocity is neglected. Changes in U may affect the wave encounter frequency by means of

$$\omega_e = \omega_w - \frac{\omega_w^2}{g} U \cos\chi, \tag{3.12}$$

where ω_w is the wave frequency.

In normal cruising conditions the ship will have the autopilot on and, hence, this will mind of keeping the forward speed as close as possible to the working point U_0. In this case the surge oscillation, induced by the longitudinal Froude-Krylov force, will resolve in a small periodic variation around U_0, which very hardly will be able to de-tune the principal parametric resonance condition. However, if the autopilot is turned off and the master does not operate the ship manually then the vessel will be left at the mercy of the wave motion, and in the limit, due to the combined action of the wave excitation forces and the ship advance resistance, it will stop. The transition from $U = U_0$ to $U = 0$ provokes instead a large variation of wave encounter frequency, and therefore it can determine the exit from the parametric resonance region. This limit situation can be translated in a more realistic scenario where the dependency of the wave encounter frequency on the ship speed can be exploited in order to bring the vessel out of the resonant motion by increasing or decreasing U.

3.2.1 Autoparametric Roll System

In the light of the qualitative description of the interactions of heave, pitch, and surge with roll for the development of the parametric roll resonance it is possible to define the autoparametric roll system according to the diagram in Fig. 3.4. According to the definition of autoparametric system given by Tondl et al. [77] the heave-pitch-roll system constitutes an autoparametric system where the heave-pitch subsystem is the primary system externally excited by the wave motion, which, hence, is in a vibrating state. The roll subsystem represents the

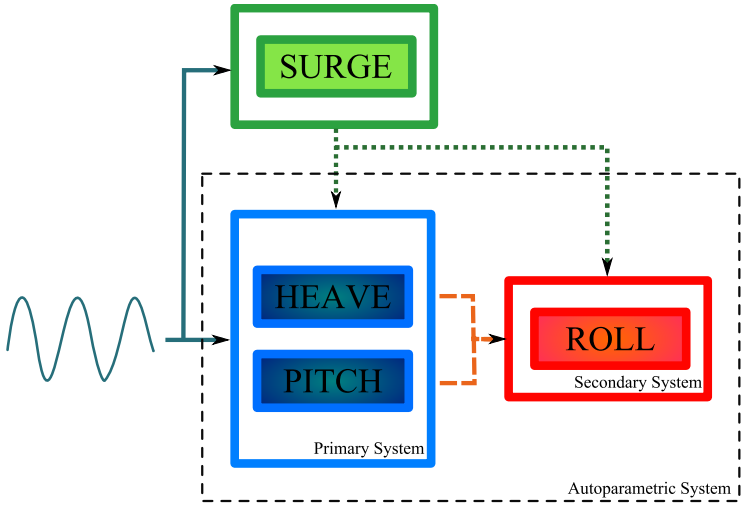

Figure 3.4: Autoparametric roll system.

secondary system initially at rest, but which enters in principal parametric resonance as soon as the energy flow coming from the modes in the vertical plane overcomes the energy dissipated through the damping.

Conversely, the surge-roll subsystem cannot be defined as an autoparametric system because, although the surge oscillations may determine that $\omega_e \approx 2\omega_\phi$, if the wavelength is not approximately equal to the ship length and, even more important, the fluctuations of the metacentric height are not big enough to cross the damping threshold, parametric roll will never onset. Nevertheless if the aforementioned conditions are all satisfied then the surge motion can contribute to trigger or de-tune the parametric resonance in roll. Therefore, if we look at the overall diagram it is possible to state that in the surge-heave-pitch-roll system the autoparametric subsystem can be brought out of the resonance condition acting on surge.

3.3 1-DOF Model: Roll Motion as the Mathieu Equation

In this section it is shown that under a sinusoidal variation in the metacentric height the roll equation can be rewritten as the Mathieu equation. This model has been used for the preliminary studies about the feasibility of stabilizing

parametric roll resonance by active control [B].

Consider a 1-DOF roll motion equation in head seas:

$$(I_{xx} - K_{\dot{p}})\ddot{\phi} + K_p\dot{\phi} + \rho g \nabla \mathrm{GM}(t)\phi = 0, \tag{3.13}$$

where I_{xx} and $K_{\dot{p}}$ are the inertia and added inertia, respectively, K_p is the linear damping, and $\mathrm{GM}(t)$ obeys to Eq. (3.9). Substituting Eq. (3.9) into Eq. (3.13) yields

$$\ddot{\phi} + \frac{K_p}{I_{xx} - K_{\dot{p}}}\dot{\phi} + \frac{\rho g \nabla}{I_{xx} - K_{\dot{p}}}(\overline{\mathrm{GM}} + \mathrm{GM}_a \cos\omega_e t)\phi = 0 \tag{3.14}$$

where it can be noticed that the two ratios

$$\frac{\rho g \nabla \overline{\mathrm{GM}}}{I_{xx} - K_{\dot{p}}}, \qquad \frac{\rho g \nabla \mathrm{GM}_a}{I_{xx} - K_{\dot{p}}}$$

are dimensionally equivalent to a frequency squared. Then defining ω_ϕ and ω_a as

$$\omega_\phi = \sqrt{\frac{\rho g \nabla \overline{\mathrm{GM}}}{I_{xx} - K_{\dot{p}}}}, \qquad \omega_a = \sqrt{\frac{\rho g \nabla \mathrm{GM}_a}{I_{xx} - K_{\dot{p}}}}$$

Eq. (3.14) reads

$$\ddot{\phi} + 2\zeta\omega_\phi\dot{\phi} + (\omega_\phi^2 + \omega_a^2 \cos\omega_e t)\phi = 0, \tag{3.15}$$

where ζ is the damping ratio. By means of the change of variable $\xi = \frac{1}{2}\omega_e t$ and introducing the dimensionless parameters

$$\delta \triangleq \frac{4\omega_\phi^2}{\omega_e^2}, \qquad \varepsilon \triangleq \frac{4\omega_a^2}{\omega_e^2}, \qquad \mu \triangleq \frac{4\zeta\omega_\phi}{\omega_e}$$

with δ being the ratio between roll natural frequency and wave encounter frequency, and ε accounting for the relative frequency variation in waves due to changes in metacentric height, then Eq. (3.15) assumes the form of the linear damped Mathieu equation (see Eq. (2.50))

$$\phi'' + \mu\phi' + (\delta + \varepsilon\cos 2\xi)\phi = 0 \tag{3.16}$$

where

$$\phi' = \frac{\mathrm{d}\phi}{\mathrm{d}\xi}, \qquad \phi'' = \frac{\mathrm{d}^2\phi}{\mathrm{d}\xi^2}.$$

This model shows unbounded roll behavior whenever the conditions for parametric resonance are fulfilled, as reported in Section 2.2.2, although the linear damping limits the growth rate. Hence in order to obtain bounded solutions,

reflecting the real behavior of the roll dynamics, the roll restoring moment is modeled as a nonlinear function of the roll angle. The standard approach is to use the Taylor expansion up to third order, as shown in [57]

$$\tau_{4,\mathrm{hs}} \approx K_\phi \phi + \frac{1}{6} K_{\phi\phi\phi} \phi^3. \tag{3.17}$$

Inserting Eq. (3.17) into Eq. (3.13) and redoing the whole procedure the following nonlinear Mathieu equation is obtained

$$\phi'' + \mu\phi' + (\delta + \varepsilon \cos 2\xi)\phi + \alpha\phi^3 = 0, \tag{3.18}$$

where $\alpha = 2K_{\phi\phi\phi}/3\omega_e^2(I_{xx} - K_{\dot{p}})$.

This allows to exploit the stability results presented in Section 2.2 in order to derive relations between the parameters of the roll mode and the parameters of the external excitation, i.e. the wave motion, that determine the onset of parametric roll.

3.4 2-DOF Model: Influence of Ship Forward Speed on Parametric Roll

A 2-DOF model based on the nonlinear coupling between surge and roll has been set up in order to first study the influence of ship forward speed on the development of parametric roll resonance and, afterwards, to develop control strategies, which could stabilize the parametric roll resonance via detuning of the frequency coupling condition $\omega_e \approx 2\omega_\phi$ (see Paper [C]).

Let $\boldsymbol{\eta} \triangleq [x,\, \phi]^T$ and $\boldsymbol{\nu} \triangleq \dot{\boldsymbol{\eta}} = [u,\, p]^T$ be the generalised position and velocity vectors, respectively. Then the nonlinear equations of motion in matrix form read as

$$\begin{aligned} \dot{\boldsymbol{\eta}} &= \boldsymbol{\nu} \\ \mathbf{M}\dot{\boldsymbol{\nu}} + \mathbf{D}(\boldsymbol{\nu})\boldsymbol{\nu} + \mathbf{K}(\boldsymbol{\eta}, \boldsymbol{\nu}, t)\boldsymbol{\eta} &= -\mathbf{e}(\boldsymbol{\nu}, t) \end{aligned} \tag{3.19}$$

where

$$\begin{aligned} \mathbf{M} &= \begin{bmatrix} m - X_{\dot{u}} & 0 \\ 0 & I_{xx} - K_{\dot{p}} \end{bmatrix} \\ \mathbf{D}(\boldsymbol{\nu}) &= -\begin{bmatrix} X_u + X_{|u|u}|\nu_1| & 0 \\ 0 & K_p + K_{|p|p}|\nu_2| \end{bmatrix} \\ \mathbf{K}(\boldsymbol{\eta}, \boldsymbol{\nu}, t) &= \begin{bmatrix} 0 \\ K_{22,\nu_1} + K_{22,\eta_2} \end{bmatrix} \end{aligned}$$

are the diagonal rigid-body generalised mass matrix, the hydrodynamic damping matrix (nonlinear in surge and roll), the nonlinear vector of restoring forces and moments (with $K_{22,\nu_1} = \rho g \nabla \mathrm{GM}(\nu_1, t)$, and $K_{22,\eta_2} = K_{\phi\phi\phi}\eta_2^2$). The vector $\mathbf{e}(\boldsymbol{\nu}, t)$ accounts for the external forces/moments generated by the wave pressure and it reads as

$$\mathbf{e}(\boldsymbol{\nu}, t) = [-F_x^{FK}(\nu_1, t),\, 0]^T, \tag{3.20}$$

where $F_x^{FK}(\nu_1, t)$ is the 1^{st}-order wave excitation force in surge, namely the longitudinal Froude-Krylov force.

The surge and roll dynamics are linked implicitly through the time-varying wave encounter frequency, which is a function of the ship forward speed, as shown in Eq. (3.12).

3.5 3-DOF Model: Heave-Pitch-Roll Autoparametric System

The 3-DOF model coupling the nonlinear dynamics of heave, pitch, and roll has been developed in order to have a benchmark model for simulating parametric roll of a container ship over a large range of ship speeds and sea states. The model, extensively presented in [A], exhibits two levels of couplings:

- hydrodynamic couplings between heave and pitch in terms of added mass and damping
- hydrostatic couplings among the three modes through the expansion of the restoring forces and moments up to the third order, including also the terms connected to the hull-wave interaction.

The nonlinear mathematical model of the container vessel is presented in agreement with the notation of Neves and Rodriguez [57]:

Let

$$\mathbf{s}(t) = \begin{bmatrix} z(t) & \phi(t) & \theta(t) \end{bmatrix}^T \tag{3.21}$$

be the generalized position vector. Then the nonlinear equations of motion can be expressed in matrix form as

$$(\mathbf{M} + \mathbf{A})\ddot{\mathbf{s}} + \mathbf{B}(\dot{\phi})\dot{\mathbf{s}} + \mathbf{c}_{\text{res}}(\mathbf{s}, \zeta) = \mathbf{c}_{\text{ext}}(\zeta, \dot{\zeta}, \ddot{\zeta}) \tag{3.22}$$

where

- $\mathbf{M} \in \mathbb{R}^{3\times3}$ is the diagonal rigid-body generalized mass matrix

$$\mathbf{M} = \begin{bmatrix} m & 0 & 0 \\ 0 & I_{xx} & 0 \\ 0 & 0 & I_{yy} \end{bmatrix} \tag{3.23}$$

- $\mathbf{A} \in \mathbb{R}^{3\times3}$ is the generalized added mass matrix

$$\mathbf{A} = \begin{bmatrix} -Z_{\ddot{z}} & 0 & -Z_{\ddot{\theta}} \\ 0 & -K_{\ddot{\phi}} & 0 \\ -M_{\ddot{z}} & 0 & -M_{\ddot{\theta}} \end{bmatrix} \tag{3.24}$$

- $\mathbf{B} \in \mathbb{R}^{3\times3}$ is the hydrodynamic damping (nonlinear in roll)

$$\mathbf{B}(\dot{\phi}) = \begin{bmatrix} -Z_{\dot{z}} & 0 & -Z_{\dot{\theta}} \\ 0 & -K_{\dot{\phi}}(\dot{\phi}) & 0 \\ -M_{\dot{z}} & 0 & -M_{\dot{\theta}} \end{bmatrix} \tag{3.25}$$

- $\mathbf{c}_{\text{res}} \in \mathbb{R}^3$ is the nonlinear vector of restoring forces and moments expressed as functions of the relative motion between ship hull and wave elevation $\zeta(t)$
- $\mathbf{c}_{\text{ext}} \in \mathbb{R}^3$ is the vector of the external wave excitation forces and moments which depends on wave heading, encounter frequency, wave amplitude and time.

This model has been validated against experimental data sets gathered in regular waves, and it showed a very good agreement of the responses of heave, pitch, and roll w.r.t. the experimental records. Due to its accuracy, it has been used for testing the nonlinear controllers developed in [C].

Chapter 4

Parametric Roll Stabilisation

The stabilisation of the large roll motion induced by the onset of parametric resonance is of primary importance in order to guarantee the safety and the integrity of the vessel. The literature survey presented in Section 1.2 showed that the development of active control strategies for counteracting parametric roll had received literally no attention at the time this research project started. Belenky et al. [3], and Shin et al. [75] had briefly investigated the potential of using passive U-tanks as a mean of reducing the susceptibility to the onset of parametric roll resonance, and they found that this kind of stabilisation device seemed to be very promising in the mitigation of the large roll oscillations provoked by parametric roll.

Roll stabilisation has been one of the focuses of the maritime community since the mid-19$^{\text{th}}$ century when remarkable changes were introduced in the design of ships. Perez [70] made a comprehensive review on the early days of ship roll stabilisation showing how the problem shifted from the developments of stabilisation concepts, since the pioneering studies of Froude [23], to the developments in control system design, which saw a theoretical boost with the introduction of the rudder as a stabilisation device in the early 1970s. In the last thirty years numerous results have been achieved in the field of roll stabilisation by means of the most refined techniques that the control theory could supply, using both fins and rudder as stabilisations devices [70]. Therefore a question to

be answered is whether the state-of-the-art of roll stabilisation could be directly used to counteract parametric roll resonance, that is if the anti-rolling devices currently available onboard, employed in the same way they are employed to stabilize synchronous roll, are capable to deliver a control action sufficient to stabilise the large roll oscillations arising from the parametric resonance phenomenon.

This chapter introduces two works developed in the control framework as answer to this question. The chapter is divided as follows:

Section 4.1 introduces the fin stabiliser as the chosen anti-roll stabilisation device, highlighting the advantages and the drawbacks with respect to another widely used stabilisation actuator, the U-tank.

Section 4.2 presents possible control strategies that may be applied in order to counteract the development of parametric roll resonance

Section 4.2.1 studies the feasibility of stabilising parametric roll resonance through the analysis of the stability conditions of the Mathieu's equation. The damping is chosen as the parameter to act on; therefore a bifurcation control is proposed by a damping injection, which will increase the stability threshold for the onset of parametric resonance. The possibility to damp the large roll oscillations is explored by implementing a P controller that actuates a fin stabiliser. The details about the proposed method can be found in Paper B.

Section 4.2.2 proposes a combined control strategy based on nonlinear control methods. Classical Lyapunov stability theory together with integrator backstepping method are exploited in order to design a speed controller joined with a fin stabiliser. The speed controller aims at detuning the frequency coupling condition, bringing the roll mode out of the resonance region, whereas the fin stabiliser is used to quickly damp the residual roll oscillations. A thorough derivation of the two controllers and performance evaluations can be found in Paper C.

4.1 Fin Stabiliser

A fin stabiliser consists of one or more pairs of hydrofoil shaped fins projected from a vessel's bilge area. Fin stabilisers can be of two kind: retractable and non-retractable (see Fig. 4.1 for an example). The control system senses through gyroscopes the ship's attitude, and it signals the stabiliser hydraulics to change the angle of incidence of the fins to counteract roll motion. The stabilisation is

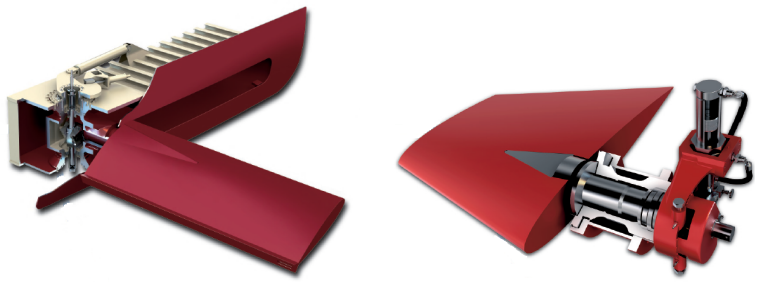

(a) (b)

Figure 4.1: Example of commercial fin stabilisers: (a) folding fin stabiliser, (b) non-retractable fin stabiliser. (`http://www.rolls-royce.com/`)

achieved through a counter-roll moment obtained as a result of the generated lift [70], which depends on vessel speed and the angle of attack of the fins. The dependency on vessel speed highlights a feature characteristic of any lifting device: the higher the ship speed the larger the stabilising moment.

At forward speeds higher than 10-15 knot, active fins are the most effective stabilising device reaching a roll reduction between 60% and 90% in root-mean-square sense. Among the drawbacks of fin stabilisers are the low effectiveness at low speed, the need for powerful hydraulic actuators, and high cost devices for installation and maintenance.

The choice of this actuator was driven by mainly two factors: the large achievable roll reduction and the relative ease of designing a control system, although advanced control strategies have to be taken into account when the ship operates in severe sea states due to the appearance of nonlinear hydrodynamic effects. On top of these aspects, if we compare fin stabiliser with anti-rolling tanks folding fin stabilisers do not require the sacrifice of cargo space, whereas U-tanks occupy large spaces in the inner part of the ship reducing the loading capability. U-tanks affect the stability of the vessel if they are not completely full due to the free-surface effects, whereas fins have no stability related issues. Moreover, U-tanks work in a narrow band of frequencies, whereas fins provide damping independent of the roll frequency.

4.2 Control Strategies

From the physical understanding about parametric resonance in general, and parametric roll in specific several control strategies could be possible. We divide them into two classes: *direct control actions*, which affect directly the roll subsystem, and *indirect control actions*, which affect the roll mode in parametric resonance acting on one or more subsystems linked with the roll motion.

The direct control actions include all the possible means of stabilising the roll motion by increasing the level of the system damping. This can be achieved by using different kind of stabilisation devices as active fin stabilisers, rudder roll stabilisation, and active U-tanks.

The indirect control actions derive from the analysis of the frequency coupling condition $\omega_e \approx 2\omega_\phi$. In order to detune this condition two ways can be pursued: to vary the ship forward speed or to vary the ship's heading. Equation (3.12) shows that U and χ are the control parameters, which can be used to change the wave encounter frequency. Therefore the indirect control actions include speed control, which links the surge subsystem with roll, and heading control, which connects the yaw subsystem with roll.

In the following the adopted control strategies are introduced. First a feasibility study about the possibility of stabilising parametric roll is presented: the critical importance of roll damping is pointed out; hence a fin stabiliser is implemented via a P controller to prove that it is possible to stabilise parametric roll by damping injection. Then this approach is integrated with the de-tuning of the frequency coupling condition, which is achieved by varying the ship forward speed. Both the speed controller and the fin stabiliser are then designed applying nonlinear control methods. A thorough discussion of the adopted control strategies can be found in Papers B-C.

4.2.1 Bifurcation Control via Increased Damping Threshold

In Section 2.2.2 we pointed out that parametric resonance in damped systems is a threshold phenomenon, i.e. the amount of damping inherent to the system sets a minimum threshold that the parametric excitation must cross in order to trigger the unstable motion. In particular we noted that if the system reduces to the Mathieu equation, the principal parametric resonance condition is characterized

by the following damping threshold

$$\varepsilon_{\min} \geqslant 2\mu. \tag{4.1}$$

This suggests that by increasing the level of the damping of the system it is possible to bring back the secondary system to the initial resting condition. Figure 4.2 shows a simulation of the damped Mathieu equation for two different levels of damping. By increasing the damping coefficient from $\mu_1 = 0.15$ to $\mu_2 = 0.3$ the damping threshold is no longer crossed since $\varepsilon < \varepsilon_{min}$; hence the unstable motion starts decaying until the trivial solution ($x(t) = 0$) is reached again.

The feasibility of stabilising parametric roll by increasing the damping threshold has been investigated in [B] where a fin stabiliser was implemented adopting a roll rate feedback. The control law provides a fin mechanical angle α which is proportional to the actual roll rate p

$$\alpha = -L_{\alpha p} \frac{\alpha_{\max}}{p_{\max}} \left(\frac{U_{\lim}}{U_{\text{nom}}} \right)^{-2} p \tag{4.2}$$

where $L_{\alpha p}$ is the controller proportional gain, and $U_{\lim} = U$ when $U \geq U_{\min}$, $U_{\lim} = U_{\min}$ otherwise.

Time history plots of the response are shown in Figs. 4.3-4.4. Control action was activated when roll amplitude was $|\phi| = 20°$ and $10°$, respectively. The roll motion decays slowly in the first case, after control has been activated, but rapidly in the second. The hydrodynamic angle of attack on the fin is large in both cases when the fin stabiliser takes the control action over, but in the first case the fins work in stall condition for a longer period and the presence of stall limits the available control torque.

The results confirmed the possibility of stabilising the roll motion after the onset of the resonant condition and limitations on the largest roll angle that could be stabilised were pointed out.

4.2.2 De-Tuning through Combined Speed Control and Fin Stabiliser

The onset of parametric roll relies on the frequency coupling between the wave encounter frequency and the roll natural frequency such that $\omega_e \approx 2\omega_\phi$. Therefore the de-tuning of this synchronization represents an important action to be taken in order to bring the system out of resonance. Theoretically this can be achieved in two ways: by varying the roll natural frequency or by changing the

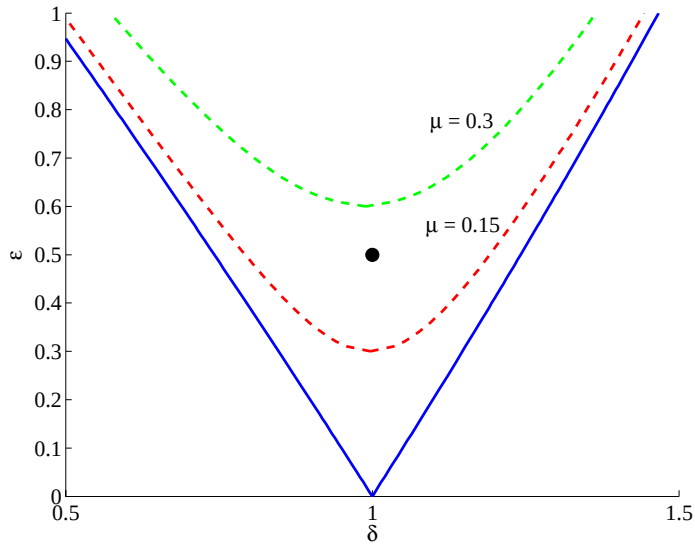

(a)

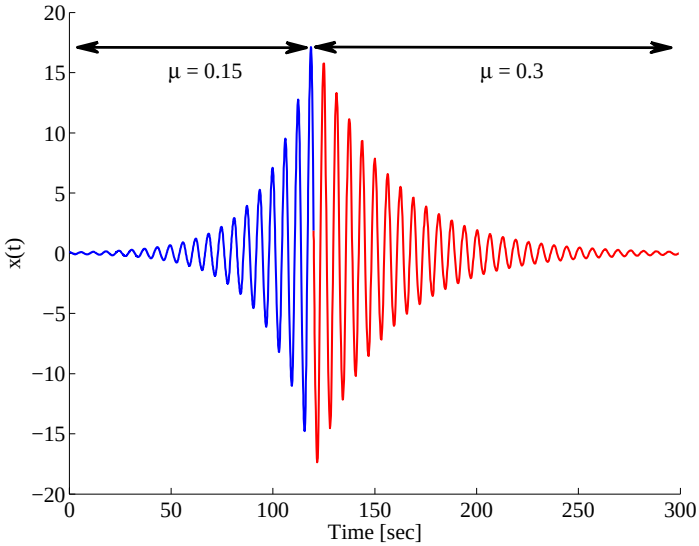

(b)

Figure 4.2: stabilisation of parametric resonant motion by increasing the damping threshold: given the excitation level $\varepsilon = 0.5$ (black dot) the Mathieu equation is in principal parametric resonance, but after increasing the level of the damping from 0.15 to 0.3 the system exits from the resonant condition.

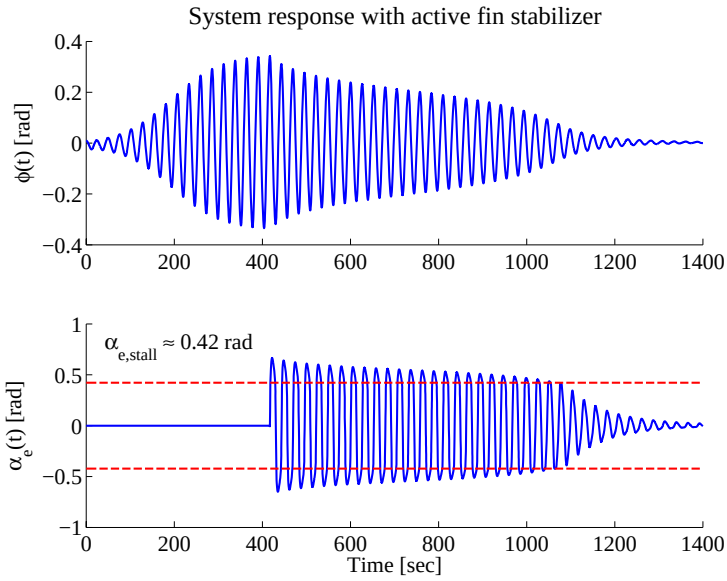

Figure 4.3: Parametric roll condition. Control is activated when roll amplitude is $|\phi| = 20°$.

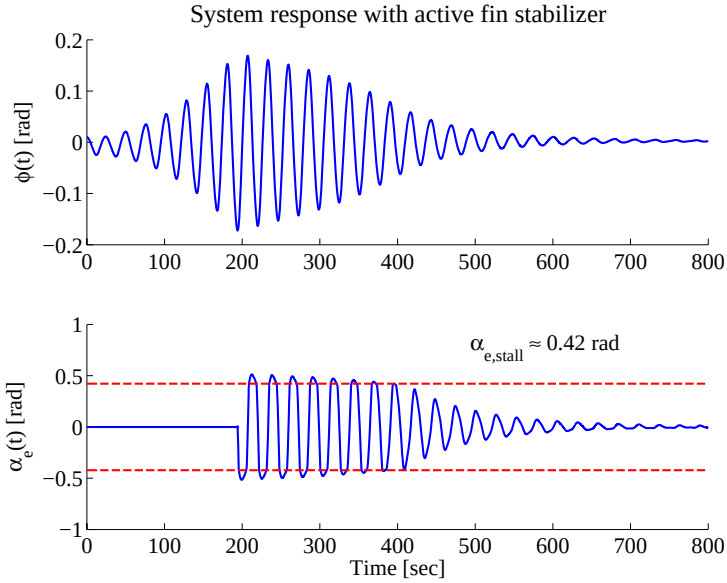

Figure 4.4: Control action by the fin stabiliser is activated at roll amplitude $|\phi| = 10°$.

wave encounter frequency. To vary ω_ϕ would require the possibility of increasing the moment of inertia, i.e. to change the distribution of the load on the ship, and it is evident that this action is impossible while the ship is sailing. Therefore the only possibility is to change ω_e.

In Section 3.2 we have seen that, given the wave frequency ω_w, the wave encounter frequency is in general a function of two parameters, i.e. $\omega_e = \omega_e(U, \chi)$. Therefore by taking proper actions on the ship forward speed, or the ship heading, or on both, it is possible to alter the ratio ω_ϕ/ω_e such that it falls out of the range $[\delta_{\min}\ ,\ \delta_{\max}]$.

In Paper C the direction pursued has been to achieve de-tuning through variation in the ship forward speed U combined with a fin stabiliser. First the 2-DOF surge-roll model introduced in Section 3.4 was extended including the control input vector $\boldsymbol{\tau} = [\tau_u,\ \tau_\phi]^{\mathrm{T}}$ and the dynamics of the fin stabiliser, as

$$\begin{aligned} \dot{\boldsymbol{\eta}} &= \boldsymbol{\nu} \\ \mathbf{M}\dot{\boldsymbol{\nu}} + \mathbf{D}(\boldsymbol{\nu})\boldsymbol{\nu} + \mathbf{K}(\boldsymbol{\eta}, \boldsymbol{\nu}, t)\boldsymbol{\eta} + \mathbf{e}(\boldsymbol{\nu}, t) &= \boldsymbol{\tau} \\ \dot{\tau}_\phi + \frac{1}{t_r}\tau_\phi &= \frac{1}{t_r}\tau_{\max}\mathrm{sat}\left(\frac{\tau_c}{\tau_{\max}}\right). \end{aligned} \tag{4.3}$$

Then the speed controller has been designed by applying classical Lyapunov stability theory. Given the surge subsystem

$$\dot{\nu}_1 = -D'_{11}(\nu_1)\nu_1 - e'_1(\nu_1, t) + \tau'_u \tag{4.4}$$

an error dynamics is defined as

$$\begin{aligned} \dot{z}_1 &= \dot{\nu}_1 - \dot{\nu}_d \\ &= -D'_{11}(\nu_1)(z_1 + \nu_d) - e'_1(\nu_1, t) + \tau'_u - \dot{\nu}_d, \end{aligned} \tag{4.5}$$

where $z_1 = \nu_1 - \nu_d$ is the tracking error and $\nu_d \in C^1$ is a bounded reference trajectory. Therefore, choosing the control Lyapunov function as

$$V_1 = \frac{1}{2}M_{11}z_1^2, \tag{4.6}$$

it is possible to demonstrate that the control input

$$\tau_u = D_{11}(\nu_1)\nu_d + M_{11}\dot{\nu}_d - \kappa_1 z_1,\ \forall\ \kappa_1 > 0 \tag{4.7}$$

guarantees that the surge speed is globally uniformly ultimately bounded if the disturbance $e(\nu, t)$ satisfies the following inequality

$$e_1(\nu_1, t) \leq 2\gamma_1\omega + 2\gamma_1 k z_1 + 2\gamma_1 k\nu_{d,\max}. \tag{4.8}$$

Last, the roll subsystem is taken into account

$$\dot{\eta}_2 = \nu_2 \tag{4.9a}$$
$$\dot{\nu}_2 = -D'_{22}(\nu_2)\nu_2 - K'_{22}\eta_2 + \tau'_\phi \tag{4.9b}$$
$$\dot{\tau}_\phi = -\frac{1}{t_r}\tau_\phi + \frac{1}{t_r}\tau_{\max}\mathrm{sat}\left(\frac{\tau_c}{\tau_{\max}}\right) \tag{4.9c}$$

and a fin stabiliser controller was designed applying the integrator backstepping technique in 3 steps:

step 1: from roll angle η_2 to roll rate ν_2 stabilisation is achieved choosing the following control input

$$\nu_2 = \psi_1(\eta_2) = -\kappa_2\eta_2, \qquad \kappa_2 > 0, \tag{4.10}$$

which guarantees the global exponential stability of Eq. (4.9a)

step 2: from ν_2 to induced fin roll moment τ_ϕ stabilisation is achieved selecting

$$\begin{aligned}\tau_\phi = \psi_2(\eta_2, z_2) = &-\kappa_3 z_2 - D_{22}(\nu_2)\kappa_2\eta_2 + K_{22,\eta_2}\eta_2 \\ &- M_{22}\kappa_2(z_2 - \kappa_2\eta_2),\ \forall\ \kappa_3 > 0\end{aligned} \tag{4.11}$$

step 3: from τ_ϕ to control torque τ_c stabilisation is achieved with τ_c given by

$$\begin{aligned}\tau_c = \psi_3(\eta_2, z_2, z_3) = &-\kappa_3 z_2 - \kappa_2 D_{22}(\nu_2)\eta_2 \\ &- M_{22}\kappa_2(z_2 - \kappa_2\eta_2) \\ &+ t_r\left(\frac{\partial\psi_2}{\partial z_2}\dot{z}_2 + \frac{\partial\psi_2}{\partial\eta_2}\dot{\eta}_2\right) - \kappa_4 z_3,\end{aligned} \tag{4.12}$$

with $\kappa_4 > 0$, which ensures the asymptotic stability of the roll subsystem in a region of attraction that is a function of $\tau_{\max}$.

The effectiveness of the combined control action has been tested in simulations on a 4-DOF surge-heave-pitch-roll model. Simulations results showed the feasibility of de-tuning the frequency coupling by both increasing and decreasing ship forward speed, as shown in Fig. 4.5-4.6. In particular, the combination of the speed controller with the fin stabiliser showed that the best stabilisation performance is achieved by increasing the ship forward speed. In fact by accelerating, the lift force produced by the fins increases, and in turn a higher roll damping can be obtained, which will quickly damp the residual roll motion.

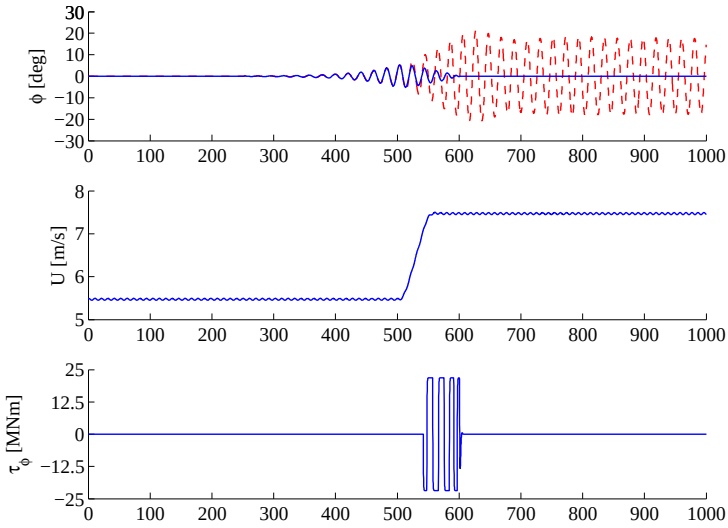

Figure 4.5: Stabilisation of roll angle ϕ using the 4-DOF model ($\Delta U = 2$ m/s, $\tau_{\phi,\max} = 21.8$ MNm). Roll in parametric resonance (red dashed curve)

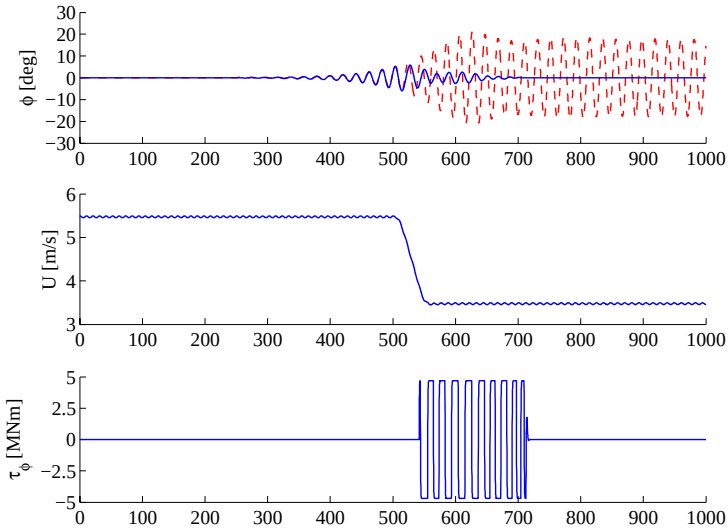

Figure 4.6: Stabilisation of roll angle ϕ using the 4-DOF model ($\Delta U = -2$ m/s, $\tau_{\phi,\max} = 4.7$ MNm). Roll in parametric resonance (red dashed curve)

Chapter 5

Parametric Roll Detection

First generation warning systems based on polar diagrams offer a great support to the master informing him about the probability that the ship has of meeting dangerous situations if it proceeds along a certain route with a certain speed. Thus the master is responsible of deciding between keeping the same route and re-scheduling the journey on the base of events that may happen in few hours from the decision time. The master, receiving information of a high probability of excessive ship motions, will be likely to decide to re-route. But what if the vessel runs into resonance conditions anyway? Could current onboard systems guarantee the safety of the vessel if the master decides to take the chance or if simply he cannot do anything else than going through the adverse weather? The answer to the latter question seems to be no. Current decision support systems are not capable to detect in a short time horizon, i.e. few minutes, if extreme events like parametric roll will develop, and therefore there is no possibility of taking appropriate control actions at proper time. The current technology cannot provide full support of the vessel safety.

In 2006 Døhlie [15] made a very clear call for the development of second generation warning systems, which must be capable to deal with the onset of parametric roll in a short predicting horizon. Dølhie stated straightforward that the time for free indemnification by insurance companies was almost over since, after 8 years from the APL China disaster, parametric roll in head seas was not an obscure phenomenon anymore. Therefore the insurance industry

loudly claimed a more evident effort from the ship owners to take steps to avoid parametric rolling.

As seen from public sources, only little has been done both in industry and in academia since the paper by Dølhie. Holden et al. [37] proposed an observer based predictor, which making use of different estimation schemes, estimates the eigenvalues of a linear second-order oscillatory system describing the roll motion. The algorithm issues a warning when those eigenvalues move into the right-half plane. The method by Holden et al. [37] works convincingly but it requires knowledge of several ship parameters for use in the observer. McCue and Bulian [52] studied the possibility of using finite time Lyapunov exponents to detect the onset of parametric roll for ships operating in irregular seas condition. The authors pointed to the possibility of identifying parametric roll by looking at the behavior of the Lyapunov exponents. McCue and Bulian [52] did not validate their method against experimental data. The author has tested similar techniques to detect exponential growth in the roll envelope but neither false alarm nor detection probabilities were satisfactory on data from model tank experiments.

This research has taken a change detection approach that is based solely on signals. A clear advantage in achieving and validating results has been access to model tests with parametric resonance.

This chapter is divided in three main sections:

Section 5.1 introduces the experimental data sets, which have been used to test the performances of the proposed detection methods.

Section 5.2 presents two novel detection methods implemented in order to detect the inception of parametric roll resonance:

Section 5.2.1 proposes a frequency-domain approach based on the nonlinear energy flow from the motions in the vertical plane (heave and pitch) to the roll motion. This energy flow is quantified by means of an energy flow coefficient, which measures how much energy is pumped by heave and/or pitch into roll about its second harmonic. The detailed discussion of the method can be found in Paper D.

Section 5.2.2 assesses the detection problem in the time-domain by performing the GLRT on a driving signal, which carries information about the phase correlation of heave/pitch with roll. The statistics of this signal has been described as Laplacian distributed and a GLRT decision function has been derived to detect a resonance condition. The proposed detection method together with its performance assessment can be found in Paper E.

Section 5.3 compares the detection performances of the two detection methods, which have been tested against two sets of experimental data.

5.1 Parametric Roll - Experimental Data

Two sets of experimental data have been gathered through experiments[1] run at the Centre for Marine Technology in Trodheim. The vessel used for the experiments is a 1:45 scale model of a container ship with length overall of 294 m, whose principal dimensions and hydrodynamic coefficients can be found in Paper A.

Two wave scenarios have been considered: regular and irregular waves. The regular wave scenario is characterized by sinusoidal waves centered at a single specific frequency, whereas the irregular wave condition, which represents the real sea motion, is generated by interference of sinusoidal waves centered at different frequencies. Tables 5.1-5.2 report the wave parameters for the sets of experiments used to validate the proposed parametric roll detectors.

Table 5.1: Regular wave experiments

Exp.	A_w [m]	ω_w [rad/s]	ω_e/ω_ϕ	$\lvert\phi_{\max}\rvert$ [deg]
1192	2.5	0.4640	1.9021	0.8944
1193	2.5	0.4640	1.9226	1.8932
1191	2.5	0.4640	1.9428	21.7800
1172	2.5	0.4640	1.9633	23.9270
1184	2.5	0.4640	1.9834	22.7810
1185	2.5	0.4640	2.0032	20.8780
1186	2.5	0.4640	2.0234	21.5640
1187	2.5	0.4640	2.0439	20.4990
1188	2.5	0.4640	2.0842	22.7190
1190	2.5	0.4640	2.1047	1.4291
1189	2.5	0.4640	2.1245	1.4368

In the regular wave condition 7 out of 11 experiments have shown parametric roll resonance, whereas the vessel experienced parametric roll only once during the irregular wave runs. It is important to stress that all the considered experiments were made to trigger parametric roll, but in the irregular wave scenario it is more difficult to have a fully developed parametric roll resonance because consecutive wave trains may not fulfil all the conditions for its existence.

[1]The experiments were performed by Dr. Drummen and Dr. Perez from CeSOS, and by Dr. Storhaug from DNV

Table 5.2: Irregular wave experiments

Exp.	H_s [m]	T_p [s]	$\lvert\phi_{\max}\rvert$ [deg]
1194	9	13.54	2.91
1195	9	13.54	17.24
1196	9	13.54	2.88
1197	7	13.54	1.68
1198	7	13.54	4.23
1199	9	13.54	1.83
1200	9	13.54	1.74
1201	9	13.54	1.45

5.2 Detection Methods

The real-time detection of the inception of parametric roll has been investigated in Papers D-E. The common root of these works is the interaction between the second harmonic of the roll motion and the first harmonic of the pitch and heave modes. Detectors capable to catch this interconnection have been implemented and tested against the two sets of experimental data presented in Section 5.1.

5.2.1 Nonlinear Energy Flow Indicator

The basic idea of the detector developed in [D] is to detect the onset of parametric roll by checking an energy flow indicator, which provides the measure of the transferred energy from the motions in the vertical plane, heave and pitch, directly excited by the waves to the motion about the transverse plane, roll. The energy indicator is based on the cross-spectrum of the following signals: the first harmonic of heave/pitch, and the second harmonic of roll. This choice has been driven by the fact that parametric roll is an autoparametric phenomenon, where the inception of large roll oscillations is provoked by the fact that the oscillation frequency of the primary system (heave/pitch) is twice the natural frequency of the secondary system (roll).

The detection problem has been set up as hypothesis testing on the cross-spectrum. In particular, given the two signals θ and ϕ^2 the detection problem is to distinguish between the following hypothesis

$$\begin{aligned} \mathscr{H}_0 &: \; P_{\phi^2\theta}(\omega) \leq \bar{P} \\ \mathscr{H}_1 &: \; P_{\phi^2\theta}(\omega) > \bar{P} \end{aligned} \tag{5.1}$$

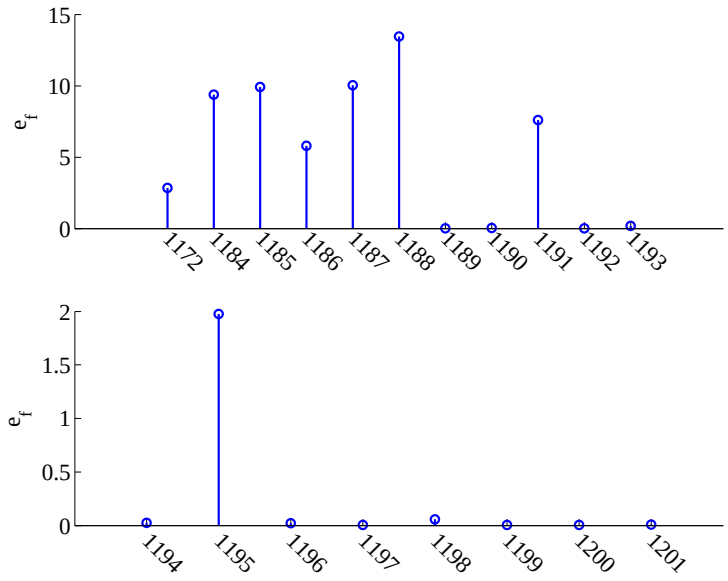

Figure 5.1: Energy flow indicator for the regular and irregular wave data sets.

where $P_{\phi^2\theta}$ is the cross-spectrum, and $\bar{P}$ is a power threshold. Instead of using directly the cross-spectrum an energy flow coefficient has been introduced, defined as

$$e_f \triangleq \frac{\sigma^2_{\phi^2\theta}}{\sqrt{\sigma^2_{\phi^2}\sigma^2_{\theta}}}, \tag{5.2}$$

where $\sigma^2_{\phi^2\theta}$ is the variance of the cross-spectrum, $\sigma^2_{\phi^2}$ is the variance of the square of the roll motion, and σ^2_{θ} is the variance of the pitch motion. In Fig. 5.1 there are the plots of e_f for each data sets considered for the performance evaluation. The plots clearly show that in those experiments where parametric roll did occur there is a significant transfer of energy from heave/pitch into roll, leading to a high value of e_f.

By means of of this energy flow indicator the detection problem can be formulated as

$$\begin{aligned} \mathscr{H}_0 &: \; e_f \leq \bar{e} \\ \mathscr{H}_1 &: \; e_f > \bar{e}, \end{aligned} \tag{5.3}$$

where $\bar{e}$ is the amount of energy required to trigger parametric roll.

To achieve real-time detection the detector was implemented in a recursive fashion. Two main parameters are important for this implementation: the window length and the window overlap. The former implies the resolution at which the power spectra are computed, and in turn, the accuracy on e_f; whereas the latter implies the time to detect. In order to obtain an acceptable resolution and a quick detection the window length was set equal to one roll period, and the window overlap equal to 75%, i.e. the spectra are recomputed every quarter of the roll period. The detector was tested on the data sets presented in Section 5.1, and its performances have been compared with a sinusoidal detector.

Figures 5.2-5.3 show two outcomes of the energy flow indicator for an experiment in regular waves where parametric roll occurred, and for an experiment in irregular waves where parametric roll did not onset. A detailed description of the achieved results can be found in [D].

Remark

For a real ship sailing in oblique short-crested seaways some forced roll with frequency equal to the encounter frequency will always occur. This does not obscure the proposed detection scheme since the energy flow coefficient is based on the cross-spectrum of the second harmonic of roll and pitch. In case of forced roll both roll and pitch will be oscillating at the same frequency; hence the cross-spectrum will be nil since the second harmonic of roll will be centered at twice the pitch frequency.

Example 5.1 *Consider pitch and roll as sinusoidal signals*

$$\begin{aligned} \theta(t) &= \theta_0 \cos(\omega_\theta t) \\ \phi(t) &= \phi_0 \cos(\omega_\phi t), \end{aligned} \tag{5.4}$$

where $\omega_\theta = \omega_e = 2\omega_\phi$*, as in parametric resonance. The energy flow coefficient* e_f *is based on the computation of the cross-spectrum* $P_{\phi^2\theta}$*, which in turn is the Fourier transform of the cross-correlation* $r_{\phi^2\theta}$*. Therefore, according to the cross-correlation theorem*

$$P_{\phi^2\theta} = \mathcal{F}(r_{\phi^2\theta}) = \mathcal{F}(\phi^2 * \theta) = \overline{\mathcal{F}(\phi^2)}\mathcal{F}(\theta) \tag{5.5}$$

where $\overline{\mathcal{F}(\phi^2)}$ *is the complex conjugate. Applying the cross-correlation theorem to the signals at hand we obtain*

$$P_{\phi^2\theta} = \frac{1}{4}\phi_0^2\theta_0\pi^2[(\delta(\omega - 2\omega_\phi) + \delta(\omega + 2\omega_\phi))]^2, \tag{5.6}$$

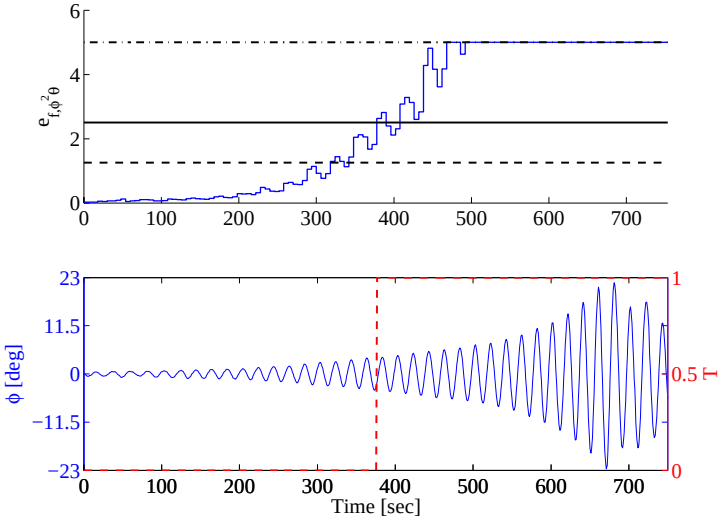

Figure 5.2: Exp. 1188: detection of parametric roll.

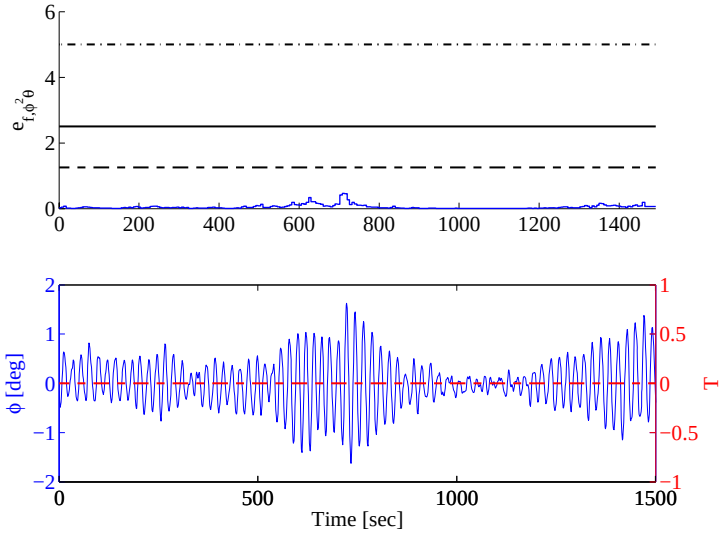

Figure 5.3: Exp. 1197: no alarm is issued.

where $\delta(\cdot)$ is the Dirac delta function. The cross-spectrum is different from zero since $\phi^2(t)$ and $\theta(t)$ are centered at the same frequency; hence the energy flow indicator is different from zero and it can be used for detecting parametric roll.

Consider now a ship sailing in near head seas condition. The lateral component of the wave force excites the roll motion directly, hence pitch and roll both respond at the same frequency ω_e of the excitation

$$\begin{aligned} \theta(t) &= \theta_0 \cos(\omega_e t) \\ \phi(t) &= \phi_0 \cos(\omega_e t). \end{aligned} \tag{5.7}$$

The cross-spectrum in this case is equal to zero, in fact

$$P_{\phi^2\theta} = \frac{1}{4}\phi_0^2\theta_0\pi^2[(\delta(\omega - 2\omega_e) + \delta(\omega + 2\omega_e))][(\delta(\omega - \omega_e) + \delta(\omega + \omega_e))] = 0 \tag{5.8}$$

since the Dirac delta function is different from zero only at $\omega = \omega_e$ or at $\omega = 2\omega_e$. Therefore the energy flow indicator will be zero, showing that the proposed detection method is insensitive to forced roll.

5.2.2 Phase Correlation and GLRT for Non-Gaussian Signals

The time-domain detection is based on the definition of a driving signal that carries the information about the phase correlation between heave/pitch and roll. Figure 5.4 shows that when parametric roll develops there is a lining up of peaks between pitch and roll, i.e. every second peak of pitch is in-phase with the peak in roll. When, instead, this alignment is lost, roll oscillations start reducing in amplitude, as seen between 150 and 250 seconds.

Consider two sinusoidal signals s_1 and s_2 given by

$$\begin{aligned} s_1 &= A_1 \cos(\omega t + \psi_1) \\ s_2 &= A_2 \cos(2\omega t + \psi_2). \end{aligned} \tag{5.9}$$

Multiplying s_1^2 by s_2, the following signal is obtained,

$$\begin{aligned} s_1^2 s_2 = A_1^2 A_2 [&\cos(2\omega t + 2\psi_1)\cos(2\omega t + \psi_2) \\ &+ \sin^2(\omega t + \psi_1)\cos(2\omega t + \psi_2)], \end{aligned} \tag{5.10}$$

which, by the change of variable $\varepsilon = 2\omega t + \psi_2$, is rewritten as,

$$s_1^2 s_2 = A_1^2 A_2 \left[\cos(\varepsilon - \psi_2 + 2\psi_1)\cos\varepsilon + \sin^2\left(\frac{\varepsilon - \psi_2}{2} + \psi_1\right)\cos(\varepsilon)\right]. \tag{5.11}$$

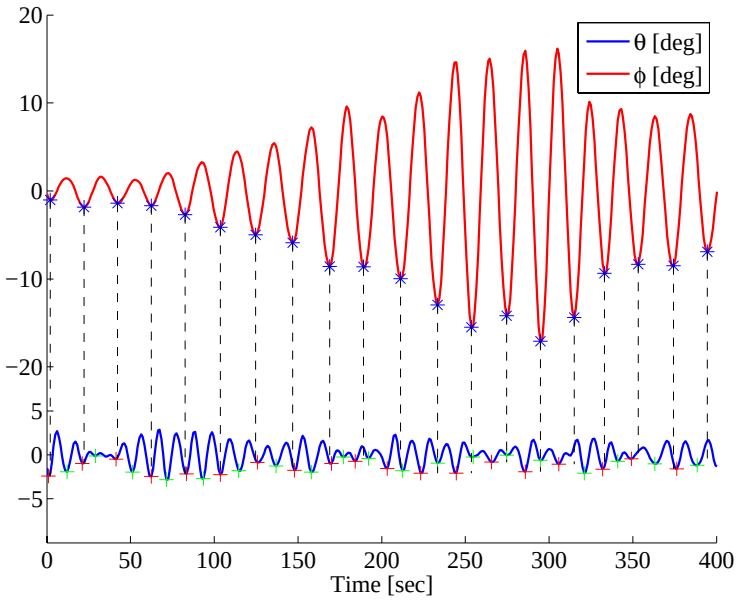

Figure 5.4: Experiment 1195: alignment of peaks between pitch θ and roll ϕ during the onset and development of parametric roll.

Equation (5.11) shows that if s_1^2 and s_2 are in-phase ($2\psi_1 - \psi_2 = 0$) then

$$s_1^2 s_2 = \frac{1}{2} A_1^2 A_2 (\cos^2 \varepsilon + \cos \varepsilon), \tag{5.12}$$

whereas if s_1^2 and s_2 are out-of-phase ($2\psi_1 - \psi_2 = \pi$) then

$$s_1^2 s_2 = -\frac{1}{2} A_1^2 A_2 (\cos^2 \varepsilon - \cos \varepsilon), \tag{5.13}$$

that means, the signal $s_1^2 s_2$ shows positive or negative peaks of maximum amplitude $A_1^2 A_2$.

Given roll angle ϕ and pitch angle θ, the signal driving the parametric resonance in roll is then defined as

$$d(t) \triangleq \phi^2(t)\theta(t), \tag{5.14}$$

and its time evolution shows that the onset and the ending of the resonant motion is addressed by large negative and positive spikes, respectively. Figure 5.5 shows an example of the behavior of the driving signal for two different

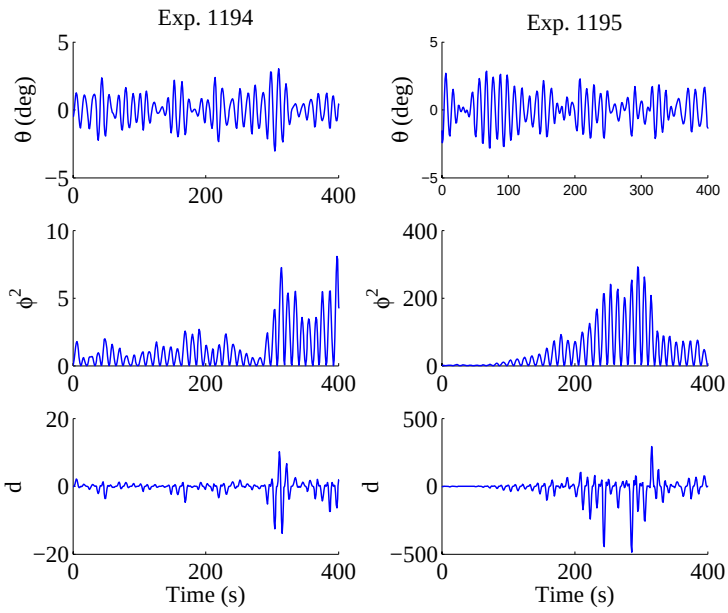

Figure 5.5: Behavior of the driving signal d in absence (left) and presence (right) of parametric roll.

experiments, one without parametric roll and one with. Furthermore, when parametric roll develops the amplitude of the negative spikes in the driving signal is much larger than those appearing when the roll motion is not in a resonance condition. Therefore, a significant change in the variance of the driving signal d could be expected from the onset of parametric roll resonance, and this jump in variance could be exploited by setting up a detector that looks for a variation of signal power in a random signal with a certain amplitude distribution.

In order to select the most suitable detection method it is of primary importance to determine the distribution of the available signals. Histograms of the driving signal have been plotted for the resonant and non resonant cases (see an example in Figs. 5.6-5.7). Two main characteristics can be pointed out: the presence of a very sharp peak in correspondence of the mean value, and long tails. Figure E.4 clearly shows that a Gaussian PDF does not fit the data since it is not able to catch the presence of the high peak in the histogram; on the other hand the Laplacian PDF better approximate the behavior of the histogram. Moreover the heavy tails of the Laplacian PDF can also explain the presence of spikes observed in the time series.

The detection problem as then been formulated as the detection of a variation

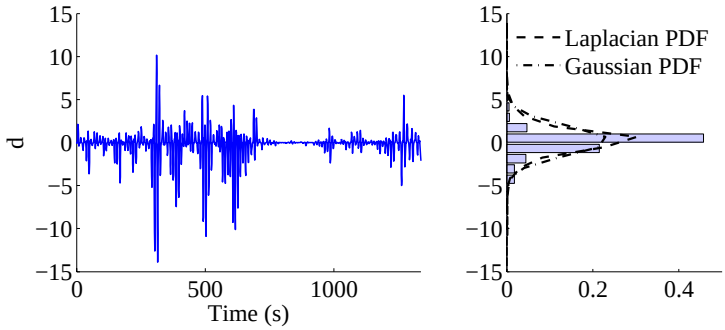

Figure 5.6: Experiment 1194: histogram of the driving signal for the non resonant case.

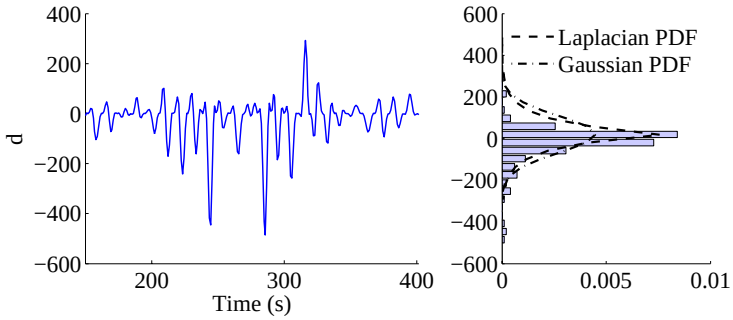

Figure 5.7: Experiment 1195: histogram of the driving signal for $150 \leq t \leq 400$ when parametric roll develops. The Laplacian PDF better approximates the histogram.

of signal power in a Laplacian distributed signal. The detection of the inception of parametric roll can be formulated as

$$\begin{array}{ll} \mathscr{H}_0 : x[n] = d[n] \ , \ \sigma_d^2 = \sigma_0^2 & n = 0, 1, \ldots, N-1 \\ \mathscr{H}_1 : x[n] = d[n] \ , \ \sigma_d^2 = \sigma_1^2 & n = 0, 1, \ldots, N-1. \end{array} \tag{5.15}$$

The GLRT decides $\mathscr{H}_1$ if

$$L_G = \frac{p\left(d; \hat{\sigma}_1^2, \mathscr{H}_1\right)}{p\left(d; \mathscr{H}_0\right)} > \gamma, \tag{5.16}$$

where $p(\cdot;\cdot)$ is the Laplacian PDF, $\hat{\sigma}_1^2$ is the MLE (maximum likelihood estimate) of σ_1^2, and γ is a threshold set by the probability of false alarms the detector is desired to have. After having determined the MLE of σ_1^2 it is possible to derive an explicit form for the detector by taking the natural logarithm of both sides of Eq. (5.16). The detector reads

$$-\frac{N}{2} \ln \hat{\sigma}_1^2 + N \frac{\hat{\sigma}_1}{\sigma_0} > \gamma'''. \tag{5.17}$$

where, $\gamma''' = \ln \gamma - \frac{N}{2} \ln \sigma_0^2 + N$.

The performance of the detection scheme has been evaluated against two sets of experimental data. The detector showed good capabilities of issuing early warning in all the runs where parametric roll occurred, triggering alarms already when roll amplitudes were less than 5°. Examples of detection for regular and irregular waves scenario are shown in Fig. 5.8-5.9. Only one possibly false alarm was issued and this happened in conditions close to parametric resonance. A detailed description of the obtained results can be found in [E].

Remark

The GLRT for non-Gaussian signals is insensitive to forced roll as well as the energy flow indicator.

Example 5.2 *Consider pitch and roll as sinusoidal signals*

$$\begin{aligned} \theta(t) &= \theta_0 \cos(\omega_\theta t + \varsigma) \\ \phi(t) &= \phi_0 \cos(\omega_\phi t). \end{aligned} \tag{5.18}$$

In forced roll condition, roll and pitch are sinusoids of the same frequency ($\omega_\theta = \omega_\phi = \omega$)*, which yields the following driving signal*

$$\begin{aligned} d(t) &= \phi^2(t)\theta(t) \\ &= \phi_0^2 \theta_0 \cos^2(\omega t) \cos(\omega t + \varsigma). \end{aligned} \tag{5.19}$$

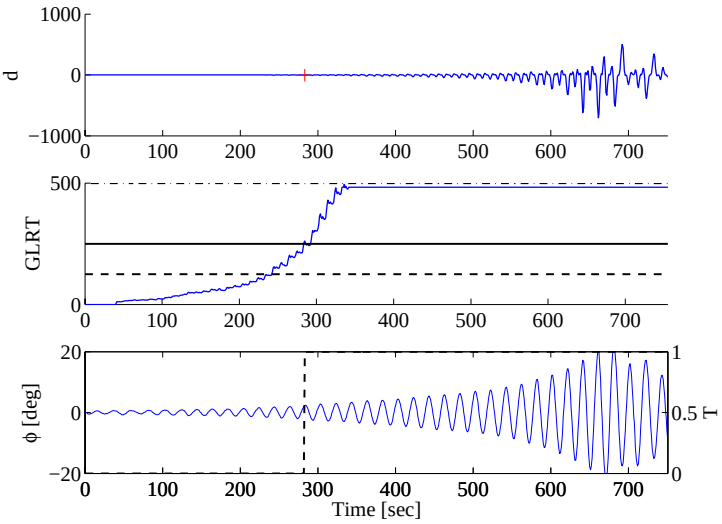

Figure 5.8: Experiment 1188: detection of parametric roll.

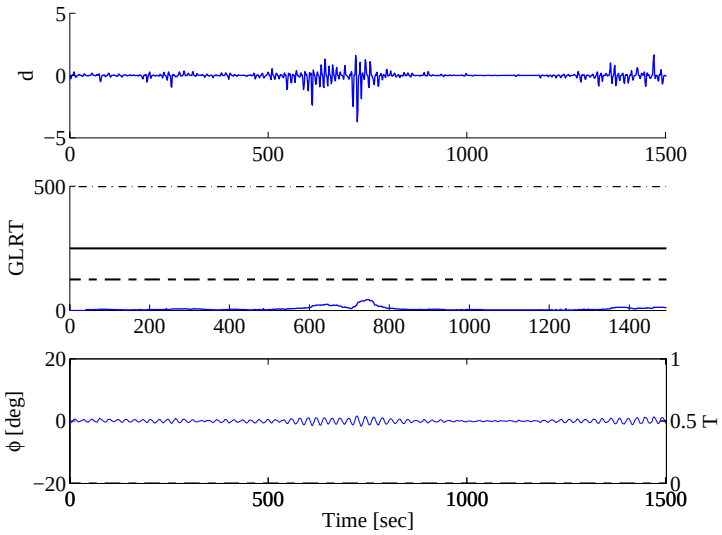

Figure 5.9: Experiment 1197: no alarm is issued.

To prove that the GLRT detector is not sensitive to forced roll, we need to demonstrate that there exists a constant Γ *such that for any* $\gamma > \Gamma$ *the detector does not trigger an alarm. In general* Γ *is function of the phase shift* ς *and of the time interval* ΔT *over which the estimate of the variance is performed.*

To find Γ *we need to prove that*

$$-\Delta T \ln\left(\frac{\sqrt{2}}{\Delta T}\int_0^{\Delta T}|d(t)|\,\mathrm{d}t\right)+\frac{\sqrt{2}}{\sigma_0}\int_0^{\Delta T}|d(t)|\,\mathrm{d}t \tag{5.20}$$

is upper bounded. The indefinite integral of $|d(t)|$ *is a periodic function given by*

$$\begin{aligned} D(t)\triangleq\int|d(t)|\,\mathrm{d}t=\frac{T}{2\pi}\phi_0^2\theta_0\Big(&\frac{1}{2}\mathrm{sgn}(\cos(\omega t))^2\mathrm{sgn}(\cos(\omega t+\varsigma))\sin(\omega t+\varsigma)\\ &+\frac{1}{4}\mathrm{sgn}(\cos(\omega t))^2\mathrm{sgn}(\cos(\omega t+\varsigma))\sin(\omega t-\varsigma)\\ &+\frac{1}{12}\mathrm{sgn}(\cos(\omega t))^2\mathrm{sgn}(\cos(\omega t+\varsigma))\sin(3\omega t+\varsigma)\Big) \end{aligned} \tag{5.21}$$

where $\mathrm{sgn}(\cdot)$ *is the signum function, and* $T=2\pi/\omega$ *is the natural roll period. For any* $\Delta T\in[0\ ,\ T]$ *we have*

$$\int_0^{\Delta T}|d(t)|\,\mathrm{d}t<\sup_{0\le\Delta T\le T}|D(t)|\le\frac{5}{6}\frac{T}{2\pi}\phi_0^2\theta_0. \tag{5.22}$$

Therefore the GLRT detector is not sensitive to forced roll if the threshold γ *is set larger than*

$$\Gamma\triangleq-\Delta T\ln\left(\frac{\sqrt{2}}{2\pi}\frac{5}{6}\frac{T}{\Delta T}\phi_0^2\theta_0\right)+\frac{\sqrt{2}}{\sigma_0}\frac{5}{6}\frac{T}{2\pi}\phi_0^2\theta_0. \tag{5.23}$$

5.3 Detection Performances Evaluation

The performances of the two proposed detectors have been compared on the base of the time to detect the onset of parametric roll and the number of false alarms issued. The comparison shows a very good potential of both detection schemes in predicting the inception of the resonant motion. The detector based on the GLRT for Laplacian distributed signals performs a quicker detection on the regular waves data set than the detector based on the energy flow indicator, but both detectors perform equally well in the irregular wave scenario.

The onset of parametric roll is detected in few roll cycles when the roll angle is, in most of the cases, less than 5°; the number of issued false alarms is very

low, if any. In particular there were no false alarms issued for the regular waves case, and only one possible false alarm was issued with the irregular waves data set.

5.3.1 Regular Waves

The detection performances of the two detectors for the regular waves data set are summarized in Table 5.3. Comparing detection time T_d and the maximum roll angle reached within the detection time $|\phi_{\max}(T_d)|$, it is possible to point out that the two detectors perform equally well issuing an early warning when the roll angle is still less than 5° in most of the cases. Moreover none of the detectors issued false alarms for the data set at hand, reaching 100% of correct detection.

Table 5.3: Regular wave experiments: detection performance

		e_f			GLRT		
Exp.	PR	T_d	$\lvert\phi_{\max}(T_d)\rvert$	Det.	T_d	$\lvert\phi_{\max}(T_d)\rvert$	Det.
1172	Yes	520 s	5.54°	C	474 s	3.15°	C
1184	Yes	364 s	5.83°	C	302 s	2.88°	C
1185	Yes	400 s	4.34°	C	353 s	2.54°	C
1186	Yes	496 s	4.56°	C	434 s	2.55°	C
1187	Yes	412 s	4.75°	C	354 s	2.51°	C
1188	Yes	400 s	4.21°	C	285 s	2.35°	C
1189	No	-	-	C	-	-	C
1190	No	-	-	C	-	-	C
1191	Yes	340 s	4.97°	C	304 s	2.61°	C
1192	No	-	-	C	-	-	C
1193	No	-	-	C	-	-	C

5.3.2 Irregular Waves

The detection performances of the two detectors for the irregular waves experiments are illustrated in Table 5.4. The detection schemes work well also in these cases, achieving a quick detection in the experiment 1195 where parametric roll did occur. The alarm triggered for the experiment 1198 has been classified as a false positive since visual inspection of the time series addressed that the resonant motion did not develop, but considering the maximum roll angle achieved when the detector issues the warning it may be possible to classify this experiment as a border case, that is, parametric roll could develop but consecutive

Table 5.4: Irregular wave experiments: detection performance

		e_f			GLRT		
Exp.	PR	T_d	$\lvert\phi_{\max}(T_d)\rvert$	Det.	T_d	$\lvert\phi_{\max}(T_d)\rvert$	Det.
1194	No	-	-	C	-	-	C
1195	Yes	94 s	3.27°	C	94 s	3.27°	C
1196	No	-	-	C	-	-	C
1197	No	-	-	C	-	-	C
1198	No	220 s	3.89°	FA	215 s	3.81°	FA
1199	No	-	-	C	-	-	C
1200	No	-	-	C	-	-	C
1201	No	-	-	C	-	-	C

wave trains did not satisfy the requirements to allow the resonant motion to keep growing.

5.3.3 Discussion

The proposed detection methods have shown very good capabilities in detecting the onset of parametric roll resonance in both wave scenarios, but it is important to point out that it was possible to test them only on a limited amount of experimental data, especially for the irregular wave case, and all experiments were run in head seas condition.

Although there is a general agreement on the fact that the roll motion in parametric resonance is not Gaussian distributed (see e.g. [3, 12]), the current literature does not provide any extensive experimental study of parametric roll in order to assess undoubtedly its statistical properties. Therefore, the Laplacian PDF, chosen to describe the amplitude distribution of the driving signal, represents one attempt to assign a certain statistical characteristics to the signals involved on the inception of parametric roll. Nevertheless, there is full awareness that the availability of more experimental runs with parametric roll in irregular wave scenario could show which distribution best describe the physical behavior of the signals at hand.

Chapter 6

Conclusions

This thesis investigated the feasibility of counteracting parametric roll resonance by combining detection and control methods.

The stability analysis of the Mathieu's equation, which was used to describe the roll motion in parametric resonance condition, showed that stabilisation of parametric roll can be achieved through two courses of action: a direct stabilisation of the roll oscillations by increasing the damping in roll, and an indirect stabilisation through de-tuning of the frequency coupling condition between the roll natural frequency and the wave encounter frequency.

As direct stabilisation, this thesis considered the increase of roll damping by using fin stabilisers. Two control approaches have been adopted to design the fin stabiliser. First a linear feedback controller from the roll rate demonstrated the feasibility of stabilising the resonant motion by increasing the damping threshold that triggers the resonance, as shown by Floquet theory. Then integrator backstepping methods were applied to design a nonlinear fin stabiliser that damps parametric roll in a region of attraction, which is a function of the maximum fin roll moment.

As indirect stabilisation, de-tuning of the frequency coupling condition was demonstrated by change in ship forward speed. The speed controller was designed using Lyapunov methods. Direct and indirect methods were then com-

bined and found to achieve roll stabilisation in few roll cycles. In particular, the effectiveness of the combined action significantly improved the separate control actions, especially when de-tuning was achieved by increase of ship forward speed, due to the dependency of the lift force on the square of the flow velocity.

Limitations on the maximum stabilisable roll angle were also analysed and linked to slew rate saturation and hydrodynamic stall characteristics of the fin stabilisers. The study on maximum stabilisable roll angle addressed the need of starting proper control action before critical oscillation magnitudes were reached.

The issue of early detection of parametric roll inception was solved by the design of two novel detectors, which work within a short-time, and was shown to detect onset of parametric roll within few roll cycles. The main idea behind these detection schemes was that of exploiting the link between the second harmonic of roll angle and the first harmonic of heave or pitch motions. A nonlinear energy flow indicator, an indicator for the transfer of energy from the first harmonic of heave or pitch into the second harmonic of roll, was at the core of the first detector. The second detector relied on a driving signal that carried information about phase correlation between pitch or heave and roll. A generalised likelihood ratio test was designed to detect a change in variance of the distribution of the driving signal. The threshold value was determined from detection theory by analysing the asymptotic performance of the GLRT detector. Nevertheless the actual implementation relied on empirical values due to the reduced amount of experimental data. The detectors were validated against experimental data of tests of a 1:45 scale model of a container ship showing good performance in terms of time to detect and false-alarm rates for both the proposed detectors.

The thesis also offered a contribution regarding modeling. A 3 degree-of-freedom nonlinear model in heave-pitch-roll of a container ship suitable for parametric roll resonance study was proposed. The model, which was developed in collaboration with other researchers, provided a benchmark for the study and simulation of parametric roll over a large range of ship speeds and sea states.

Results of this research were published in papers enclosed in this thesis and a patent application was filed on the detection schemes and their implementations.

Bibliography

[1] ABS, "Assessment of parametric roll resonance in the design of container carriers," American Bureau of Shipping, Tech. Rep., September 2004.

[2] V. Belenky, H. Yu, and K. Weems, "Numerical procedures and practical experience of assessment of parametric roll of container carriers," in *Proceedings of the 9th International Conference on Stability of Ships and Ocean Vehicles*, 2006.

[3] V. L. Belenky, K. M. Weems, W. M. Lin, and J. R. Paulling, "Probabilistic analysis of roll parametric resonance in head seas," in *Proceedings of the 8th International Conference on Stability of Ships and Ocean Vehicles*, 2003.

[4] G. Blanch, *Handbook of Mathematical Functions: with Formulas, Graphs, and Mathematical Tables*, 1972, ch. 20, pp. 722–746.

[5] M. Blanke and A. G. Jensen, "Dynamic properties of a container vessel with low metacentric height," *Trans Inst Measurement and Control*, vol. 19(2), pp. 78–93, 1997.

[6] M. Blanke, K. P. Lindegaard, and T. I. Fossen, "Dynamic model for thrust generation of marine propellers," in *Proceedings of the IFAC Conference on Manoeuvreing of Marine Craft*, 2000.

[7] M. Blanke, M. Kinnaert, J. Lunze, and M. Staroswiecki, *Diagnosis and Fault-Tolerant Control - Second Edition.* Springer, 2006.

[8] W. Blocki, "Ship safety in connection with the parametric resonance of the roll," *International ShipBuilding Progress*, vol. 27, pp. 36–53, 1980.

[9] G. Bulian, "Nonlinear parametric rolling in regular waves - a general procedure for the analytical approximation of the gz curve and its use in the time domain simulations," *Ocean Engineering*, vol. 32, pp. 309–330, 2005.

[10] ——, "Development of nonlinear analytical models for parametric roll and hydrostatic restoring variations in regular and irregular waves," Ph.D. dissertation, Università degli Studi di Trieste, 2006.

[11] G. Bulian, A. Francescutto, and C. Lugni, "On the nonlinear modelling of parametric rolling in regular and irregular waves," *International ShipBuilding Progress*, vol. 51, pp. 173–203, 2004.

[12] G. Bulian, A. Francescutto, N. Umeda, and H. Hashimoto, "Qualitative and quantitative characteristics of parametric ship rolling in random waves," *Ocean Engineering*, vol. 35, pp. 1661–1675, 2008.

[13] S. M. Carmel, "Study of parametric rolling event on a panamax container vessel," *Journal of the Transportation Research Board*, vol. 1963, pp. 56–63, 2006.

[14] DNV, "Parametric rolling simulation," *DNV Container Ship Update*, vol. 1, p. 15, 2007.

[15] K. A. Døhlie, "Parametric rolling – a problem solved?" *DNV Container Ship Update*, vol. 1, pp. 12–15, 2006.

[16] EMSA, *Maritime Accident Review 2008*. European Maritime Safety Agency, 2009.

[17] M. Faraday, "On a peculiar class of acoustical figures; and on certain forms assumed by groups of particles upon vibrating elastic surfaces," *Philosophical Transactions of the Royal Society of London*, vol. 121, pp. 299–340, 1831.

[18] G. Floquet, "Sur les équations différentielles linéaires à coefficients périodiques," *Annales Scientifiques de l'École Normale Supérieure*, vol. 12, pp. 47–89, 1883.

[19] T. I. Fossen, *Marine Control Systems: guidance, navigation and control of ships, rigs and underwater vehicles*. Marine Cybernetics, 2002.

[20] W. N. France, M. Levadou, T. W. Treakle, J. R. Paulling, R. K. Michel, and C. Moore, "An investigation of head-sea parametric rolling and its influence on container lashing systems," in *SNAME Annual Meeting*, 2001.

[21] A. Francescutto, "An experimental investigation of parametric rolling in head waves," *Journal of Offshore Mechanics and Arctic Engineering*, vol. 123, pp. 65–69, 2001.

[22] A. Francescutto and G. Bulian, "Nonlinear and stochastic aspects of parametric rolling modelling," in *Proceedings of the 6th International Ship Stability Workshop*, 2002.

[23] W. Froude, "On the rolling of ships," *Transaction of the Institution of Naval Architects*, vol. 2, pp. 180–227, 1861.

[24] ——, "Remarks on Mr. Scott Russel's paper on rolling," *Transactions of the Institution of Naval Architects*, vol. 4, pp. 232–275, 1863.

[25] R. Galeazzi and M. Blanke, "On the feasibility of stabilizing parametric roll with active bifurcation control," in *Proceedings of the 7th IFAC Conference on Control Applications in Marine Systems*, 2007.

[26] R. Galeazzi, J. Vidic-Perunovic, M. Blanke, and J. J. Jensen, "Stability analysis of the parametric roll resonance under non-constant ship speed," in *Proceedings of the 9th Biennial ASME Conference on Engineering Systems Design and Analysis*, 2008.

[27] R. Galeazzi, M. Blanke, and N. K. Poulsen, "Detection of parametric roll resonance on ships from indication of nonlinear energy flow," in *Proc. 7th IFAC Symp. on Fault Detection, Supervision and Safety of Technical Processes, SAFEPROCESS'2009*, 2009.

[28] R. Galeazzi, C. Holden, M. Blanke, and T. I. Fossen, "Stabilization of parametric roll resonance by combined speed and fin stabilizer control," in *Submitted to European Control Conference*, 2009.

[29] S. Ginsberg, "Lawsuits rock APL's boat – Cargo goes overboard; insurance lawyers surface," San Francisco Business Times, November 1998. [Online]. Available: http://www.bizjournals.com/sanfrancisco/stories/1998/11/23/story1.html

[30] G. C. Goodwin, S. F. Graebe, and M. E. Salgado, *Control System Design*. Prentice Hall, 2001.

[31] R. Grimshaw, *Nonlinear Ordinary Differential Equations*. CRC Press, 1993.

[32] H. Gunderson, H. Rigas, and F. S. A. van Vleck, "Technique for determining stability regions for the damped Mathieu equation," *SIAM Journal on Applied Mathematics*, vol. 26, pp. 345–349, 1974.

[33] H. Hashimoto and N. Umeda, "Nonlinear analysis of parametric rolling in longitudinal and quartering seas with realistic modelling of roll-restoring moment," *Journal of Marine Science and Technology*, vol. 9, pp. 117–126, 2004.

[34] G. W. Hill, "On the part of the lunar perigee which is a function of the mean motions of the sun and moon," *Acta Mathematica*, vol. 8, pp. 1–36, 1886.

[35] Y. Himeno, "Prediction of ship roll damping - state of the art," Department of Naval Architecture and Marine Engineering, The University of Michigan, Tech. Rep., 1981.

[36] C. Holden, R. Galeazzi, C. Rodríguez, T. Perez, T. I. Fossen, M. Blanke, and M. A. S. Neves, "Nonlinaer container ship model for the study of parametric roll resonance," *Modeling, Identification and Control*, vol. 28, pp. 87–113, 2007.

[37] C. Holden, T. Perez, and T. I. Fossen, "Frequency-motivated observer design for the prediction of parametric roll resonance," in *Proceedings of the 7th IFAC Conference on Control Applications in Marine Systems*, 2007.

[38] C. Holden, R. Galeazzi, T. Perez, and T. I. Fossen, "Stabilization of parametric roll resonance with active U-tanks via Lyapunov control design," in *Submitted to European Control Conference*, 2009.

[39] IMO, "Guidance to the master for avoiding dangerous situations in following and quartering seas," International Maritime Organization, Tech. Rep. MSC/Circ. 707, 1995.

[40] ——, "Revised guidance to the master for avoiding dangerous situations in adverse weather and sea conditions," International Maritime Organization, Tech. Rep. MSC.1/Circ.1228, January 2007.

[41] J. J. Jensen, *Load and global response of ships*. Elsevier, 2001.

[42] ——, "Effcient estimation of extreme non-linear roll motions using the first-order reliability method (FORM)," *Journal of Marine Science and Technology*, vol. 12, pp. 191–202, 2007.

[43] J. J. Jensen and P. T. Pedersen, "Critical wave episodes for the assessment of parametric roll," in *Proceedings of the 9th International Marine Design Conference*, 2006.

[44] J. J. Jensen, J. Vidic-Perunovic, and P. T. Pedersen, "Influence of surge motion on the probability of parametric roll in a stationary sea state," in *Proceedings of the 10th International Ship Stability Workshop*, 2007.

[45] J. J. Jensen, P. T. Pedersen, and J. Vidic-Perunovic, "Estimation of parametric roll in stochastic seaway," in *Proceedings of IUTAM Symposium on Fluid-Structure Interaction in Ocean Engineering*, 2008.

[46] S. M. Kay, *Fundamental of Statistical Signal Processing vol II: Detection Theory.* Prentice Hall, 1998.

[47] J. E. Kerwin, "Notes on rolling in longitudinal waves," *International Ship-Building Progress*, vol. 2(16), pp. 597–614, 1955.

[48] H. K. Khalil, *Nonlinear Systems – third edition.* Prentice Hall, 2002.

[49] M. Levadou and L. Palazzi, "Assessment of operational risks of parametric roll," in *SNAME Annual Meeting 2003*, 2003.

[50] Lloyd's Register, "Head-sea parametric rolling of container ships," *Marine Service Information Sheet*, 2003.

[51] E. Mathieu, "Mémoire sur le movement vibratoire d'une membrane de forme elliptique," *Journal de Mathématiques Pures et Appliquées*, vol. 13, pp. 137–203, 1868.

[52] L. S. McCue and G. Bulian, "A numerical feasibility study of a parametric roll advance warning system," *Journal of Offshore Mechanics and Arctic Engineering*, vol. 129, pp. 165–175, 2007.

[53] F. Melde, "Über erregung stehender wellen eines fadenförmigen körpers," *Annalen der Physik und Chemie*, vol. 109, pp. 193–215, 1859.

[54] MSS, "Marine Systems Simulator - Matlab/Simulink Toolbox," <www.marinecontrol.org>, 2007, accessed November 30.

[55] A. H. Nayfeh and D. T. Mook, *Nonlinear Oscillations.* WILEY-VCH, 2004.

[56] M. A. S. Neves, "On the excitation of combination modes associated with parametric resonance in waves," in *Proceedings of the 6th International Ship Stability Workshop*, 2002.

[57] M. A. S. Neves and C. A. Rodriguez, "A coupled third order model of roll parametric resonance," in *Maritime Transportation and Exploitation of Ocean and Coastal Resources*, C. G. Soares, Y. Garbatov, and N. Fonseca, Eds. Taylor & Francis, 2005, pp. 243–253.

[58] ——, "An investigation on roll parametric resonance in regular waves," in *Proceedings of the 9th International Conference on Stability of Ships and Ocean Vehicles*, 2006.

[59] ——, "On unstable ship motions resulting from strong non-linear coupling," *Ocean Engineering*, vol. 33, pp. 1853–1883, 2006.

[60] ——, "Influence of non-linearities on the limits of stability of ship rolling in head seas," *Ocean Engineering*, vol. 34, pp. 1618–1630, 2007.

[61] M. A. S. Neves, N. A. Perez, and L. Valerio, "Stability of small fishing vessels in longitudinal waves," *Ocean Engineering*, vol. 26, pp. 1389–1419, 1999.

[62] J. N. Newman, *Marine Hydrodynamics*. The MIT Press, 1977.

[63] J. K. Nielsen, N. H. Pedersen, J. Michelsen, U. D. Nielsen, J. Baatrup, J. J. Jensen, and E. S. Petersen, "SeaSense - real-time onboard decision support," in *World Maritime Technology Conference*, 2006.

[64] I. G. Oh, A. H. Nayfeh, and D. T. Mook, "Theoretical and experimental study of the nonlinearly coupled heave, pitch, and roll motions of a ship in longitudinal waves," in *Proceedings of the 14th Biennial Conference on Mechanical Vibration and Noise*, 1993.

[65] ——, "A theoretical and experimental investigations of indirectly excited roll motion in ships," *Philosophical Transactions: Mathematical, Physical and Engineering Sciences*, vol. 358, pp. 1853–1881, 2000.

[66] M. Palmquist and C. Nygren, "Recording of head-sea parametric rolling on a PCTC," International Maritime Organization, Tech. Rep., 2004.

[67] R. Panko, "Cast away: cargo losses at sea are becoming more expensive to marine writers," *Best's Review*, 2003.

[68] J. R. Paulling, "The transverse stability of a ship in a longitudinal seaway," *Journal of Ship Research*, vol. 4(4), pp. 37–49, 1961.

[69] J. R. Paulling and R. M. Rosenberg, "On unstable ship motions resulting from nonlinear coupling," *Journal of Ship Research*, vol. 3(1), pp. 36–46, 1959.

[70] T. Perez, *Ship Motion Control*. Springer, 2005.

[71] S. Ribeiro e Silva, T. A. Santos, and C. Guedes Soares, "Parametrically excited roll in regular and irregular head seas," *International Shipbuilding Progress*, vol. 51, pp. 29–56, 2005.

[72] C. A. Rodríguez, C. Holden, T. Perez, I. Drummen, M. A. S. Neves, and T. I. Fossen, "Validation of a container ship model for parametric rolling," in *Proc. of the 9th International Ship Stability Workshop*, 2007.

[73] N. Salvesen, O. E. Tuck, and O. Faltinsen, "Ship motions and sea loads," *Transactions of SNAME*, vol. 78, pp. 250–287, 1970.

[74] N. E. Sanchez and A. H. Nayfeh, "Nonlinear rolling motions of ships in longitudinal waves," *International ShipBuilding Progress*, vol. 37(411), pp. 247–272, 1990.

[75] Y. S. Shin, V. L. Belenky, J. R. Paulling, K. M. Weems, and W. M. Lin, "Criteria for parametric roll of large containeships in longitudinal seas," *Transactions of SNAME*, vol. 112, 2004.

[76] K. J. Spyrou, I. Tigkas, G. Scanferla, N. Pallikaropoulos, and N. Themelis, "Prediction potential of the parametric rolling behaviour of a post-panamax container ship," *Ocean Engineering*, vol. 35, pp. 1235–1244, 2008.

[77] A. Tondl, T. Ruijgrok, F. Verhulst, and R. Nabergoj, *Autoparametric Resonance in Mechanical Systems*. Cambridge University Press, 2000.

[78] N. Umeda, H. Hashimoto, D. Vassalos, S. Urano, and K. Okou, "Nonlinear dynamics on parametric roll resonance with realistic numerical modelling," *International ShipBuilding Progress*, vol. 51, pp. 205–220, 2004.

[79] N. Umeda, H. Hashimoto, S. Minegaki, and A. Matsuda, "An investigation of different methods for the prevention of parametric rolling," *Journal of Marine Science and Technology*, vol. 13, pp. 16–23, 2008.

[80] UNCTAD secretariat, *Review of Maritime Transport 2008*. United Nations, 2008.

[81] J. van Amerongen, P. G. M. van der Klugt, and H. R. van Nauta Lemke, "Rudder roll stabilization for ships," *Automatica*, vol. 26(4), pp. 679–690, 1990.

Paper A

Nonlinear Container Ship Model for the Study of Parametric Roll Resonance

Published in *Modeling, Identification and Control*, **28**, pp.87-113, 2007.
Available at `http://www.mic-journal.no/`.

Abstract: Parametric roll is a critical phenomenon for ships, whose onset may cause roll oscillations up to $\pm 40°$, leading to very dangerous situations and possibly capsizing. Container ships have been shown to be particularly prone to parametric roll resonance when they are sailing in moderate to heavy head seas.

A Matlab/Simulink® parametric roll benchmark model for a large container ship has been implemented and validated against a wide set of experimental data. The model is a part of a Matlab/Simulink Toolbox [54]. The benchmark implements a 3rd-order nonlinear model where the dynamics of roll is strongly coupled with the heave and pitch dynamics. The implemented model has shown good accuracy in predicting the container ship motions, both in the vertical plane and in the transversal one. Parametric roll has been reproduced for all the data sets in which it happened, and the model provides realistic results which are in good agreement with the model tank experiments.

Keywords: Parametric roll resonance; Nonlinear systems; Model validation; Parameter identification; Ships

A.1 Introduction

Parametric roll is an autoparametric resonance phenomenon whose onset causes a sudden rise in roll oscillations. The resulting heavy roll motion, which can reach 30-40 degrees of roll angle, may bring the vessel into conditions dangerous for the ship, the cargo, and the crew. The origin of this unstable motion is the time-varying geometry of the submerged hull, which produces periodic variations of the transverse stability properties of the ship.

Parametric roll is known to occur when a ship sails in moderate to heavy longitudinal or oblique seas; the wave passage along the hull and the wave excited vertical motions result in variations of the intercepted waterplane area, and in turn, in relevant changes in the restoring characteristics. The onset and build-up of parametric roll is due to the occurrence of concomitant conditions: the wave length is close to the ship length ($\lambda_w \approx L_{\mathrm{PP}}$), the ship approaches waves with encounter frequency almost twice the roll natural frequency ($\omega_e \approx 2\omega_0$), and the wave height is greater than a ship-dependent threshold ($h_w > \overline{h}_s$).

The risk of parametric roll has been known to the maritime community since the early fifties, but only for small vessels with marginal stability – e.g. fishing boats – sailing in following seas. However, the phenomenon has recently attracted significant interest by the scientific community after accidents occurred with container ships sailing in head seas, incidents that involved significant damage to cargo as well as structural damages for millions of dollars [13, 20].

Several different types of vessel have reported to experience parametric roll in head seas, e.g. destroyers [21], ro-ro paxes [22] and PCTC [66]. Container carriers, however, are the most prone to parametric roll because of the current particular hull shape, i.e. large bow flare and stern overhang, and hence abrupt variation in the intercepted water-plane area when a wave crest or trough is amidships.

This has called for deep investigations into the nature of parametric roll in head/near head seas, and for the development of mathematical models able to capture and reproduce the physical aspects driving the resonant motion. In the last six years mathematical models of different complexity have been proposed by the scientific community, most of them relying on the Mathieu Equation to describe the dynamics of the ship subject to parametric resonance.

One-DOF models considering the uncoupled roll motion have been widely used to analyze the critical parameters of the phenomenon and derive stability conditions. Examples can be found in the papers by France et al. [20] and Shin et al. [75] where the authors employed the 1-DOF roll equation to show that, in regular waves, the Mathieu Equation can explain the onset of heavy roll motion in head seas.

Bulian [10] proposed a 1.5-DOF model where the dynamic interaction between the vertical motions and the roll oscillation was relaxed by the assumption of quasi-static heave and pitch. Moreover, that assumption allowed an analytical description of the GZ curve that was approximated as a surface varying with roll angle and wave crest position. This model is considered valid for moderate ship speed in head seas, and has lead to reasonable results in predicting parametric roll.

A 3-DOF nonlinear fully coupled model was first developed by Neves [56]. A first attempt was done by using Taylor series expansion up to 2^{nd}-order to describe the coupled restoring forces and moments in heave, pitch and roll. This model, although it provided a quite thorough description of the nonlinear interactions among the different modes, tended to overestimate the roll oscillation above the stability threshold. Neves and Rodriguez [57] proposed a 3^{rd}-order analytical model where the couplings among the three modes are expressed as a 3^{rd}-order Taylor series expansion. In this new model the nonlinear coefficients are mathematically derived as a functions of the characteristics of the hull shape. This 3-DOF model has been applied for the prediction of parametric roll to a transom stern fishing vessel [58, 59] providing outcomes which better match the experimental results than the 2^{nd}-order model.

It is noted that the above-mentioned literature have attempted to model parametric roll from an analytical points of view. Jensen [42] takes a statis-

tical approach instead, motivated by the difficulties inherent in describing the interaction between a 3-dimensional wave pattern and the motion of a ship hull. He shows how the statistical distribution of nonlinear ship responses can be estimated very accurately using a first-order reliability method. A commercial implementation in a system to predict parametric roll (SeaSense®) was reported in Nielsen et al. [63].

The direction of this paper is the analytical one, aiming at providing simulation tools that could e.g. be used in studies of active stabilization and control. The model proposed by Neves and Rodriguez [57] is applied to describe the dynamics of a container vessel subject to parametric roll resonance conditions. The model parameters are identified based upon the ship line drawings and the loading conditions. A Matlab/ Simulink implementation of the above model is then presented. The reliability of the implemented model in simulating parametric resonance behavior is validated against experimental data. The validation has shown good agreement with the experimental results for roll both in the experiments where parametric roll resonance occurred, and in the experiments where it did not occur.

The main goal of this work is to provide a benchmark for simulating parametric roll of a container ship over a large range of ship speeds and sea states. This benchmark has been designed to be a fully integrated part of Matlab/Simulink Toolbox for marine systems [54]. The availability of such a powerful tool opens up a great wealth of opportunities, notably the design and testing of novel model-based roll motion stabilizers.

A.2 Mathematical Model for Parametric Roll

The proposal and the adoption of an analytical model for representing a specific phenomenon should be driven by a trade-off between complexity and agreement with physical laws governing that phenomenon and/or experimental results.

Tondl et al. [77] define an autoparametric system as follows:

Definition A.1 Autoparametric systems are vibrating systems that consist of at least two constituting subsystems. One is the *primary system* that will usually be in a vibrating state. This primary system can be externally forced, self-excited, parametrically excited, or a combination of these. The second constituting subsystem is called the *secondary system*. The secondary system is coupled to the primary system in a nonlinear way, but such that the secondary system can be at rest while the primary system is vibrating.

An autoparametric system is, hence, characterized by these main aspects:

1. two nonlinearly coupled subsystems;
2. a normal mode where the primary system is in a vibrating state and the secondary system is at rest;
3. the presence of instability regions where the normal mode becomes unstable;
4. in the region of instability of the normal mode the overall system is in autoparametric resonance: the secondary system is parametrically excited by the vibrations of the primary system and it will not be at rest anymore.

Considering Definition A.1, 1 DOF models have too little complexity to describe an autoparametric system, since the roll motion for a ship sailing in longitudinal seas represents only the secondary system. They are useful to obtain insight in the parametric roll resonance phenomenon, but they will have difficulty predicting the real amplitude of the oscillations about the transverse plane.

The model proposed by Neves and Rodriguez [57] is complex enough to capture the dynamics of a container vessel behaving as an autoparametric system; it includes both the primary system (heave and pitch dynamics) which is externally excited by the wave motion, and the secondary system (roll dynamics) which is parametrically excited by the primary.

A.2.1 Equations of Motion

The 3-DOF nonlinear mathematical model of the container vessel is presented in the following way (using the notation of Neves and Rodriguez [57]):

Let

$$\mathbf{s}(t) = \begin{bmatrix} z(t) & \phi(t) & \theta(t) \end{bmatrix}^T \tag{A.1}$$

be the generalized coordinate vector, where z is the heave displacement, ϕ is the roll angle, and θ is the pitch angle, as shown in Figure A.1.

Then the nonlinear equations of motion can be expressed in matrix form as

$$(\mathbf{M} + \mathbf{A})\ddot{\mathbf{s}} + \mathbf{B}(\dot{\phi})\dot{\mathbf{s}} + \mathbf{c}_{\text{res}}(\mathbf{s}, \zeta) = \mathbf{c}_{\text{ext}}(\zeta, \dot{\zeta}, \ddot{\zeta}) \tag{A.2}$$

where

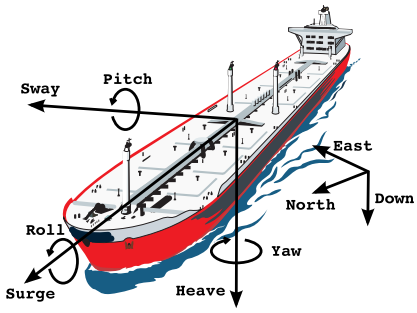

Figure A.1: Definition of motions.

- $\mathbf{M} \in \mathbb{R}^{3\times3}$ is the diagonal rigid-body generalized mass matrix;
- $\mathbf{A} \in \mathbb{R}^{3\times3}$ is the generalized added mass matrix;
- $\mathbf{B} \in \mathbb{R}^{3\times3}$ is the hydrodynamic damping (nonlinear in roll);
- $\mathbf{c}_{\text{res}} \in \mathbb{R}^3$ is the nonlinear vector of restoring forces and moments expressed as functions of the relative motion between ship hull and wave elevation $\zeta(t)$;
- $\mathbf{c}_{\text{ext}} \in \mathbb{R}^3$ is the vector of the external wave excitation forces and moments which depends on wave heading, encounter frequency, wave amplitude and time.

Generalized Mass, Added Mass and Damping

The generalized mass matrix can be written as

$$\mathbf{M} = \begin{bmatrix} m & 0 & 0 \\ 0 & I_x & 0 \\ 0 & 0 & I_y \end{bmatrix} \tag{A.3}$$

where m is the ship mass, I_x is inertia in roll and I_y is inertia in pitch.

The hydrodynamic added mass and damping matrices are expressed as

$$\mathbf{A} = \begin{bmatrix} -Z_{\ddot{z}} & 0 & -Z_{\ddot{\theta}} \\ 0 & -K_{\ddot{\phi}} & 0 \\ -M_{\ddot{z}} & 0 & -M_{\ddot{\theta}} \end{bmatrix} \tag{A.4}$$

$$\mathbf{B}(\dot{\phi}) = \begin{bmatrix} -Z_{\dot{z}} & 0 & -Z_{\dot{\theta}} \\ 0 & -K_{\dot{\phi}}(\dot{\phi}) & 0 \\ -M_{\dot{z}} & 0 & -M_{\dot{\theta}} \end{bmatrix} \tag{A.5}$$

where all entries except $K_{\dot{\phi}}(\dot{\phi})$ can be evaluated by means of potential theory [73].

The hydrodynamic damping in roll may be expressed as

$$K_{\dot{\phi}}(\dot{\phi})\dot{\phi} = K_{\dot{\phi}}\dot{\phi} + K_{\dot{\phi}|\dot{\phi}|}\dot{\phi}|\dot{\phi}| \tag{A.6}$$

where the linear term represents the potential and linear skin friction, whereas the nonlinear term takes into account viscous effects. The coefficients $K_{\dot{\phi}}$ and $K_{\dot{\phi}|\dot{\phi}|}$ can be calculated by the formulae given in Himeno [35]. The roll damping characteristics may also be derived from data of roll decaying tests at appropriate forward speeds of the vessel.

Waves

In regular seas, the incident wave elevation according to the Airy linear theory, see [62], is defined as

$$\zeta(x, y, t; \chi) = A_w \cos(kx \cos\chi - ky \sin\chi - \omega_e t) \tag{A.7}$$

where A_w is the wave amplitude, k is the wave number, χ is the wave heading, and ω_e is the encounter wave frequency. For head seas ($\chi = 180°$), the wave elevation reads as

$$\zeta(x, t) = A_w \cos(kx + \omega_e t). \tag{A.8}$$

Nonlinear Restoring Forces and Moments

The nonlinear restoring actions are given by the combination of the effects of the vessel motion in calm water and the effect of the wave elevation along the hull. Therefore, the vector of restoring forces and moments can be written, up

to 3rd-order terms, as

$$\begin{aligned}\mathbf{c}_{\text{pos}} \approx\ & \mathbf{c}_{\text{pos},\mathbf{s}} + \mathbf{c}_{\text{pos},\zeta} \\ & + \mathbf{c}_{\text{pos},\mathbf{s}^2} + \mathbf{c}_{\text{pos},\mathbf{s}\zeta} + \mathbf{c}_{\text{pos},\zeta^2} \\ & + \mathbf{c}_{\text{pos},\mathbf{s}^3} + \mathbf{c}_{\text{pos},\mathbf{s}^2\zeta} + \mathbf{c}_{\text{pos},\mathbf{s}\zeta^2} + \mathbf{c}_{\text{pos},\zeta^3}\end{aligned} \tag{A.9}$$

where $\mathbf{c}_{\text{pos},\mathbf{s}^i\zeta^j} = \frac{\partial^{i+j}\mathbf{c}_{\text{pos}}}{\partial\mathbf{s}^i\partial\zeta^j}\mathbf{s}^i\zeta^j$.

The 1st, 2nd and 3rd-order components in (A.9), which are independent of the displacement vector $\mathbf{s}$, must be included in the external forces and moments acting on the vessel. These terms describe the linear and nonlinear Froude-Krylov forces/moments.

The 2nd and 3rd-order nonlinear effects due to hull-wave interactions must, instead, be included in the restoring vector $\mathbf{c}_{\text{res}}$ because of their affinity, from the mathematical point of view, with the hydrostatic actions. Then the restoring force and moments due to body motion are given by

$$\mathbf{c}_{\text{res}}(\mathbf{s},\zeta) = \mathbf{c}_{\text{pos}}(\mathbf{s},\zeta) - \mathbf{c}_{\text{ext,FK}}(\zeta) \tag{A.10}$$

where $\mathbf{c}_{\text{ext,FK}}(\zeta) = \mathbf{c}_{\text{pos},\zeta} + \mathbf{c}_{\text{pos},\zeta^2} + \mathbf{c}_{\text{pos},\zeta^3}$.

Therefore the restoring force/moments in each degree of freedom are given by the following terms:

- 1st-order body motions ($\mathbf{c}_{\text{pos},\mathbf{s}}$)

$$\begin{aligned}Z_b^{(1)} &= Z_z z + Z_\phi\phi + Z_\theta\theta \\ K_b^{(1)} &= K_z z + K_\phi\phi + K_\theta\theta \\ M_b^{(1)} &= M_z z + M_\phi\phi + M_\theta\theta\end{aligned} \tag{A.11}$$

- 2nd-order body motions ($\mathbf{c}_{\text{pos},\mathbf{s}^2}$)

$$\begin{aligned}Z_b^{(2)} &= \frac{1}{2}(Z_{zz}z^2 + 2Z_{z\phi}z\phi + 2Z_{z\theta}z\theta \\ &\quad + 2Z_{\phi\theta}\phi\theta + Z_{\phi\phi}\phi^2 + Z_{\theta\theta}\theta^2) \\ K_b^{(2)} &= \frac{1}{2}(K_{zz}z^2 + 2K_{z\phi}z\phi + 2K_{z\theta}z\theta \\ &\quad + 2K_{\phi\theta}\phi\theta + K_{\phi\phi}\phi^2 + K_{\theta\theta}\theta^2) \\ M_b^{(2)} &= \frac{1}{2}(M_{zz}z^2 + 2M_{z\phi}z\phi + 2M_{z\theta}z\theta \\ &\quad + 2M_{\phi\theta}\phi\theta + M_{\phi\phi}\phi^2 + M_{\theta\theta}\theta^2)\end{aligned} \tag{A.12}$$

- 2^{nd}-order hull-wave interactions ($\mathbf{c}_{\text{pos},\mathbf{s}\zeta}$)

$$\begin{aligned} Z_{h/w}^{(2)} &= Z_{\zeta z}(t)z + Z_{\zeta\phi}(t)\phi + Z_{\zeta\theta}(t)\theta \\ K_{h/w}^{(2)} &= K_{\zeta z}(t)z + K_{\zeta\phi}(t)\phi + K_{\zeta\theta}(t)\theta \\ M_{h/w}^{(2)} &= M_{\zeta z}(t)z + M_{\zeta\phi}(t)\phi + M_{\zeta\theta}(t)\theta \end{aligned} \tag{A.13}$$

- 3^{rd}-order body motions ($\mathbf{c}_{\text{pos},\mathbf{s}^3}$)

$$\begin{aligned} Z_b^{(3)} = \frac{1}{6}\big(&Z_{zzz}z^3 + Z_{\phi\phi\phi}\phi^3 + Z_{\theta\theta\theta}\theta^3 \\ &+ 3Z_{zz\phi}z^2\phi + 3Z_{zz\theta}z^2\theta + 3Z_{\phi\phi z}\phi^2 z \\ &+ 3Z_{\phi\phi\theta}\phi^2\theta + 3Z_{\theta\theta z}\theta^2 z \\ &+ 3Z_{\theta\theta\phi}\theta^2\phi + 6Z_{z\phi\theta}z\phi\theta\big) \\ K_b^{(3)} = \frac{1}{6}\big(&K_{zzz}z^3 + K_{\phi\phi\phi}\phi^3 + K_{\theta\theta\theta}\theta^3 \\ &+ 3K_{zz\phi}z^2\phi + 3K_{zz\theta}z^2\theta + 3K_{\phi\phi z}\phi^2 z \\ &+ 3K_{\phi\phi\theta}\phi^2\theta + 3K_{\theta\theta z}\theta^2 z \\ &+ 3K_{\theta\theta\phi}\theta^2\phi + 6K_{z\phi\theta}z\phi\theta\big) \\ M_b^{(3)} = \frac{1}{6}\big(&M_{zzz}z^3 + M_{\phi\phi\phi}\phi^3 + M_{\theta\theta\theta}\theta^3 \\ &+ 3M_{zz\phi}z^2\phi + 3M_{zz\theta}z^2\theta + 3M_{\phi\phi z}\phi^2 z \\ &+ 3M_{\phi\phi\theta}\phi^2\theta + 3M_{\theta\theta z}\theta^2 z \\ &+ 3M_{\theta\theta\phi}\theta^2\phi + 6M_{z\phi\theta}z\phi\theta\big) \end{aligned} \tag{A.14}$$

- 3^{rd}-order hull-wave interactions ($\mathbf{c}_{\text{pos},\mathbf{s}^2\zeta} + \mathbf{c}_{\text{pos},\mathbf{s}\zeta^2}$)

$$\begin{aligned} Z_{h/w}^{(3)} &= Z_{\zeta zz}(t)z^2 + Z_{\zeta\phi\phi}(t)\phi^2 + Z_{\zeta\theta\theta}(t)\theta^2 \\ &\quad + Z_{\zeta z\phi}(t)z\phi + Z_{\zeta z\theta}(t)z\theta \\ &\quad + Z_{\zeta\phi\theta}(t)\phi\theta + Z_{\zeta\zeta z}(t)z \\ &\quad + Z_{\zeta\zeta\phi}(t)\phi + Z_{\zeta\zeta\theta}(t)\theta \\ K_{h/w}^{(3)} &= K_{\zeta zz}(t)z^2 + K_{\zeta\phi\phi}(t)\phi^2 + K_{\zeta\theta\theta}(t)\theta^2 \\ &\quad + K_{\zeta z\phi}(t)z\phi + K_{\zeta z\theta}(t)z\theta \\ &\quad + K_{\zeta\phi\theta}(t)\phi\theta + K_{\zeta\zeta z}(t)z \\ &\quad + K_{\zeta\zeta\phi}(t)\phi + K_{\zeta\zeta\theta}(t)\theta \end{aligned} \tag{A.15}$$

$$
\begin{aligned}
M^{(3)}_{h/w} = {} & M_{\zeta zz}(t)z^2 + M_{\zeta\phi\phi}(t)\phi^2 + M_{\zeta\theta\theta}(t)\theta^2 \\
& + M_{\zeta z\phi}(t)z\phi + M_{\zeta z\theta}(t)z\theta \\
& + M_{\zeta\phi\theta}(t)\phi\theta + M_{\zeta\zeta z}(t)z \\
& + M_{\zeta\zeta\phi}(t)\phi + M_{\zeta\zeta\theta}(t)\theta
\end{aligned}
$$

The time varying terms depend explicitly on the wave elevation $\zeta(t)$ and thus implicitly on the time t.

Looking at the 1st, 2nd and 3rd-order coefficients, a strong cross-coupling between all three degrees of freedom becomes evident.

External Forcing

The interaction between ship motion and wave passage is modeled as a variation of the geometry of the submerged hull defined by the instantaneous wave position. The external forcing vector $\mathbf{c}_{\text{ext}}(\zeta, \dot{\zeta}, \ddot{\zeta})$ includes only contributions independent of ship motions, such that

$$\mathbf{c}_{\text{ext}}(\zeta, \dot{\zeta}, \ddot{\zeta}) = \boldsymbol{\tau}_{1\text{w}} + \boldsymbol{\tau}_{2\text{w}}. \tag{A.16}$$

$\boldsymbol{\tau}_{1\text{w}}$ represents the 1st-order wave excitation forces generated by the wave motion. These forces are characterized by two contributions: the first one is due to Froude-Krylov forces, which are caused by incident waves considering the hull restrained from moving and that the presence of the hull does not influence the wave field. The second contribution gives the diffraction forces, which provide the corrections necessary for the variation of the flow field produced by the hull.

$\boldsymbol{\tau}_{2\text{w}}$ are the 2nd-order wave excitation forces which include three important components. The first contribution is given by the mean wave drift forces caused by nonlinear wave potential effects; the second one is due to low-frequency wave drift forces caused by nonlinear elements in the wave loads; and the third component is given by high-frequency wave drift forces.

In the present analysis the external force and moments are defined as being proportional to the first order wave motion, whereas higher order terms are neglected. Therefore the external force/moments vector $\mathbf{c}_{\text{ext}}$ reads as

$$\mathbf{c}_{\text{ext}}(\zeta, \dot{\zeta}, \ddot{\zeta}) \approx \boldsymbol{\tau}_{1\text{w}} = \mathbf{c}_{\text{ext,FK}} + \mathbf{c}_{\text{ext,Dif}}. \tag{A.17}$$

The wave excitation forces are defined by the wave-force response amplitude operator (force RAO) for each degree of freedom. The Force RAO is computed

[70] as

$$F_i(\omega_e, \chi) = \left| \frac{\tilde{\tau}_{1\mathrm{w}i}(\omega_e, \chi)}{\tilde{\zeta}} \right| e^{j \arg[\tilde{\tau}_{1\mathrm{w}i}(\omega_e, \chi)]} \tag{A.18}$$

where $\tilde{\tau}_{1\mathrm{w}i}$ is the complex 1^{st}-order wave excitation forces, and $\tilde{\zeta}$ is the complex wave elevation. Since the model only considers head seas, (A.18) simplifies to

$$\bar{F}_i(\omega_e) = \left| \frac{\bar{\tau}_{1\mathrm{w}i}(\omega_e)}{\tilde{\zeta}} \right| e^{j \arg[\bar{\tau}_{1\mathrm{w}i}(\omega_e)]}. \tag{A.19}$$

With these force RAOs, it is possible to obtain the wave excitation loads in each degree of freedom as

$$\tau_{1\mathrm{w}i}(t) = |\bar{F}_i(\omega_e)| A_w \cos(\omega_e t + \alpha_i) \tag{A.20}$$

for $i = 3, 4, 5$, where $\alpha_i = \arg[\bar{F}_i(\omega_e)]$. For example, the external force acting on heave is given by

$$Z_{\mathrm{ext}}(t) = |\bar{F}_3(\omega_e)| A_w \cos(\omega_e t + \alpha_3). \tag{A.21}$$

A.3 Identification of Model Parameters from Hull Form and Wave Characteristics

The identification of model parameters is completely based upon the hull shape of the container vessel and upon the wave characteristics. In this section the formulas are presented. The numerical values of those parameters, computed for the considered container ship, can be found in Appendix A.8.

In Table A.1 the main characteristics of the containership are reported.

Table A.1: Main characteristics of the container ship

Quantity	Sym.	Value
Length between perpendiculars	L_{PP}	281 m
Beam amidships	B	32.26 m
Draught amidships	T	11.75 m
Displacement	∇	76468 m^3
Roll radius of gyration	r_x	12.23 m
Transverse metacentric height	GM_t	1.84 m

A.3.1 Body Motion Coefficients

The 1st-order body motion coefficients refer to calm water hydrostatics and are given by

$$\begin{aligned} Z_z &= \rho g A_0 \\ Z_\theta &= -\rho g A_0 x_{f_0} \\ K_\phi &= \nabla G M_t \\ M_z &= -\rho g A_0 x_{f_0} \\ M_\theta &= \nabla \mathrm{GM}_l \end{aligned} \tag{A.22}$$

where ρ is the water density, g is the acceleration of gravity, A_0 is the waterplane area, x_{f_0} is the longitudinal coordinate of the centre of floatation, and GM_l is the longitudinal metacentric height.

The 2nd and 3rd-order body motion coefficients correspond to the variations in the restoring characteristics of the ship due to the changes in pressure related to the vessel motions. In order to compute them numerically, it is necessary to express the nonlinear hydrostatic actions as function of the three modes heave, pitch, and roll. In particular, it is possible to demonstrate that

$$\begin{aligned} Z(z,\phi,\theta) &= \rho g(\nabla_1 - \nabla_0) \\ K(z,\phi,\theta) &= \rho g[\nabla_0 z_G \sin\phi \\ &\quad + \nabla_1(y_{B_1}\cos\phi - z_{B_1}\sin\phi)] \\ M(z,\phi,\theta) &= \rho g[\nabla_0 z_G \cos\phi \sin\theta - \nabla_1(x_{B_1}\cos\theta \\ &\quad + y_{B_1}\sin\phi\cos\theta + z_{B_1}\cos\phi\sin\theta)] \end{aligned} \tag{A.23}$$

where ∇_0 is the mean displacement, $\nabla_1 = \nabla_1(z,\phi,\theta)$ is the instantaneous displacement, z_G is the vertical coordinate of the centre of gravity, x_{B_1}, y_{B_1}, and z_{B_1} are the coordinates of the instantaneous centre of buoyancy.

Tables A.2-A.3 show the 2nd and 3rd-order coefficients for each degree of freedom.

A.3.2 Hull-Wave Interaction Coefficients

Under the assumption of regular waves, the periodic wave passage along the hull produces cyclic variation in the restoring characteristics of the vessel. These changes are taken into account by the 2nd and 3rd-order coefficients included in the nonlinear interactions $\mathbf{c}_{\mathrm{pos},\mathbf{s}\zeta}$ and $\mathbf{c}_{\mathrm{pos},\mathbf{s}^2\zeta} + \mathbf{c}_{\mathrm{pos},\mathbf{s}\zeta^2}$.

Table A.2: 2nd-order hydrostatic restoring coefficients

Heave	Roll	Pitch
$Z_{zz} = -\frac{\partial^2 Z}{\partial z^2}$	$K_{zz} = 0$	$M_{zz} = -\frac{\partial^2 M}{\partial z^2}$
$Z_{z\phi} = 0$	$K_{z\phi} = -\frac{\partial^2 K}{\partial z \partial \phi}$	$M_{z\phi} = 0$
$Z_{z\theta} = -\frac{\partial^2 Z}{\partial z \partial \theta}$	$K_{z\theta} = 0$	$M_{z\theta} = -\frac{\partial^2 M}{\partial z \partial \theta}$
$Z_{\phi\phi} = -\frac{\partial^2 Z}{\partial \phi^2}$	$K_{\phi\phi} = 0$	$M_{\phi\phi} = -\frac{\partial^2 M}{\partial \phi^2}$
$Z_{\phi\theta} = 0$	$K_{\phi\theta} = -\frac{\partial^2 K}{\partial \phi \partial \theta}$	$M_{\phi\theta} = 0$
$Z_{\theta\theta} = -\frac{\partial^2 Z}{\partial \theta^2}$	$K_{\theta\theta} = 0$	$M_{\theta\theta} = -\frac{\partial^2 M}{\partial \theta^2}$

Table A.3: 3rd-order hydrostatic restoring coefficients

Heave		
$Z_{zzz} = -\frac{\partial^3 Z}{\partial z^3}$	$Z_{zz\phi} = 0$	$Z_{zz\theta} = -\frac{\partial^3 Z}{\partial z^2 \partial \theta}$
$Z_{\phi\phi z} = -\frac{\partial^3 Z}{\partial z \partial \phi^2}$	$Z_{\phi\phi\phi} = 0$	$Z_{\phi\phi\theta} = -\frac{\partial^3 Z}{\partial \phi^2 \partial \theta}$
$Z_{\theta\theta z} = -\frac{\partial^3 Z}{\partial z \partial \theta^2}$	$Z_{\theta\theta\phi} = 0$	$Z_{\theta\theta\theta} = -\frac{\partial^3 Z}{\partial \theta^3}$
Roll		
$K_{zzz} = 0$	$K_{zz\phi} = -\frac{\partial^3 K}{\partial z^2 \partial \phi}$	$K_{zz\theta} = 0$
$K_{\phi\phi z} = 0$	$K_{\phi\phi\phi} = -\frac{\partial^3 K}{\partial \phi^3}$	$K_{\phi\phi\theta} = 0$
$K_{\theta\theta z} = 0$	$K_{\theta\theta\phi} = -\frac{\partial^3 K}{\partial \phi \partial \theta^2}$	$K_{\theta\theta\theta} = 0$
Pitch		
$M_{zzz} = -\frac{\partial^3 M}{\partial z^3}$	$M_{zz\phi} = 0$	$M_{zz\theta} = -\frac{\partial^3 M}{\partial z^2 \partial \theta}$
$M_{\phi\phi z} = -\frac{\partial^3 M}{\partial z \partial \phi^2}$	$M_{\phi\phi\phi} = 0$	$M_{\phi\phi\theta} = -\frac{\partial^3 M}{\partial \phi^2 \partial \theta}$
$M_{\theta\theta z} = -\frac{\partial^3 M}{\partial z \partial \theta^2}$	$M_{\theta\theta\phi} = 0$	$M_{\theta\theta\theta} = -\frac{\partial^3 M}{\partial \theta^3}$
Heave-roll-pitch coupling		
$Z_{z\phi\theta} = 0$	$K_{z\phi\theta} = -\frac{\partial^3 K}{\partial z \partial \phi \partial \theta}$	$M_{z\phi\theta} = 0$

Table A.4: 2nd-order hydrostatic restoring coefficients due to wave passage

Heave	Roll	Pitch
$Z_{\zeta z}(t) = -\frac{\partial F_3^{FK_1}}{\partial z}$	$K_{\zeta z}(t) = 0$	$M_{\zeta z}(t) = -\frac{\partial F_5^{FK_1}}{\partial z}$
$Z_{\zeta\phi}(t) = 0$	$K_{\zeta\phi}(t) = -\frac{\partial F_4^{FK_1}}{\partial \phi}$	$M_{\zeta\phi}(t) = 0$
$Z_{\zeta\theta}(t) = -\frac{\partial F_3^{FK_1}}{\partial \theta}$	$K_{\zeta\theta}(t) = 0$	$M_{\zeta\theta}(t) = -\frac{\partial F_5^{FK_1}}{\partial \theta}$

In order to determine the hull-wave interaction coefficients, the Froude-Krylov forces must be defined. The velocity potential for the undisturbed wave, as defined in (A.7), is given by

$$\varphi_I = \frac{A_w g}{\omega_e} e^{kz} \sin(kx\cos\chi - ky\sin\chi - \omega_e t). \tag{A.24}$$

Therefore, the 1st and 2nd-order Froude-Krylov forces are:

$$F_j^{FK_1}(t) = \rho \iint \frac{\partial \varphi_I}{\partial t} n_j \,\mathrm{d}S \tag{A.25}$$

$$F_j^{FK_2}(t) = \frac{1}{2}\rho \iint (\nabla\varphi_I \cdot \nabla\varphi_I)\, n_j \,\mathrm{d}S \tag{A.26}$$

where n is the normal to the hull surface and j addresses the specific mode for which the force is computed. The coefficients are then given by the formulas is Tables A.4–A.5.

Due to the assumption of regular waves, the coefficients can be described as a sum of a sine and a cosine term. For instance, the 2nd-order term $K_{\zeta\phi}(t)$, which is proportional to wave amplitude, can be written as

$$K_{\zeta\phi}(t) = A_w(K_{\zeta\phi c}\cos\omega_e t + K_{\zeta\phi s}\sin\omega_e t) \tag{A.27}$$

where $K_{\zeta\phi c}$ and $K_{\zeta\phi s}$ are constants.

Analogously, the 3rd-order terms $K_{\zeta z\phi}(t)$ and $K_{\zeta\phi\theta}(t)$ are given by

$$K_{\zeta z\phi}(t) = A_w(K_{\zeta z\phi c}\cos\omega_e t + K_{\zeta z\phi s}\sin\omega_e t) \tag{A.28}$$

$$K_{\zeta\phi\theta}(t) = A_w(K_{\zeta\phi\theta c}\cos\omega_e t + K_{\zeta\phi\theta s}\sin\omega_e t). \tag{A.29}$$

These functions play an important role since they parametrically excite the coupled system, being multiplied with, respectively, $z(t)\phi(t)$ and $\phi(t)\theta(t)$.

The 3rd-order term $K_{\zeta\zeta\phi}(t)$, which is proportional to the wave amplitude squared, is given by

$$\begin{aligned} K_{\zeta\zeta\phi}(t) = A_w^2(&K_{\zeta\zeta\phi 0} + K_{\zeta\zeta\phi c}\cos 2\omega_e t \\ &+ K_{\zeta\zeta\phi s}\sin 2\omega_e t) \end{aligned} \tag{A.30}$$

Table A.5: 3rd-order hydrostatic restoring coefficients due to wave passage

Heave		
$Z_{\zeta\zeta z}(t) = -\frac{\partial F_3^{FK_2}}{\partial z}$	$Z_{\zeta\zeta\phi}(t) = 0$	$Z_{\zeta\zeta\theta}(t) = -\frac{\partial F_3^{FK_2}}{\partial \theta}$
$Z_{\zeta zz}(t) = -\frac{\partial^2 F_3^{FK_1}}{\partial z^2}$	$Z_{\zeta z\phi}(t) = 0$	$Z_{\zeta z\theta}(t) = -\frac{\partial^2 F_3^{FK_1}}{\partial z \partial \theta}$
$Z_{\zeta\phi\phi}(t) = -\frac{\partial^2 F_3^{FK_1}}{\partial \phi^2}$	$Z_{\zeta\theta\theta}(t) = -\frac{\partial^2 F_3^{FK_1}}{\partial \theta^2}$	$Z_{\zeta\phi\theta}(t) = 0$
Roll		
$K_{\zeta\zeta z}(t) = 0$	$K_{\zeta\zeta\phi}(t) = -\frac{\partial F_4^{FK_2}}{\partial \phi}$	$K_{\zeta\zeta\theta}(t) = 0$
$K_{\zeta zz}(t) = 0$	$K_{\zeta z\phi}(t) = -\frac{\partial^2 F_4^{FK_1}}{\partial z \partial \phi}$	$K_{\zeta z\theta}(t) = 0$
$K_{\zeta\phi\phi}(t) = 0$	$K_{\zeta\theta\theta}(t) = 0$	$K_{\zeta\phi\theta}(t) = -\frac{\partial^2 F_4^{FK_1}}{\partial \phi \partial \theta}$
Pitch		
$M_{\zeta\zeta z}(t) = -\frac{\partial F_5^{FK_2}}{\partial z}$	$M_{\zeta\zeta\phi}(t) = 0$	$M_{\zeta\zeta\theta}(t) = -\frac{\partial F_5^{FK_2}}{\partial \theta}$
$M_{\zeta zz}(t) = -\frac{\partial^2 F_5^{FK_1}}{\partial z^2}$	$M_{\zeta z\phi}(t) = 0$	$M_{\zeta z\theta}(t) = -\frac{\partial^2 F_5^{FK_1}}{\partial z \partial \theta}$
$M_{\zeta\phi\phi}(t) = -\frac{\partial^2 F_5^{FK_1}}{\partial \phi^2}$	$M_{\zeta\theta\theta}(t) = -\frac{\partial^2 F_5^{FK_1}}{\partial \theta^2}$	$M_{\zeta\phi\theta}(t) = 0$

where it can be noticed the presence of a constant term plus a super-harmonic term of double the encounter frequency.

A.3.3 Nonlinear Restoring Forces and Moments Redux

Rewriting the restoring forces and moments (A.11)–(A.15), according to the equations derived in this section gives:

- 1st-order body motions ($\mathbf{c}_{\text{pos,s}}$)

$$\begin{aligned} Z_b^{(1)} &= Z_z z + Z_\theta \theta \\ K_b^{(1)} &= K_\phi \phi \\ M_b^{(1)} &= M_z z + M_\theta \theta \end{aligned} \tag{A.31}$$

- 2^{nd}-order body motions ($\mathbf{c}_{\text{pos},\mathbf{s}^2}$)

$$\begin{aligned} Z_b^{(2)} &= \frac{1}{2}(Z_{zz}z^2 + 2Z_{z\theta}z\theta + Z_{\phi\phi}\phi^2 + Z_{\theta\theta}\theta^2) \\ K_b^{(2)} &= K_{z\phi}z\phi + K_{\phi\theta}\phi\theta \\ M_b^{(2)} &= \frac{1}{2}(M_{zz}z^2 + 2M_{z\theta}z\theta + M_{\phi\phi}\phi^2 + M_{\theta\theta}\theta^2) \end{aligned} \tag{A.32}$$

- 2^{nd}-order hull-wave interactions ($\mathbf{c}_{\text{pos},\mathbf{s}\zeta}$)

$$\begin{aligned} Z_{h/w}^{(2)} &= A_w(Z_{\zeta zc}z + Z_{\zeta\theta c}\theta)\cos\omega_e t + A_w(Z_{\zeta zs}z + Z_{\zeta\theta s}\theta)\sin\omega_e t \\ K_{h/w}^{(2)} &= A_w(K_{\zeta\phi c}\cos\omega_e t + K_{\zeta\phi s}\sin\omega_e t)\phi \\ M_{h/w}^{(2)} &= A_w(M_{\zeta zc}z + M_{\zeta\theta c}\theta)\cos\omega_e t + A_w(M_{\zeta zs}z + M_{\zeta\theta s}\theta)\sin\omega_e t \end{aligned} \tag{A.33}$$

- 3^{rd}-order body motions ($\mathbf{c}_{\text{pos},\mathbf{s}^3}$)

$$\begin{aligned} Z_b^{(3)} &= \frac{1}{6}\big(Z_{zzz}z^3 + Z_{\theta\theta\theta}\theta^3 + 3Z_{zz\theta}z^2\theta \\ &\quad + 3Z_{\phi\phi z}\phi^2 z + 3Z_{\phi\phi\theta}\phi^2\theta + 3Z_{\theta\theta z}\theta^2 z\big) \\ K_b^{(3)} &= \frac{1}{6}\big(K_{\phi\phi\phi}\phi^3 + 3K_{zz\phi}z^2\phi + 3K_{\theta\theta\phi}\theta^2\phi + 6K_{z\phi\theta}z\phi\theta\big) \\ M_b^{(3)} &= \frac{1}{6}\big(M_{zzz}z^3 + M_{\theta\theta\theta}\theta^3 + 3M_{zz\theta}z^2\theta \\ &\quad + 3M_{\phi\phi z}\phi^2 z + 3M_{\phi\phi\theta}\phi^2\theta + 3M_{\theta\theta z}\theta^2 z\big) \end{aligned} \tag{A.34}$$

- 3^{rd}-order hull-wave interactions ($\mathbf{c}_{\text{pos},\mathbf{s}^2\zeta} + \mathbf{c}_{\text{pos},\mathbf{s}\zeta^2}$)

$$\begin{aligned} Z_{h/w}^{(3)} &= Z_{\zeta zz}(t)z^2 + Z_{\zeta\phi\phi}(t)\phi^2 + Z_{\zeta\theta\theta}(t)\theta^2 \\ &\quad + Z_{\zeta z\theta}(t)z\theta + Z_{\zeta\zeta z}(t)z + Z_{\zeta\zeta\theta}(t)\theta \\ K_{h/w}^{(3)} &= K_{\zeta z\phi}(t)z\phi + K_{\zeta\phi\theta}(t)\phi\theta + K_{\zeta\zeta\phi}(t)\phi \\ M_{h/w}^{(3)} &= M_{\zeta zz}(t)z^2 + M_{\zeta\phi\phi}(t)\phi^2 + M_{\zeta\theta\theta}(t)\theta^2 \\ &\quad + M_{\zeta z\theta}(t)z\theta + M_{\zeta\zeta z}(t)z + M_{\zeta\zeta\theta}(t)\theta \end{aligned} \tag{A.35}$$

A.4 Matlab Implementation of the Model

A Matlab/Simulink model for the container ship model was developed for the purposes of simulating parametric roll resonance, based on the model of Section A.2.

For each time instant and system state, a function generates the instantaneous value of $[\dot{\mathbf{s}}^{\mathrm{T}}\ \ddot{\mathbf{s}}^{\mathrm{T}}]^{\mathrm{T}}$. Numerically integrating with an explicit Runge-Kutta method of order 4, with the fixed time step $h = 1$ s, the state $[\mathbf{s}^{\mathrm{T}}\ \dot{\mathbf{s}}^{\mathrm{T}}]^{\mathrm{T}}$ is calculated for any given time instant.

The parameters used in the calculations are listed in Appendix A.8. While this was not done for the results presented in this paper, for other encounter frequencies than the ones used in the experiments, interpolation can be applied to calculate approximate parameter values.

The code is part of the Marine Systems Simulator [54].

A.5 Validation of the Model Against Experimental Data

A comparison of the simulation and the experimental results can be seen in Figures A.2–A.24.

The experiments were conducted with a 1:45 scale model ship in a towing tank. The experiments were done with varying forward speed, and wave frequency and height. This is summarized in Table A.6. All data in the table and in the figures are in full scale.

The simulations were done with the code described in Section A.4. All simulations were made ballistically. Initial conditions can be found in Table A.7. Initial conditions not listed in the table (θ, $\dot{z}$, $\dot{\phi}$ and $\dot{\theta}$) were all zero. The experiments were all assumed to start at $t = 0$.

A comparison of the simulation results with the experimental results can be seen in Table A.8. The first column is the experiment number. The second column is wave amplitude A_w. The third column is wave frequency ω. The fourth column is the ratio of encounter frequency to natural roll frequency (ω_e/ω_0). The fifth column is maximum roll amplitude for the simulations ($\max|\phi_{\mathrm{sim}}|$). The sixth is maximum roll amplitude for the experiments ($\max|\phi_{\mathrm{exp}}|$). The seventh and final column is the percentage error given by

$$100\frac{\max|\phi_{\mathrm{sim}}| - \max|\phi_{\mathrm{exp}}|}{\max|\phi_{\mathrm{exp}}|},$$

rounded to integer value. Note that most of the experiments were stopped before the final steady-state roll angle could be achieved due to fear of vessel capsizing.

Figures A.2–A.23 show heave, roll and pitch as functions of time, both experimental and simulated.

In Figure A.24, we can see the maximum roll angle achieved in the simulations and experiments for certain conditions, plotted against the ratio of encounter frequency to natural roll frequency (ω_e/ω_0). The data in the figure is all for $A_w = 2.5$ m, and $\omega = 0.4640$ rad/s.

Table A.6: Experimental conditions

Exp.	U [m/s]	ω [rad/s]	A_w [m]	ω_e [rad/s]
1172	5.4806	0.4640	2.5	0.5844
1173	5.4806	0.4425	2.5	0.5519
1174	5.4806	0.4764	2.5	0.6031
1175	5.4806	0.4530	2.5	0.5677
1176	5.4806	0.4893	2.5	0.6231
1177	5.4806	0.4640	1.5	0.5844
1178	5.4806	0.4699	1.5	0.5933
1179	5.4806	0.4583	1.5	0.5756
1180	5.4806	0.4640	3.5	0.5844
1181	5.4806	0.4425	3.5	0.5519
1182	5.4806	0.4893	3.5	0.6231
1183	5.4806	0.4530	3.5	0.5677
1184	5.7556	0.4640	2.5	0.5904
1185	6.0240	0.4640	2.5	0.5963
1186	6.2990	0.4640	2.5	0.6023
1187	6.5740	0.4640	2.5	0.6084
1188	7.1241	0.4640	2.5	0.6204
1189	7.6675	0.4640	2.5	0.6324
1190	7.3991	0.4640	2.5	0.6265
1191	5.2056	0.4640	2.5	0.5783
1192	4.6555	0.4640	2.5	0.5662
1193	4.9305	0.4640	2.5	0.5723

A.6 Analysis of the Model Based Upon the Validation Results

The 3$^{\text{rd}}$-order model developed for the 281m long container ship shows high capabilities in reproducing the vertical and transversal dynamics of the vessel under parametric resonance conditions, as shown by the comparison of the

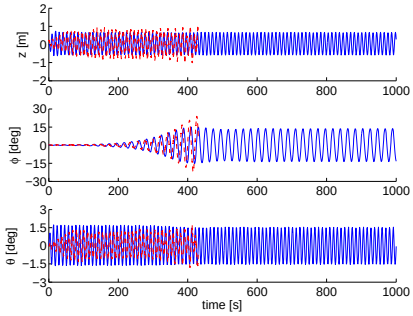

Figure A.2: Exp. 1172. Exp. dashed red, sim. solid blue.

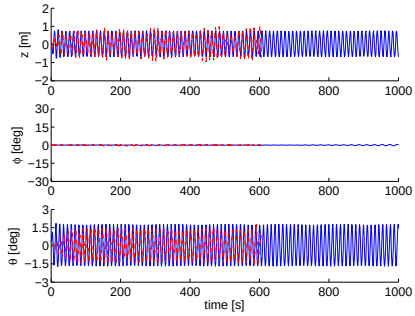

Figure A.3: Exp. 1175. Exp. dashed red, sim. solid blue.

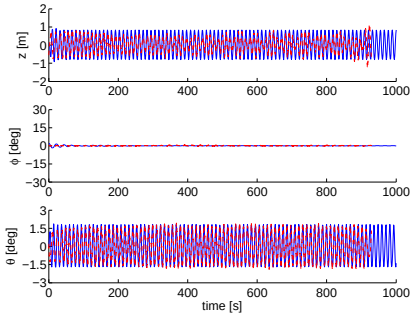

Figure A.4: Exp. 1173. Exp. dashed red, sim. solid blue.

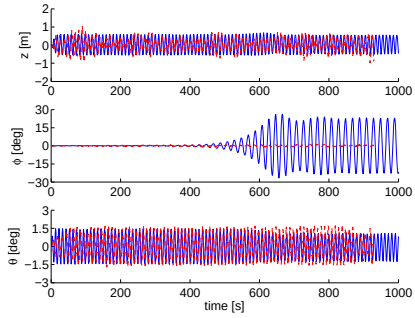

Figure A.5: Exp. 1176. Exp. dashed red, sim. solid blue.

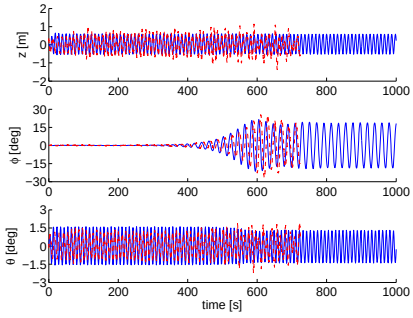

Figure A.6: Exp. 1174. Exp. dashed red, sim. solid blue.

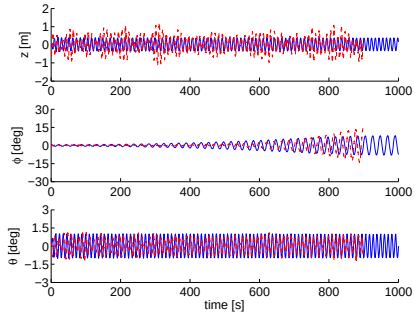

Figure A.7: Exp. 1177. Exp. dashed red, sim. solid blue.

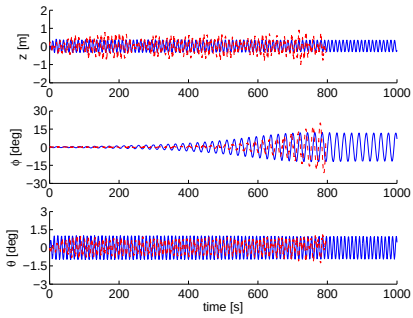

Figure A.8: Exp. 1178. Exp. dashed red, sim. solid blue.

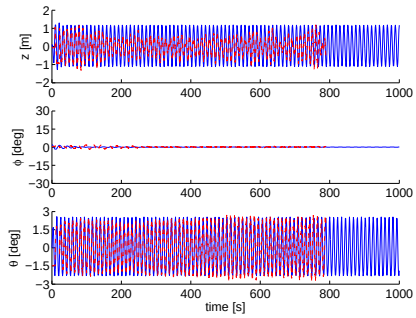

Figure A.9: Exp. 1181. Exp. dashed red, sim. solid blue.

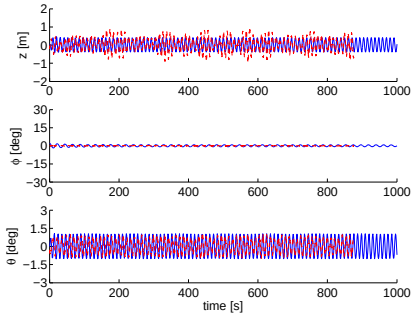

Figure A.10: Exp. 1179. Exp. dashed red, sim. solid blue.

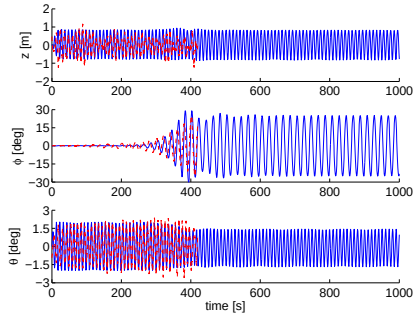

Figure A.11: Exp. 1182. Exp. dashed red, sim. solid blue.

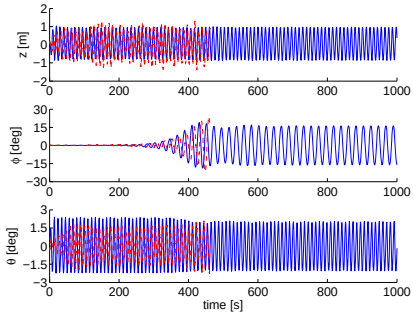

Figure A.12: Exp. 1180. Exp. dashed red, sim. solid blue.

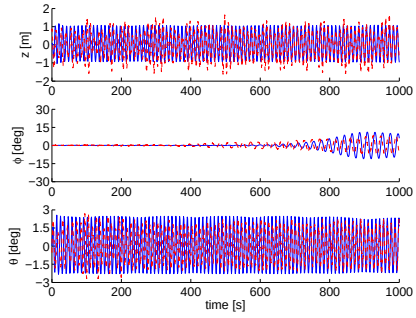

Figure A.13: Exp. 1183. Exp. dashed red, sim. solid blue.

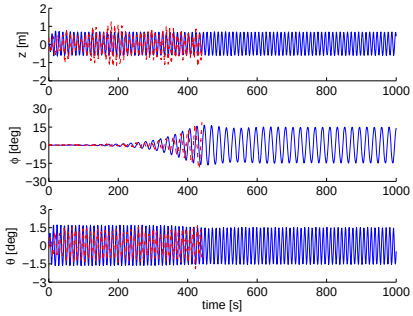

Figure A.14: Exp. 1184. Exp. dashed red, sim. solid blue.

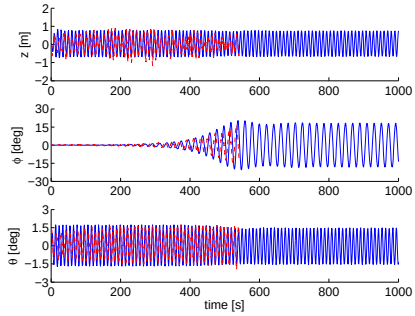

Figure A.15: Exp. 1187. Exp. dashed red, sim. solid blue.

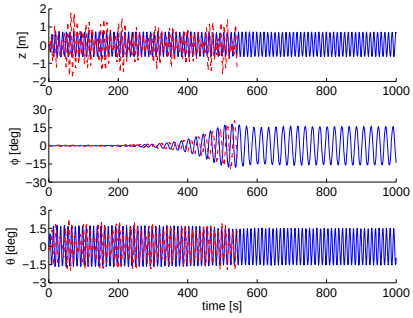

Figure A.16: Exp. 1185. Exp. dashed red, sim. solid blue.

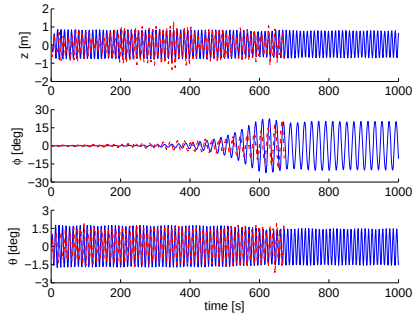

Figure A.17: Exp. 1188. Exp. dashed red, sim. solid blue.

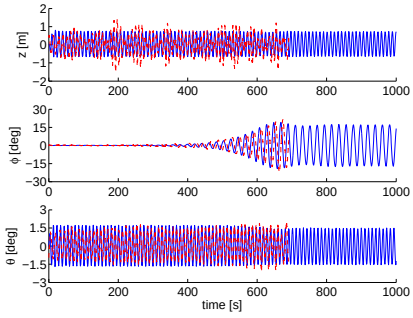

Figure A.18: Exp. 1186. Exp. dashed red, sim. solid blue.

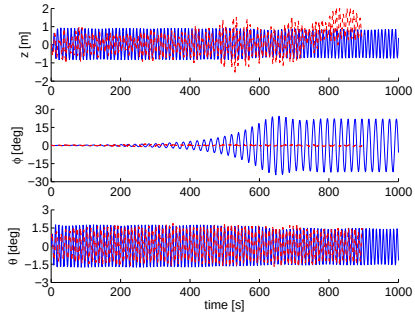

Figure A.19: Exp. 1189. Exp. dashed red, sim. solid blue.

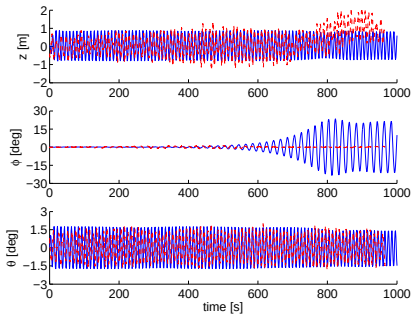

Figure A.20: Exp. 1190. Exp. dashed red, sim. solid blue.

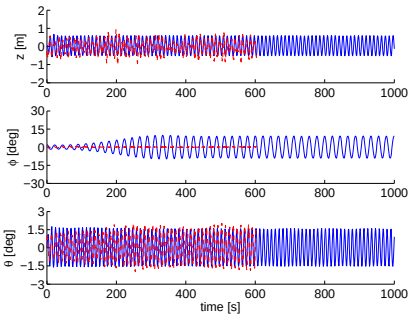

Figure A.21: Exp. 1192. Exp. dashed red, sim. solid blue.

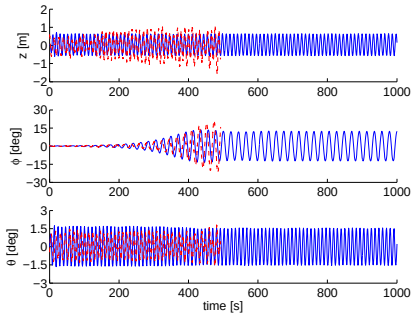

Figure A.22: Exp. 1191. Exp. dashed red, sim. solid blue.

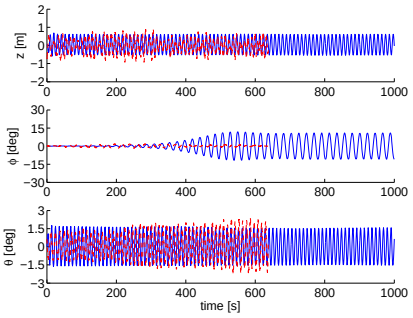

Figure A.23: Exp. 1193. Exp. dashed red, sim. solid blue.

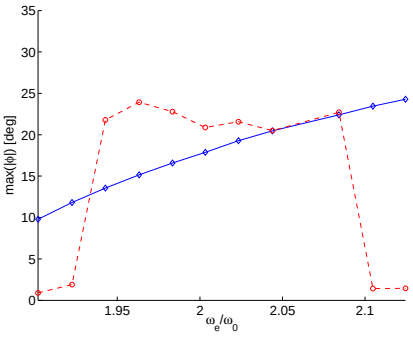

Figure A.24: Max. roll angle vs ω_e/ω_0 for $A_w = 2.5$ m, $\omega = 0.4640$ rad/s. Exp. dashed red, sim. solid blue.

Table A.7: Simulation initial conditions

Exp.	z_0 [m]	ϕ_0 [rad]
1172	0.0250	3.4907E-3
1173	0.0500	3.4907E-2
1174	0.0500	3.4907E-5
1175	0.0500	1.7453E-4
1176	0.0500	1.7453E-5
1177	0.0500	1.3963E-2
1178	0.0500	8.7266E-3
1179	0.0500	3.4907E-2
1180	0.0500	8.7266E-5
1181	0.0500	3.4907E-2
1182	0.0500	1.7453E-5
1183	0.0500	8.7266E-6
1184	0.0500	1.7453E-3
1185	0.0500	5.2360E-4
1186	0.0500	8.7266E-5
1187	0.0500	5.2360E-4
1188	0.0500	5.2360E-4
1189	0.0500	2.4435E-3
1190	0.0500	1.7453E-4
1191	0.0500	3.4907E-3
1192	0.0500	3.4907E-2
1193	0.0500	1.7453E-3

experimental results (Figures A.2–A.24).

Considering the 13 experiments where parametric resonance did occur, the implemented model performs well: starting from similar initial conditions and being subjected to the same excitation forces used during the experiments, the model develops parametric resonance within the same time frame as the 1:45 scale model ship in most of the cases.

The most obvious differences between the simulation and the experimental results consists of the amplitude of the oscillations. In all the experiments where parametric resonance occurred, the peak value of the roll oscillations is higher than the saturation level at which the model settles. Although the model has a general tendency to underestimate the peak value of the roll motion, the gap is relatively small in most cases.

Considering the 9 experiments where parametric roll did not occur, the model

Table A.8: Simulation results

Exp.	A_w	ω	ω_e/ω_0	$\max\lvert\phi_{\text{sim}}\rvert$	$\max\lvert\phi_{\text{exp}}\rvert$	Error %
1179	1.5	0.4583	1.9337	2.0000	0.4729	323
1177	1.5	0.4640	1.9633	8.0982	17.1140	-53
1178	1.5	0.4699	1.9932	12.0995	22.5530	-46
1173	2.5	0.4425	1.8541	2.0000	0.7142	180
1175	2.5	0.4530	1.9072	0.6084	0.7215	-16
1192	2.5	0.4640	1.9021	9.7799	0.8944	993
1193	2.5	0.4640	1.9226	11.8080	1.8932	524
1191	2.5	0.4640	1.9428	13.5465	21.7800	-38
1172	2.5	0.4640	1.9633	15.1622	23.9270	-37
1184	2.5	0.4640	1.9834	16.5792	22.7810	-27
1185	2.5	0.4640	2.0032	17.8812	20.8780	-14
1186	2.5	0.4640	2.0234	19.2712	21.5640	-11
1187	2.5	0.4640	2.0439	20.4611	20.4990	0
1188	2.5	0.4640	2.0842	22.4097	22.7190	-1
1190	2.5	0.4640	2.1047	23.4472	1.4291	1541
1189	2.5	0.4640	2.1245	24.2884	1.4368	1590
1174	2.5	0.4764	2.0261	21.4924	26.6960	-19
1176	2.5	0.4893	2.0933	26.7459	1.2581	2026
1181	3.5	0.4425	1.8541	2.0000	2.0352	-2
1183	3.5	0.4530	1.9072	11.0859	8.9410	24
1180	3.5	0.4640	1.9633	18.8898	23.9530	-21
1182	3.5	0.4893	2.0933	30.2110	24.9870	21

produced 5 false positive cases developing resonant motion. In order to understand this disagreement between model behavior and experimental results, the tuning factor ω_e/ω_0 must be taken into consideration. In fact all the 5 false-positive cases occur with a tuning factor close to the limits of the first instability region of the Hill-Mathieu Equation ($\omega_e \approx 2\omega_0$), as shown in Figure A.24. Looking at the peak value of the roll oscillations (Figure A.24 and Table A.8), it is seen that the largest differences are in the region of high tunings ($\frac{\omega_e}{\omega_0} \geqslant 2.1$) for which the model predicts large roll motion whereas the experiments showed no amplification. It seems obvious that when the experimental conditions are close to the limits of stability the model does not match exactly the frequency at which the abrupt variation in roll motion take place.

The errors indicated in tests 1173, 1179 and 1181 have no real physical meaning, since the initial condition of 2 degrees was chosen arbitrarily high in

order to indicate a decaying motion.

For all 22 experiments, heave and pitch dynamics have shown relatively good agreement with the experiments. In all the test runs the two modes oscillates at the excitation frequency, matching the experimental records. The amplitude of the oscillations is close to that of the experimental values.

A.7 Conclusions

A Matlab/Simulink benchmark for the simulation of parametric roll resonance for a large container ship has been implemented and validated against experimental results. The implementation reflects the coupled 3^{rd}-order nonlinear model for parametric roll first introduced by [57].

The mathematical model for the container ship at hand, already presented in [72], has been reviewed, illustrating in details the ship dynamics that has been taken into account. 1^{st}, 2^{nd} and 3^{rd}-order contributions have been described and analytical formulas of all the couplings coefficients due to heave, roll, pitch, and wave motion have been given. Furthermore, numerical values of all coefficients are computed based upon the hull geometry and wave characteristics.

The benchmark has been tested on a set of 22 different conditions, which have been chosen to match the experimental conditions. Each test run differs from the previous for at least the value of one parameter among ship speed, wave frequency, and wave height. The heave and pitch dynamics described by the model are in good accordance with the experimental results. The model seems to reproduce the pitch motion slightly better, catching the right amplitude in most of the cases.

The results obtained in roll have shown good agreement with the records of the experiments. In particular, the model agrees with the experiments in all the cases where parametric roll occurred, although the amplitude of the roll oscillations does not quite reach the experimental peak value in most cases.

For the experiments where there was no parametric roll, then the model produces false positives in about 50% of the cases. This disagreement between the simulation and the experimental results is believed to be related to the specific values of the tuning factor ω_e/ω_0 which were too close to the limits of the first instability region of the Hill-Mathieu Equation. In these cases, it is very difficult to get the correct response with ballistic simulations.

The availability of this benchmark offers a wide range of opportunities for development of new model-based control strategies for counteracting or preventing parametric roll resonance.

A.8 Tables of Coefficients

The parameters can be found in Tables A.9–A.16. All numbers are given in the kg-m-s (SI) system. Only non-zero numbers are listed.

Table A.9 contains the rigid body inertia matrix, and Table A.10 the added mass. Table A.11 contains the hydrodynamic damping parameters, while Table A.12 contains the body motion parameters. Table A.13 contains the wave motion parameters for heave. Table A.14 contains the wave motion parameters for roll. Table A.15 contains the wave motion parameters for pitch. Table A.16 contains the external wave excitation parameters. Note that α_3 and α_5 are given in radians.

Table A.9: Rigid body inertia

m	I_x	I_y
7.72E7	1.41E10	2.99E11

Table A.10: Added mass

ω_e	$Z_{\ddot{z}}$	$Z_{\ddot{\theta}}$	$K_{\ddot{\phi}}$	$M_{\ddot{z}}$	$M_{\ddot{\theta}}$
0.5519	8.4377E7	5.2986E8	2.17E9	2.2140E9	4.3227E11
0.5662	8.3596E7	6.8658E8	2.17E9	2.0263E9	4.2368E11
0.5677	8.3515E7	5.7142E8	2.17E9	2.1383E9	4.2519E11
0.5723	8.3266E7	6.5957E8	2.17E9	2.0402E9	4.2169E11
0.5756	8.3077E7	5.9056E8	2.17E9	2.1017E9	4.2161E11
0.5783	8.2935E7	6.3403E8	2.17E9	2.0526E9	4.1972E11
0.5844	8.2604E7	6.0987E8	2.17E9	2.0637E9	4.1775E11
0.5904	8.2273E7	5.8702E8	2.17E9	2.0734E9	4.1579E11
0.5933	8.2112E7	6.2852E8	2.17E9	2.0255E9	4.1376E11
0.5963	8.1955E7	5.6623E8	2.17E9	2.0816E9	4.1392E11
0.6023	8.0509E7	5.2790E8	2.17E9	2.0821E9	4.0685E11
0.6031	8.1568E7	6.4758E8	2.17E9	1.9849E9	4.0935E11
0.6084	8.0003E7	5.0546E8	2.17E9	2.0875E9	4.0410E11
0.6204	7.9811E7	4.7712E8	2.17E9	2.1003E9	4.0240E11
0.6231	8.0481E7	6.8112E8	2.17E9	1.9082E9	4.0059E11
0.6265	7.9714E7	4.6449E8	2.17E9	2.1051E9	4.0155E11
0.6324	7.9491E7	4.5092E8	2.17E9	2.1082E9	4.0014E11

Table A.11: Hydrodynamic damping

ω_e	$Z_{\dot{z}}$	$Z_{\dot{\theta}}$	$K_{\dot{\phi}}$	$K_{\dot{\phi}\lvert\dot{\phi}\rvert}$	$M_{\dot{z}}$	$M_{\dot{\theta}}$
0.5519	4.6790E7	1.1900E9	3.1951E8	2.9939E8	2.6485E8	2.7431E11
0.5662	4.6121E7	1.1146E9	3.0467E8	3.7433E8	3.3617E8	2.7151E11
0.5677	4.6051E7	1.1830E9	3.1951E8	2.9939E8	2.6733E8	2.7254E11
0.5723	4.5838E7	1.1351E9	3.0962E8	3.4696E8	3.1392E8	2.7124E11
0.5756	4.5676E7	1.1795E9	3.1951E8	2.9939E8	2.6859E8	2.7166E11
0.5783	4.5554E7	1.1555E9	3.1456E8	3.2205E8	2.9184E8	2.7097E11
0.5844	4.5271E7	1.1757E9	3.1951E8	2.9939E8	2.6995E8	2.7071E11
0.5904	4.4987E7	1.1956E9	3.2445E8	2.7877E8	2.4824E8	2.7045E11
0.5933	4.4849E7	1.1717E9	3.1951E8	2.9939E8	2.7136E8	2.6973E11
0.5963	4.4714E7	1.2147E9	3.2921E8	2.6067E8	2.2754E8	2.7020E11
0.6023	4.4749E7	1.2312E9	3.3415E8	2.4348E8	2.1714E8	2.7166E11
0.6031	4.4383E7	1.1673E9	3.1951E8	2.9939E8	2.7292E8	2.6866E11
0.6084	4.4524E7	1.2498E9	3.3910E8	2.2779E8	1.9803E8	2.7167E11
0.6204	4.3839E7	1.2892E9	3.4898E8	2.0031E8	1.5198E8	2.7044E11
0.6231	4.3451E7	1.1585E9	3.1951E8	2.9939E8	2.7605E8	2.6654E11
0.6265	4.3497E7	1.3088E9	3.5393E8	1.8826E8	1.2903E8	2.6982E11
0.6324	4.3198E7	1.3274E9	3.5878E8	1.7741E8	1.0805E8	2.6943E11

Table A.12: Restoring force (motions)

Heave	Roll	Pitch
Z_z = 7.9882E7	K_ϕ = 1.4340E9	M_z = 7.6622E8
Z_θ = 7.6622E8	$K_{\phi\phi\phi}$= 1.7844E10	M_θ = 4.1365E11
Z_{zz} =-3.0014E6	$K_{z\phi}$ =-8.4268E7	M_{zz} =-2.4985E8
$Z_{z\theta}$ =-2.4986E8	$K_{\phi\theta}$ =-1.4090E10	$M_{z\theta}$ =-4.9230E10
$Z_{z\phi}$ =-2.9468E8	$K_{zz\phi}$ = 7.9738E7	$M_{z\phi}$ =-2.0614E10
$Z_{\theta\theta}$ =-4.9230E10	$K_{\phi\theta\theta}$ = 1.5400E11	$M_{\theta\theta}$ =-4.8730E12
$Z_{z\phi\phi}$= 2.8817E8		$M_{z\phi\phi}$= 2.7052E10
$Z_{\phi\phi\theta}$= 2.7052E10		$M_{\phi\phi\theta}$= 4.1064E12
$Z_{\theta\theta\theta}$ = 1.5324E9		$M_{\theta\theta\theta}$ = 8.5664E11

Table A.13: Restoring force heave (wave)

ω	$Z_{\zeta zc}$	$Z_{\zeta zs}$	$Z_{\zeta\theta c}$	$Z_{\zeta\theta s}$	$Z_{\zeta\phi\phi c}$	$Z_{\zeta\phi\phi s}$
0.4425	-2.3750E6	6.6977E5	-2.4465E8	2.9599E8	8.1275E7	-5.4920E7
0.4530	-2.5435E6	3.2979E5	-2.5538E8	2.5518E8	9.8517E7	-3.6843E7
0.4583	-2.6145E6	2.0307E5	-2.5920E8	1.3333E8	9.1601E7	-3.3192E7
0.4640	-2.6795E6	1.6335E5	-2.6201E8	1.0901E8	9.4449E7	-2.0234E7
0.4699	-2.7334E6	-1.1570E5	-2.6345E8	1.8304E8	10.6854E7	-1.7722E7
0.4764	-2.7763E6	-2.5049E5	-2.6320E8	1.5364E8	10.8827E7	-0.6161E7
0.4893	-2.8063E6	-6.1952E5	-2.5674E8	-0.9361E8	10.0490E7	1.3270E7

Table A.14: Restoring force roll (wave)

ω	$K_{\zeta\phi c}$	$K_{\zeta\phi s}$
0.4425	-2.0159E8	5.0131E7
0.4530	-2.2088E8	3.9835E7
0.4583	-2.2955E8	2.9048E7
0.4640	-2.3800E8	1.7097E7
0.4699	-2.4571E8	-1.4401E7
0.4764	-2.5289E8	-2.0107E7
0.4893	-2.6271E8	-5.1159E7

Table A.15: Restoring force pitch (wave)

ω	$M_{\zeta zc}$	$M_{\zeta zs}$	$M_{\zeta\theta c}$	$M_{\zeta\theta s}$	$M_{\zeta\phi\phi c}$	$M_{\zeta\phi\phi s}$
0.4425	-2.4465E8	2.9599E8	-4.1210E10	13.4180E9	1.2085E10	-8.3843E9
0.4530	-2.5538E8	2.5518E8	-4.3826E10	9.9360E9	1.2758E10	-6.7092E9
0.4583	-2.5920E8	1.3333E8	-4.4896E10	7.5627E9	1.3023E10	-5.8125E9
0.4640	-2.6201E8	1.0901E8	-4.5844E10	4.9408E9	1.3246E10	-4.8142E9
0.4699	-2.6345E8	1.8304E8	-4.6590E10	1.1646E9	1.3407E10	-3.7486E9
0.4764	-2.6320E8	1.5364E8	-4.7118E10	-2.0510E9	1.3496E10	-2.5428E9
0.4893	-2.5674E8	-0.9361E8	-4.7200E10	-8.7894E9	1.3384E10	-0.0820E9

Table A.16: External wave forces

ω_e	$\bar{F}_3$	α_3	$\bar{F}_5$	α_5
0.5519	1.1189E7	-0.0000	2.9506E9	4.8904
0.5662	0.5271E7	-0.2025	2.6579E9	4.8730
0.5677	0.8123E7	-0.0750	2.8144E9	4.8817
0.5723	0.5222E7	-0.2147	2.6552E9	4.8730
0.5756	0.6653E7	-0.1361	2.7384E9	4.8764
0.5783	0.5175E7	-0.2269	2.6525E9	4.8712
0.5844	0.5130E7	-0.2391	2.6500E9	4.8695
0.5904	0.5086E7	-0.2496	2.6475E9	4.8695
0.5933	0.3709E7	-0.4189	2.5538E9	4.8642
0.5963	0.5157E7	-0.2478	2.6549E9	4.8712
0.6023	0.5138E7	-0.2548	2.6545E9	4.8695
0.6031	0.2489E7	-0.8186	2.4424E9	4.8573
0.6084	0.5105E7	-0.2653	2.6528E9	4.8695
0.6204	0.4957E7	-0.2950	2.6423E9	4.8660
0.6231	0.2816E7	-2.1398	2.1973E9	4.8381
0.6265	0.4886E7	-0.3107	2.6373E9	4.8642
0.6324	0.4838E7	-0.3229	2.6341E9	4.8642

Acknowledgements

The authors would like to thank MARINTEK for having provided the experimental facilities and the financial support. Many thanks are due to Dr. Ingo Drummen for having collected the experimental data. This work was partially supported in Brazil by CNPq within the STAB project (Nonlinear Stability of Ships), by LabOceano-COPPE/UFRJ and CAPES, and in Norway by CESOS (Centre of Excellence for Ships and Ocean Structures).

Paper B

On the Feasebility of Stabilizing Parametric Roll with Active Bifurcation Control

---

Published in *Proceedings of the 7th IFAC Conference on Control Application in Marine Systems*, 2007.

Abstract: When parametric resonance occurs on a ship, large roll motion develops rapidly and severe damage on cargo is likely. Some vessels have even capsized in moderate seas for reasons believed to be parametric resonance. This paper revisits the analysis of parametric resonance and assess the possibility to dynamically modify the instability region where parametric roll can occur. It is shown how a control strategy for roll stabilization could be modified to change a bifurcation in roll motion and stabilize the motion, even after parametric resonance has started. The paper addresses issues of achievable performance and demonstrates the approach on a yaw-sway-roll-surge model of a containership.

Keywords: Parametric resonance, Parametric roll, Ship motion control.

B.1 Introduction

Parametric roll is a well known critical phenomenon characterized by a sudden and quick rise of roll oscillations, which may bring the ship into conditions dangerous for the ship, the cargo and the crew. Recent casualties, as that happened in 1998 to a post-Panamax C11 class containership ([20]), have brought a raising attention of the scientific community on analyzing the nature of parametric roll in head sea in order to determine the principal conditions which origin the phenomenon itself. In the last six years there has been a very profitable effort by many different research-tanks ([20]; [21]; [22]; [75]) which ended up in defining major requirements to be met in order to make parametric roll happen. Particular conditions need to be fulfilled for this resonant motion to develop: the vessel sails in extreme head/near head sea; the ship has small roll damping due to reduced speed; moderate to heavy sea causes a periodic variation in the transverse stability of the ship.

Investigations have been carried out for different kinds of vessels ranging from containerships ([20]; [75]; [71]; [43]), through Destroyer and Ro-Ro pax ([21]; [22]), to fishing boats ([57]; [58]; [59]). Nevertheless, considering the requirements stated above, the last factor plays a particular important role when container carrier is the vessel class taken into consideration. Nowadays, containerships are characterized by bow flare and stern overhang which bring about dramatic variations in intercepted water-plane area, when a wave crest or trough is close to amidships position.

The roll damping appears a natural means to exploit in order to either counteract the growth of parametric roll or, if possible, prevent the origin of the critical situation. If the reduction of roll oscillations amplitude is greater than

the rise caused by the change of stability, then the roll mode will not increase and parametric roll will not occur. The onset of the resonant phenomenon is, hence, related to a damping threshold (see [31]; [22]; [75]) and the aim is to keep the roll damping larger than the threshold.

Although to this day the literature has been enriched of valuable papers describing the nature of the critical phenomenon and analyzing very carefully different scenarios, i.e. regular and irregular waves (see [11]; [71]) or linear and nonlinear behaviors (see [75]; [59]), there seems to be a lack of proposals regarding the possibility and feasibility of counteracting parametric roll by active control.

Two ways could increase the ship's roll damping: increase the cruising speed significantly or perform a control action by means of available control surfaces like fins and rudder. Only the latter approach is applicable, since the extreme sea conditions might not allow to increase vessel speed. Roll damping control systems using fin stabilizers have been available for a century and rudder-roll stabilization was developed from 1970s and onwards. The achievable performance of both approaches is well documented, see [70] and references herein.

This paper, starting from a short and accurate analysis of linear and nonlinear behavior of parametric roll, assess the possibility to modify in a dynamic fashion the shape of the instability region, where autoparametric resonance may occur. In particular, a fin stabilization technique is employed to demonstrate the feasibility to change the bifurcation in roll mode and stabilize the motion, even after the onset of parametric roll. Finally, the approach is shown simulated on a yaw-sway-roll-surge model of a containership.

B.2 Parametric roll

In this section the attention is focused on the analysis of the onset of resonant phenomena: linear and nonlinear Mathieu's equation is exploit in order to show the presence of bifurcation points in the dynamics of physical systems and how it is possible to bring back resonant behaviors to stable ones acting on the damping of the system.

Parametric roll is an unstable resonant phenomenon whose onset is strictly related to the time-varying submerged hull geometry and to particular sea conditions. When a ship sails in moderate to heavy head sea, the wave motion determines variations in the intercepted waterplane area, and in turn, in the transverse metacentric height GM_t. The fluctuation has a peak when a wave

trough is nearby amidships position. The periodic variation of transverse metacentric height changes the stability properties of the vessel through the roll restoring moment ($\tau_\phi \triangleq f(t, GM_t, \phi)$). In particular, the stability increases when a wave trough is midships ($GM_{tr} > GM_{sw}$) and decreases when the wave crest is midships ($GM_{cr} < GM_{sw}$).

A fast development of parametric roll can happen when conditions are: the ship approaches waves with encounter frequency almost twice the natural roll frequency ($\omega_e \approx 2\omega_\phi$), the wavelength is almost equal to ship length ($\lambda_w \approx L_{PP}$) and a disturbance in roll occurs when stability is raising.

B.2.1 Mathematical model: linear and nonlinear Mathieu's equation

Consider a one degree of freedom roll motion equation in head sea:

$$(I_{xx} - K_{\dot{p}})\,\ddot{\phi} + K_p\dot{\phi} + \rho g \nabla GM(t)\,\phi = 0 \tag{B.1}$$

where $K_{\dot{p}}$ is the added mass, K_p is the linear damping and $\rho g \nabla GM(t)\,\phi$ is the time-varying restoring moment. Under the assumption of regular waves and considering the vessel as a linear time invariant (LTI) system, the GM changes can be assumed sinusoidal

$$GM(t) = \overline{GM} + GM_a \cos(\omega_e t) \tag{B.2}$$

where $\overline{GM}$ is the mean value of the metacentric height, GM_a is the amplitude of the variations of the metacentric height in waves and ω_e is the frequency of encounter of the wave. Substituting (B.2) into (B.1) yields, with $\alpha_1 = \frac{K_p}{(I_{xx}-K_{\dot{p}})}$ and $\alpha_2 = \frac{\rho g \nabla}{(I_{xx}-K_{\dot{p}})}$,

$$\ddot{\phi} + \alpha_1\dot{\phi} + \alpha_2\left(\overline{GM} + GM_a\cos(\omega_e t)\right)\phi = 0 \tag{B.3}$$

where it can be seen that the two ratios $\frac{\rho g \nabla \overline{GM}}{(I_{xx}-K_{\dot{p}})}$, $\frac{\rho g \nabla GM_a}{(I_{xx}-K_{\dot{p}})}$ are dimensionally equivalent to a frequency squared. Then defining ω_ϕ and ω_a,

$$\omega_\phi = \sqrt{\frac{\rho g \nabla \overline{GM}}{(I_{xx} - K_{\dot{p}})}}, \quad \omega_a = \sqrt{\frac{\rho g \nabla GM_a}{(I_{xx} - K_{\dot{p}})}} \tag{B.4}$$

(B.3) can be written in the following form

$$\ddot{\phi} + 2\zeta\omega_\phi\dot{\phi} + \left(\omega_\phi^2 + \omega_a^2\cos(\omega_e t)\right)\phi = 0. \tag{B.5}$$

Introducing a variable $\xi = \frac{1}{2}\omega_e t$ and the dimensionless parameters

$$\delta = \frac{4\omega_\phi^2}{\omega_e^2}, \qquad \epsilon = \frac{4\omega_a^2}{\omega_e^2}, \qquad \nu = \frac{4\zeta\omega_\phi}{\omega_e} \tag{B.6}$$

where δ is the ratio between natural roll frequency and encounter wave frequency, and ϵ is the relative frequency variation in waves due to variation in GM, then (B.5) assumes the form of the well-known, linear damped Mathieu's equation ([31])

$$\phi'' + \nu\phi' + (\delta + \epsilon\cos 2\xi)\,\phi = 0. \tag{B.7}$$

where

$$\phi' = \frac{d\phi}{d\xi}, \qquad \phi'' = \frac{d^2\phi}{d\xi^2}.$$

This equation with periodic coefficient has bounded and unbounded solutions depending on the values of the pair (δ, ϵ). The stable and unstable regions of the Mathieu's equation are visualized through the Ince-Strutt diagram (Figure B.1), which represents the transition curves in the δ-ϵ plane. These curves origin from a point $\delta = n^2$ $(n \in \mathbb{N})$ and define regions of instability usually referred to as tongues. If (δ, ϵ) is inside one of these tongues then the solution is unbounded and grows exponentially. When (δ, ϵ) falls outside the tongues the solution is bounded and is a quasiperiodic function of time. The damping term v in the Mathieu's equation results in a detachment of the tongues from the δ-axis, determining an enlargement of the areas of stability. Hence, the damping introduces a minimum value for ϵ to be reached before resonance phenomena can develop.

In the presence of nonlinearities, which basically detune the resonance, mechanical systems do not exhibit unbounded behavior but has a tendency to limit the amplitude of motion. To include such nonlinear contributions Mathieu's equation is extended by a nonlinear term,

$$\phi'' + v\phi' + (\delta + \epsilon\cos 2\xi)\,\phi + \epsilon\alpha\phi^3 = 0. \tag{B.8}$$

The nonlinear Mathieu's equation (B.8) has a cubic function that physically represents the righting moment of roll. The action carried out by this nonlinear term is to saturate the resonant phenomenon, defining a limit for the roll angle that cannot be overcome, unless capsizing occurs.

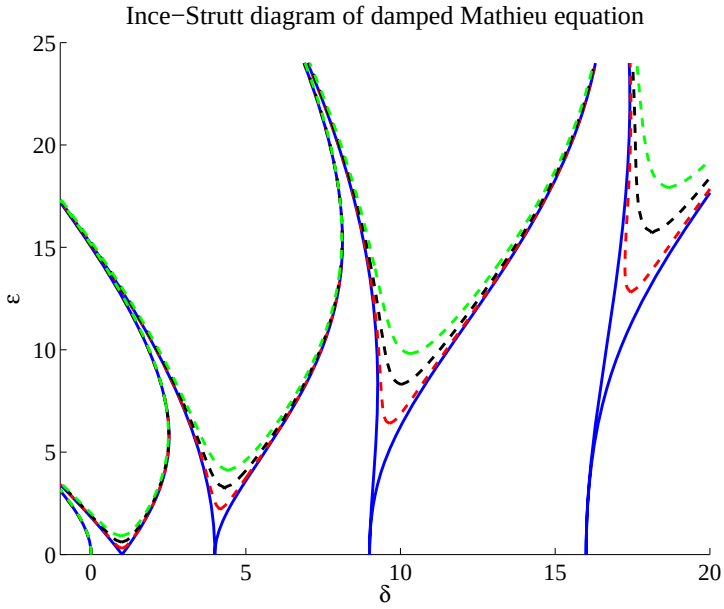

Figure B.1: Ince-Strutt diagram of the damped linear Mathieu's equation. The continuous lines represent the transition curves for the undamped case, while the dashed lines refer to damping values equal to 0.15, 0.3, 0.45.

B.3 Active bifurcation control

Since parametric resonance in theory was avoided if the shape of the tongues could be modified such that (δ, ϵ) is in the stable part, it is tempting to attempt a detuning of parametric roll, even after it has occurred, by increasing the value of the system damping through active control. As a test case, the 4-DOF (yaw-sway-roll-surge) nonlinear model of the containership Luna Maersk from 1982 is employed, see [5], although this particular ship was never reported to exhibit parametric roll. This vessel was chosen since it is one of the few ships for which both model tests with roll-sway-yaw and full scale identification results are available. Assuming a variation of GM in waves, which is believed to be realistic, however without performing a scrutiny of the ship's lines, the parametric roll is simulated in the nonlinear model showing how, even in head sea condition where no roll motion is expected, the resonant phenomenon could occur.

B.3.1 Nonlinear and linear ship model

The considered ship model is a yaw-sway-roll-surge nonlinear model of a containership whose principal dimensions are stated in Table B.1 (taken from [5]).

Table B.1: Main data for containership Luna Maersk (1982) - at even keel

Quantity	**Symbol**	**Measure**
Length bt perpendiculars	L_{pp}	230m
Beam	B	32m
Draft fore	D_f	10.7m
Draft aft	D_a	10.7m
Displacement	∇	46000m^3
Nominal speed	U_0	12.7m / s
x coordinate of CG	x_G	-0.5m
z coordinate of CG	z_G	-3.5m
Metacentric height	GM	0.55÷0.90m
Nondim. inertia in roll	I'_{xx}	1.32
Nondim. inertia in yaw	I'_{zz}	43.25

In absence of external moments due to waves and/or actuators, and with a righting arm, under the assumption of regular waves,

$$G'_z(\phi') = \left(\overline{GM}' + GM'_a \cos(\omega_e t)\right) \sin(\phi') \tag{B.9}$$

the nonlinear nondimensional roll equation is given in (B.10)

$$\begin{aligned}\left(I'_{xx} - K'_{\dot{p}}\right)\ \dot{p}' - (m' z'_G\ cos\,(\phi) + K'_{\dot{v}})\,\dot{v}' - K'_{\dot{r}}\dot{r}' &= K'_v v' + K'_{vv} v'^{\,2} \\ &+ K'_{v|v|} v'\,|v'| + K'_{v|r|} v'\,|r'| + K'_{vrr} v' r'^{\,2} + m' z'_G \cos(\phi)\ u' r' \\ &+ K'_r\ r' - \rho' g' \nabla' G'_z(\phi') + K'_{r|r|} r'\,|r'| + K'_{rrr} r'^{\,3} + K'_{rvv} r' v'^{\,2} \\ &+ K'_{r|v|} r'\,|v'| + K'_p p' + K'_{p|p|} p'\,|p'| + K'_{ppp} p'^{\,3} + K'_{pu} p' u'_a \\ &+ K'_{pu|pu|} p' u'_a\,|p' u'_a| + K'_{v\phi} v'\,\phi' + K'_{v\phi\phi} v' \phi'^{\,2} + K'_{\phi vv} \phi' v'^{\,2} \\ &+ K'_0 + K'_{0u} u'_a \end{aligned} \tag{B.10}$$

If the frequency coupling condition holds and assuming $GM_a = 0.5\,\mathrm{m}$, then a roll motion starts to build up and, approximately in 10 roll periods, it has already reached critical values around $\pm 0.45\,\mathrm{rad}$ ($\sim \pm 25.5°$), as shown in Figure B.2. As predicted through the analysis of the nonlinear Mathieu's equation, the roll response shows saturation.

The linear time varying model is derived from the nonlinear one assuming a

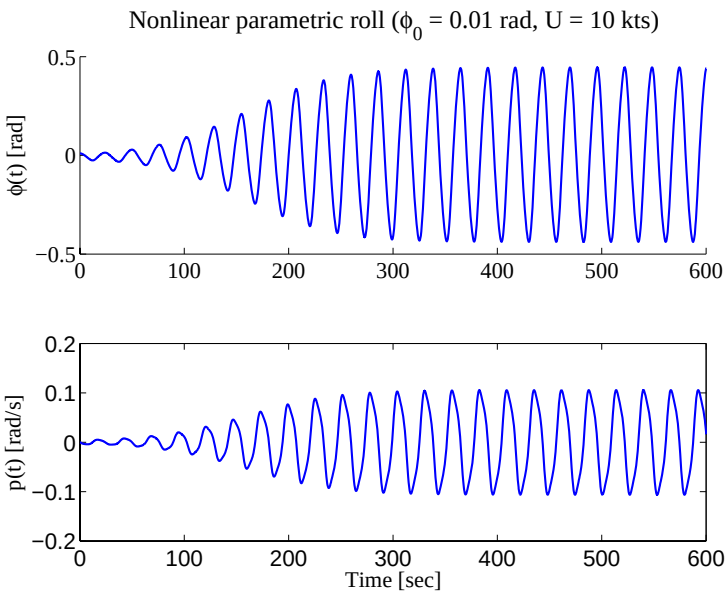

Figure B.2: Containership model experiencing parametric roll in head sea.

metacentric height $GM = 0.83\,\mathrm{m}$ and a forward speed $U = 10$ kt:

$$\dot{\mathbf{x}} = \begin{bmatrix} -0.0047 & -0.0020 & -1.3303 & a_{14}(\omega_e t) & 0 \\ 0.0015 & -0.0341 & 0.0395 & a_{24}(\omega_e t) & 0 \\ -0.0004 & 0.0014 & -0.0912 & a_{34}(\omega_e t) & 0 \\ 0 & 1 & 0 & 0 & 0 \\ 0 & 0 & 1 & 0 & 0 \end{bmatrix} \mathbf{x}$$
$$\mathbf{y} = \begin{bmatrix} 0 & 1 & 0 & 0 & 0 \\ 0 & 0 & 0 & 1 & 0 \end{bmatrix} \mathbf{x} \tag{B.11}$$

where the state vector is $\mathbf{x} = \begin{bmatrix} v & p & r & \phi & \psi \end{bmatrix}^T$ and the output vector is $\mathbf{y} = \begin{bmatrix} p & \phi \end{bmatrix}^T$. The $\mathbf{A}$ matrix is dependent on the frequency of the encounter of waves and on time, through the linearized righting arm $G'_z(\omega_e t)$. This gives rise to the unbounded response of the roll motion when the frequency coupling condition holds. Comparing the linear and nonlinear response in roll it is possible to see how the absence of detuning produces an exponential linear roll response whereas the nonlinear model exhibits the bounded response, shown in Figure B.3. It is noted that these simulations focus solely on the parametric resonance in roll and do not include roll induced by usual wave excitation, as this is insignificant in head seas.

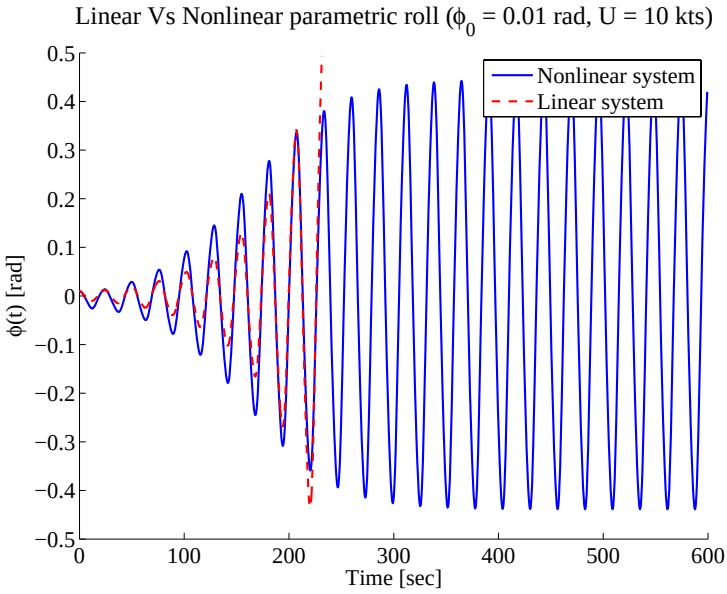

Figure B.3: Linear and nonlinear response in roll when parametric resonance has occurred.

B.3.2 Bifurcation control by fin stabilizer

As the origin and the growth of parametric roll could be counteracted by change of the envelope of instability tongues in Figure B.1, the achievement of a value of the damping coefficient larger than a damping threshold should prevent the parametric resonance. For the first region of instability, the value of the threshold was approximated by [31], obtaining

$$\nu_T \approx \sqrt{\frac{\epsilon^2}{4} - (\delta - 1)^2}. \tag{B.12}$$

If the bifurcation point $\delta = 1$ is chosen, the threshold is $\frac{\epsilon}{2}$ means that, when $\omega_e = 2\omega_\phi$, the variation of GM must be at least the double of the actual damping in order to get autoparametric resonance, see Fig.B.4. Hence, if the actual damping ν is larger than ν_T then the resonant phenomena could not develop, even if the frequency condition holds. Moreover, since both ϵ and δ are strictly related to system parameters, the knowledge of a threshold value for the damping gives the possibility to counteract parametric roll when it has already occurred, by increasing the value of the damping to beyond ν_T. Figure B.5 shows

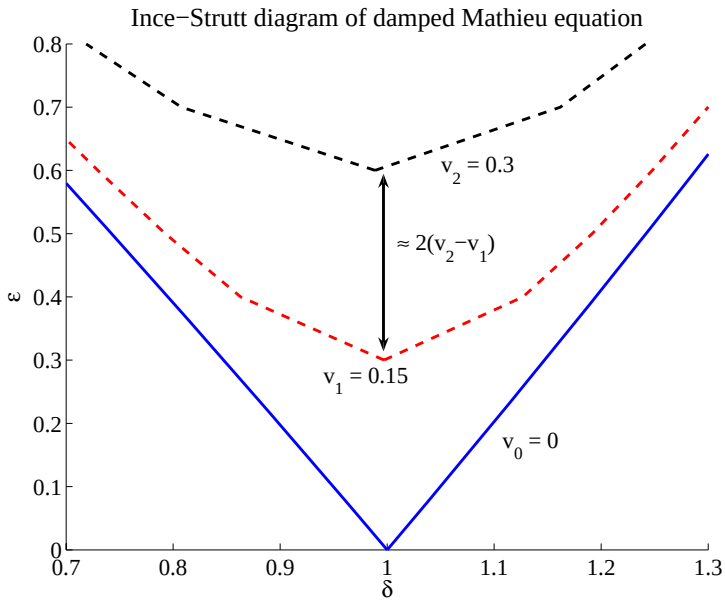

Figure B.4: Damping effect on the first instability region.

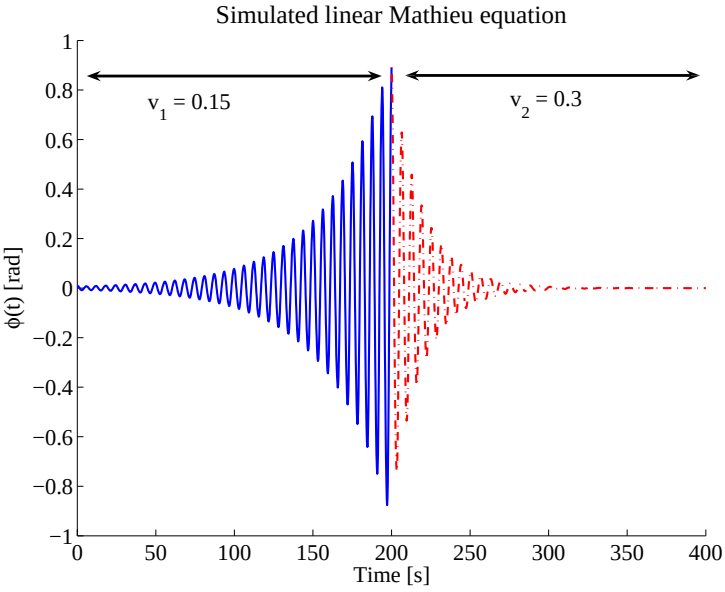

Figure B.5: Resonant phenomenon stabilized by increasing the damping in the system.

Table B.2: Characteristics of the fins.

Quantity	**Symbol**	**Measure**
Area	A_R	7.8 m^2
Aspect ratio	a	2.4
Max. angle	$\alpha_{\max}$	20deg
Max. rate	$\dot{\alpha}_{\max}$	15.8deg / s
Hyd. prop. band	α_{pb}	5deg
Tilt angle	β	35deg
Lift coefficient (estimated)	C_L	1.2
Nominal lift at service speed	L_{nom}	518kN

the feasibility to damp out parametric roll even if the resonance phenomenon has already started, by increasing the value of damping in the equation.

Moving the bifurcation point of the parametric resonance could in practice be obtained by increasing the actual level of roll damping. This is shown through the design of a fin stabilizer which takes the control action over when parametric roll has already developed. The characteristics of the vessel's fins are stated in Table B.2.

Fins give rise to forces and moments acting on sway, roll and yaw given as

$$\begin{aligned} \tau_v &= -\tau_f \sin\beta \\ \tau_\phi &= 2\tau_f r_f \\ \tau_\psi &= x_{FCG}\tau_f \sin\beta \end{aligned} \tag{B.13}$$

where τ_f is the normal component of the total hydrodynamic force resulting from lift and drag forces acting on the centre of pressure of the fin; β is the tilt angle of the fin; r_f is the fin roll arm; x_{FCG} is the distance in the longitudinal direction between the centre of pressure of the fin and the centre of gravity of the ship. The magnitude of the fin-induced moment in roll is related to the angle of attack α_e of the fin, that in turn depends upon the mechanical angle α. Due to particular sea conditions taken into consideration, moderate to heavy sea, it is necessary to consider unsteady hydrodynamics characteristics of the foils and in particular the so-called foil motion ([70]) in order to determine the real angle of attack. In fact, α_e is given by the combination of the mechanical angle α commanded by the controller and the flow angle α_{fl} due to the interaction between the roll-induced velocity and the forward speed U of the ship; in particular following the notation of Perez [70]

$$\alpha_e = \alpha - \alpha_{fl}. \tag{B.14}$$

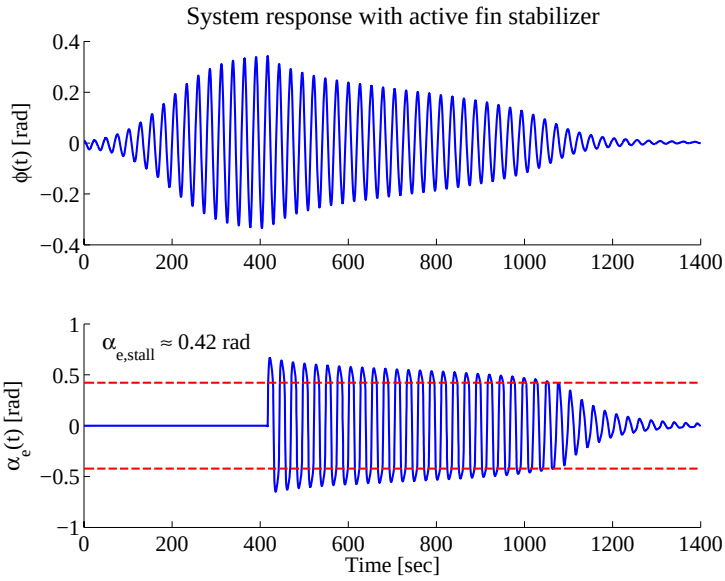

Figure B.6: Parametric roll condition with $GM_a = 0.42\,\mathrm{m}$. Control is activated when roll amplitude is $|\phi| = 20\,\mathrm{deg}$.

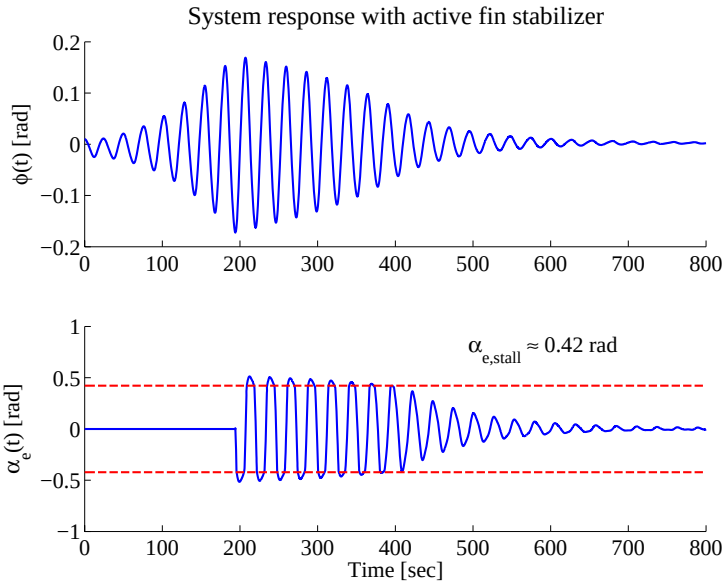

Figure B.7: Control action by the fin stabilizer is activated at roll amplitude $|\phi| = 10\,\mathrm{deg}$.

Table B.3: Poles and damping without and with fin stabilizer.

A		**A − BLC**	
Poles	**Damp**	**Poles**	**Damp**
0	−	0	−
−0.00068	1	−0.00068	1
$-0.016 \pm 0.23i$	0.07	$-0.0385 \pm 0.222i$	0.17
−0.098	1	−0.098	1

To demonstrate the ability to stabilize the resonant roll motion, a roll-rate feedback is considered. The control law provides a mechanical angle α which is proportional to the actual roll rate p

$$\alpha = -L_{\alpha p} \frac{\alpha_{\max}}{p_{\max}} \left(\frac{U_{\lim}}{U_{nom}} \right)^{-2} p \tag{B.15}$$

where $U_{\lim} = U$ when $U \geq U_{\min}, U_{\lim} = U_{\min}$ otherwise. The control action moves the complex poles increasing the system damping of one order of magnitude (see Table B.3 where the pole positions are stated for the average system damping).

Time history plots of the response are shown in Figures B.6 and B.7 where $GM_a = 0.42\,\text{m}$ was used. Control action was activated when roll amplitude was $|\phi| = 20\,\text{deg}$ and 10 deg, respectively. The roll motion is seen to decay slowly in the first case, after control has been activated, but rapidly in the second. The hydrodynamic angle of attack on the fin is large in both cases when the fin stabilizer takes the control action over, but in the first case the fins work in stall condition for a longer period and the presence of stall limits the available control torque.

The rate of decay in roll is associated with damping of the periodically excited system. The constraint of the hydraulic machinery on the actual α_e is also an issue, but this is not pursued in this context.

B.4 Rate of Decay

When the nonlinear system (B.8) is subject to periodic variation, the rate of decay can be assessed by Floquet theory. The response of the nonlinear system (B.8), is approximately, applying the two variable expansion method with $\xi = t$

being the fast time, and $\eta = \epsilon t$ being the slow time ([31]),

$$\begin{aligned}\phi(t,\epsilon) &= \phi_0(\xi,\eta) + \epsilon\phi_1(\xi,\eta) + O\left(\epsilon^2\right) \\ &= A_0(\eta)\cos\xi + B_0(\eta)\sin\xi \\ &+ A_1(\eta)\,\epsilon\cos\xi + B_1(\eta)\,\epsilon\sin\xi \\ &+ \frac{A_0(\eta)}{16}\epsilon\cos 3\xi + \frac{B_0(\eta)}{16}\epsilon\sin 3\xi + O\left(\epsilon^2\right).\end{aligned} \tag{B.16}$$

The functions $A(\eta)$ and $B(\eta)$ are the envelopes of the sinusoidal response; in particular

$$A_0(\eta) = A_0 e^{\mu\eta}, \quad B_0(\eta) = B_0 e^{\mu\eta} \tag{B.17}$$

where $\mu = -\frac{1}{2}\frac{v}{\epsilon} \pm \frac{1}{2}\sqrt{\frac{1}{4} - \left(\frac{\delta-1}{\epsilon}\right)^2}$ is the characteristic exponent found as the eigenvalue of the slow motion equations.

When the system

$$\phi'' + v\phi' + (\delta + \epsilon\cos 2\xi)\,\phi + \epsilon\alpha\phi^3 = \tau \tag{B.18}$$

is forced using a feedback control

$$\tau = -c\phi' \tag{B.19}$$

the characteristic exponents (B.17) are

$$\mu = -\frac{1}{2}\frac{v+c}{\varepsilon} \pm \frac{1}{2}\sqrt{\frac{1}{4} - \left(\frac{\delta-1}{\epsilon}\right)^2} \tag{B.20}$$

hence, with $a_1 = \left(\frac{4\zeta\omega_\phi}{\omega_e} + c\right)$ and $a_2 = \left(\frac{4\omega_\phi^2 - \omega_e^2}{4\omega_a^2}\right)$

$$\mu = -\frac{1}{8}\frac{\omega_e^2}{\omega_a^2}a_1 \pm \frac{1}{2}\sqrt{\frac{1}{4} - a_2^2}. \tag{B.21}$$

Considering the value of the damping after the fin stabilizer has been activated, $v + c \simeq 0.34$, and $\epsilon \simeq 0.51$, corresponding to $GM_a = 0.42\,\mathrm{m}$, the envelopes of the sinusoidal response are both decreasing exponential functions since $\mu_1 = -0.08$ and $\mu_2 = -0.58$. This shows the efficiency of the control action in inverting the tendency of the roll motion of exponentially increasing, as addressed by the positive value of one characteristic exponent ($\mu_1 = 0.12$) when the fin stabilizer is not activated.

B.4.1 Required Control Action

With the stability condition from (B.21) $\mu < 0$, parameters $\zeta \geq 0$, $\omega_e \neq 0$ and at resonance, the control gain c need to satisfy

$$-\frac{1}{2}\frac{\omega_\phi^2}{\omega_a^2}(2\zeta + c) \pm \frac{1}{4} < 0 \Leftrightarrow \tag{B.22}$$
$$\frac{1}{2}\frac{\omega_a^2}{\omega_\phi^2} - 2\zeta < c.$$

When the non-dimensional acceleration is achieved by control torque as

$$\tau = \frac{1}{(I_{xx} - K_{\dot{p}})\,\omega_\phi^2} K_f(p, \phi) \tag{B.23}$$

then, in the resonance condition, damping can be achieved if and only if

$$\rho g \nabla \overline{GM} \left(\frac{1}{2}\frac{GM_a}{\overline{GM}} - 2\zeta \right) < \frac{\partial}{\partial p} K_f(p, \phi). \tag{B.24}$$

This Floquet theory result is valid when a linear control action can be assumed, according to (B.19). In Figure B.7, this is the response seen after $t = 400s$, when fin operation gets out of the stall region.

Given a fin size, the inequality (B.24) can be used to determine the maximum roll angle that can be damped by the fin stabilizer within the linear region of operation. In fact, assuming a sinusoidal variation in roll angle and multiplying both sides of (B.24) by the roll rate

$$\rho g \nabla \overline{GM} \left(\frac{1}{2}\frac{GM_a}{\overline{GM}} - 2\zeta \right) \phi_0 \omega_\phi < K_{f,\max} \tag{B.25}$$

where $K_{f,\max} = \frac{\partial}{\partial p} K_f(p, \phi) p$ is the actual maximum control torque. Disregarding the drag force acting on the fin, the control torque can be expressed as

$$K_{f,\max} = 2 r_f L(\alpha, p) = r_f \rho C_L A_f V_f^2 \tag{B.26}$$

then the maximum roll angle that can be damped, according to the Floquet theory result, is

$$\phi_{0,\max} = \left(\rho g \nabla \overline{GM} \left(\frac{1}{2}\frac{GM_a}{\overline{GM}} - 2\zeta \right) \omega_\phi \right)^{-1} K_{f,\max} \tag{B.27}$$

Considering the physical characteristics of the actual fins, the maximum roll angle for linear damping is in the range $\phi_{0,\max} \approx 0.14 - 0.31$ rad at ship speed 5 m/ s. This is a pessimistic estimate of the capabilities of the fin stabilizer, however. The reason is that damping is also possible in the region where stall appears, as illustrated by the simulations, but a scrutiny of this is outside the scope of the present paper.

B.5 Conclusions

This paper analyzed the theoretical possibilities to stabilize parametric roll by influencing the location of the bifurcation point in the nonlinear Mathieu equation for parametric resonance. The feasibility of the approach was demonstrated theoretically and by simulation using a four degree of freedom model of a container vessel. The real container vessel was not reported to have experiences of parametric roll, but simulations showed a possibility thereof, given the variation in GM in regular seas was 0.5 m and the frequency conditions of parametric resonance were met. The parametric resonance was demonstrated to be stabilized using the fins of the vessel. Further, assessment was made of the efficiency of the control action, showing through Floquet theory that the characteristic exponents of the Mathieu equation satisfy the stability condition after the fin stabilizer was activated. Finally, an evaluation of the required fin torque was made and the limits of linear control action was assessed.

Acknowledgements

The kind permission from Maersk Lines to use and publish vessel data are gratefully acknowledged. The advice on hydrodynamic issues from Prof. Jørgen Juncher Jensen and Dr. Jenena Vidic-Perunovic from DTU are also gratefully acknowledged.

Paper C

Stabilisation of Parametric Roll Resonance by Combined Speed and Fin Stabiliser Control

Published in *Proceedings of the 10th European Control Conference*, 2009.

Abstract: Parametric roll resonance on a ship is a condition where large roll motion develops rapidly in moderate head or following seas. The phenomenon is caused by bifurcation in the nonlinear equations of motion when a restoring moment is subject to periodic variation. This paper analyzes the stability of the nonlinear system and suggests active control of both ship speed and fin stabilizers to stabilise the roll resonance condition. Lyapunov and backstepping designs are employed to achieve two nonlinear controllers, which are proved to stabilise the nonlinear system. The designed controllers are validated employing a high fidelity simulation model. The combined speed and fin stabiliser control is shown to efficiently drive the vessel out of the bifurcation condition and to quickly damp the residual roll motion.

C.1 Introduction

Auto-parametric resonance is a de-stabilising effect, which can arise in mechanical systems consisting of two or more vibrating components [77]. This phenomenon can be described by

$$\ddot{x} + b(\dot{x})\dot{x} + a(t)x = 0 \tag{C.1}$$

where the parameter $a(t)$ is periodic, $a(t+T) = a(t)$. The conservative system (i.e $b = 0$) is recognised as the Hill-Mathieu's equation [31]. Equation (C.1) is subject to instabilities, which can occur when there is resonance between the imposed period T and the natural period T_0. The resonance condition is that T, or $2T$, is an integer multiple of T_0.

Parametric roll is an auto-parametric resonance phenomenon whose onset causes a sudden and quick rise in roll oscillations. The resulting large roll motion, which can reach 30-40 degrees of roll angle, may bring the vessel into conditions dangerous for the ship, the cargo, and the crew. The origin of this unstable motion is the time-varying geometry of the submerged hull, which produces periodic variations of the transverse stability properties of the ship. Container ships are known to be particularly prone to this phenomenon due to the hull shape – i.e. bow flare and stern overhang – which brings about dramatic variations in intercepted water-plane area when a wave crest or trough is close to amidships position. Incidents have been reported with significant damage to the cargo as well as to the ship [20], [13].

Parametric roll is known to occur when a ship sails in moderate to heavy longitudinal or oblique seas; the wave passage along the hull and the wave excited vertical motions result in variations of the intercepted waterplane area, and in turn, in relevant changes in the roll restoring characteristics. The onset and

buildup of parametric roll is due to the occurrence of concomitant conditions: the wave length is close to the ship length ($\lambda_w \approx L_s$), the ship approaches waves with encounter frequency of about twice the roll natural frequency ($\omega_e \approx 2\omega_\phi$), and the wave height is greater than a ship-dependent threshold ($h_w > \overline{h}_s$).

This work aims at designing a control strategy that is capable of stabilising the parametric roll motion to zero when the foregoing conditions are met. Different methods are available in order to stabilise the phenomenon using different actuators; e.g. active U-tanks are employed in [38] in order to drive the roll motion to zero.

The control strategy proposed in this paper relies on two factors: to vary the forward speed of the vessel in order to de-tune the frequency coupling condition ($\omega_e \approx 2\omega_\phi$), and to increase the roll damping by means of the fins. The two controllers are designed applying Lyapunov stability theory.

The analytical results are tested by simulations, using the benchmark model of [36].

C.2 Model

A nonlinear coupled surge-roll model is set up where the interaction between the two modes is presented in terms of a time-varying wave encounter frequency.

The standard definition of wave encounter frequency is based on the assumption of constant ship forward speed U

$$\omega_e \triangleq \omega - kU\cos\chi, \tag{C.2}$$

where ω is the wave frequency, k is the wave number, and χ is the encounter angle. The definition (C.2) was shown to be valid also when a time-varying forward speed is taken into account [26].

Some important assumptions for the development of the model are:

- the vessel is sailing in head seas ($\chi = 180°$);
- sway motion is neglected, therefore the time-varying forward speed U can be approximated as

$$U(t) = \sqrt{u(t)^2 + v(t)^2} \approx u(t), \tag{C.3}$$

  where u and v are the surge and sway velocities, respectively;

- the 1st-order wave excitation forces are considered only in terms of the Froude-Krylov forces, disregarding the diffraction forces.

C.2.1 Surge mode

For a vessel sailing in head seas, the forces acting along the longitudinal direction are: the inertial forces due to mass and added mass, the drag forces due to wave resistance, the thrust supplied by the propeller, and the external forces due to the incident waves under the assumption that the hull is restrained from moving. The non-linear surge dynamics is, to a first order approximation, where wave pressure generated forces are considered and thrust deduction from propeller flow around the stern are included but wave reflection and drag terms from hull motions and the rudder are disregarded,

$$(m - X_{\dot{u}})\dot{u} = R(u) + (1 - t_d)T_p + F_x^{FK}, \tag{C.4}$$

where m is the ship's mass, $-X_{\dot{u}} > 0$ the added mass term, $R(u)$ the ship's non-linear hydrodynamic resistance, T_p the propeller thrust, $t_d \in [0\ ,\ 1]$ the thrust deduction factor, and F_x^{FK} the longitudinal Froude-Krylov force created by wave pressure integrated over the hull. The latter is a nonlinear term since wave pressure increases with wave elevation and the area over which to integrate forces also increase by wave elevation.

The ship resistance function $R(u)$ provides damping in surge and consists of linear laminar skin friction $X_u u$, and of nonlinear quadratic drag $X_{|u|u}\,|u|\,u$ [6]

$$R(u) = X_u u + X_{|u|u}\,|u|\,u < 0. \tag{C.5}$$

Higher order terms in $R(u)$ occur due to wave making in the high end of range of ship speed, but this is not essential in this context.

According to linear airy theory [62], the wave induced force in surge is taken as the longitudinal Froude-Krylov force, considering the incident wave pressure in a regular wave. Therefore, the 1st-order wave excitation force in surge is given according to [45] by

$$\begin{aligned} F_x^{FK} &= \int_V \frac{\partial p(X, Z, t)}{\partial x}\,\mathrm{d}V \\ &= \gamma_1 \omega_e(t)\Big[\sin\Big(\omega t + kL_s + k\int_0^t U(\tau)\,\mathrm{d}\tau\Big) \\ &\quad - \sin\Big(\omega t + k\int_0^t U(\tau)\,\mathrm{d}\tau\Big)\Big]. \end{aligned} \tag{C.6}$$

where $\gamma_1 = B\frac{\rho g\bar{\zeta}}{k\omega}(1-e^{-kT})$, ρ is the water density, $\bar{\zeta}$ the wave amplitude, L_s the ship length, B the ship breadth, and T the ship draught.

C.2.2 Roll mode

Models of different complexity have been presented in literature in order to describe the roll mode in parametric resonance condition. The simplest way to model parametric roll is to consider the uncoupled non-linear equation of roll

$$(I_{xx} - K_{\ddot{\phi}})\ddot{\phi} + \bar{K}_{\dot{\phi}}(\dot{\phi})\dot{\phi} + mg\mathrm{GM}(t)\phi + K_{\phi^3}\phi^3 = 0 \tag{C.7}$$

and to recast it as the nonlinear damped Mathieu's Equation, as shown in [25]. In (C.7) I_{xx} is the ship's inertia, $-K_{\ddot{\phi}} > 0$ the added inertia, $\bar{K}_{\dot{\phi}}(\dot{\phi})\dot{\phi}$ the hydrodynamic damping that can be expressed as

$$\bar{K}_{\dot{\phi}}(\dot{\phi})\dot{\phi} = -(K_{\dot{\phi}}\dot{\phi} + K_{|\dot{\phi}|\dot{\phi}}|\dot{\phi}|\dot{\phi}) > 0, \tag{C.8}$$

$K_{\phi^3} > 0$ the nonlinear spring term. The time-varying restoring moment is $mg\mathrm{GM}(t)$, with the metacentric height defined as

$$\mathrm{GM}(t) \triangleq \overline{\mathrm{GM}} + \mathrm{GM}_a \cos(\omega_e t) \tag{C.9}$$

where $\overline{\mathrm{GM}}$ is the still water metacentric height, and GM_a is the amplitude of the variation of the metacentric height in waves.

A 3$^{\mathrm{rd}}$-order nonlinear coupled model has been developed in [36], where roll is fully coupled with the motions in the vertical plane. Let $\xi = [z,\, \phi,\, \theta]^{\mathrm{T}}$ be the generalised coordinate vector, where z is the heave displacement, ϕ is the roll angle, and θ is the pitch angle. Then the nonlinear equation of motion in matrix form are given by

$$(\mathbf{M} + \mathbf{A})\ddot{\xi} + \mathbf{D}(\dot{\phi})\dot{\xi} + \mathbf{c}_{\mathrm{res}}(\xi, t) = \mathbf{c}_{\mathrm{ext}}(t). \tag{C.10}$$

Further details – included numerical values of model parameters for a 281 m, 76500 tonnes container ship – can be found in [36]. This model is used to verify the designed control law.

C.2.3 Fins model

Fins give rise to a moment acting on roll [70] given as

$$\tau_\phi = 2Nr_f, \tag{C.11}$$

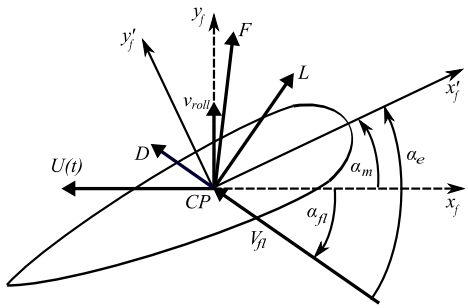

Figure C.1: Fin motion induced by roll motion

where N is the normal component of the total hydrodynamic force F resulting from lift force L and drag force D acting on the centre of pressure (CP) of the fin (see Fig. C.1), and r_f is the fin roll arm. The magnitude of τ_ϕ is related to the effective angle of attack α_e of the fin. The normal component of F is given by

$$N = L\cos\alpha_e + D\sin\alpha_e, \tag{C.12}$$

where the lift force L is

$$L = \frac{1}{2}\rho V_f^2 S C_L(\alpha_e) \tag{C.13}$$

with V_f being the flow velocity, S the fin surface, and C_L the lift coefficient, and D is the drag force.

The fins are commanded by hydraulic machinery that can be modeled as a first order system with saturation effects (see [70, 81]). Therefore, it is assumed that a first order model can be employed in order to dynamically describe the generation of the fin-induced roll moment τ_ϕ

$$\dot{\tau}_\phi + \frac{1}{t_r}\tau_\phi = \frac{1}{t_r}\tau_{\max}\text{sat}\left(\frac{\tau_c}{\tau_{\max}}\right), \tag{C.14}$$

where $\tau_{\max}$ is the maximum moment that can be produced by the fins taking into account saturation effects on the mechanical angle and on the lift coefficient, and τ_c is the moment commanded by the controller. The time constant t_r is assumed to be the same as that of the hydraulic machinery since the moment cannot be changed at a rate faster than the fins can move.

C.2.4 Resulting models

Two models are then employed for the design and the analysis of the control system. A reduced model, where roll is only coupled with surge, is first used to design a controller capable of varying the ship forward speed and drive the roll motion to zero. Then, a 4-DOF surge-heave-roll-pitch high fidelity model is employed to evaluate the performance of the controllers.

Plant model

The plant is described by a 4-DOF model based upon the 3rd-order model developed in [36], where surge, heave, roll, and pitch are coupled together. Let $\bar{\xi} = [x, \xi^T]^{\mathrm{T}}$ be the generalised coordinate vector, then the equation of motions in matrix form are

$$(\bar{\mathbf{M}} + \bar{\mathbf{A}})\ddot{\bar{\xi}} + \bar{\mathbf{D}}(u, \dot{\phi})\dot{\bar{\xi}} + \bar{\mathbf{c}}_{\mathrm{res}} = \bar{\mathbf{c}}_{\mathrm{ext}} + \mathbf{f} \tag{C.15}$$
$$\dot{\tau}_\phi + \frac{1}{t_r}\tau_\phi = \frac{1}{t_r}\tau_{\max}\mathrm{sat}\left(\frac{\tau_c}{\tau_{\max}}\right)$$

where

$$\begin{aligned}
\bar{\mathbf{M}} &= \mathrm{diag}(m, m, I_{xx}, I_{yy}) \\
\bar{\mathbf{A}} &= -\begin{bmatrix} X_{\dot{u}} & \mathbf{0}_{1\times 3} \\ \mathbf{0}_{3\times 1} & \mathbf{A} \end{bmatrix} > 0 \\
\bar{\mathbf{D}}(u, \dot{\phi}) &= -\begin{bmatrix} R(u) & \mathbf{0}_{1\times 3} \\ \mathbf{0}_{3\times 1} & \mathbf{D}(\dot{\phi}) \end{bmatrix} > 0 \\
\bar{\mathbf{c}}_{\mathrm{res}} &= [0,\, \mathbf{c}_{\mathrm{res}}(\xi, \dot{\xi}, t)]^{\mathrm{T}} \\
\bar{\mathbf{c}}_{\mathrm{ext}} &= [F_x^{FK}(\dot{\xi}, t),\, \mathbf{c}_{\mathrm{ext}}(t)]^{\mathrm{T}} \\
\mathbf{f} &= [f_1(u_d, \dot{u}_d, u),\, 0,\, f_2(\phi, \dot{\phi}, \ddot{\phi}),\, 0]^{\mathrm{T}}.
\end{aligned}$$

Nominal model

The nominal model is based on a surge-roll coupled system where the coupling between the two modes is given by the time-varying encounter frequency.

Let $\eta \triangleq [x,\, \phi]^{\mathrm{T}}$ and $\nu \triangleq \dot{\eta} = [u,\, p]^{\mathrm{T}}$ be the generalised position and velocity vectors, respectively. Then, with $\tau = [\tau_u,\, \tau_\phi]^{\mathrm{T}}$ being the control input vector,

the control model reads

$$\begin{aligned} \dot{\eta} &= \nu \\ \mathcal{M}\dot{\nu} + \mathcal{D}(\nu)\nu + \mathcal{K}(\eta,\nu,t)\eta + e(\nu,t) &= \tau \\ \dot{\tau}_\phi + \frac{1}{t_r}\tau_\phi &= \frac{1}{t_r}\tau_{\max}\mathrm{sat}\left(\frac{\tau_c}{\tau_{\max}}\right) \end{aligned} \tag{C.16}$$

where

$$\begin{aligned} \mathcal{M} &= \begin{bmatrix} m - X_{\dot{u}} & 0 \\ 0 & I_{xx} - K_{\ddot{\phi}} \end{bmatrix} \\ \mathcal{D}(\nu) &= -\begin{bmatrix} X_u + X_{|u|u}|\nu_1| & 0 \\ 0 & K_{\dot{\phi}} + K_{|\dot{\phi}|\dot{\phi}}|\nu_2| \end{bmatrix} \\ \mathcal{K}(\eta,\nu,t) &= \begin{bmatrix} 0 & 0 \\ 0 & \mathcal{K}_{22,\nu_1} + \mathcal{K}_{22,\eta_2} \end{bmatrix} \\ e(\nu,t) &= \begin{bmatrix} -F_x^{FK}(\nu_1,t) \\ 0 \end{bmatrix} \end{aligned}$$

where $\mathcal{K}_{22,\nu_1} = mg\mathrm{GM}(\nu_1,t)$, and $\mathcal{K}_{22,\eta_2} = K_{\phi^3}\eta_2^2$.

C.3 Analysis and design

The design of the speed controller is done by applying classical Lyapunov stability theory, whereas the fin stabiliser is designed by applying backstepping [48].

C.3.1 Speed controller

Given the surge subsystem

$$\dot{\nu}_1 = -\mathcal{D}'_{11}(\nu_1)\nu_1 - e'_1(\nu_1,t) + \tau'_u \tag{C.17}$$

where $\mathcal{D}'_{11}(\nu_1) = \frac{\mathcal{D}_{11}(\nu_1)}{\mathcal{M}_{11}}$, $e'_1(\nu_1,t) = \frac{e_1(\nu_1,t)}{\mathcal{M}_{11}}$, and $\tau'_u = \frac{\tau_u}{\mathcal{M}_{11}}$. The control goal is to design the controller τ'_u capable of varying the forward speed $U(t)$ so that the parametric resonance condition $\omega_e \approx 2\omega_\phi$ is avoided. This will push the system out of the instability region where parametric roll can occur.

Defining the error dynamics as

$$z_1 = \nu_1 - \nu_d, \tag{C.18}$$

where z_1 is the tracking error and $\nu_d \in C^1$ is a bounded reference trajectory, then (C.17) can be rewritten as

$$\begin{aligned}\dot{z}_1 &= \dot{\nu}_1 - \dot{\nu}_d \\ &= -\mathcal{D}'_{11}(\nu_1)(z_1 + \nu_d) - e'_1(\nu_1, t) + \tau'_u - \dot{\nu}_d.\end{aligned} \tag{C.19}$$

The control Lyapunov function for the system (C.19) is

$$V_1 = \frac{1}{2}\mathcal{M}_{11} z_1^2, \tag{C.20}$$

which is positive definite and radially unbounded; hence there exist class $\mathcal{K}_\infty$ functions α_1 and α_2 such that V_1 satisfies the following relationship globally

$$\alpha_1(|z_1|) \leq V_1 \leq \alpha_2(|z_1|). \tag{C.21}$$

The derivative of V_1 along the trajectories of the system is given by

$$\begin{aligned}\dot{V}_1 = z_1(&-\mathcal{D}_{11}(\nu_1)(z_1 + \nu_d) - e_1(\nu_1, t) + \tau_u \\ &- \mathcal{M}_{11}\dot{\nu_d}).\end{aligned} \tag{C.22}$$

Choosing the control input τ_u to be

$$\tau_u = \mathcal{D}_{11}(\nu_1)\nu_d + \mathcal{M}_{11}\dot{\nu}_d - \kappa_1 z_1, \ \forall\ \kappa_1 > 0 \tag{C.23}$$

gives

$$\dot{V}_1 = -(\kappa_1 + \mathcal{D}_{11}(\nu_1))z_1^2 - e_1(\nu_1, t)z_1. \tag{C.24}$$

The disturbance $e_1(\nu_1, t)$ satisfies the following relationship (see Appendix C.5)

$$e_1(\nu_1, t) \leq 2\gamma_1\omega + 2\gamma_1 k z_1 + 2\gamma_1 k\nu_{d,\max}. \tag{C.25}$$

Therefore, the following inequality holds

$$\begin{aligned}\dot{V}_1 &\leq -(\mathcal{D}_{11}(\nu_1) + \kappa_1 - 2\gamma_1 k)z_1^2 \\ &\quad + 2\gamma_1(\omega + k\nu_{d,\max})|z_1| \\ &\leq -(1-\theta_1)(\mathcal{D}_{11}(\nu_1) + \kappa_1 - 2\gamma_1 k)z_1^2 \\ &\quad - \theta_1(\mathcal{D}_{11}(\nu_1) + \kappa_1 - 2\gamma_1 k)z_1^2 + 2\gamma_1(\omega + k\nu_{d,\max})|z_1| \\ &\leq -(1-\theta_1)(\mathcal{D}_{11}(\nu_1) + \kappa_1 - 2\gamma_1 k)z_1^2 \\ &\leq -(1-\theta_1)(-X_u + \kappa_1 - 2\gamma_1 k)z_1^2\end{aligned} \tag{C.26}$$

$\forall\ |z_1| > \mu$ and $\forall \kappa_1 > X_u + 2\gamma_1 k$, where $\mu \triangleq \frac{2\gamma 1(\omega + k\nu_{d,\max})}{\theta_1(-X_u+\kappa_1-2\gamma_1 k)}$, and $\theta_1 \in (0,1)$. Hence, the solutions are globally uniformly ultimately bounded [48, Theorem 4.18]. In order to find the ultimate bound the functions $\alpha_1(|z_1|)$ and $\alpha_2(|z_1|)$ must be determined. Using

$$\alpha_1(|z_1|) = \alpha_2(|z_1|) = \frac{1}{2}\mathcal{M}_{11} z_1^2, \tag{C.27}$$

then the ultimate bound is given by

$$b = \alpha_1^{-1}(\alpha_2(\mu)) = \mu. \tag{C.28}$$

C.3.2 Fin stabiliser

Given the roll subsystem

$$\dot{\eta}_2 = \nu_2 \tag{C.29a}$$
$$\dot{\nu}_2 = -\mathcal{D}'_{22}(\nu_2)\nu_2 - \mathcal{K}'_{22}\eta_2 + \tau'_\phi \tag{C.29b}$$
$$\dot{\tau}_\phi = -\frac{1}{t_r}\tau_\phi + \frac{1}{t_r}\tau_{\max}\mathrm{sat}\left(\frac{\tau_c}{\tau_{\max}}\right) \tag{C.29c}$$

where $\mathcal{D}'_{22}(\nu_2) = \frac{\mathcal{D}_{22}(\nu_2)}{\mathcal{M}_{22}}$, $\mathcal{K}'_{22} = \frac{\mathcal{K}_{22}}{\mathcal{M}_{22}}$, and $\tau'_\phi = \frac{\tau_\phi}{\mathcal{M}_{22}}$, the control goal is to stabilise the roll angle η_2 to zero.

First step

For the system (C.29a) the state variable ν_2 is considered as virtual control input. The control Lyapunov function is

$$V_1(\eta_2) = \frac{1}{2}c_1\eta_2^2 \tag{C.30}$$
$$\dot{V}_1 = c_1\eta_2\nu_2, \tag{C.31}$$

where c_1 is a positive real constant. Therefore, choosing

$$\nu_2 = \psi_1(\eta_2) = -\kappa_2\eta_2, \tag{C.32}$$

with $\kappa_2 > 0$ gives

$$\dot{V}_1 = -\kappa_2 c_1 \eta_2^2 < 0 \tag{C.33}$$

and the origin of (C.29a) is globally exponentially stable [48].

Second step

The subsystem (C.29a), (C.29b) is considered. The new state variable $z_2 = \nu_2 - \psi_1(\eta_2) = \nu_2 + \kappa_2\eta_2$ is introduced. Its time derivative is $\dot{z}_2 = \dot{\nu}_2 + \kappa_2\nu_2$. The control Lyapunov function is chosen as

$$V_2(\eta_2, z_2) = V_1(\eta_2) + \frac{1}{2}\mathcal{M}_{22}z_2^2 \tag{C.34}$$

$$\begin{aligned}\dot{V}_2 = &-\kappa_2 c_1\eta_2^2 + z_2(-\mathcal{D}_{22}(\nu_2)(z_2 - \kappa_2\eta_2) \\ &- \mathcal{K}_{22}\eta_2 + \tau_\phi + \mathcal{M}_{22}\kappa_2(z_2 - \kappa_2\eta_2)).\end{aligned} \tag{C.35}$$

Hence, choosing the fin-induced roll moment to be

$$\begin{aligned}\tau_\phi = \psi_2(\eta_2, z_2) = &-\kappa_3 z_2 - \mathcal{D}_{22}(\nu_2)\kappa_2\eta_2 + \mathcal{K}_{22,\eta_2}\eta_2 \\ &- \mathcal{M}_{22}\kappa_2(z_2 - \kappa_2\eta_2),\ \forall\ \kappa_3 > 0\end{aligned} \tag{C.36}$$

then $\dot{V}_2$ reads

$$\begin{aligned}\dot{V}_2 = &-\kappa_2 c_1\eta_2^2 - (\mathcal{D}_{22}(\nu_2) + \kappa_3)z_2^2 \\ &- \mathcal{K}_{22,\nu_1}\eta_2 z_2.\end{aligned} \tag{C.37}$$

Defining $\gamma_2 \triangleq mg\overline{\mathrm{GM}} > 0$ and $\gamma_3 \triangleq mg\mathrm{GM}_a > 0$, then the roll restoring moment $K_{22}(\nu_1, t)$ satisfies the following inequality

$$\mathcal{K}_{22,\nu_1} \leq \gamma_2 + \gamma_3|\cos((\omega + k\nu_1)t)| \leq \gamma_4, \tag{C.38}$$

where $\gamma_4 = \gamma_2 + \gamma_3$. Therefore $\dot{V}_2$ reads

$$\begin{aligned}\dot{V}_2 &\leq -\kappa_2 c_1\eta_2^2 - (\mathcal{D}_{22}(\nu_2) + \kappa_3)z_2^2 + \gamma_4|\eta_2||z_2| \\ &= -(1-\theta_2)\kappa_2 c_1\eta_2^2 - \theta_2\kappa_2 c_1\eta_2^2 - (\mathcal{D}_{22}(\nu_2) + \kappa_3)z_2^2 \\ &\quad + \gamma_4|\eta_2||z_2| \\ &= -(1-\theta_2)\kappa_2 c_1\eta_2^2 - \left(\sqrt{\theta_2\kappa_2 c_1}|\eta_2| - \frac{\gamma_4}{2\sqrt{\theta_2\kappa_2 c_1}}|z_2|\right)^2 \\ &\quad + \frac{\gamma_4^2}{4\theta_2\kappa_2 c_1}z_2^2 - (\mathcal{D}_{22}(\nu_2) + \kappa_3)z_2^2 \\ &\leq -(1-\theta_2)\kappa_2 c_1\eta_2^2 - \left(\mathcal{D}_{22}(\nu_2) + \kappa_3 - \frac{\gamma_4^2}{4\theta_2\kappa_2 c_1}\right)z_2^2 \\ &\leq -(1-\theta_2)\kappa_2 c_1\eta_2^2 - \left(-K_{\dot{\phi}} + \kappa_3 - \frac{\gamma_4^2}{4\theta_2\kappa_2 c_1}\right)z_2^2.\end{aligned} \tag{C.39}$$

that is negative definite for $\forall\ \kappa_3 > \frac{\gamma_4^2}{4\theta_2\kappa_2 c_1} + K_{\dot{\phi}}$ with $\theta_2 \in (0, 1)$.

Third step

The subsystem (C.29a), (C.29b), (C.29c) is finally taken into account. To backstep the change of variable

$$\begin{aligned} z_3 &= \tau_\phi - \psi_2(\eta_2, z_2) \\ &= \tau_\phi + \kappa_3 z_2 + \mathcal{D}_{22}(\nu_2)\kappa_2\eta_2 + \mathcal{M}_{22}\kappa_2(z_2 - \kappa_2\eta_2) \\ &\quad + \mathcal{K}_{22,\eta_2}\eta_2 \end{aligned} \tag{C.40}$$

$$\dot{z}_3 = \dot{\tau}_\phi - \frac{\partial\psi_2}{\partial\eta_2}\dot{\eta}_2 - \frac{\partial\psi_2}{\partial z_2}\dot{z}_2 \tag{C.41}$$

is applied, where

$$\frac{\partial\psi_2}{\partial\eta_2} = -\kappa_2(\mathcal{D}_{22}(\nu_2) - \mathcal{M}_{22}\kappa_2) + 3\mathcal{K}_{22,\eta_2} \tag{C.42}$$

$$\frac{\partial\psi_2}{\partial z_2} = -(\kappa_3 + \mathcal{M}_{22}\kappa_2). \tag{C.43}$$

After introducing z_3, the system reads

$$\begin{aligned} \dot{\eta}_2 &= \nu_2 \\ \dot{\nu}_2 &= -\mathcal{D}'_{22}(\nu_2)\nu_2 - \mathcal{K}'_{22}\eta_2 + \tau'_\phi \\ \dot{z}_3 &= -\frac{1}{t_r}\tau_\phi + \frac{1}{t_r}\tau_{\max}\mathrm{sat}\left(\frac{\tau_c}{\tau_{\max}}\right) - \frac{\partial\psi_2}{\partial\eta_2}\dot{\eta}_2 - \frac{\partial\psi_2}{\partial z_2}\dot{z}_2. \end{aligned}$$

Substituting (C.40) into $\dot{z}_3$ gives

$$\begin{aligned} \dot{z}_3 = &\frac{1}{t_r}\tau_{\max}\mathrm{sat}\left(\frac{\tau_c}{\tau_{\max}}\right) - \frac{\partial\psi_2}{\partial\eta_2}\dot{\eta}_2 - \frac{\partial\psi_2}{\partial z_2}\dot{z}_2 \\ &- \frac{1}{t_r}(z_3 - \kappa_3 z_2 - \mathcal{D}_{22}(\nu_2)\kappa_2\eta_2 + \mathcal{K}_{22,\eta_2}\eta_2 \\ &- \mathcal{M}_{22}\kappa_2(z_2 - \kappa_2\eta_2)). \end{aligned} \tag{C.44}$$

Using the composite Lyapunov function

$$V_3(\eta_2, z_2, z_3) = V_2(\eta_2, z_2) + \frac{1}{2}z_3^2 \tag{C.45}$$

$$\begin{aligned} \dot{V}_3 &= \dot{V}_2 + z_3\dot{z}_3 \\ &\leq -(1-\theta_2)\kappa_2 c_1\eta_2^2 - z_3\left(\frac{\partial\psi_2}{\partial z_2}\dot{z}_2 + \frac{\partial\psi_2}{\partial\eta_2}\dot{\eta}_2\right) \\ &\quad + \frac{1}{t_r}z_3(\tau_c - z_3 + \kappa_3 z_2 + \mathcal{D}_{22}(\nu_2)\kappa_2\eta_2 \\ &\quad + \mathcal{M}_{22}\kappa_2(z_2 - \kappa_2\eta_2)) \\ &\quad - \left(-K_{\dot{\phi}} + \kappa_3 - \frac{\gamma_4^2}{4\theta_2\kappa_2 c_1}\right)z_2^2 \end{aligned} \tag{C.46}$$

Table C.1: Simulation Parameters

Fin	Controllers
$S = 16.6\ \mathrm{m}^2$	$\kappa_1 = 10^8\ \mathrm{kgms}^{-1}$
$\dot{\alpha}_{\max} = 15.8\,\mathrm{deg\ s}^{-1}$	$c_1 = 6.5 \cdot 10^7\ \mathrm{kgm}^2\mathrm{s}^{-2}$
$\alpha_{\mathrm{pb}} = 5\,\mathrm{deg}$	$\kappa_2 = 1\ \mathrm{s}^{-1}$
$t_r = \alpha_{\mathrm{pb}}/\dot{\alpha}_{\max} \approx 0.32\ \mathrm{s}$	$\kappa_3 \approx 3.24 \cdot 10^{10}\ \mathrm{kgm}^2\mathrm{s}^{-2}$
	$\kappa_4 = 1$

assuming $|\tau_c| \leq \tau_{\max}$. Selecting the control input τ_c as

$$\begin{aligned}\tau_c = \psi_3(\eta_2, z_2, z_3) = &-\kappa_3 z_2 - \kappa_2 \mathcal{D}_{22}(\nu_2)\eta_2 \\ &- \mathcal{M}_{22}\kappa_2(z_2 - \kappa_2\eta_2) \\ &+ t_r\left(\frac{\partial \psi_2}{\partial z_2}\dot{z}_2 + \frac{\partial \psi_2}{\partial \eta_2}\dot{\eta}_2\right) - \kappa_4 z_3\end{aligned} \tag{C.47}$$

with $\kappa_4 > 0$, gives

$$\begin{aligned}\dot{V}_3 \leq &-(1-\theta_2)k_2 c_1 \eta_2^2 - \frac{1}{t_r}(1+k_4)z_3^2 \\ &- \left(-K_{\dot{\phi}} + k_3 - \frac{\gamma_3^2}{4\theta_2 k_2 c_1}\right) z_2^2\end{aligned} \tag{C.48}$$

which is negative definite. Hence the origin of (C.44) is asymptotically stable [48, Lemma 14.2] with a region of attraction that is a function of $\tau_{\max}$. Note that in (C.47) $\dot{z}_2$ is computed based upon the knowledge of only the states of the roll subsystem. In fact $\dot{z}_2 = \dot{\nu}_2 + \kappa_2\nu_2$, where $\dot{\nu}_2$ is given by (C.29b).

C.4 Simulations

The designed control laws were tested carrying out simulations with the plant model. Some simulations parameters are listed in Table C.1, where $\dot{\alpha}_{\max}$ is the slew rate saturation, and α_{pb} is the hydraulic proportional band. The parameters referring to the container vessel can be found in [36].

The efficacy of the combined control action was evaluated comparing the responses of the plant model when only either the fin stabiliser or the speed controller were active (Figs. C.2-C.3). The control action is activated when the

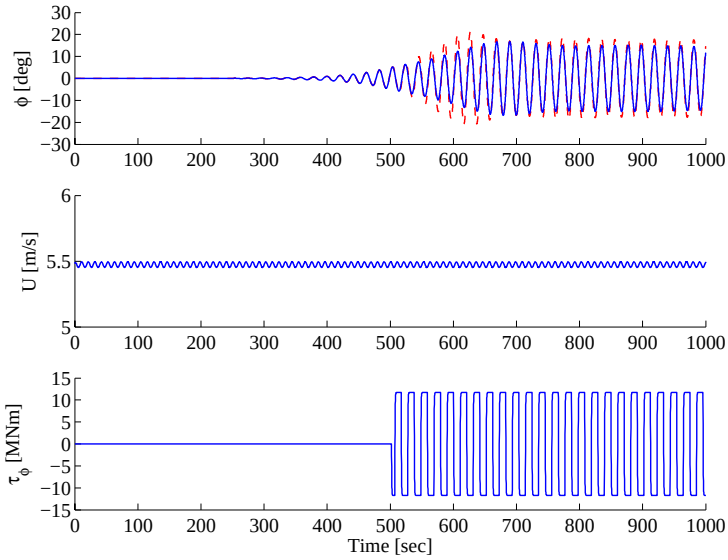

Figure C.2: Stabilisation of roll angle ϕ with only fin stabiliser active. Roll in parametric resonance (red dashed curve)

roll angle ϕ is about 5°. Fig. C.2 clearly shows that the control torque supplied by the fins is not enough to damp out the motion, but only a small reduction in roll oscillations can be achieved. Conversely, a small variation in ship forward ($\Delta U = 0.5$ m/s) speed has a stronger influence in the development of parametric roll, as Fig. C.3 illustrates, but it is not sufficient to bring the roll motion to zero.

Figs. C.4-C.5 are examples of how the combined control action works. First the speed controller is activated when the roll angle is about 5°, and the ship forward speed is increased or decreased according to the new set-point. When the new forward speed set-point is about to be reached the fin stabiliser takes over driving the roll motion to zero. The efficacy and the velocity of the control action is strictly dependent on the new value of the ship forward speed. In fact, by comparing Fig. C.4 with Fig. C.5 it can be noticed that even if $|\Delta U| = 2$ m/s in both cases, increasing or decreasing the speed determine a different performance of the fin stabiliser, as shown by the control torque τ_ϕ supplied by the fins.

The control torque τ_ϕ depends on the amount of lift that the fins are able to produce, and this in turn is proportional to the square of the flow velocity. Therefore, increasing the ship forward speed makes the overall control law more

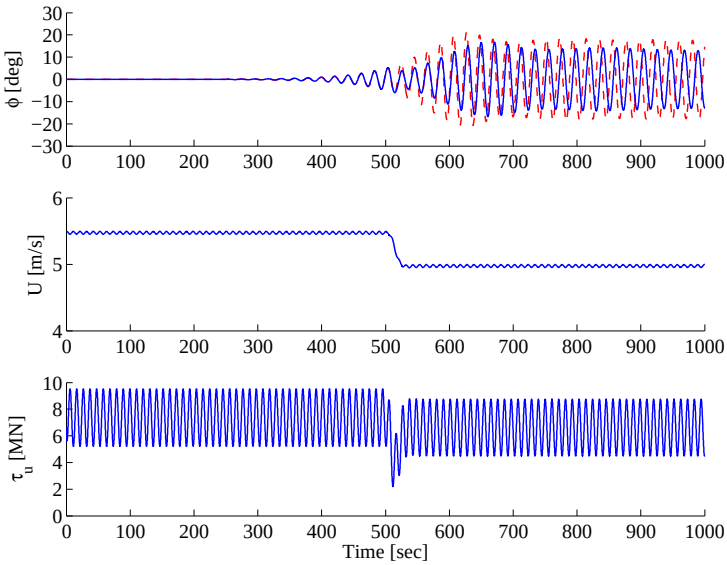

Figure C.3: Stabilisation of roll angle ϕ with only speed controller active. Roll in parametric resonance (red dashed curve)

effective; in addition to de-tuning the frequency coupling condition $\omega_e \approx 2\omega_\phi$, it increases the maximum control torque that the fin stabiliser can supply to damp out the roll motion.

C.5 Conclusions

A combined speed and fin stabiliser controller was developed applying nonlinear control methods.

A nonlinear backstepping-based fin stabiliser was developed, capable of driving the roll motion asymptotically to zero in a region of attraction that is a function of the maximum control moment the fins can supply.

A speed controller was developed applying classical Lyapunov stability theory. In the presence of a permanent time-varying disturbance (i.e. waves) this controller guarantees that the surge speed is globally uniformly ultimately bounded, where the ultimate bound is a function of the disturbance amplitude.

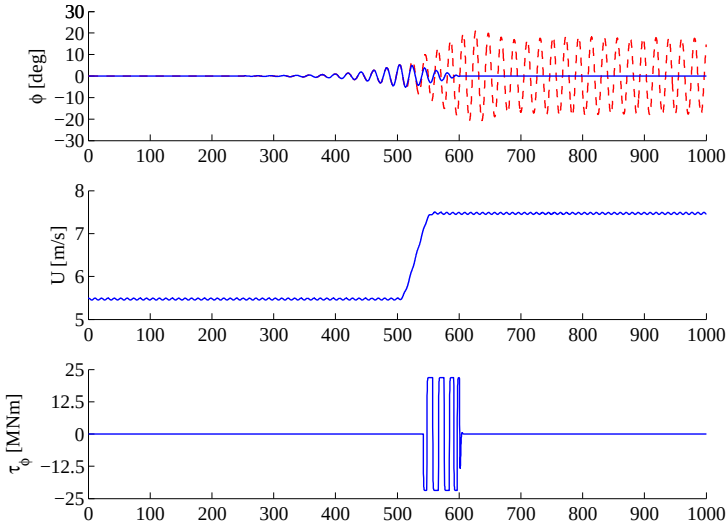

Figure C.4: Stabilisation of roll angle ϕ using the plant model ($\Delta U = 2$ m/s, $\tau_{\phi,\max} = 21.8$ MNm). Roll in parametric resonance (red dashed curve)

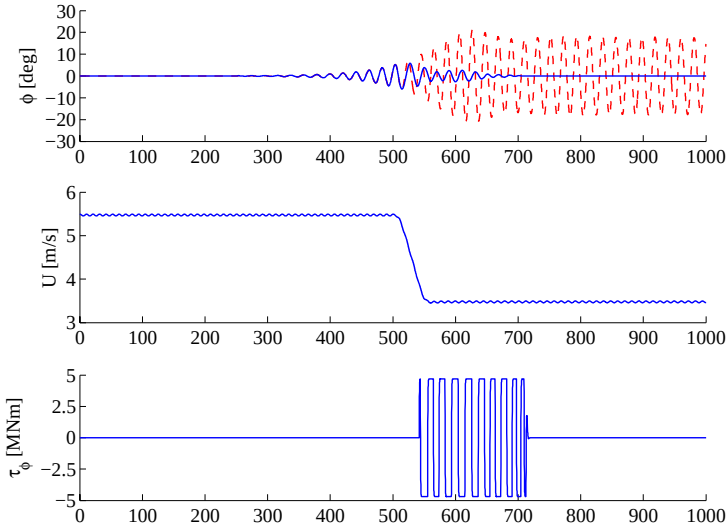

Figure C.5: Stabilisation of roll angle ϕ using the plant model ($\Delta U = -2$ m/s, $\tau_{\phi,\max} = 4.7$ MNm). Roll in parametric resonance (red dashed curve)

The combined action of the two controllers stabilised the roll motion in parametric resonance condition. Moreover, the performance of the fin stabiliser was improved by the speed controller, because positive variations in forward speed allowed for a larger control torque.

These results were verified by simulating the combined control law with a high fidelity model.

Appendix

Time-varying disturbance

The disturbance acting on the surge subsystem is given by

$$\begin{aligned} e_1(\nu_1, t) &= F_x^{FK} \\ &= \gamma_1(\omega + k\nu_1)[\sin(\omega t + kL_s + k\eta_1) \\ &\quad - \sin(\omega t + k\eta_1)] \\ &= \gamma_1\omega[\sin(\omega t + kL_s + k\eta_1) - \sin(\omega t + k\eta_1)] \\ &\quad + \gamma_1 kz_1[\sin(\omega t + kL_s + k\eta_1) - \sin(\omega t + k\eta_1)] \\ &\quad + \gamma_1 k\nu_d[\sin(\omega t + kL_s + k\eta_1) - \sin(\omega t + k\eta_1)]. \end{aligned} \tag{C.49}$$

Since the following trigonometry relationship holds

$$\sin\alpha - \sin\beta \leq |\sin\alpha - \sin\beta| \leq |\sin\alpha| + |-\sin\beta| \leq 2,$$

then the time-varying disturbance satisfies the following inequality

$$\begin{aligned} e_1(\nu_1, t) &\leq 2\gamma_1\omega + 2\gamma_1 kz_1 + 2\gamma_1 k\nu_d \\ &\leq 2\gamma_1\omega + 2\gamma_1 kz_1 + 2\gamma_1 k\nu_{d,\max} \end{aligned} \tag{C.50}$$

where $\nu_{d,\max}$ is the upper bound of the reference trajectory.

Paper D

Parametric Roll Resonance Detection on Ships from Nonlinear Energy Flow Indicator

---

Published in *Proceedings of the 7th IFAC International Symposium on Fault Detection, Supervision and Safety of Technical Processes*, 2009.

Abstract: The detection of the onset of parametric roll resonance on ships is of a central importance in order to activate specific control strategies able to counteract the large roll motion. One of the main priorities is to have detectors with a small detection time, such that warnings can be issued when the roll oscillations are about 5°. This paper proposes two different detection approaches: the first one based on sinusoidal detection in white gaussian noise; the second one utilizes an energy flow indicator in order to catch the onset of parametric roll based upon the transfer of energy from heave and pitch to roll. Both detectors have been validated against experimental data of a scale model of a container vessel excited with both regular and irregular waves. The detector based on the energy flow indicator proved to be very robust to different scenarios (regular/irregular waves) since it does not rely on any specific assumption on the signal to be detected.

Keyword: Statistical methods; Marine systems; Parametric resonance; Roll resonance

D.1 Introduction

Parametric roll is a well known critical phenomenon characterized by a sudden and quick rise of roll oscillations, which may bring the ship into conditions dangerous for the ship, the cargo and the crew. Recent casualties involving damages and losses for million of dollars, as those reported by [20] and [13], have brought a raising attention of the scientific community on analyzing the nature of parametric roll in head sea, in order to determine the principal conditions which origin the phenomenon itself.

Parametric roll is known to occur when a ship sails in moderate to heavy longitudinal or oblique seas; the wave passage along the hull and the wave excited vertical motions result in variations of the intercepted waterplane area, and in turn, in relevant changes in the restoring characteristics. The onset and buildup of parametric roll is due to the occurrence of concomitant conditions: the wave length is close to the ship length ($\lambda_w \approx L_{PP}$), the ship approaches waves with encounter frequency almost twice the roll natural frequency ($\omega_e \approx 2\omega_\phi$), and the wave height is greater than a ship-dependent threshold ($h_w > \overline{h}_s$).

In order to counteract the development of parametric roll control actions must be taken at proper time. Valuable control strategies have been proposed using different actuators – e.g. fin stabilizers and cruise control ([28]); active U-tanks ([38]) – but the effectiveness of the control action has been shown to be very much related to the readiness of the controller in taking over. In fact the

available actuators can deliver a finite control action proportional to actuator dimensions and to other physical variables, e.g. ship forward speed for fin-induced roll moment; therefore they are not able to damp out the roll motion if its magnitude has already overcome an actuator related threshold. Then it is important to have detection tools, which are able to ensure an early warning when the parametric roll has still to onset or, anyway, before the roll oscillations reach critical values. Considering that this resonant phenomenon takes about 10 roll periods before being fully developed, it is crucial to have a detector that can carry out detection at least 5 roll periods before critical oscillations take place.

The possibility of detecting the onset of the resonant motion appears then to be a critical factor in order to perform the proper control action at the proper time. To the author's knowledge very little contribution has been provided from the scientific community to this aspect of the problem. Holden et al. [36] proposed an observer based predictor, which making use of different estimation schemes, estimates the eigenvalues of a linear second-order oscillatory system describing the roll motion and issues a warning when those move into the right-half plane. McCue and Bulian [52] studied the possibility of using finite time Lyapunov exponents to detect the onset of parametric roll for ships operating in irregular seas condition. The authors pointed out the opportunity of identifying warnings of parametric roll inception by looking at the behavior of the Lyapunov exponents. It is also worth to mention that some commercial on-board warning system are available, as the SeaSense ([63]) and the Amarcon's OCTOPUS Resonance[1], which support the officer-on-watch by polar diagrams displaying the dangerous sea areas for the ship with an horizon of prediction of some hours.

This works aims at detecting the onset of parametric roll in a short time horizon by using of statistical change detection tools. Two scenarios are taken into consideration: regular and irregular longitudinal seas induced parametric roll. Due to the particular sailing condition, the roll motion is not directly excited by the wave motion, but the parametric resonance takes place because of a transfer of energy from the vertical ship motions, i.e. heave and pitch, to the transverse motion of the ship. Therefore the design of detection schemes based only upon the roll motion seems unlikely to provide the early warning needed in order to apply ad-hoc control strategies.

The proposed detection schemes operate in the frequency domain, focusing on the evolution of the power spectrum of the signals at hand over time. Heave and pitch, which are directly excited by the sea motion, are monitored in order

[1] http://www.amarcon.com/products/index.html?main=http://www.amarcon.com/products/resonance.html

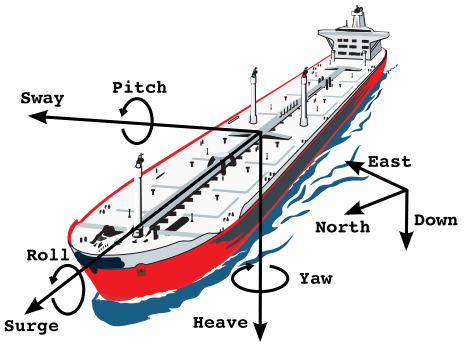

Figure D.1: Ship motions (by courtesy of [36]).

to determine if the vessel is approaching waves with encounter frequency that could trigger parametric roll. If this turns to be the case the spectrum of the roll motion is analyzed to evaluate if there is an increase of energy.

The efficacy of the proposed detectors is validated against a set of experimental data of a 1:45 scale model of container ship with a length overall of 294 m.

Part of the results in this paper are covered by a pending patent[2].

D.2 Heave-Pitch-Roll motion

This section shortly introduces a simplified model of heave-pitch-roll motion in order to give the general understanding of how parametric roll resonance develops. The simplified model is presented referring to [77], who employ a two mass-spring-damper system connected to a pendulum in order to describe the couplings between the three degrees of freedom.

Let $[z\ ,\ \phi\ ,\ \theta]$ be the generalized position vector, where z is heave, ϕ is roll, and θ is pitch (see Fig. D.1). The equation of motions in dimensionless form

[2]EP: 09157857.5, US: 61/169,154

are given as ([77])

$$\begin{aligned}
&\bar{z}'' + \kappa_1 \bar{z}' + q_1^2 \bar{z} + \mu_1(\phi'' \sin\phi + \phi'^2 \cos\phi) = a\eta^2 \cos\eta\tau \\
&\bar{\theta}'' + \kappa_2 \bar{\theta}' + q_2^2 \bar{\theta} + \mu_2(\phi'' \sin\phi + \phi'^2 \cos\phi) = a\eta^2 \cos(\eta\tau - \psi) \\
&\phi'' + \kappa_0 \phi' + \sin\phi + \frac{1}{2}[\bar{z}'' - a\eta^2 \cos\eta\tau \\
&\qquad + \bar{\theta}'' - a\eta^2 \cos(\eta\tau - \psi)] = 0,
\end{aligned} \tag{D.1}$$

where $\bar{z} = z/l$, $\bar{\theta} = \theta/l$, l is the length of the pendulum rod, $\eta = \omega_e/\omega_\phi$ is the ratio between the frequency of the external excitation and the natural roll frequency, and differentiation is done with respect to $\tau = \sqrt{g/l}t = \omega_\phi t$, i.e. $z' = \mathrm{d}z/\mathrm{d}\tau$. For the details about the other constant coefficients refer to ([77]).

The steady-state solution of the system (D.1) is

$$\begin{aligned}
\bar{z}_0(t) &= (A_1 \cos\omega_e t + B_1 \sin\omega_e t) \\
\bar{\theta}_0(t) &= (A_2 \cos\omega_e t + B_2 \sin\omega_e t) \\
\phi_0(t) &= 0,
\end{aligned} \tag{D.2}$$

and its stability can be studied by perturbations methods. It can be shown ([77]) that the perturbed system has the following form

$$\begin{aligned}
z_1'' + \kappa_1 z_1' + q_1^2 z_1 &= 0 \\
\theta_1'' + \kappa_2 \theta_1' + q_2^2 \theta_1 &= 0 \\
\phi_1'' + \kappa_0 \phi_1' + \phi_1 - \frac{1}{2} a\eta^2 (E\cos\eta\tau + F\sin\eta\tau)\phi_1 &= 0,
\end{aligned} \tag{D.3}$$

where z_1, θ_1, ϕ_1 are the perturbations in heave, pitch and roll, respectively, $E = f(A_j, \psi)$, and $F = f(B_j, \psi)$. The first two equations of system (D.3) are asymptotically stable, whereas the third equation is a Mathieu equation, which is known to be instable for $\eta \approx 2$. The instability of the trivial solution in roll arises from a transfer of energy from heave and pitch into the second harmonic of roll; in fact $\eta \approx 2$ means that the external excitation driving the system is approximately at a frequency twice the natural roll frequency.

D.3 Frequency-based detection

Two detection schemes are proposed in the following, both work in the frequency domain. The first detector performs sinusoidal detection in white gaussian noise; the second checks for the transfer of energy between the motion in the vertical plane and the transverse plane making use of the cross-spectrum of pitch and

the second harmonic of roll. Although the two detectors use different methods in order to determine the possibility of the onset of parametric roll, both detection schemes have as first step the estimation of the encounter frequency ω_e in order to evaluate if it is in a range where parametric roll resonance is likely to happen.

D.3.1 Encounter frequency estimation

The estimation of ω_e is carried out exploiting the heave and pitch motions. Assuming that the sea motion can be modeled as regular waves, then the wave elevation is

$$\zeta(t) = A_w \sin(\omega_e t + \psi_w), \tag{D.4}$$

where A_w is the wave amplitude, and ψ_w is the phase. The responses in heave and pitch have the first harmonic centered at the frequency of the excitation

$$z(t) = A_z \sin(\omega_e t + \psi_z) + \text{h.o.h.} \tag{D.5}$$
$$\theta(t) = A_\theta \sin(\omega_e t + \psi_\theta) + \text{h.o.h.}, \tag{D.6}$$

where A_z, A_θ are heave and pitch amplitudes, and ψ_z, ψ_θ are heave and pitch phases, respectively. Computing the power spectrum of heave and pitch and maximizing them over the frequency, an estimation of ω_e can be obtained

$$\hat{\omega}_e = \arg\max(Z(\omega), \Theta(\omega)), \tag{D.7}$$

where $Z(\omega)$ and $\Theta(\omega)$ are the power spectra of heave and pitch, respectively. If $\hat{\omega}_e \in [\omega_{e,\min}\ ,\ \omega_{e,\max}]$, that is the range of frequencies in which parametric roll can develop, then a low level warning is issued.

D.3.2 Sinusoidal detection in WGN

Applying perturbation methods to the Mathieu equation (see [31], [25]) an approximate solution to the roll motion in parametric resonance can be found as

$$\phi(t) \approx C_\phi(t) \cos\left(\frac{1}{2}\omega_e t + \psi_\phi\right) + \text{h.o.h.} \tag{D.8}$$

where $C_\phi(t)$ is the envelope of the sinusoidal motion, and ψ_ϕ is the roll phase angle. Therefore, the roll response in parametric resonance can be modeled as a sinusoid whose amplitude grows over time.

The parametric roll detection can then be seen as the detection of a sinusoidal signal with amplitude and phase unknown in white gaussian noise (WGN). As shown in ([46]), the detection problem can be formulated as

$$\begin{aligned} \mathscr{H}_0 &: \; x[n] = w[n] \\ \mathscr{H}_1 &: \; x[n] = C_\phi \cos(\omega_\phi n + \psi_\phi) + w[n] \;\; n = 0, \ldots, N-1 \end{aligned} \tag{D.9}$$

where the unknown parameters C_ϕ and ψ_ϕ are deterministic, the frequency ω_ϕ is equal to $\frac{1}{2}\hat{\omega}_e$, $w[n]$ is WGN with known variance σ^2, and $N-1$ is the number of samples of the signal that are taken into account.

Using the GLRT (Generalized Likelihood Ratio Test), the detector decides $\mathscr{H}_1$ if

$$\frac{p(\mathbf{x}; \hat{C}_\phi, \hat{\psi}_\phi, \mathscr{H}_1)}{p(\mathbf{x}; \mathscr{H}_0)} > \gamma, \tag{D.10}$$

where $\hat{C}_\phi$ and $\hat{\psi}_\phi$ are the MLE (Maximum Likelihood Estimate) of the true parameters, and γ is a threshold set by the probability of false alarms P_{FA} the detector is desired to have.

Kay [46] showed that, once the MLE of amplitude and phase shift have been obtained, the detector decides $\mathscr{H}_1$ if

$$\Phi(\omega_\phi) > \sigma^2 \ln \gamma = \gamma', \tag{D.11}$$

where $\Phi(\omega)$ is the power spectrum of roll. Therefore, the detection of the onset of parametric roll resolves in computing the power spectrum of roll and evaluating if, at $\omega_\phi = \frac{1}{2}\hat{\omega}_e$, it overcomes a given threshold. The threshold γ' can be found in terms of P_{FA} as ([46])

$$\gamma' = -\sigma^2 \ln(P_{\text{FA}}). \tag{D.12}$$

D.3.3 Energy flow detection using cross-spectrum

Since the onset and development of parametric roll is due to the transfer of energy from the motions in the vertical plane, directly excited by the wave motion, to the motion in the transverse plane, at a frequency about twice the natural roll frequency. Therefore, an increase of power about the second harmonic in roll can be used as a measure of the development of parametric roll.

Given two signals, e.g. $\phi(t)$ and $\theta(t)$, the cross-correlation provides a measure of similarity of the two waveforms as a function of time lag. If the two signals

are discrete sequences then the cross-correlation is defined as

$$r_{\phi\theta}[k] \triangleq \sum_{k=-\infty}^{\infty} \phi^*[k]\theta[n+k], \tag{D.13}$$

where k is the time lag, and ϕ^* denotes the complex conjugate of ϕ. The cross-correlation function carries information about which frequency components are held in common between the two signals. In order to have a clear interpretation of the shared frequency content the cross-spectrum must be computed. The cross-spectrum is defined as the Fourier transform of the cross-correlation function

$$P_{\phi\theta}(\omega) \triangleq \sum_{k=-\infty}^{\infty} r_{\phi\theta}[k]e^{-j\omega k}. \tag{D.14}$$

The magnitude of the cross-spectrum describes which frequency components of $\phi[n]$ are associated with large or small amplitudes at the same frequency of $\theta[n]$. Since the frequency component carrying useful information about the onset of parametric roll resonance is the second harmonic in roll, the detection problem can be cast as thresholding of the cross-spectrum of $\phi^2[n]$ and $\theta[n]$.

The parametric roll detection problem is then formulated as

$$\begin{aligned} \mathscr{H}_0 &: \; P_{\phi^2\theta}(\omega) \leq \bar{P} \\ \mathscr{H}_1 &: \; P_{\phi^2\theta}(\omega) > \bar{P} \end{aligned} \tag{D.15}$$

where $\bar{P}$ is a threshold in power. Instead of using directly the cross-spectrum, an energy flow coefficient could be exploited, defined as

$$e_f \triangleq \frac{\sigma^2_{\phi^2\theta}}{\sqrt{\sigma^2_{\phi^2}\sigma^2_{\theta}}}. \tag{D.16}$$

The detection problem can then be rewritten as

$$\begin{aligned} \mathscr{H}_0 &: \; e_f \leq \bar{e} \\ \mathscr{H}_1 &: \; e_f > \bar{e} \end{aligned} \tag{D.17}$$

where $\bar{e}$ is the minimum level of energy to be transferred in order to trigger parametric roll.

D.3.4 Recursive implementation

Both the proposed methods have been implemented in a recursive fashion in order to allow real-time detection. Since both the sinusoidal detector and the

energy flow detector are based on the computation of some spectra, which is done applying the FFT (Fast Fourier Transform) to the data series at hand, it is important to fix the window length such that an acceptable frequency resolution is achieved.

The window length was chosen as a multiple integer of the natural roll period, i.e. $N = rT_\phi$ where T_ϕ is the roll period and $r \in \mathbb{N}$. Moreover, in order to achieve a quick detection, the computation of the spectra is updated every quarter of the window length, i.e. there is 75% overlap between two consecutive windows.

D.4 Detection schemes validation

The proposed detection schemes have been validated against a set of experimental data of a 1:45 scale model of a container vessel with a length overall of 294 m. The experiments were conducted in a towing tank with both regular and irregular waves, varying wave frequency and height, and ship forward speed. Eleven runs were considered for the regular wave case (see Table E.1 for the experiment parameters), and eight runs for the irregular wave case (see Table D.2 for the experiment parameters). Figure D.2 shows a time series for regular waves excitation.

Table D.1: Regular wave experiments

Exp.	A_w [m]	ω_w [rad/s]	ω_e/ω_ϕ	$\lvert\phi_{\max}\rvert$ [deg]
1192	2.5	0.4640	1.9021	0.8944
1193	2.5	0.4640	1.9226	1.8932
1191	2.5	0.4640	1.9428	21.7800
1172	2.5	0.4640	1.9633	23.9270
1184	2.5	0.4640	1.9834	22.7810
1185	2.5	0.4640	2.0032	20.8780
1186	2.5	0.4640	2.0234	21.5640
1187	2.5	0.4640	2.0439	20.4990
1188	2.5	0.4640	2.0842	22.7190
1190	2.5	0.4640	2.1047	1.4291
1189	2.5	0.4640	2.1245	1.4368

For the sinusoidal detection in WGN the probability of false alarms P_{FA} was computed as the reciprocal of the desired time between false alarms T_{FA}. Setting $T_{\text{FA}} = 6$ months, the probability of false alarms is $P_{\text{FA}} = 1/T_{\text{FA}} \approx 6.5 \cdot 10^{-8}$. The variance σ^2 of the noise $w[n]$ was chosen as the weighted mean value of the variances of the roll angle in those experiments where parametric roll did not

Table D.2: Irregular wave experiments

Exp.	H_s [m]	T_p [s]	$\lvert\phi_{\max}\rvert$ [deg]
1194	9	13.54	2.91
1195	9	13.54	17.24
1196	9	13.54	2.88
1197	7	13.54	1.68
1198	7	13.54	4.23
1199	9	13.54	1.83
1200	9	13.54	1.74
1201	9	13.54	1.45

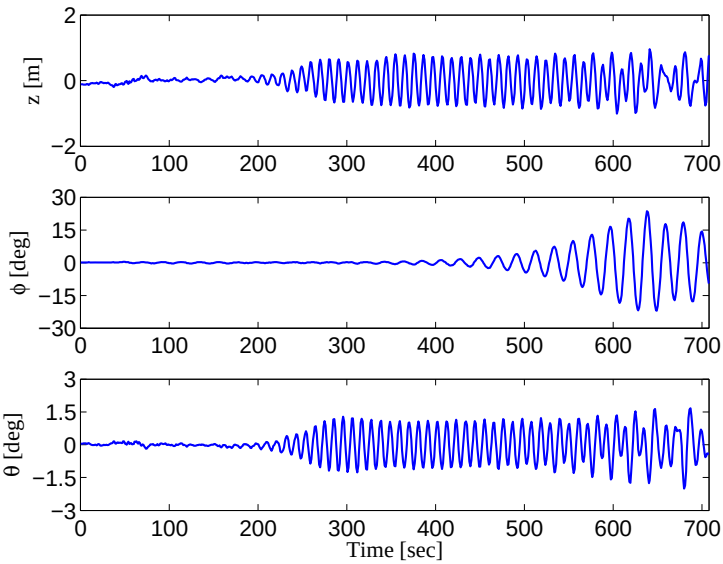

Figure D.2: Exp. 1172: parametric roll did occur.

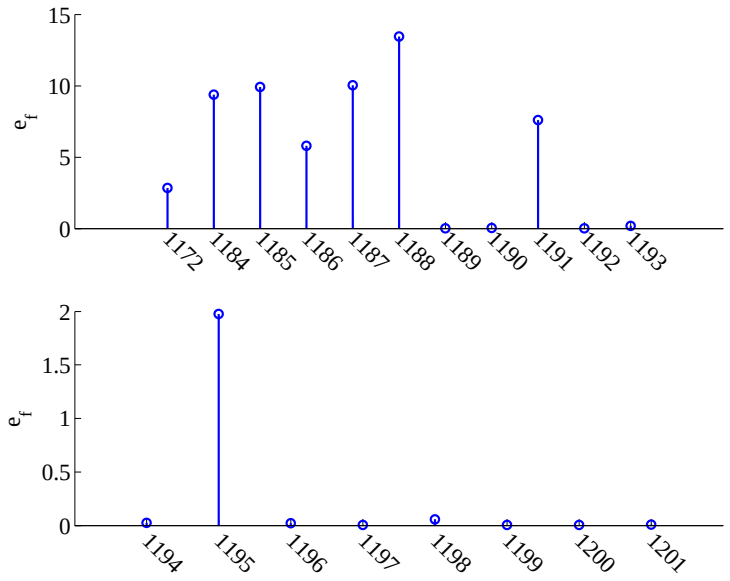

Figure D.3: e_f coeff. for regular (t) and irregular (b) waves exp.

occur, that is

$$\sigma^2 = E[\sigma_\phi^2] = \frac{\sum_{j=1}^{M} w_j \sigma_{\phi_j}^2}{\sum_{j=1}^{M} w_j}, \tag{D.18}$$

where $E[\cdot]$ is the function expected value, $\sigma_{\phi_j}^2$ is the variance of the roll motion of the j-th experiment, $w_j = 1/L_j$ is the weight given as the reciprocal of the time series length L_j, and M is the number of experiments where parametric roll did not occur.

For the energy flow detection the threshold $\bar{e}$ was instead chosen according to the trend of the e_f coefficient over the set of experiments. Figure D.3 shows that there is a very large gap in values of e_f between the experiments where parametric roll occur and those where the resonant motion did not onset, both for regular and irregular waves. Note that due to the non stationarity of the process ϕ^2 the range of variability of the energy flow coefficient e_f is much larger than for a cross-correlation coefficient, which usually takes values in the interval $[-1, 1]$.

D.4.1 Regular waves

The detection performances of the two detectors for the regular waves data set are summarized in Tables E.3-D.4 for window length $N = T_\phi \approx 21$ s. Comparing detection time T_d and the maximum roll angle reached within the detection time $|\phi_{\max}(T_d)|$, it is possible to point out that the sinusoidal detector performs a quicker detection than the energy flow detector, issuing an early warning when the roll angle is still less than 5°. Moreover, none of the detectors issued false alarms for the data set at hand, reaching 100% of correct detection. An example of parametric roll detection using the sinusoidal and the energy flow detectors is shown in Figs. D.4-D.5.

Table D.3: Sinusoidal detection: regular waves

Exp.	T_d [s]	$\lvert\phi_{\max}(T_d)\rvert$ [deg]	PR	Detection
1172	454	2.21	Yes	Correct
1184	274	2.31	Yes	Correct
1185	340	2.02	Yes	Correct
1186	430	2.20	Yes	Correct
1187	340	2.24	Yes	Correct
1188	286	2.35	Yes	Correct
1189	-	-	No	Correct
1190	-	-	No	Correct
1191	286	2.45	Yes	Correct
1192	-	-	No	Correct
1193	-	-	No	Correct

Table D.4: Energy flow detection: regular waves

Exp.	T_d [s]	$\lvert\phi_{\max}(T_d)\rvert$ [deg]	PR	Detection
1172	520	5.54	Yes	Correct
1184	364	5.83	Yes	Correct
1185	400	4.34	Yes	Correct
1186	496	4.56	Yes	Correct
1187	412	4.75	Yes	Correct
1188	400	4.21	Yes	Correct
1189	-	-	No	Correct
1190	-	-	No	Correct
1191	340	4.97	Yes	Correct
1192	-	-	No	Correct
1193	-	-	No	Correct

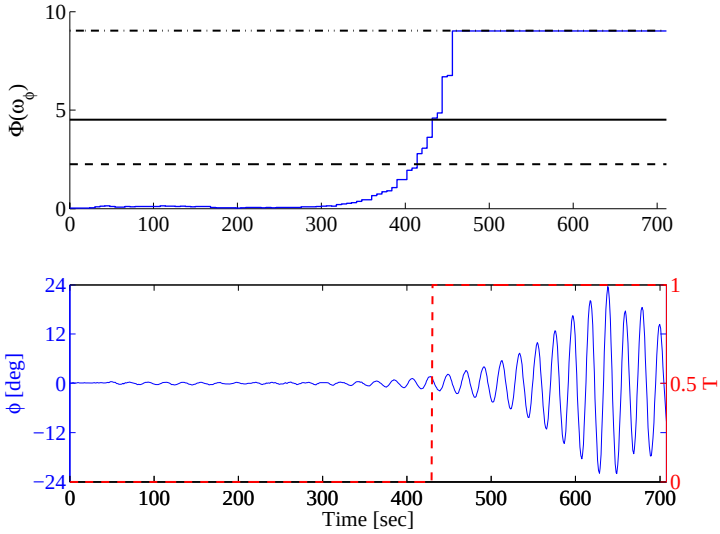

Figure D.4: Exp. 1172: detection using the sinusoidal detector.

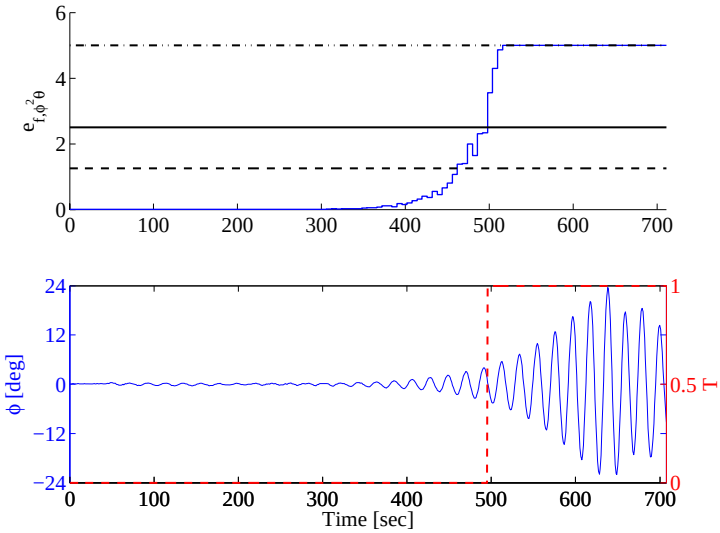

Figure D.5: Exp. 1172: detection using the energy flow detector.

D.4.2 Irregular waves

The detection performances of the two detectors for the irregular waves experiments are illustrated in Tables E.4-D.6 for window length $N = T_\phi \approx 21$ s. The performances of the two detectors are very much comparable: a quick detection of the onset of parametric roll in experiment 1195 is achieved by both detectors (see Figs. D.6-D.7), and only in one experiment false alarms are issued (see Fig. D.8).

Table D.5: Sinusoidal detection: irregular waves

Exp.	T_d [s]	$\lvert\phi_{\max}(T_d)\rvert$ [deg]	PR	Detection
1194	-	-	No	Correct
1195	106	4.14	Yes	Correct
1196	-	-	No	Correct
1197	-	-	No	Correct
1198	202	3.40	No	2 False Pos.
1199	-	-	No	Correct
1200	-	-	No	Correct
1201	-	-	No	Correct

Table D.6: Energy flow detection: irregular waves

Exp.	T_d [s]	$\lvert\phi_{\max}(T_d)\rvert$ [deg]	PR	Detection
1194	-	-	No	Correct
1195	94	3.27	Yes	Correct
1196	-	-	No	Correct
1197	-	-	No	Correct
1198	220	3.89	No	False pos.
1199	-	-	No	Correct
1200	-	-	No	Correct
1201	-	-	No	Correct

D.4.3 Detector robustness

The performances of the two detectors were evaluated for increasing length of the computational window N with r ranging from 1 to 4. Table D.7 summarizes the detection performances in terms of number of experiments where false alarms were issued by the sinusoidal detector (SD) and the energy flow detector (EF). It is clear that increasing the window length the performances of the sinusoidal detector gradually degraded, whereas the energy flow detector appeared to be very robust, improving its detection rate for the irregular wave data set indeed.

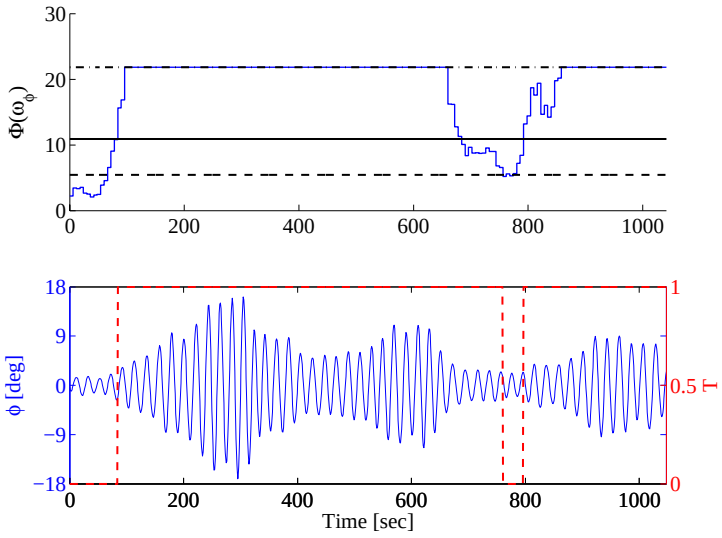

Figure D.6: Exp. 1195: detection using the sinusoidal detector.

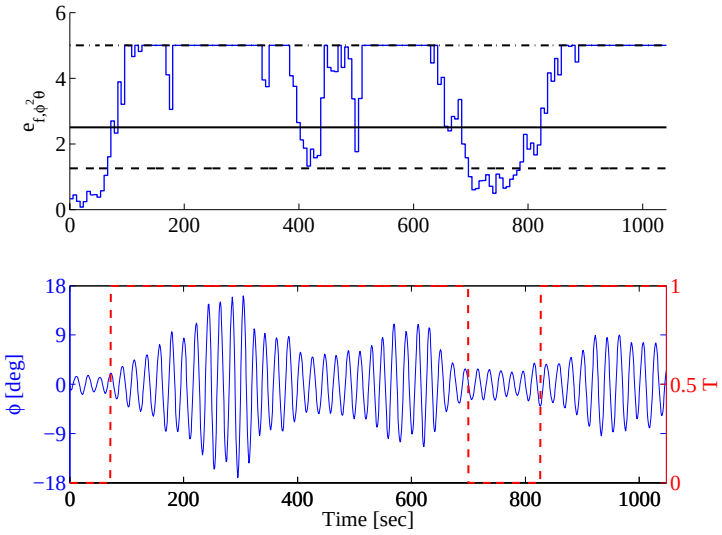

Figure D.7: Exp. 1195: detection using the energy flow detector.

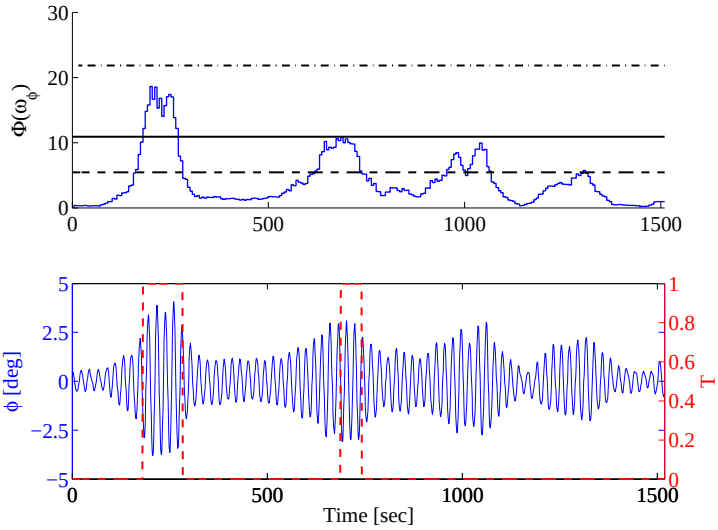

Figure D.8: Exp. 1198: false alarms issued by the sinusoidal detector.

Table D.7: Detection robustness

	Regular waves		Irregular waves	
r	SD	EF	SD	EF
1	0	0	1	1
2	3	0	4	1
3	3	0	4	0
4	3	0	7	0

D.5 Conclusions

Two detection approaches have been proposed to determine when parametric roll resonance occurs on ships. The two detectors have been validated against experimental data of a 1:45 scale model of a container vessel, excited both with regular and irregular waves. The detection performances are summarized in Table D.8, which refers to the results showed in Tables E.3-D.6.

The two detectors performs equally well in terms of detection rate, which in total is equal to 94.7%. The sinusoidal detector showed good detection performances – small detection time T_d, no false alarms – on the experiments run with regular waves. The energy flow indicator showed a higher detection time in all the regular waves experiments than the sinusoidal detector, whereas it performs better for the irregular waves experiments.

When increasing the window length for the computation of the detection indexes, the detection rate of the sinusoidal detector worsened, while the energy flow detector improves its detection performances. The robustness of this detection scheme is believed to reside in the fact that the detector looks at the energy flow from the vertical modes of the ship (heave and pitch) to the roll mode, without taking directly into account any particular model for the signals at hand.

Table D.8: Comparison of detectors: accuracy

	Sinusoidal Det.	Energy Flow Det.
Total accuracy	94.7%	94.7%
Reg. wave accuracy	100.0%	100.0%
Irreg. wave accuracy	87.5%	87.5%

Acknowledgements

The authors are thankful to Dr. Drummen and Dr. Perez from CeSOS, and to Dr. Storhaug from DNV for performing the experiments at the Centre for Marine Technology in Trondheim.

Paper E

Parametric Roll Resonance Detection using Phase Correlation and Log-likelihood Testing Techniques

---

Published in *Proceedings of the 8th IFAC International Conference on Manoeuvring and Control of Marine Craft*, 2009.

This paper has been awarded as the "Best Regular Paper" of the conference.

Abstract: Real-time detection of parametric roll is still an open issue that is gathering an increasing attention. A first generation warning systems, based on guidelines and polar diagrams, showed their potential to face issues like long-term prediction and risk assessment. This paper presents a second generation warning system the purpose of which is to provide the master with an onboard system able to trigger an alarm when parametric roll is likely to happen within the immediate future. A detection scheme is introduced, which is able to issue a warning within five roll periods after a resonant motion started. After having determined statistical properties of the signals at hand, a detector based on the generalised log-likelihood ratio test (GLRT) is designed to look for variation in signal power. The ability of the detector to trigger alarms when parametric roll is going to onset is evaluated on two sets of experimental data, covering both regular and irregular seas in a model basin.

Keyword: Change detection, Parametric roll resonance, Phase correlation, GLRT

E.1 Introduction

Parametric roll is a resonant motion characterised by a sudden and quick rise of roll oscillation that may bring the vessel into conditions dangerous for the cargo, the crew and the hull integrity. Parametric roll is known to occur when a ship sails in moderate to heavy longitudinal or oblique seas; the wave passage along the hull and the wave excited vertical motions result in variations of the intercepted waterplane area and in turn, changes the roll restoring characteristics. The onset and further development of parametric roll has been thoroughly analysed by the scientific community and major conditions have been identified that trigger this dangerous phenomenon: the wave length is close to the ship length ($\lambda_w \approx L_{PP}$), the ship approaches waves with encounter frequency almost twice the roll natural frequency ($\omega_e \approx 2\omega_\phi$), and the wave height is greater than a ship-dependent threshold ($h_w > \bar{h}$).

This phenomenon, well-known since the 1950's for fishing vessels sailing in following seas, caught a renewed attention 10 years ago when the container ship *APL China* experienced parametric rolling in extremely high head seas caused by typhoon-type weather conditions in the north Pacific Ocean. As reported by France et al. [20] the post-Panamax C11 experienced roll motion up to 40° together with extreme pitching, which caused devastation of the cargo: one third of the containers on deck were lost overboard and another third were in various conditions of damage. Back in 2003 Carolina Mærsk, a Panamax container ship, encountered a storm in the north Atlantic Ocean and suffered roll motion up to 47° [13]. Losses counted about 133 containers and water damages of different

severity were reported on another 50 containers. Price tag: more than 4 millions of dollars for cargo claims.

Two questions recently came to the attention of the technical/scientific community:

- Why is the detection of parametric roll needed?
- What kind of warning systems are needed now?

Døhlie [15] gave a very clear answer to the first question stating: "the insurance industry has also put pressure on the ship owners to take steps to avoid parametric rolling. At first, when it was comparatively unknown, claims for this could be successfully submitted, but now that there is greater knowledge of this, it may not be an obvious insurance claim". Moreover, Dølhie pointed out the necessity to develop *second generation warning systems*, capable to deal with the critical phenomenon in a short prediction horizon, to be integrated with the first generation warning systems based on guidelines for mariners and polar diagrams (as the SeaSense [63] and the Amarcon's OCTOPUS Resonance [1]).

Only little contribution has been provided from the scientific community in the direction suggested by Dølhie. Holden et al. [36] proposed an observer based predictor, which making use of different estimation schemes, estimates the eigenvalues of a linear second-order oscillatory system describing the roll motion and issues a warning when those move into the right-half plane. McCue and Bulian [52] studied the possibility of using finite time Lyapunov exponents to detect the onset of parametric roll for ships operating in irregular sea conditions and mentioned the possibility of issuing warnings of parametric roll from the behaviour of the Lyapunov exponents.

This paper takes an entirely different route and considers designing a detector capable to catch the energy flow from the vertical modes (heave and pitch) to the roll mode. The idea of assessing parametric excitation by a function introduced as energy flow, was proposed in [27]. This paper suggests a new detection scheme based on the GLRT (generalised likelihood ratio test) for non-Gaussian signals. Galeazzi et al. [27] showed that the onset of the parametric roll may be detected looking at the transfer of energy from the first harmonic of pitch and/or heave, which are directly excited by the wave motion, to the second harmonic of roll. This coupling between pitch and roll is further exploited in this paper, generating a driving signal that carries the information of how the pitch motion excites the roll motion determining the development of the resonant motion.

[1] `http://www.amarcon.com/products/index.html?main=http://www.amarcon.com/products/resonance.html`

Using a set of experimental data, the paper presents a statical analysis to find the distribution of the driving signal, which is shown to be non-Gaussian. A dedicated change detector is then designed implementing a recursive GLRT for the specific distributions found in the signals. The performance of the proposed detection scheme is tested on a set of experimental data of a 1:45 scale model of container ship with a length overall of 294 m, demonstrating the features and quality of the new detector.

Methods presented in this paper are covered by patents pending: EP 09157857.5 and US 61/169,154.

E.2 Driving Signal

In order to obtain detection of parametric roll in the time domain it is crucial to find a suitable signal that can characterise the presence/absence of the resonant motion. When parametric roll develops there is a lining up of peaks between the pitch motion and the roll motion, pointed out by [15], that is, every second peak of pitch is in-phase with the peak in roll, as illustrated in Fig. E.1. Figure E.1 also shows that when this alignment is temporarily lost, roll oscillations start decaying, as seen between 150 and 250 seconds and after 300 seconds in the Figure. Therefore, a signal that carries phase information of pitch and roll could be exploited for solving the detection problem.

Consider two sinusoidal signals s_1 and s_2 given by

$$\begin{aligned} s_1 &= A_1 \cos(\omega t + \psi_1) \\ s_2 &= A_2 \cos(2\omega t + \psi_2)\,. \end{aligned} \tag{E.1}$$

Computing the square of s_1 gives a new signal that has one component at 2ω and one at ω

$$s_1^2 = A_1^2 \cos^2(\omega t + \psi_1) \tag{E.2}$$

$$= A_1^2 \left[\cos(2\omega t + 2\psi_1) + \sin^2(\omega t + \psi_1)\right]. \tag{E.3}$$

Multiplying s_1^2 by s_2, the following signal is obtained,

$$\begin{aligned} s_1^2 s_2 = A_1^2 A_2 [&\cos(2\omega t + 2\psi_1)\cos(2\omega t + \psi_2) \\ &+ \sin^2(\omega t + \psi_1)\cos(2\omega t + \psi_2)], \end{aligned} \tag{E.4}$$

which, by the change of variable $\varepsilon = 2\omega t + \psi_2$, is rewritten as,

$$\begin{aligned} s_1^2 s_2 = A_1^2 A_2 [&\cos(\varepsilon - \psi_2 + 2\psi_1)\cos\varepsilon \\ &+ \sin^2\left(\frac{\varepsilon - \psi_2}{2} + \psi_1\right)\cos(\varepsilon)]. \end{aligned} \tag{E.5}$$

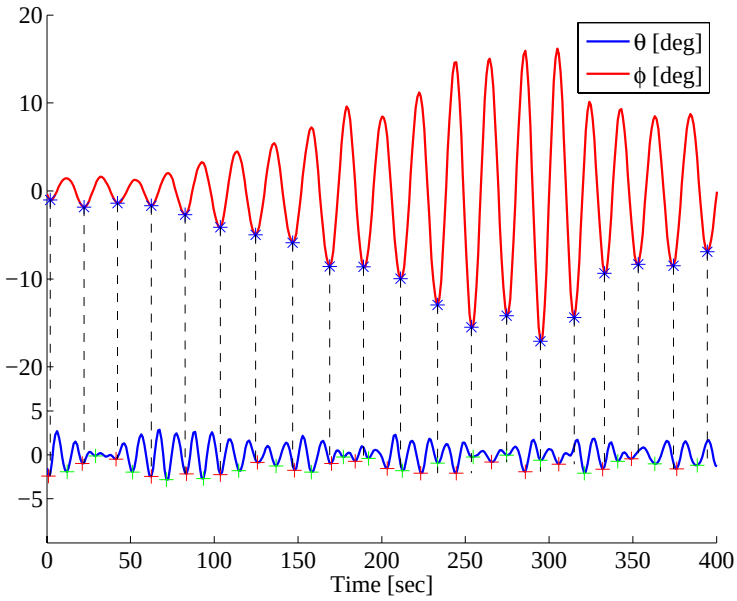

Figure E.1: Experiment 1195: alignment of peaks between pitch θ and roll ϕ during the onset and development of parametric roll.

Equation (E.5) shows that if s_1^2 and s_2 are in-phase ($2\psi_1 - \psi_2 = 0$) then,

$$s_1^2 s_2 = \frac{1}{2} A_1^2 A_2 (\cos^2 \varepsilon + \cos \varepsilon), \tag{E.6}$$

whereas if s_1^2 and s_2 are out-of-phase ($2\psi_1 - \psi_2 = \pi$) then,

$$s_1^2 s_2 = -\frac{1}{2} A_1^2 A_2 (\cos^2 \varepsilon - \cos \varepsilon), \tag{E.7}$$

that means, the signal $s_1^2 s_2$ shows positive or negative peaks of maximum amplitude $A_1^2 A_2$.

Given roll angle ϕ and pitch angle θ, the signal driving the parametric resonance in roll is then defined as,

$$d(t) \triangleq \phi^2(t)\, \theta(t). \tag{E.8}$$

Considering Fig. E.2, where $\theta(t)$, $\phi^2(t)$ and $d(t)$ are plotted for one experiment without parametric roll (Exp. 1194) and another with parametric roll (Exp. 1195), the driving signal d seems to characterise quite well the way the amplitude

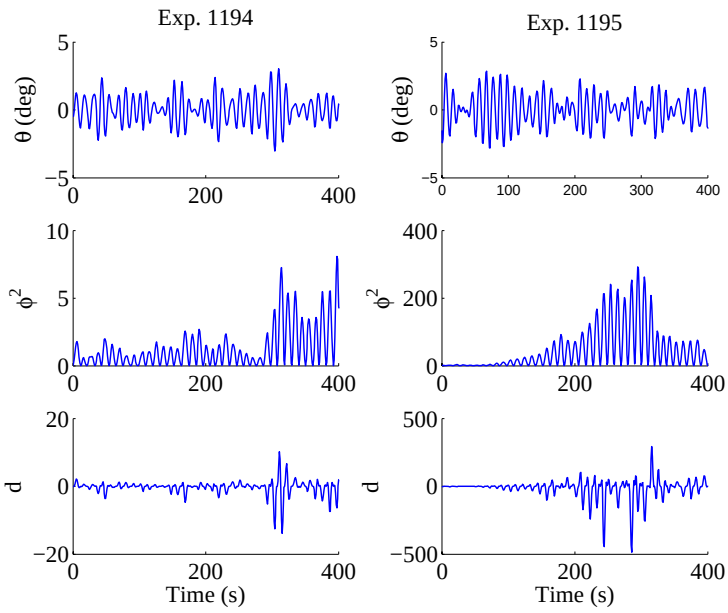

Figure E.2: Negative and positive peaks in d address how the amplitude of the roll oscillations increases and decreases.

grows or decays inside the signal ϕ^2. In particular it is possible to notice that when the amplitude of ϕ^2 abruptly grows, a sequence of negative spikes appear up in the driving signal. In contrast, when the amplitude of ϕ^2 decreases, positive spikes reflect this condition in the driving signal.

Moreover, when parametric roll is developing, the magnitudes of negative spikes in the driving signal are much larger then those appearing when the roll mode is not in a resonant condition. Therefore, a remarkable variation in the variance of the driving signal d could be expected from the inception of parametric roll. A jump in variance could be exploited by setting up a detector that looks for variation of signal power in a random signal with a certain amplitude distribution. Several detection schemes are present in literature, which differ by the nature of the signal we wish to detect (deterministic/stochastic) and by the distribution of noise atop the signal (Gaussian/non-Gaussian). A fairly complete survey about detection theory can be found in [46] and references therein. The literature on change detection also advise on general methods to assess probabilities of detection and false alarm given amplitude distributions and detection methods. To select the most appropriate detection scheme it is of paramount importance to know the distribution of the signals at hand.

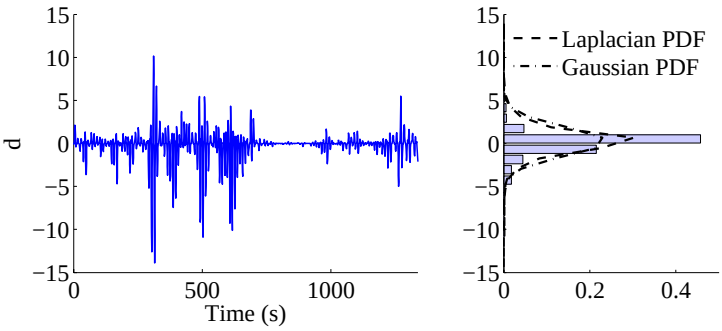

Figure E.3: Experiment 1194: histogram of the driving signal for the non resonant case.

Histograms of the driving signal have been plotted for the resonant and non resonant cases (see an example in Figs. E.3-E.4). Two main characteristics can be pointed out: the presence of a very sharp peak in correspondence of the mean value, and long tails. Figure E.4 clearly shows that a Gaussian probability density function (PDF) does not fit the data since it is not able to catch the presence of the high peak in the histogram; on the other hand the Laplacian PDF better approximate the behaviour of the histogram. Moreover the heavy tails of the Laplacian PDF can also explain the presence of spikes observed in the time series.

The Laplacian distribution was chosen to describe the nature of the driving signal. It has the probability density function,

$$p\left(d\right) = \frac{1}{\sqrt{2\sigma_0^2}} \exp\left(-\sqrt{\frac{2}{\sigma_0^2}}\left|d-\mu_0\right|\right), \tag{E.9}$$

where μ_0 is the mean value, and σ_0^2 is the variance or signal power.

The histograms also suggest that a good way to discriminate between resonant and non resonant cases is to look for a variation in signal power. Ideally, in the non resonant case the variance of the driving signal would be zero because no roll motion is expected when a ship sails in head seas. In real life, instead, the wave train approaches the ship with a certain spreading factor, resulting in an excitation also along the transversal plane of the ship. This excitation induces small roll oscillations, which in turn gives a driving signal d with power different from zero (as shown in Fig. E.3). Therefore a detector which looks for abrupt changes in signal power is designed.

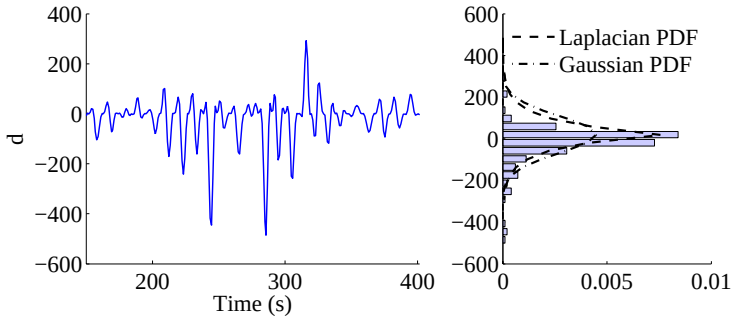

Figure E.4: Experiment 1195: histogram of the driving signal for $150 \leq t \leq 400$ when parametric roll develops. The laplacian PDF better approximates the histogram.

E.3 GLRT for Laplacian Signals

Established the distribution describing the driving signal $d(t)$, it is possible to see the detection problem as the detection of a variation of signal power σ^2 in a Laplacian distributed signal.

The detection of parametric roll can be formulated as

$$\begin{aligned} \mathcal{H}_0 &: x[n] = d[n] \ , \ \sigma_d^2 = \sigma_0^2 \qquad n = 0, 1, \ldots, N-1 \\ \mathcal{H}_1 &: x[n] = d[n] \ , \ \sigma_d^2 = \sigma_1^2 \qquad n = 0, 1, \ldots, N-1 \end{aligned} \tag{E.10}$$

where σ_1^2 is an unknown variation in the signal power, and d is Laplacian distributed with probability density function given by equation (E.9), where μ_0 and σ_0 are known. The generalised likelihood ratio test (GLRT) decides $\mathcal{H}_1$ if

$$L_G = \frac{p\left(d; \hat{\sigma}_1^2, \mathcal{H}_1\right)}{p\left(d; \mathcal{H}_0\right)} > \gamma, \tag{E.11}$$

where $\hat{\sigma}_1^2$ is the maximum likelihood estimate (MLE) of σ_1^2, and γ is a threshold set by the probability of false alarms the detector is desired to have. The first step in this approach is therefore to find the MLE of the unknown parameter.

To find the MLE of σ_1 it corresponds to the maximisation over σ_1 of,

$$p(d) = \left(\frac{1}{2\sigma_1^2}\right)^{\frac{N}{2}} \exp\left(-\sqrt{\frac{2}{\sigma_1^2}} \sum_{n=0}^{N-1} |d[n] - \mu_0|\right), \tag{E.12}$$

that means to determine for which value of $\sigma_1 > 0$ the partial derivative of $p(d)$ w.r.t. σ_1 is equal to zero,

$$\frac{\partial p}{\partial \sigma_1} = 0 \Rightarrow \hat{\sigma}_1 = \frac{\sqrt{2}}{N} \sum_{n=0}^{N-1} |d[n] - \mu_0| . \tag{E.13}$$

Having determined the MLE $\hat{\sigma}_1$ it is then possible to derive an explicit form for the detector. By taking the natural logarithm of both sides of equation (E.11),

$$\begin{aligned} \ln \frac{p\left(d; \hat{\sigma}_1^2, \mathcal{H}_1\right)}{p\left(d; \mathcal{H}_0\right)} > \ln \gamma \Rightarrow \\ \frac{N}{2} \ln \left(\frac{\sigma_0^2}{\hat{\sigma}_1^2} \right) + \sqrt{2} \left(\frac{\hat{\sigma}_1 - \sigma_0}{\sigma_0 \hat{\sigma}_1} \right) \sum_{n=0}^{N-1} |d[n] - \mu_0| > \gamma' \Rightarrow \\ -\frac{N}{2} \ln \hat{\sigma}_1^2 + N \left(\frac{\hat{\sigma}_1 - \sigma_0}{\sigma_0 \hat{\sigma}_1} \right) \hat{\sigma}_1 > \gamma'', \end{aligned} \tag{E.14}$$

where $\gamma'' = \gamma' - \frac{N}{2} \ln \sigma_0^2$. Simplifying equation (E.14), the detector reads,

$$-\frac{N}{2} \ln \hat{\sigma}_1^2 + N \frac{\hat{\sigma}_1}{\sigma_0} > \gamma'''. \tag{E.15}$$

where, $\gamma''' = \gamma'' + N$.

E.3.1 Recursive implementation

A recursive implementation of the detector allows to perform a real-time estimation of when parametric roll starts developing. If $M = nT_\phi$ is the window length, where T_ϕ is the roll period and $n \in \mathbb{N}$, then the GLRT decision function can be written as ([7]),

$$\mathrm{GLRT}(k) = \max_{k-M+1 \le j \le k} S_j^k \left(\hat{\sigma}_1 (j,k) \right), \tag{E.16}$$

where $S_j^k \left(\hat{\sigma}_1 (j,k) \right)$ is the log-likelihood between the hypothesis $\mathcal{H}_0$ and $\mathcal{H}_1$

$$S_j^k \left(\hat{\sigma}_1 (j,k) \right) = \sum_{i=j}^{k} \ln \frac{p\left(d(i); \hat{\sigma}_1^2, \mathcal{H}_1\right)}{p\left(d(i); \mathcal{H}_0\right)}. \tag{E.17}$$

If at the sample k the GLRT(k) is greater than the chosen threshold γ''', then the hypothesis $\mathcal{H}_1$ is accepted and an alarm is triggered at the alarm time $k_a = k$. The estimated time of the onset of parametric roll can then be computed as,

$$\hat{k}_o = \arg \left\{ \max_{k_a - M + 1 \le j \le k_a} S_j^k \left(\hat{\sigma}_1 (j, k_a) \right) \right\}. \tag{E.18}$$

E.3.2 Threshold determination

Two methods can be taken into consideration in order to determine the threshold γ against which the decision function has to be compared:

- asymptotic analysis of the performance of the GLRT detector;
- empirical method based on the set of experimental data at hand.

[46] showed that, given a PDF $p(d,\theta)$ where θ is a vector of unknown parameters, for large data records or asymptotically (as $N \to \infty$) the modified GLRT statistic $2L_G(d)$ has the PDF,

$$2L_G(d) \overset{a}{\sim} \begin{cases} \chi_r^2 & \text{under } \mathcal{H}_0 \\ \chi_r'^2(\lambda) & \text{under } \mathcal{H}_1 \end{cases} \tag{E.19}$$

where χ_r^2 is a chi-squared PDF with r degrees of freedom, and $\chi_r'^2(\lambda)$ is a non-central chi-squared PDF with r degrees of freedom and non-centrality parameter λ, which is a function of the parameter vector θ. Under the hypothesis $\mathcal{H}_0$ the asymptotic PDF does not depend on θ, hence the threshold required to achieve a constant probability of false alarms P_{FA} can be determined. This detector is therefore referred as a constant false alarm rate (CFAR) detector.

According to [46], the probability of false alarms can be determined by observing that a random variable x, with $x \sim \chi_1'^2(\lambda)$, is equal to the square of a random variable y, with $y \sim \mathcal{N}\left(\sqrt{\lambda}, 1\right)$. Hence under the hypothesis $\mathcal{H}_0$

$$\begin{aligned} P_{FA} &= \Pr\{x > \gamma'; \mathcal{H}_0\} \\ &= \Pr\left\{y > \sqrt{\gamma'}; \mathcal{H}_0\right\} + \Pr\left\{y > -\sqrt{\gamma'}; \mathcal{H}_0\right\} \\ &= 2Q\left(\sqrt{\gamma'}\right). \end{aligned} \tag{E.20}$$

Therefore the threshold is given by

$$\gamma' = \left[Q^{-1}\left(\frac{1}{2}P_{FA}\right)\right]^2 \tag{E.21}$$

where $Q(\cdot)$ is the complementary cumulative distribution function. Substituting γ' into γ''' we obtain

$$\gamma''' = \left[Q^{-1}\left(\frac{1}{2}P_{FA}\right)\right]^2 - \frac{N}{2}\ln\sigma_0^2 + N, \tag{E.22}$$

where it should be noted that for a desired P_{FA} the threshold increases with the amount of data samples we take into consideration.

With limited experimental data available, empirical determination of the threshold had to be chosen. Inspecting the behaviour of the GLRT decision function for the set of available experimental data, the threshold was set to a value that ensures a low probability of false alarms, yet still allowing a quick detection of the onset of parametric resonance.

E.4 Detection Scheme Validation

The parametric roll detector based on the GLRT for Laplacian distributed signals was validated against a set of experimental data of a 1:45 scale model of a container vessel with a length overall of 294 m ([36]). The experiments were conducted in a towing tank with regular and irregular waves, varying wave frequency and height, and ship forward speed. Tables E.1-E.2 summarise the characteristics of the different runs, where A_w is the wave amplitude, ω_w is the wave frequency, ω_e is the wave encounter frequency, H_s is the significant wave height, T_p is the peak period of the wave, and $\phi_{\max}$ is the maximum roll angle reached during the run. For the regular wave data set, out of 11 experiments 7 reported parametric roll; whereas only in the experiment 1195 parametric roll occurred for the irregular wave data set.

Table E.1: Regular wave experiments

Exp.	A_w [m]	ω_w [rad/s]	ω_e/ω_ϕ	$\lvert\phi_{\max}\rvert$ [deg]
1192	2.5	0.4640	1.9021	0.8944
1193	2.5	0.4640	1.9226	1.8932
1191	2.5	0.4640	1.9428	21.7800
1172	2.5	0.4640	1.9633	23.9270
1184	2.5	0.4640	1.9834	22.7810
1185	2.5	0.4640	2.0032	20.8780
1186	2.5	0.4640	2.0234	21.5640
1187	2.5	0.4640	2.0439	20.4990
1188	2.5	0.4640	2.0842	22.7190
1190	2.5	0.4640	2.1047	1.4291
1189	2.5	0.4640	2.1245	1.4368

The parameters of the GLRT for Laplacian signals have been set up using the time series of the experiments where parametric roll did not occur. In particular

Table E.2: Irregular wave experiments

Exp.	H_s [m]	T_p [s]	$\lvert\phi_{\max}\rvert$ [deg]
1194	9	13.54	2.91
1195	9	13.54	17.24
1196	9	13.54	2.88
1197	7	13.54	1.68
1198	7	13.54	4.23
1199	9	13.54	1.83
1200	9	13.54	1.74
1201	9	13.54	1.45

the mean value μ_0 was chosen as

$$\mu_0 = E[\mu_d] = \frac{\sum_{j=1}^{M} w_j \mu_{d_j}}{\sum_{j=1}^{M} w_j}, \tag{E.23}$$

and the standard deviation σ_0 was chosen as

$$\sigma_0 = E[\sigma_d] = \frac{\sum_{j=1}^{M} w_j \sigma_{d_j}}{\sum_{j=1}^{M} w_j}, \tag{E.24}$$

where $E[\cdot]$ is expected value, $(\mu_{d_j}, \sigma_{d_j})$ are the mean value and the standard deviation of the driving signal of the j-th experiment, respectively, and $w_j = 1/L_j$ is the weight given as the reciprocal of the time series length L_j. M is the number of experiments where parametric roll did not occur.

The recursive implementation of the change detector has been provided with a constraint (dash-dotted line) set to 2γ, which limits the maximum value the GLRT decision function can reach. An out-of-resonance threshold (dashed line) is set to 0.5γ, which determines when the critical condition can be considered overcome.

E.4.1 Regular waves

The detection performance of the detector for the regular waves data set is summarised in Table E.3.

Looking at the maximum roll angle reached within the detection time T_d it is seen that the proposed detector is capable to trigger an early warning when the roll oscillations are still small (less than 5°). Moreover, the detector did not

Table E.3: Regular wave experiments: sinusoidal detection

Exp.	T_d [s]	$\lvert\phi_{\max}(T_d)\rvert$ [deg]	PR	Detection
1172	474	3.15	Yes	Correct
1184	302	2.88	Yes	Correct
1185	353	2.54	Yes	Correct
1186	434	2.55	Yes	Correct
1187	354	2.51	Yes	Correct
1188	285	2.35	Yes	Correct
1189	-	-	No	Correct
1190	-	-	No	Correct
1191	304	2.61	Yes	Correct
1192	-	-	No	Correct
1193	-	-	No	Correct

issue any false alarms, hence providing exact detection for all 11 runs. Examples of detection can be seen in Figs. E.5-E.6.

E.4.2 Irregular waves

Table E.4 presents detection performance of the parametric roll detector on the set of experiments in irregular waves.

Table E.4: Irregular wave experiments: sinusoidal detection

Exp.	T_d [s]	$\lvert\phi_{\max}(T_d)\rvert$ [deg]	PR	Detection
1194	-	-	No	Correct
1195	94	3.27	Yes	Correct
1196	-	-	No	Correct
1197	-	-	No	Correct
1198	215	3.81	No	1 False Pos.
1199	-	-	No	Correct
1200	-	-	No	Correct
1201	-	-	No	Correct

The detection scheme works well also in these cases, achieving a quick detection in the experiment 1195 where parametric roll did occur. The alarm triggered for the experiment 1198 has been classified as a false positive since visual inspection of the time series addressed that the resonant motion did not develop, but considering the maximum roll angle achieved when the detector issues the warning it may be possible to classify this experiment as a border case, that is parametric roll could develop but all the sudden the next wave train did not satisfy the requirements to allow the resonant motion to keep growing. The

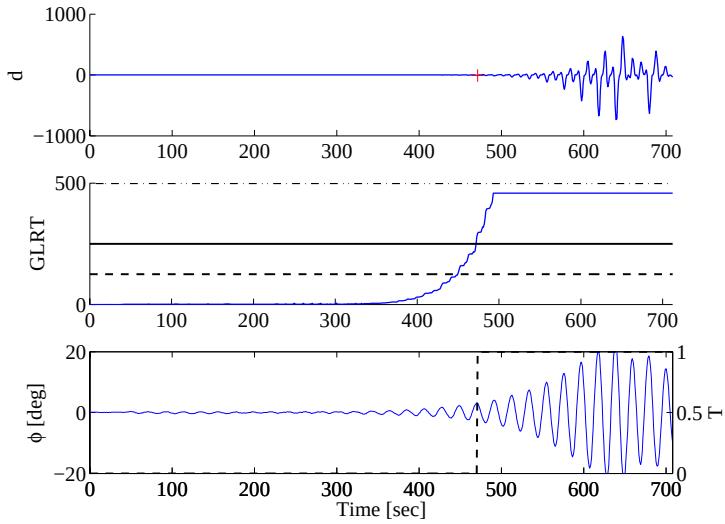

Figure E.5: Experiment 1172: detection of parametric roll.

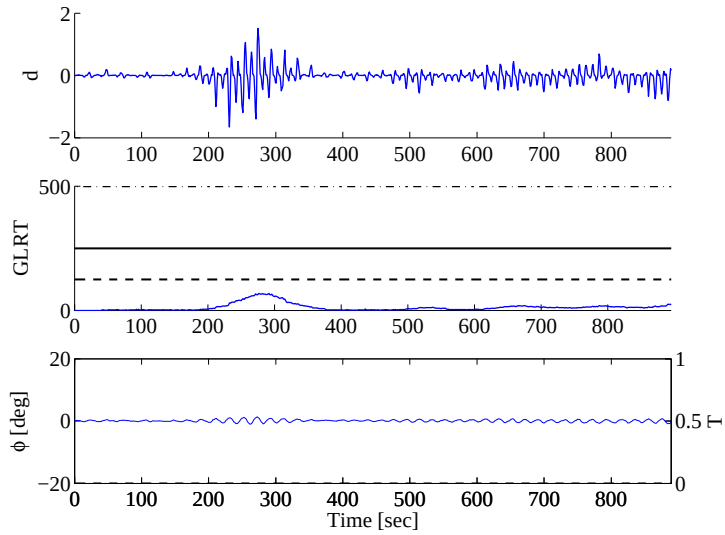

Figure E.6: Experiment 1189: the GLRT never crosses the threshold.

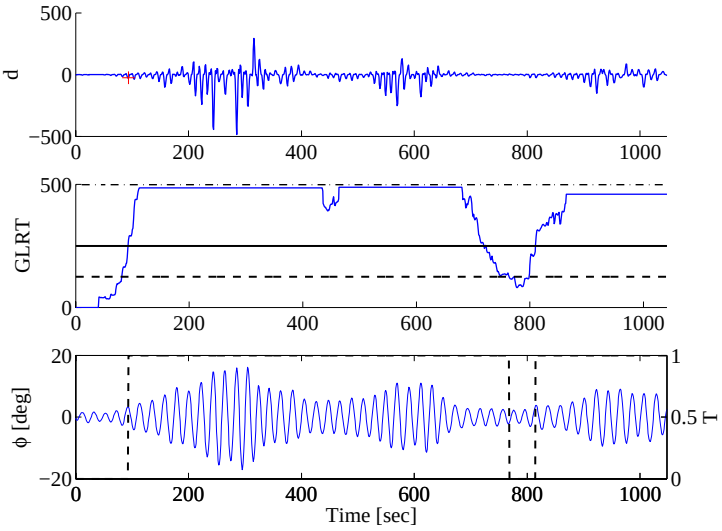

Figure E.7: Experiment 1195: detection of parametric roll.

results of the detection performance are also shown in Figs. E.7-E.8.

E.5 Conclusions

Early detection of parametric roll resonance was considered and a detector based on the GLRT for the particular non-Gaussian distributed signals was proposed. A driving signal carrying the information about phase correlation between pitch and roll was chosen. A detector was derived that looks for variation in the power of this signal using a generalised log-likelihood ratio test, and a recursive change detector was implemented, allowing real-time detection of parametric roll.

The performance of the new detection scheme was evaluated against two sets of experimental data. The detector showed good capabilities of issuing early warning in all the runs where parametric roll occurred, triggering alarms already when roll amplitudes were less than 5°. Only one possibly false alarm was issued and this happened in conditions close to parametric resonance.

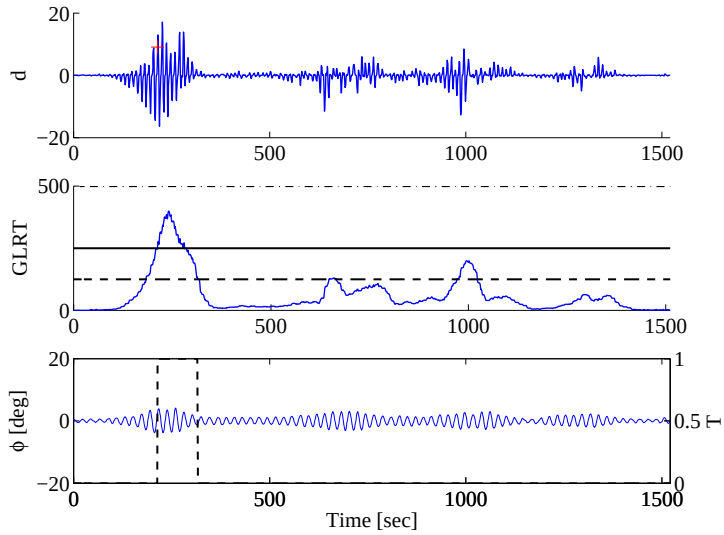

Figure E.8: Experiment 1198: false alarm.

Acknowledgements

The authors are grateful to Dr. Drummen and Dr. Perez from CeSOS, and to Dr. Storhaug from DNV for performing the experiments at the Centre for Marine Technology in Trondheim.

[This page intentionally left blank]

www.elektro.dtu.dk
Department of Electrical Engineering
Automation and Control
Technical University of Denmark
Ørsteds Plads
Building 348
DK-2800 Kgs. Lyngby
Denmark
Tel: (+45) 45 25 38 00
Fax: (+45) 45 93 16 34
Email: info@elektro.dtu.dk

ISBN 978-87-92465-16-0